DOT/FAA/TC-17/6

Federal Aviation Administration
William J. Hughes Technical Center
Aviation Research Division
Atlantic City International Airport
New Jersey 08405

Mode I (GIC) Fracture Toughness of Composite Sandwich Structures for Use in Damage Tolerance Design and Analysis: Vol. II: Fatigue Testing, Including Effects of Fluid Ingression

October 2017

Final Report

U.S. Department of Transportation
Federal Aviation Administration

NOTICE

Technical Report Documentation Page

1. Report No.	2. Government Accession No.	3. Recipient's Catalog No.
DOT/FAA/TC-17/6		

4. Title and Subtitle	5. Report Date
MODE I (GIC) FRACTURE TOUGHNESS OF COMPOSITE SANDWICH STRUCTURES FOR USE IN DAMAGE TOLERANCE DESIGN AND ANALYSIS: VOL. II: FATIGUE TESTING, INCLUDING EFFECTS OF FLUID INGRESSION	October 2017
	6. Performing Organization Code

7. Author(s)	8. Performing Organization Report No.
John S. Tomblin, Waruna Seneviratne, and Shawn Denning	

9. Performing Organization Name and Address	10. Work Unit No. (TRAIS)
National Institute for Aviation Research Wichita State University Wichita, KS 67260	
	11. Contract or Grant No.

12. Sponsoring Agency Name and Address	13. Type of Report and Period Covered
FAA Northwest Mountain Regional Office 1601 Lind Ave SW Renton, WA 98057	14. Sponsoring Agency Code AIR-100

15. Supplementary Notes

The FAA William J. Hughes Technical Center Aviation Research Division CORs were Curtis Davies and Lynn Pham.

16. Abstract

This report, Volume II, contains results of Mode I fatigue testing of composite sandwich structures. This report is the second of a set of three volumes. The first volume contained results of Mode I static testing, and the third volume will contain supplemental results of Mode I static testing of sandwich variables not tested in Volume I.

In this volume, the influence of sandwich parameters, such as facesheet thickness, core type, cell size, and core density, on the onset and damage growth rate of sandwich composites was investigated using single-cantilever beam fatigue testing for Mode I fracture toughness of the core-facesheet disbond. To investigate the influence of fluid ingression and entrapped fluids in sandwich structures, test specimens were conditioned in a hydraulic oil (Skydrol®) and water mixture. In general, fluid-ingressed specimens experienced faster crack growth than baseline specimens. The information gathered through this research will be instrumental in developing analytical methods and validating finite element analysis procedures to further investigate the damage growth mechanics in composite sandwich structures. The data can also be used in design for composite sandwich structures constructed of similar materials and geometries tested here.

17. Key Words	18. Distribution Statement
Progressive damage growth, Composite sandwich, GAG cycle, Fluid ingression, Mode I testing	This document is available to the U.S. public through the National Technical Information Service (NTIS), Springfield, Virginia 22161. This document is also available from the Federal Aviation Administration William J. Hughes Technical Center at actlibrary.tc.faa.gov.

19. Security Classif. (of this report)	20. Security Classif. (of this page)	21. No. of Pages	22. Price
Unclassified	Unclassified	197	

ACKNOWLEDGEMENTS

This research program was funded by the FAA William J. Hughes Technical Center in Atlantic City, NJ. The authors would like to thank Curtis Davies of the FAA William J. Hughes Technical Center and Dr. Larry Ilcewicz of the FAA Seattle Aircraft Certification Office for their technical guidance. In addition, the support provided by Cessna Aircraft, Bombardier Aerospace, Hawker Beechcraft, and Spirit Aerosystems was appreciated.

The authors would also like to thank the National Institute for Aviation Research Composites and Structures Laboratory staff for their commitment and hard work. Specifically, we would like to thank Upul Palliyaguru, Janith Senaratne, Tharindu Jayaratne, Chee-Kuen Chan, Jason Koehn, Errick Robles, Jeffery Robles, and Benjamin Coon for their support during fabrication, testing, and data reduction.

TABLE OF CONTENTS

LIST OF FIGURES

LIST OF TABLES

LIST OF ACRONYMS

da/dn	Crack growth rate
GIC	Mode I fracture toughness
G_{Imax}	Strain energy release rate during cyclic loading
G_{Ith}	Threshold strain energy release rate
A	Adhesive interface disbond failure
C	Tensile core failure
CDT	Critical damage threshold
DCB	Double-cantilever beam
F	Modified correction factor
GAG	Ground-air-ground
HX	Hexagonal core
NIAR	National Institute for Aviation Research
OX	Overexpanded core
PO	Adhesive pullout failure
RTD	Room temperature dry
RTW	Room temperature wet
S	Interlaminar facesheet delamination failure
SCB	Single-cantilever beam
SERR	Strain energy release rate

EXECUTIVE SUMMARY

The influence of sandwich parameters (such as facesheet thickness, core type, cell size, and core density) on the onset and damage growth rate of sandwich composites was investigated using single-cantilever beam fatigue testing for Mode I fracture toughness of the core-facesheet disbond. To investigate the influence of fluid ingression and entrapped fluids in sandwich structures, test specimens were conditioned in a hydraulic oil (Skydrol®) and water mixture. The fluid-ingression phenomenon in composites is a concern relative to sandwich structures. Inadequate design details and poor material selection can result in microcracks during ground-air-ground (GAG) cycling that consequently coalesce to form transverse matrix cracks leading to moisture ingression into the subsequent composite and adhesive layers and finally into the core. Impact damage to sandwich structures exacerbates the fluid-ingression phenomenon as a result of localized transverse cracks, delaminations, disbonds, and core damages. Thermo-mechanical loads during GAG cycling could cause local buckling on the compression side of sandwich structures, which results in localized Mode I stresses that may result in further delamination/disbond growth, thereby creating more passageways for fluid migration. In addition, trapped water in sandwich cells translates into vapor during high temperatures, thereby increasing the internal pressure and causing core disbonds or fractures. In some cases, the damage growth resulting from these two mechanisms is stable and occurs over a period of several flights, but it may not be readily detected on the ground when the thermo-mechanical and internal vapor pressure loads are released. Though the damage size continues to grow in such cases, the structure will continue to carry loads until it reaches a critical damage threshold (CDT), whereupon the unstable damage growth triggers catastrophic failure. Unless such damage is detected and repaired prior to reaching the CDT, GAG cycling effects will increase the size of damage and threaten the structural integrity and safety of the aircraft. Ingressed fluid increases the rate of crack growth of specimens when compared to baseline specimens. The information gathered through this research will be instrumental in developing analytical methods and validating finite element analysis procedures to further investigate the damage growth mechanics of composite sandwich structures. The data can also be used in design for composite sandwich structures constructed of the similar materials and geometries tested here.

1. INTRODUCTION

Over the past 25 years, the use of advanced composite materials in aircraft primary structures has increased significantly. In 1994, with the Advanced General Aviation Transport Experiments program, NASA and the FAA revitalized the use of composites in both general and commercial aviation. Driven by the demand for fuel-efficient, lightweight, and high-stiffness structures with fatigue durability and corrosion resistance, large modern commercial aircraft are now designed with more than 50% composite materials. Because of the key differences between metal and composite damage mechanics and durability concerns, the certification philosophy for composites must meet rigorous structural integrity, safety, and durability requirements. Despite the many advantages of composites, composite structural certification becomes challenging because of a lack of experience with large-scale structures, complex interactive failure mechanisms, sensitivity to temperature and moisture, and scatter in the data, especially fatigue.

The current research effort was designed to investigate the fluid-ingression phenomenon in sandwich structures and the resulting progressive damage growth due to ground-air-ground (GAG) cycling. Inadequate design details and poor material selection as well as operational damages can cause fluid ingression into the core. Impact damage on sandwich structures exacerbates the fluid-ingression phenomenon as a result of localized transverse cracks, delaminations, disbonds, and core damages. Thermo-mechanical loads during GAG cycling could cause local buckling on the compression side of a sandwich structure, resulting in localized Mode I stresses that may result in further delamination/disbond growth, thereby creating more passageways for fluid migration. In addition, trapped water in sandwich cells translates into vapor during high temperatures, thereby increasing the internal pressure and causing core disbonds or fractures. In some cases, the damage growth resulting from these two mechanisms is stable and occurs over a period of several flights, but it may not be readily detected on the ground when the thermo-mechanical and internal vapor pressure loads are released. Though the damage size continues to grow in such cases, the structure will continue to carry loads until it reaches a critical damage threshold (CDT), whereupon the unstable damage growth triggers catastrophic failure. Unless such damage is detected and repaired prior to reaching the CDT, GAG cycling effects will increase the size of damage and threaten the structural integrity and safety of the aircraft.

This investigation used single-cantilever beam (SCB) fatigue testing for Mode I fracture toughness of core-facesheet constructions because the failure modes included core, disbonds, and adhesive. The influence of sandwich parameters (such as facesheet thickness, core size, core density, and cell size) on the onset and damage growth rate (da/dn) of sandwich composites was investigated. Furthermore, the influence of the fluid-ingression phenomenon and progressive damage growth due to entrapped fluids in sandwich structures was investigated. The figure 1 flow chart shows how the data generated in this program will result in guidance for durability and damage tolerance of sandwich composite structures.

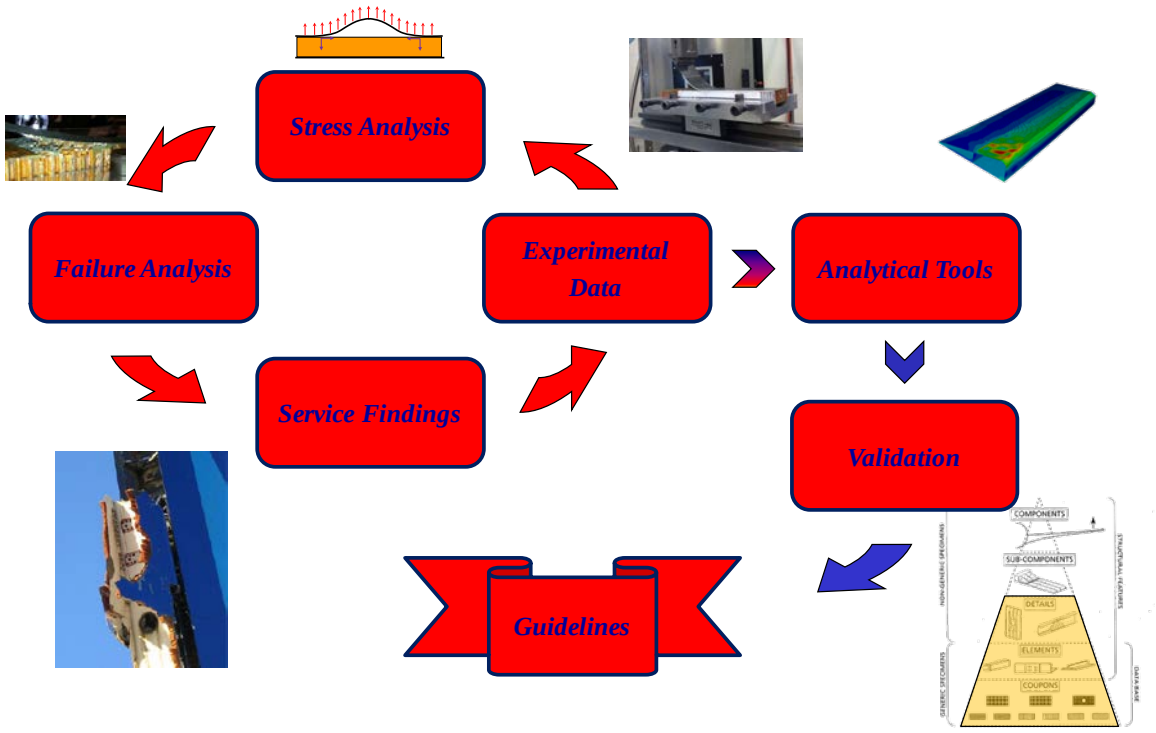

Figure 1. Objective of current research program

The onset of damage propagation and the CDT are a function of the stress level for a particular damage configuration. Typically, certification programs adopt a "no-growth" damage-tolerant design concept, whereby a composite structure is required to demonstrate the ability to contain intrinsic manufacturing defects, and the maximum allowable service damage(s) in adverse operational conditions and throughout the design life of the structure (i.e., the allowable damage limit) is selected so that the fatigue stress level corresponding to the limit load of the structure will not cause the onset of damage propagation prior to a life corresponding to the design service goal. In contrast, a "stable-growth" damage-tolerant design concept must consider damage growth only if the following apply:

- Damage growth is stable or an arrest mechanism is in place prior to the damage reaching the CDT.
- Damage growth can be predicted through analysis and can be verified by testing.
- If applicable, two inspection intervals occur prior to the damage reaching the CDT.

Because the onset of damage propagation depends on several design parameters (e.g., load spectrum/severity, damage configuration, damage location with respect to the primary load path, environmental exposure, facesheet thickness, core density or cell size of sandwich construction, fracture toughness, etc.), the application of load-enhancement factors to a structure that exhibits stable damage growth during testing may significantly alter its fatigue life. Damage-tolerance substantiation through a stable-growth approach for a specific structure requires great confidence at the onset (initiation) and during the growth rate (propagation), as well as knowledge of the factors influencing both initiation and propagation. The literature revealed that, through

experimental validation, the fracture toughness of an adhesive or the core can be used to predict crack initiation [1]. The influence of key parameters (e.g., initial damage configuration, fracture toughness at different altitudes and environmental conditions, facesheet thickness, core type, cell size, and core density both at initiation and during propagation) must be studied in detail and incorporated into the certification process to mitigate risks associated with a stable-growth approach. The data contained in this and the preceding report and the following volumes encompass the information regarding the fracture toughness of sandwich structures and the influence of core and facesheet parameters and provide an understanding of the sandwich structure design space and the failure mechanism.

Crack growth can be characterized by three fracture modes [2, 3]: Mode I (opening mode), Mode II (sliding or in-plane shear mode), and Mode III (tearing or out-of-plane shear mode), as shown in figure 2. It is common that combinations of these three modes are present at a crack tip unless care is taken to isolate them, especially during coupon-level testing. This volume focuses on Mode I fracture toughness of sandwich structures under fatigue.

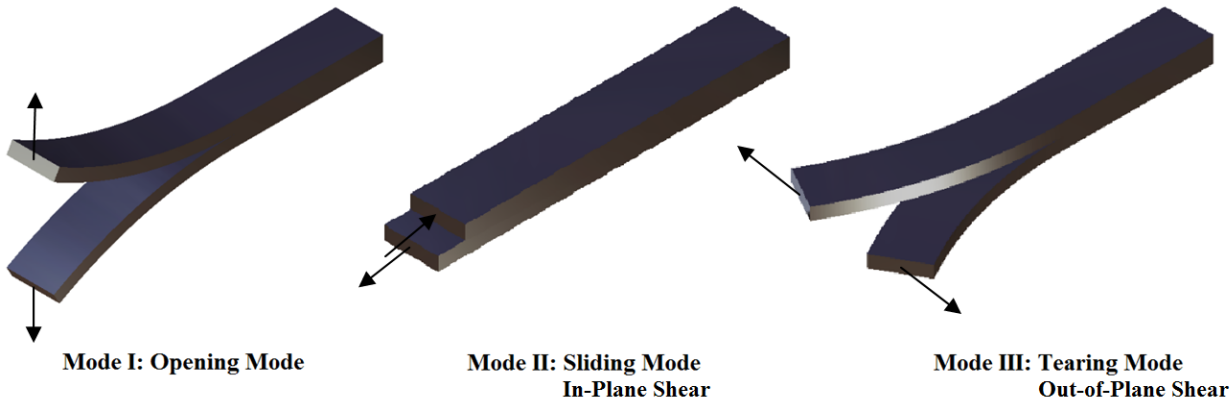

Figure 2. Fracture modes of crack growth

Mode I (GIC) opening mode is considered a material property. For the tests performed here, GIC has a broader meaning. It should be understood more as a structural property of a given sandwich construction. Different failure modes are encountered, so a strict definition of a material property does not apply.

2. EXPERIMENTAL PROCEDURE

The primary objective of this program was to determine Mode I fracture toughness of several sandwich composite material systems. Therefore, it was imperative to develop and use a test configuration that isolated Mode I crack propagation and mitigated Mode II-/Mode III-induced crack growth. Because of the lack of standardized test methods and validated data reduction techniques involving Mode I tests of sandwich structures, a preliminary investigation was conducted to evaluate the feasibility of two test configurations: (1) double-cantilever beam (DCB) and (2) SCB, which are shown in figure 3. The DCB fatigue test for a sandwich structure is a modification of the existing ASTM standard D5528, Mode I Interlaminar Fracture Toughness of Unidirectional Fiber-Reinforced Polymer Matrix Composites and round robin testing conducted at the National Institute for Aviation Research (NIAR) at Wichita State University. Because the round robin data-reduction technique is not directly applicable to the current sandwich specimen, it required modification to address the current test procedure. Therefore, the existing data-reduction methodologies for similar specimens [4–6] were reviewed and modified to suit the sandwich test configurations.

(a) (b)

Figure 3. Test configurations for (a) DCB and (b) SCB [7]

Preliminary DCB tests indicated large rotation of the free end because of the asymmetric nature of the sandwich specimen configuration (i.e., crack along the facesheet-core interface, as shown in figure 4). This potentially added a significant amount of Mode II stresses, resulting in mixed-mode loading at the crack tip. When the free end was stabilized by two rollers to prevent rotation, unsymmetrical bending loads caused core rupture through the thickness and crack propagation along the lower facesheet, a failure known as kinking, which can be seen in figure 5. Both of these DCB test configurations were deemed unacceptable for sandwich specimen testing.

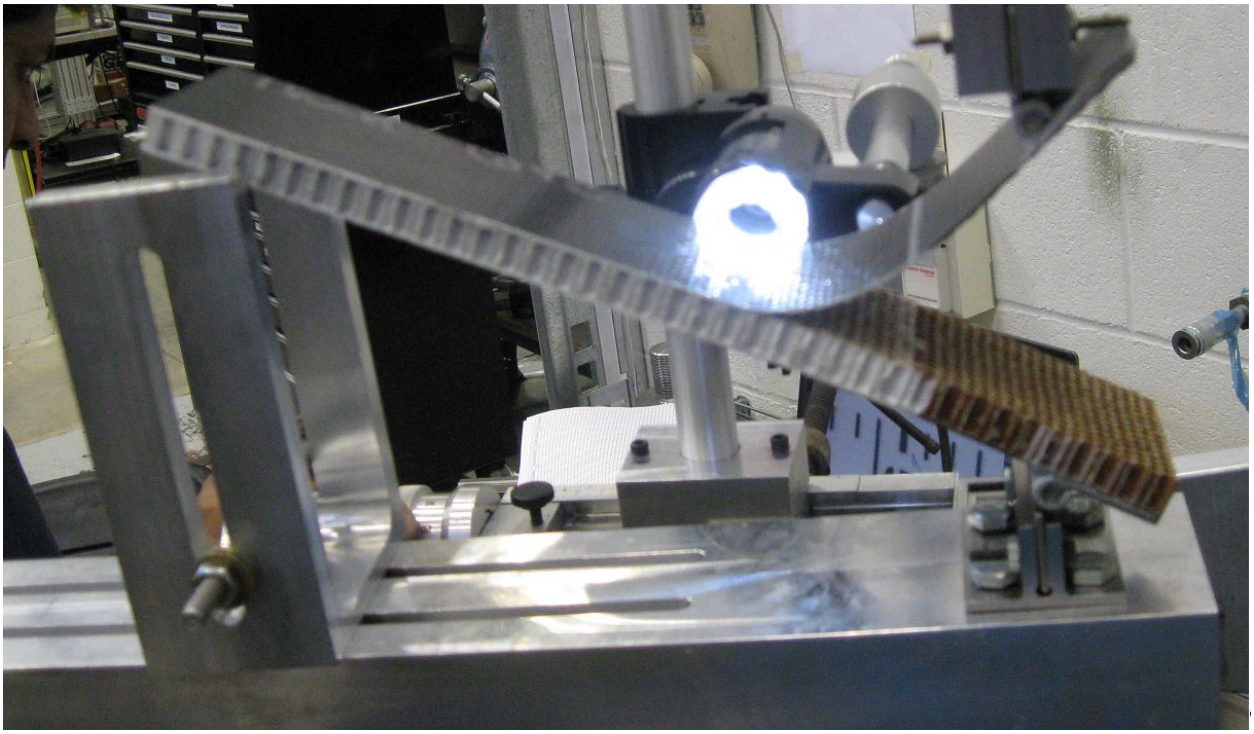

Figure 4. Large rotation of an unstabilized DCB test on sandwich structure

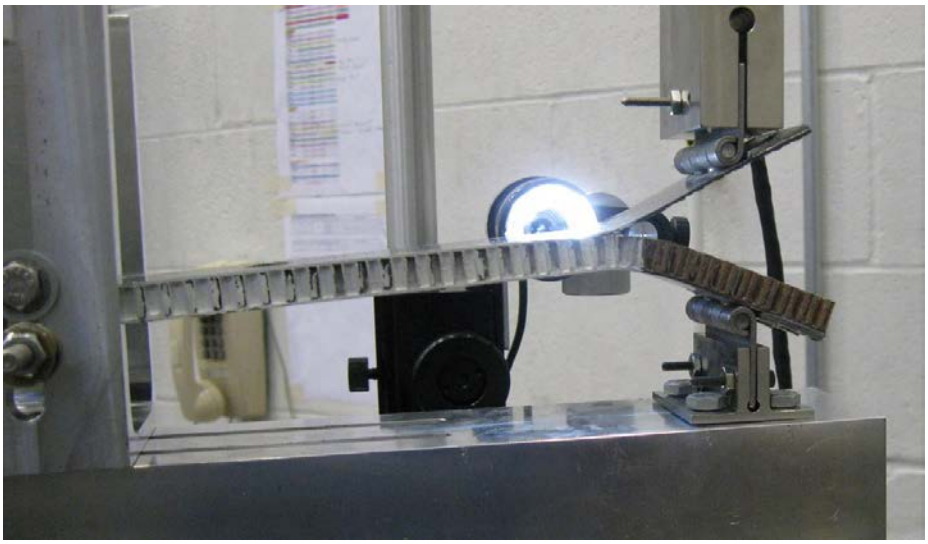

(a)

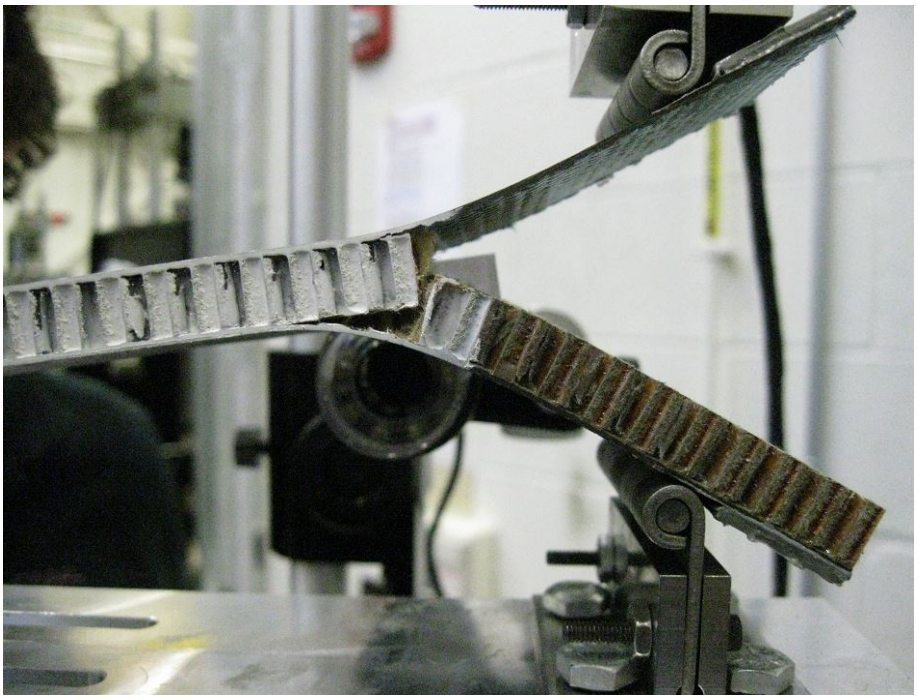

(b)

Figure 5. Kinking of stabilized DCB test on sandwich structure: (a) test setup and (b) kinking and core rupture

After preliminary DCB trials, SCB tests (based on the work of Cantwell and Davies [8, 9]) and round robin testing at NIAR were selected for the remainder of the tests included in the current phase of the research, and the specimen sizing guidelines presented by Ratcliffe [10] were evaluated to determine the valid range of crack lengths for each specimen configuration. The sandwich SCB test configuration used for this research program is discussed in detail here.

Because of the complex damage mechanics, a detailed failure analysis was conducted for each test specimen. Preliminary tests conducted on the sandwich specimens indicated that failure initiation can occur either along the bondline or within the core, right below the fillets. Though it is possible that the crack could initiate within the composite facesheet, this was unlikely, given that the facesheet fracture toughness is significantly higher than that of the core. Furthermore, preliminary tests revealed that two primary progressive fracture paths are possible, as shown in figure 6:

1. Crack propagation along the bondline (core-facesheet interface)
2. Crack propagation along the bondline for a short distance, then migration into the core right below the fillets

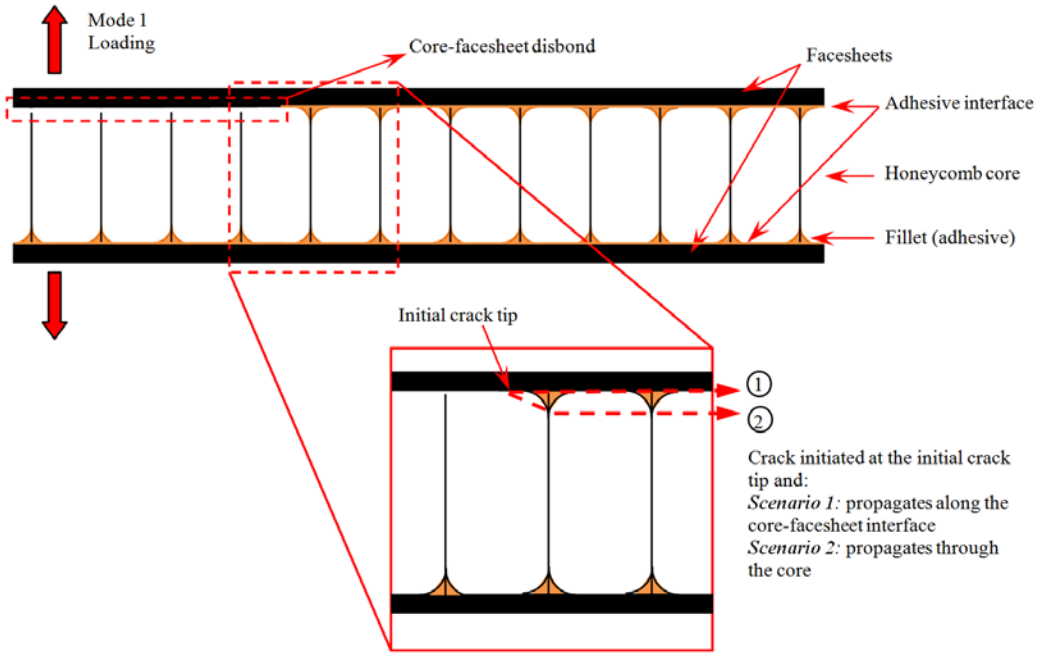

Figure 6. Primary progressive fracture paths for sandwich structures

In addition to these two primary failure modes, the following secondary failure modes were observed:

- Adhesive pullout: flatwise tensile failure of adhesive underneath the fillet region (very common)
- Kinking: crack propagation along the bondline for a short distance, core rupture through the thickness, and crack propagation along the opposite bondline (common in DCB tests but not in SCB tests)
- Core pullout or adhesive failure of the cell wall interface (not common)
- Delamination of the facesheet (not common)

Because of the complex nature of progressive damage growth, any combination of the above-mentioned primary failure modes is possible. Detailed failure modes for the sandwich

specimen configurations studied in this investigation are discussed in the results section of this report.

2.1 SCB TEST ON SANDWICH STRUCTURE

The primary difference between SCB and DCB test configurations on sandwich structures is that the underside of the SCB specimen is secured to a sliding foundation, whereas the top facesheet is loaded out-of-plane (Mode I), as shown in figure 7.

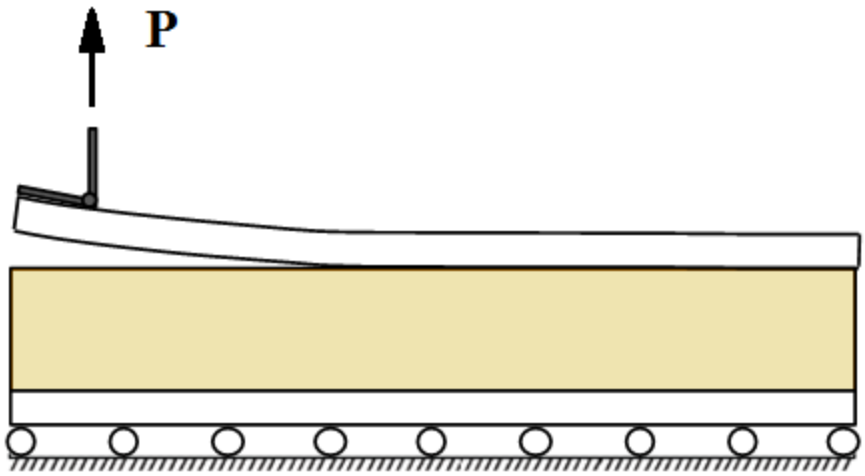

Figure 7. SCB test configuration on sandwich structure

2.1.1 Test Fixture

The SCB diminishes the effects of unsymmetrical loading of sandwich specimens and the effects of stiffness mismatch. It also reduces the effects of mode mixity, which can be further mitigated by creating a very long loading arm, thereby reducing the component of force in the shear direction or by placing the specimen on a sliding foundation, which releases the force in the shear direction every time it overcomes static friction. The latter method was used in designing this test configuration. The clamping method could be carried out in many ways. For example, each specimen could be perfectly bonded to the sliding foundation; however, this is illogical and time and cost intensive. Instead, an adjustable clamping system was used, as shown in figure 8. The test fixture holds the bottom facesheet while loading the hinge bonded to the top facesheet where the prescribed crack is located, as shown in figure 9.

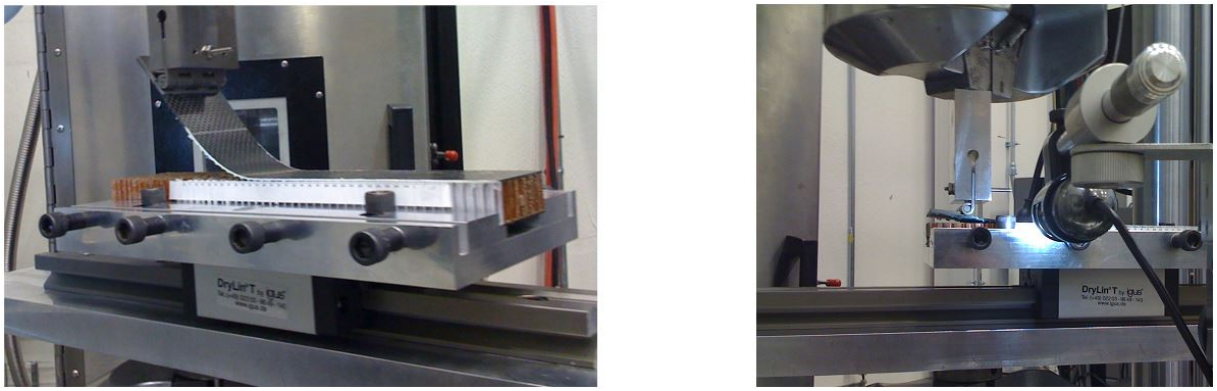

Figure 8. Sliding SCB test fixture design

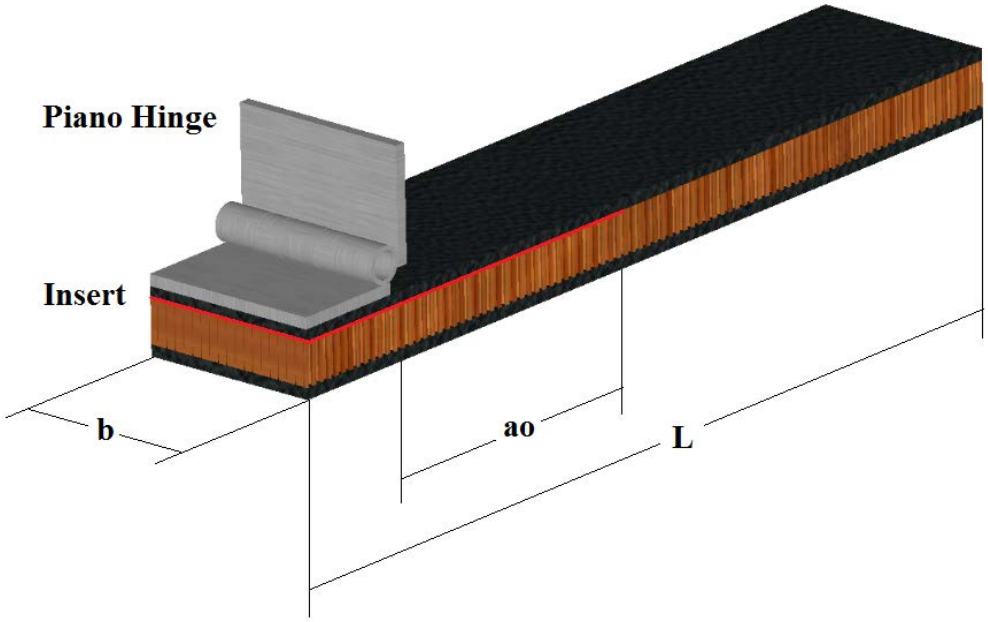

Figure 9. SCB geometry of sandwich specimen

2.1.2 Specimen Sizing

The 4-ply facesheet specimens underwent large displacements during static testing. The modified correction factor (F), based on the ASTM D5528 test configuration, could properly adjust the Mode I fracture toughness (GIC); however, it does not adjust the corresponding displacements. Because nonlinear displacements are required to properly determine the maximum and minimum displacements for cyclic loading, an additional adjustment was needed.

To reduce the large deflection and attain an accurate nonlinear displacement, coupons were resized to reduce the prescribed crack length, thereby prolonging the onset of large deflection if the prescribed crack length was still long enough to ensure that bending was the primary form of loading. Methods presented by Ratcliffe [10] were used to determine a modified prescribed crack length (a_o) of the shortened specimens. A new prescribed crack length of 1″, referred to as "shortened," was selected. These specimens are represented in the master summary by an asterisk

and italicized data. The sizing study, shown in figure 10, indicates the length of cracks with the black lines as the initial crack length (a_o), as per Ratcliffe [10].

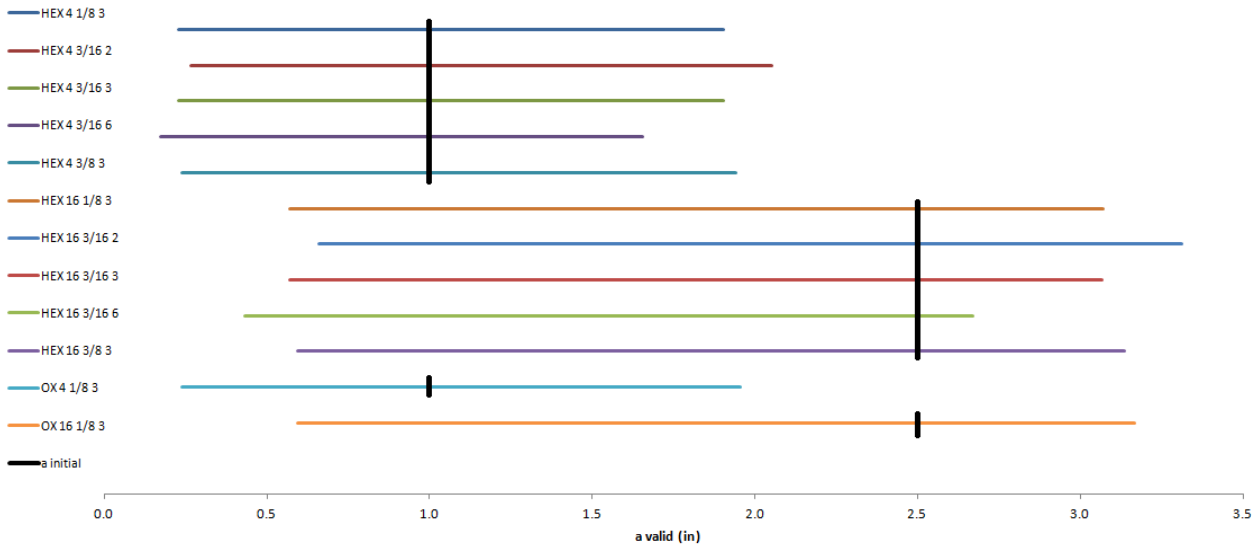

Figure 10. Valid crack growth range for 4-ply sandwich specimens

2.2 TEST MATRIX

Experiments proposed in the current task were carried out using Cytec AS4/E7K8 plain weave facesheets bonded to Hexcel HexWeb HRH-10 aramid fiber/phenolic honeycomb with Cytec FM300 film adhesive. Table 1 shows the test matrix for determining the Mode I fracture growth rates of sandwich specimens using the SCB test configuration.

Table 1. Test matrix for SCB sandwich specimens

Core Material	Core Type	Core Thickness (in)	Facesheet Layup	Cell Size [in]	Core Density [lb/ft^3]	Number of Fatigue Test Specimens	
						Baseline	Fluid-Ingressed
HRH-10	HX	0.5	4-ply $[0/45]_S$	1/8	2.0*		
					3.0*	6	6
					6.0*		
				3/16	2.0*	6	6
					3.0*	6	6
					6.0*	6	6
				3/8	2.0*		
					3.0*	6	6
					6.0*		
			16-ply $[0/45]_{4S}$	1/8	2		
					3	6	3
					3**		4
					6		
				3/16	2	6	1
					2**		6
					3	6	3
					3**		5
					6	6	4
					6**		4
				3/8	2		
					3	6	6
					6		
	OX	0.5	4-ply	3/16	2		
					3	6	6
					6		
			16-ply	3/16	2		
					3	6	6
					6		
Total Specimens					150		

a_o = 1″; δ_{max} from static FI results; HX = hexagonal core; OX = over-expanded core

As shown in table 1, two different core types (hexagonal and over-expanded), three different cell sizes (1/8″, 3/16″, and 3/8″), and three different core densities (2, 3, and 6 pcf) were selected with two different facesheet thicknesses (4 and 16 plies). This matrix includes as-fabricated (baseline) and fluid-ingressed specimens. Fluid-ingressed specimens were conditioned in a mixture of water and Skydrol® LD-4 hydraulic oil, as outlined in the procedure described in appendix A. An additional subtask determined the appropriate conditioning parameters. The test matrix was reduced so that a design of the experiment model could be used for evaluating other (untested) combinations within the design space considered in table 1. The nomenclature shown in figure 11 was used to uniquely identify different specimen configurations.

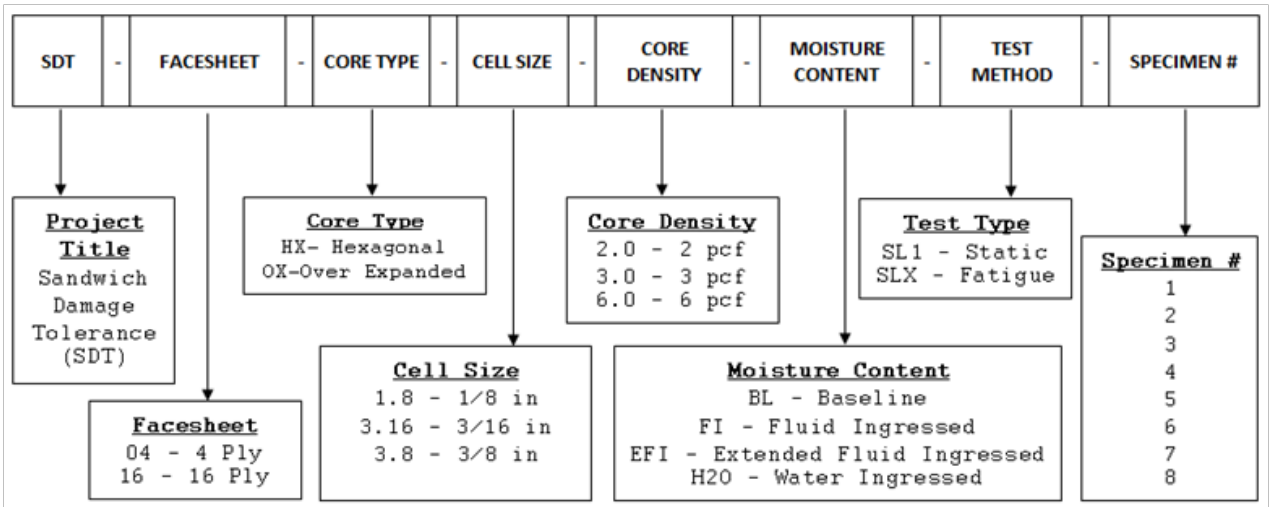

Figure 11. Sandwich specimen nomenclature

SCB sandwich specimens with 4-ply facesheets were 2″ x 8.5″ with a prescribed length (a_o) of 1″. SCB sandwich specimens with 16-ply facesheets were 2″ x 10″ with a prescribed length (a_o) of 2.5″.

Figure 12 shows the basic core geometry for both a hexagonal core (HX) and an overexpanded core (OX). Note that the OX cell size is the normal HX cell size before expansion to a rectangular shape. The typical nomenclature for core designation is material-cell size density (i.e., HRH-10-1/8-3.0), indicating HRH-10 hexagonal honeycomb material with 1/8″ cell size and 3.0 lb/ft^3 (pcf) density. It is important to recognize that the mechanical properties of the sandwich structure are influenced by the ribbon direction in addition to the above-mentioned core parameters.

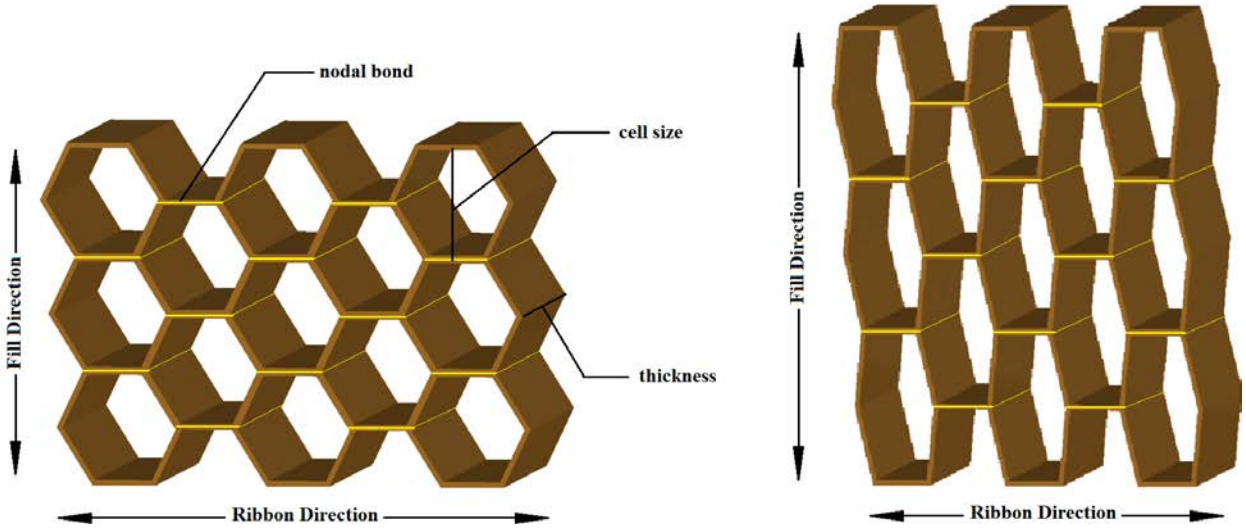

(a) (b)

Figure 12. Core geometry: (a) HX and (b) OX

2.2.1 Environmental Conditioning

Baseline specimens were tested as fabricated with no drying or additional fluid ingression. Fluid-ingressed specimens were conditioned in a Skydrol-water solution for 45 days.

When hydraulic oil was mixed with water and exposed to elevated temperatures (i.e., above 120°F) for an extended period of time, a chemical reaction released phosphoric acid, which deteriorated the adhesive interface in the bonded structures. Aircraft control surfaces that extensively use sandwich structures are frequently exposed to hydraulic oil, and the above-mentioned conditions are highly probable. Therefore, it was vital to determine the effect of this volatile mixture on exposed sandwich structures.

To produce a viable solution, water and Skydrol were mixed in a 50:50 ratio by volume, placed in an elevated temperature of 160°F for preconditioning, and agitated for 2 weeks. The mixture was then kept at room temperature, and the acidity level was monitored daily. During preconditioning, the elevated temperature acted as a catalyst and accelerated the chemical reaction that produced phosphoric acid. Following preconditioning, the solution maintained a steady pH level of approximately 3 at room temperature, indicating a stable fluid mixture for conditioning the fluid-ingressed specimens (see figure 13). Details can be found in appendix A.

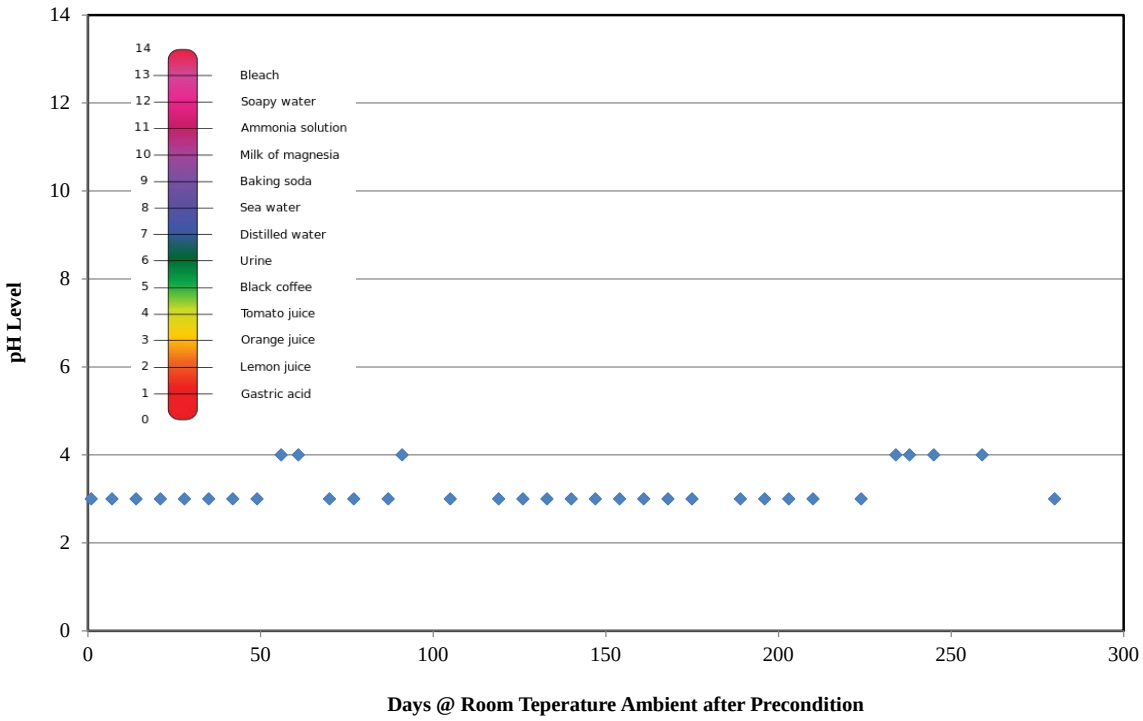

Figure 13. Acidity of Skydrol-water mixture used for environmental conditioning

2.2.2 Supplemental Testing

In addition to the sandwich SCB tests outlined in table 1, DCB test configurations were selected for determining the fracture growth rate of the composite material and the adhesive system used for sandwich construction. Table 2 shows the test matrix for evaluating the fracture growth rate of the laminate and adhesive using a modified ASTM D5528 test configuration. Note that it includes the baseline specimens tested at room temperature dry (RTD) and fluid-ingressed specimens tested at room temperature wet (RTW). DCB fatigue tests were carried out using a procedure developed for ASTM round robin testing conducted at NIAR for determining crack propagation. The results of these tests are found in appendix F.

Table 2. Test matrix for DCB laminate and adhesive fracture toughness

Material	Description	Layup Sequence	Test Condition	Number of Fatigue Test Specimens	
				Baseline	Fluid-Ingressed
AS4/E7K8 PW	Laminate	$[0/45]_{4S}$	RTD	6	
			RTW		6
AS4/E7K8 PW and FM300	Adhesive	$[0/45/0/45/FM300]_S$	RTD	6	
			RTW		6
Total Specimens				24	

2.3 TEST PROCEDURE

The procedure involved in testing sandwich composite specimens for damage growth rate has no engineering standard dictating proper methodology. Therefore, a new procedure was developed by modifying the existing procedure for testing laminate DCB specimens and round robin testing conducted at NIAR.

2.3.1 Fatigue Test Procedure

The fatigue test procedure was based on ASTM 6115 and round robin testing conducted at NIAR. Excluding the test specimen configuration (SCB vs. DCB) and data-reduction method, the test procedures were very similar. As GAG cycles on essentially constant amplitude, all tests here were constant amplitude.

Similar to the practices prescribed in the NIAR procedure, the side of each specimen was painted white so that the crack propagation could be clearly visible. Because the edge was not planar but instead contoured with the honeycomb core, shadowing and depth played a part in visually determining the crack tip location and crack propagation; therefore, crack length was a subjective measurement. Crack tip was monitored using a traveling digital microscope set at a magnification of 20x, as shown in figure 8.

One key difference in the test setup was the SCB test fixture. Specimens were clamped into the test fixture in a widthwise direction at two different torque values, which were determined after several trials, so that the facesheets would not be damaged. The clamping torque for thick-facesheet specimens was 35 in-lbs, and for thin-facesheet specimens was 20–25 in-lbs.

Maximum fatigue displacement ($\delta_{\max}$) was determined by evaluating the average non-linear displacements from quasi-static tests in Volume I (δ_{nl}) and by using equation 1. The unknown δ_{nl} in equation 1 is determined by the displacement corresponding to the nonlinear point of load-displacement curve, as shown in figure 15 in Volume I of this report series). Once this value was plugged into equation 1 and solved for $\delta_{\max}$, the minimum displacement, $\delta_{\min}$, was found by applying a displacement ratio of 0.1 (equation 2). Initially, the baseline static non-linear displacements were analyzed to determine the baseline fatigue displacements, and the fluid-ingressed static non-linear displacements were analyzed to determine the fluid-ingressed fatigue displacements. However, after a few specimens were tested, it was decided to use the static baseline non-linear displacements to determine both the baseline and fluid-ingressed fatigue displacements to better compare the results. Maximum and minimum displacements can be found in table 3. Those specimens that used fluid-ingressed non-linear displacements are indicated with a double asterisk (**).

$$\frac{\delta^2{}_{\max}}{\left[\delta_{nl}\right]^2} = \frac{G_{\mathrm{Im}ax}}{G_{Ic}} = 0.9 \qquad (1)$$

$$\frac{\delta_{min}}{\delta_{max}} = 0.1 \quad (2)$$

Table 3. Maximum and minimum displacements

Specimen	Maximum δ [in]	Minimum δ [in]	Maximum δ [mm]	Minimum δ [mm]
SDT-04-HX-1.8-3-BL-SLX-X (shortened)	0.191	0.019	4.845	0.485
SDT-04-HX-3.16-2-BL-SLX-X (shortened)	0.186	0.019	4.734	0.473
SDT-04-HX-3.16-3-BL-SLX-X (shortened)	0.165	0.016	4.180	0.418
SDT-04-HX-3.16-6-BL-SLX-X (shortened)	0.162	0.016	4.121	0.412
SDT-04-HX-3.8-3-BL-SLX-X (shortened)	0.139	0.014	3.524	0.352
SDT-04-OX-3.16-3-BL-SLX-X (shortened)	0.223	0.022	5.670	0.567
SDT-16-HX-1.8-3-BL-SLX-X	0.141	0.014	3.581	0.358
SDT-16-HX-3.16-2-BL-SLX-X	0.148	0.015	3.761	0.376
SDT-16-HX-3.16-3-BL-SLX-X	0.138	0.014	3.496	0.350
SDT-16-HX-3.16-6-BL-SLX-X	0.162	0.016	4.111	0.411
SDT-16-HX-3.8-3-BL-SLX-X	0.135	0.014	3.440	0.344
SDT-16-OX-3.16-3-BL-SLX-X	0.178	0.018	4.524	0.452
SDT-04-HX-1.8-3-FI-SLX-X (shortened)	0.191	0.019	4.845	0.485
SDT-04-HX-3.16-2-FI-SLX-X (shortened)	0.186	0.019	4.734	0.473
SDT-04-HX-3.16-3-FI-SLX-X (shortened)	0.165	0.016	4.180	0.418
SDT-04-HX-3.16-6-FI-SLX-X (shortened)	0.162	0.016	4.121	0.412
SDT-04-HX-3.8-3-FI-SLX-X (shortened)	0.139	0.014	3.524	0.352
SDT-04-OX-3.16-3-FI-SLX-X (shortened)	0.223	0.022	5.670	0.567
SDT-16-HX-1.8-3-FI-SLX-X	0.141	0.014	3.581	0.358
SDT-16-HX-1.8-3-FI-SLX-X**	0.123	0.012	3.115	0.312
SDT-16-HX-3.16-2-FI-SLX-X	0.148	0.015	3.761	0.376
SDT-16-HX-3.16-2-FI-SLX-X**	0.149	0.015	3.789	0.379
SDT-16-HX-3.16-3-FI-SLX-X	0.138	0.014	3.496	0.350
SDT-16-HX-3.16-3-FI-SLX-X**	0.133	0.013	3.374	0.337
SDT-16-HX-3.16-6-FI-SLX-X	0.162	0.016	4.111	0.411
SDT-16-HX-3.16-6-FI-SLX-X**	0.137	0.014	3.479	0.348
SDT-16-HX-3.8-3-FI-SLX-X	0.135	0.014	3.440	0.344
SDT-16-OX-3.16-3-FI-SLX-X	0.178	0.018	4.524	0.452

**specimens that used fluid-ingressed non-linear displacements

Several initial fatigue test specimens underwent 3 million cycles. As shown in figure 14, it was later determined that 1 to 2 million cycles were sufficient at 5Hz with regularly scheduled visual inspections to determine crack length. The inspection schedule is presented in table 4. If significant crack growth was not observed after 1 million cycles, the fatigue test was stopped.

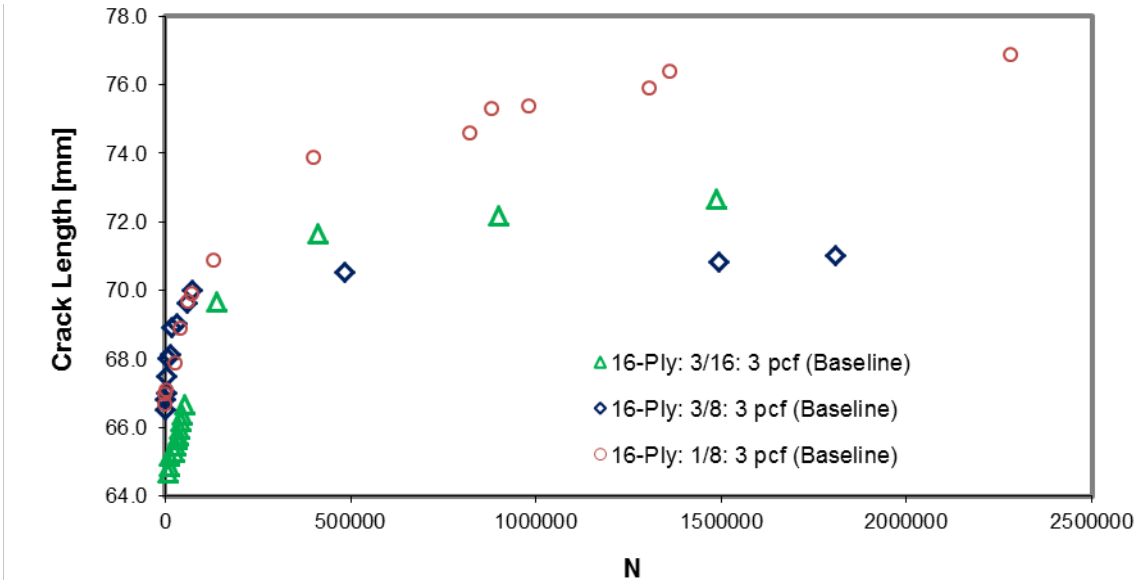

Figure 14. Examples of SCB crack growth data

Table 4. Inspection schedule

Cycle Count	Inspection Interval (cycles)
0–5,000	500
5,000–10,000	1,000
10,000–25,000	2,500
25,000–50,000	5,000
50,000–100,000	10,000
100,000–250,000	25,000
250,000–1,000,000	50,000
1,000,000–2,000,000	100,000

2.4 DATA REDUCTION

2.4.1 Crack Growth Rate Derivation

The crack growth rate (da/dn) was determined by dividing the change in crack length by the change in cycle count, in which the cycle count is prescribed by the inspection schedule in table 4 [3]:

$$\frac{da}{dn} = \frac{a_{i+1} - a_i}{n_{i+1} - n_i} \tag{3}$$

2.4.2 G_{Imax} Derivation

The strain energy release rate (SERR) was determined using the modified beam-bending theory and was derived in Volume I of this report. The only difference was the use of an average crack length [3]:

$$G_{\mathrm{Im}\,ax} = \frac{3P_{\max}\delta_{\max}}{2b\left(\overline{a} + |\Delta|_{av}\right)} \tag{4}$$

where:

$$\overline{a} = \frac{1}{2}\left(a_{i+1} + a_i\right) \tag{5}$$

The correction factor F was not used.

2.4.3 Shaping Parameters of Paris Region

The crack growth rate (da/dn) and strain energy release rate (G_{Imax}) were then plotted on a logarithmic scale, as shown in figure 15. The corresponding plot was divided into three regions. The first region represents no growth and consists of any loading that results in an SERR less than the threshold SERR (G_{Ith}). The third region signifies instant failure and constitutes any loading that results in a SERR that exceeds the critical SERR, or GIC. The second or middle region is of most interest, because it characterizes stable crack growth. This region is often referred to as the Paris region and consists of all loadings that result in an SERR between G_{Ith} and GIC.

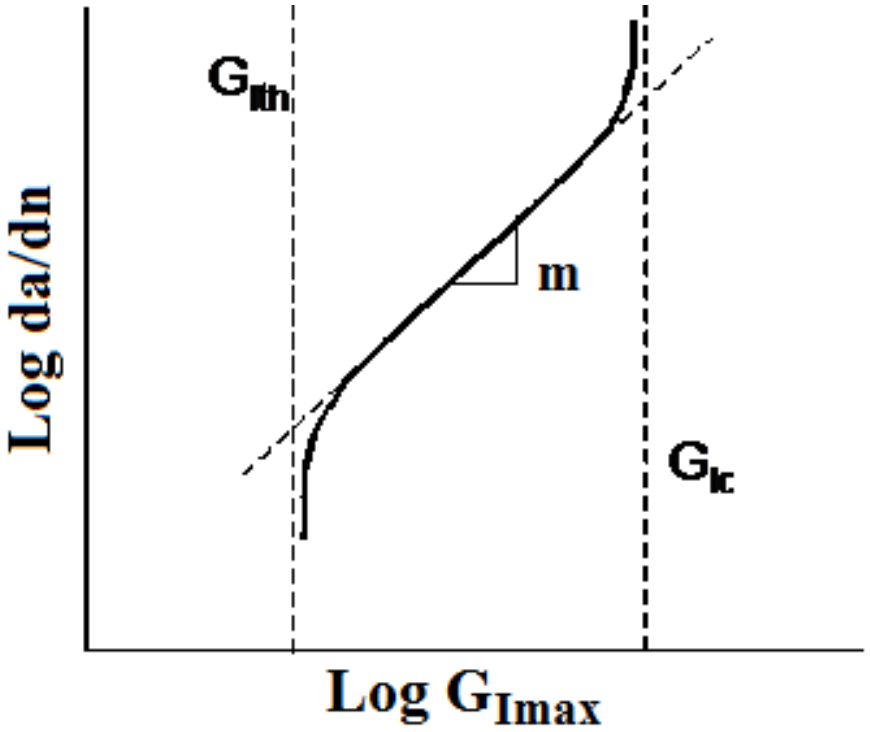

Figure 15. Log plot of da/dn vs. G_{Imax}

The Paris region is characterized with a power curve consisting of two shaping parameters, *m* and *B* [3]:

$$\frac{da}{dn} = B[(1-R)G_{\mathrm{Im}ax}]^m \tag{6}$$

where:

$$R = \frac{G_{\min}}{G_{\max}} = \left(\frac{\delta^2_{\min}}{\delta^2_{\max}}\right) = .01 \tag{7}$$

Therefore, (1-*R*) is neglected and the final equation takes the form:

$$\frac{da}{dn} = BG^m_{\mathrm{Im}ax} \tag{8}$$

The shaping parameter, *m*, represents the load sensitivity of the crack propagation rate and was determined by curve fitting experimental data within the Paris region. Generally, a small value of *m* is preferred for fatigue crack growth resistance. Therefore, the shaping parameters for different sandwich configurations were used for comparison purposes. The shaping parameter, *B*, was also determined by curve fitting experimental data and can be found in the appendices. These are insufficient data with large scatter to plot *m* as a function of the increasing number of fatigue cycles.

Three distinct solutions for the shaping parameter, *m*, were determined:

- A curve fit was applied to each specimen's data, and the corresponding shaping parameters for each set of data (typically six specimens per set) were averaged. This was called the average "individual" shaping parameter.
- A curve fit was applied to the entire set of specimen data. This was called the average "all" shaping parameter.
- Each specimen's data were linearly interpolated with respect to predetermined G_{Imax}'s (G_{Imax} = 10 x *i*, where *i*= 1,2,3…and G_{Imax} was in [j/m^2]), and those results were averaged for each particular configuration G_{Imax} (as long as at least two specimens were accounted for). This was called the average "interpolated" shaping parameter.

2.5 FAILURE MODES

2.5.1 Adhesive Interface Disbond

An adhesive interface disbond, or adhesion failure, occurs when a crack forms between the adhesive and the facesheet (see figure 16). This failure mode is typically an indication of poor bonding of the film adhesive to the prepreg material during the co-cure process. In this report, such a failure is identified by the letter A.

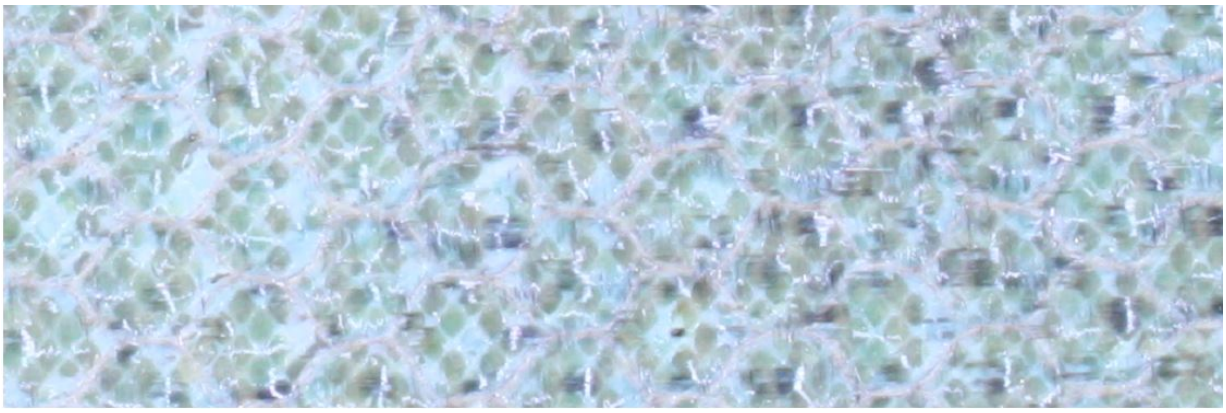

(a)

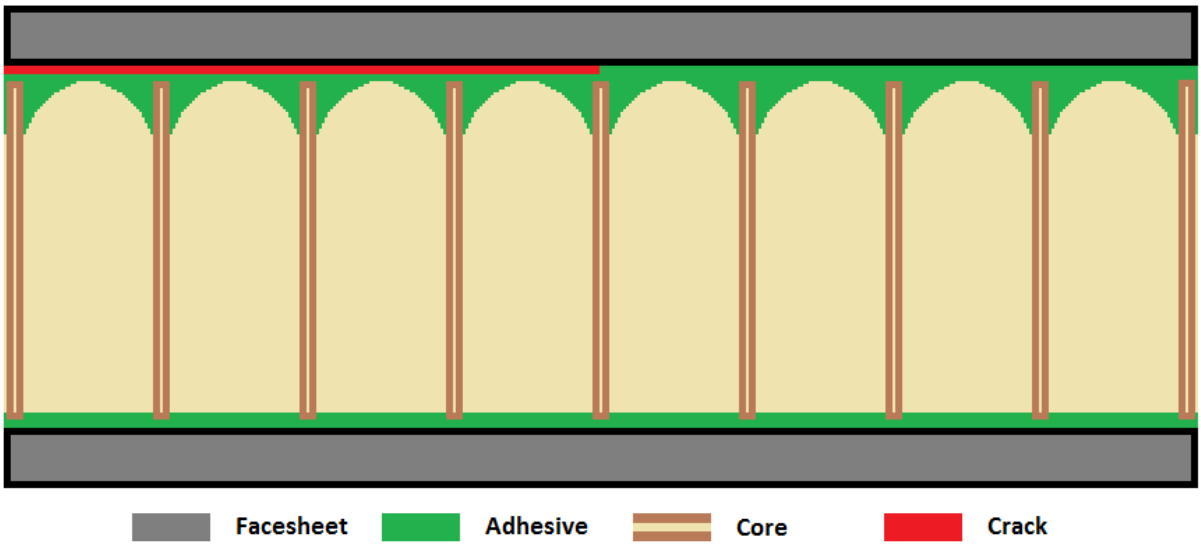

(b)

Figure 16. Image of adhesive interface disbond (A): (a) adhesive interface failure surface and (b) side view

2.5.2 Adhesive Pullout Failure

Adhesive pullout failure (PO), or simply pullout failure, occurs when a crack forms within the adhesive (see figure 17). This type of failure rarely takes place on its own and most often is in combination with an adhesive interface disbond.

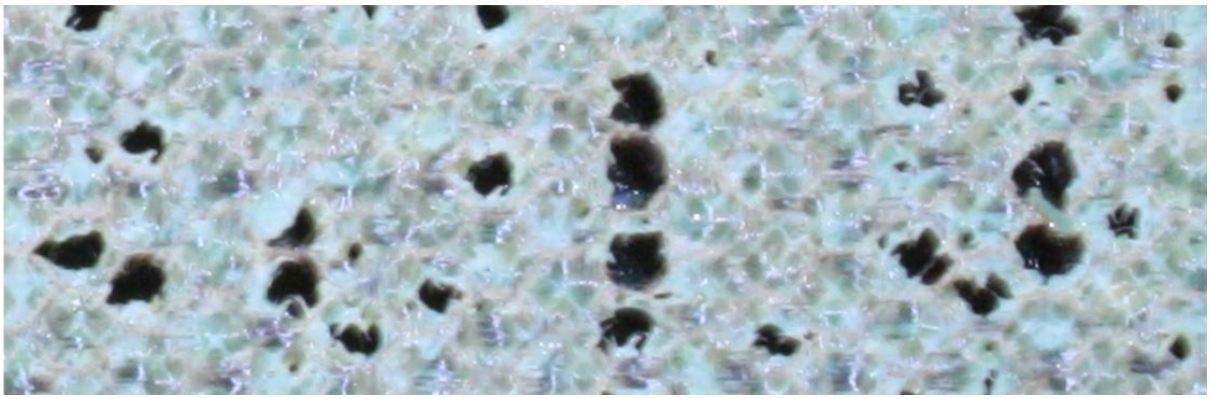

(a)

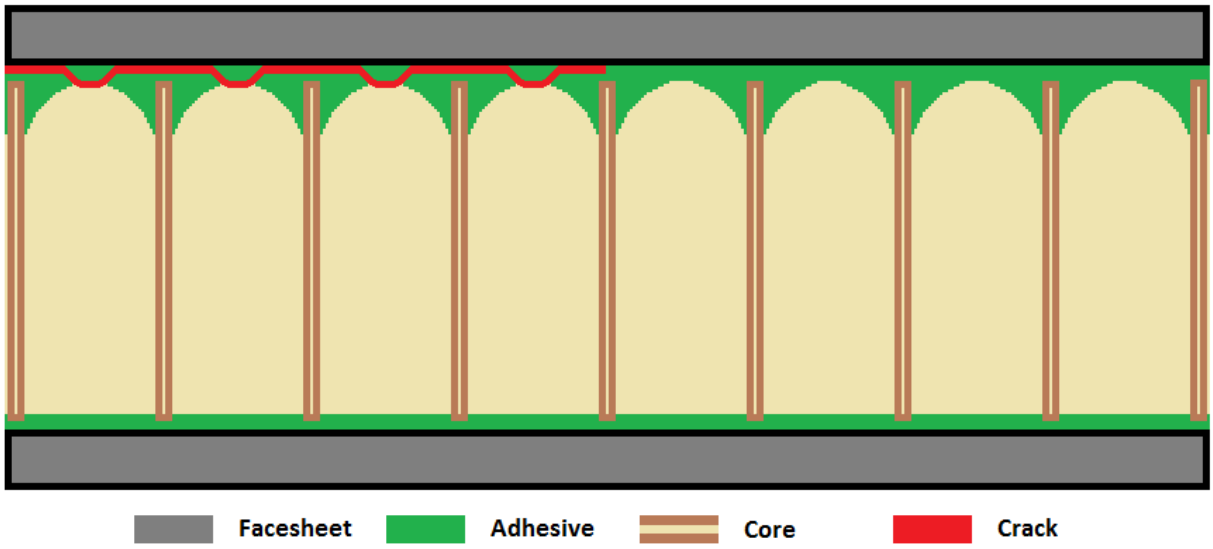

(b)

Figure 17. PO: (a) surface and (b) side view

2.5.3 Tensile Core Failure

Tensile core failure (C), or simply core failure, occurs when a crack forms within the core (see figure 18). Soon after initiation, the crack propagates into the core and often stays there.

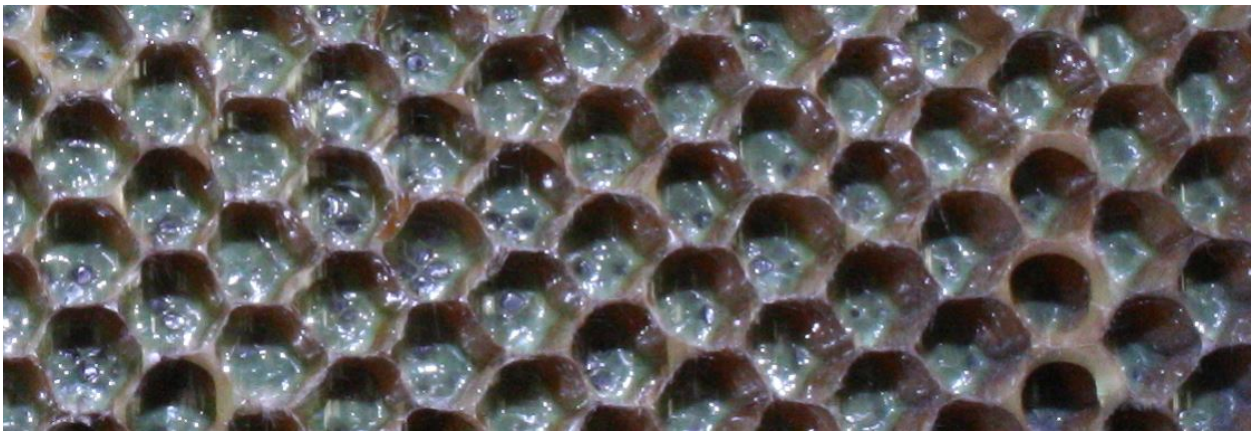

(a)

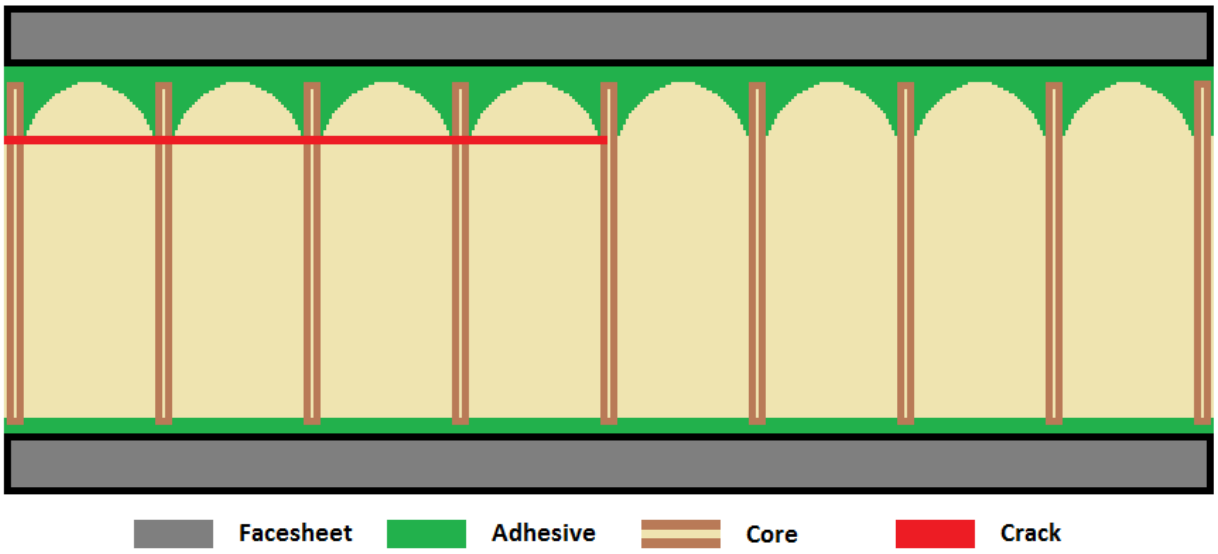

(b)

Figure 18. Tensile core failure (C): (a) tensile core failure surface and (b) side view

2.5.4 Tensile Core Pullout Failure

Tensile core PO occurs when a crack forms between the adhesive and the core (see figure 19). This type of failure mode was not seen during this investigation but can result from improper core preparation (i.e., rough cut/dry sanded core).

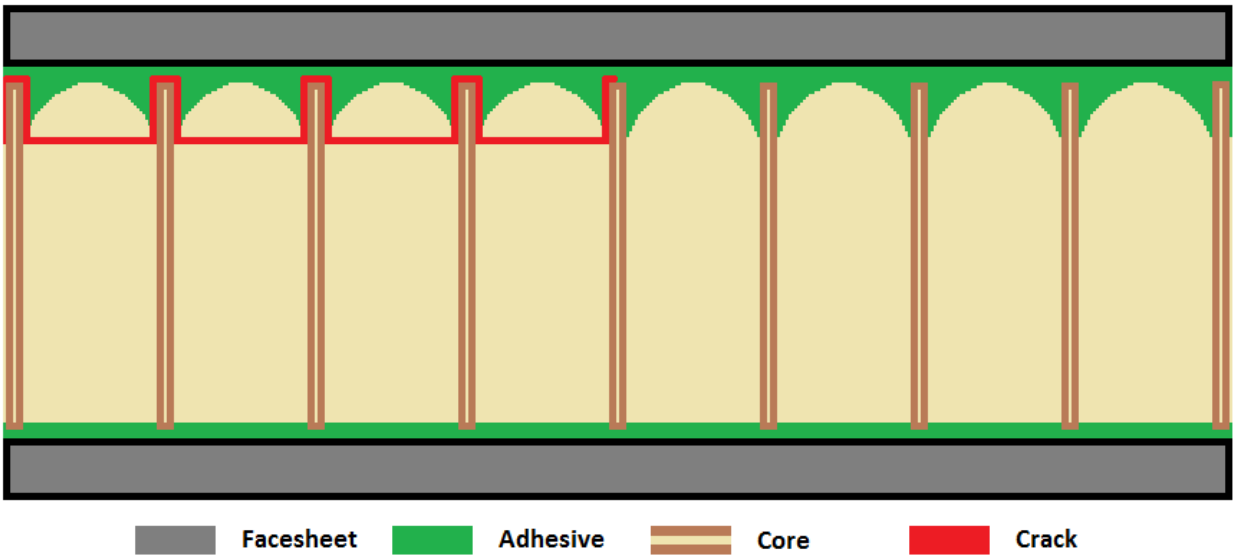

Figure 19. Tensile core PO

2.5.5 Adherend First-Ply Facesheet Delamination

An adherend first-ply facesheet delamination, or adherend failure, is very rare and occurs when a crack forms within the first-ply of the composite facesheet and propagates through the laminate.

2.5.6 Interlaminar Facesheet Delamination

Typically, interlaminar facesheet delamination (S) forms on very thick facesheets (see figure 20) and occurs when a crack forms within the laminate. This crack is predominantly caused by shear (Mode II) loads during the bending of a facesheet.

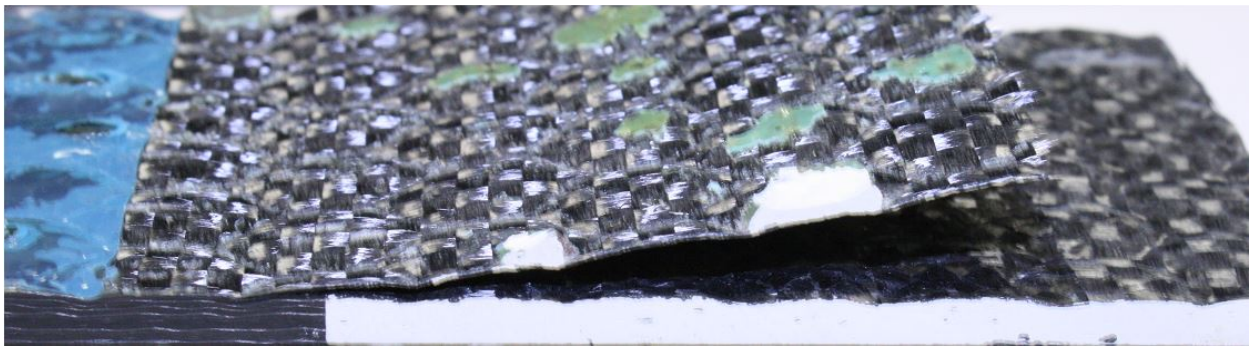

(a)

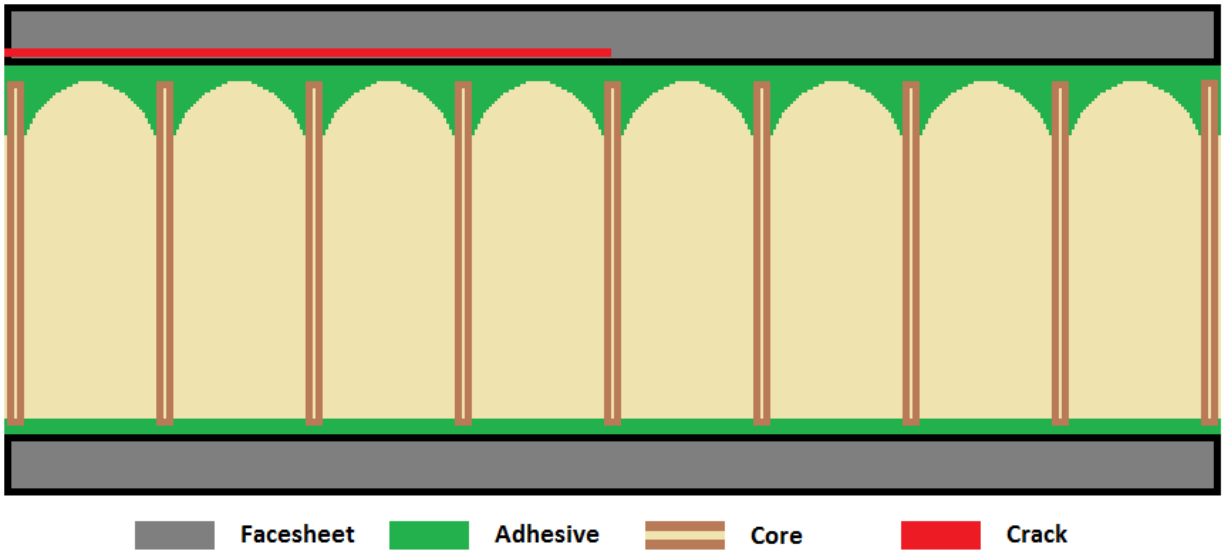

(b)

Figure 20. Interlaminar facesheet delamination (S): (a) failure surface and (b) side view

3. RESULTS AND DISCUSSION

Table 5 shows the average shaping parameter, *m*, obtained for different sandwich parameters and environmental conditions. Higher *m* results in faster crack growth. Figures 21–24 show a graphical comparison of these results. Test data include the shaping parameter, *m*, for different facesheet thicknesses, core types, cell sizes, core densities, and environments. Several other variables can contribute to the shaping parameter, *m*, (e.g., ribbon direction, fabrication technique, prescribed crack location with respect to cell walls, etc.). Therefore, the discussion and conclusions here are solely based on the results included in this report. Detailed results, including failure modes, are found in appendices B–E for 4-ply HX, 16-ply HX, 4-ply OX, and 16-ply OX, respectively.

Table 5. Master summary

Core Type	Facesheet	Cell Size (in)	Core Density (lb/ft^3)	Baseline			Fluid-Ingressed		
				AVERAGE INDIVIDUAL	AVERAGE ALL	AVERAGE INTERPOLATED	AVERAGE INDIVIDUAL	AVERAGE ALL	AVERAGE INTERPOLATED
HX	4-ply [0/45]S	1/8	2.0*						
			3.0*	6.389	5.483	5.678	3.297	1.859	2.286
			6.0*						
		3/16	2.0*	4.059	3.045	3.441	4.318	3.704	4.026
			3.0*	6.770	5.767	6.833	4.823	4.447	5.000
			6.0*	9.891	7.934	8.528	13.654	3.733	4.434
		3/8	2.0*						
			3.0*	6.828	3.399	4.419	11.770	6.007	7.296
			6.0*						
	16-ply $[0/45]_{4S}$	1/8	2						
			3	9.739	7.297	8.039	38.823	N/A	N/A
			3**				58.739	N/A	N/A
			6						
		3/16	2	2.837	2.519	2.397	20.461	20.461	N/A
			2**				3.596	2.638	2.213
			3	14.258	6.044	5.516	48.758	9.068	7.396
			3**				35.113	N/A	28.134
			6	14.287	7.555	10.032	31.568	12.562	11.570
			6**				58.162	N/A	N/A
		3/8	2						
			3	23.081	4.136	14.947	42.943	1.803	11.481
			6						
OX	4-ply [0/45]S	3/16	2.0*						
			3.0*	3.407	3.159	3.235	2.254	1.686	1.903
			6.0*						
	16-ply [0/45]4S	3/16	2						
			3	2.774	2.368	2.316	3.831	1.529	2.254
			3**						
			6						

* ao = 1 ″; ** δ_{max} from static FI results

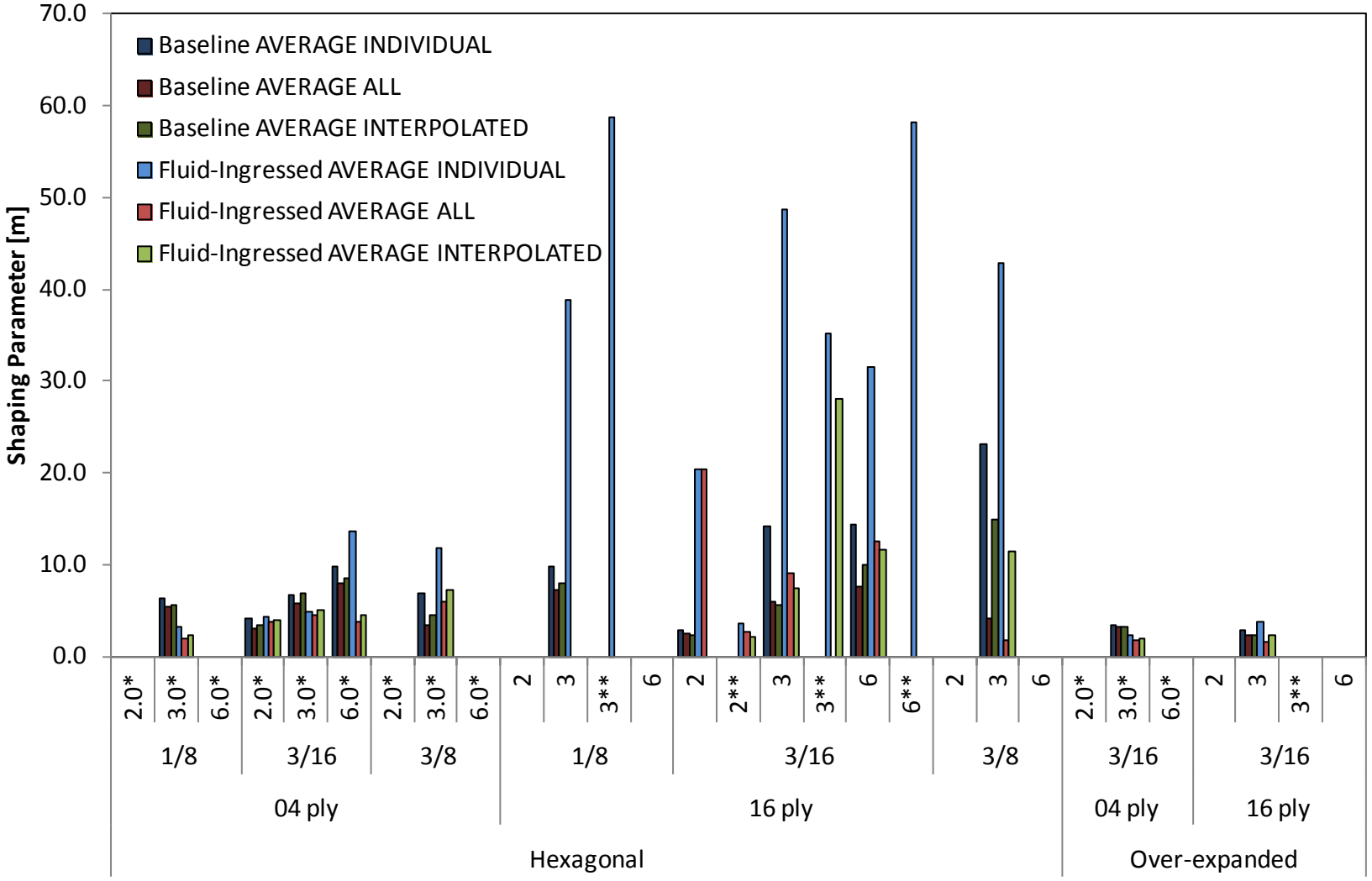

Figure 21. Master summary of shaping parameter, *m*

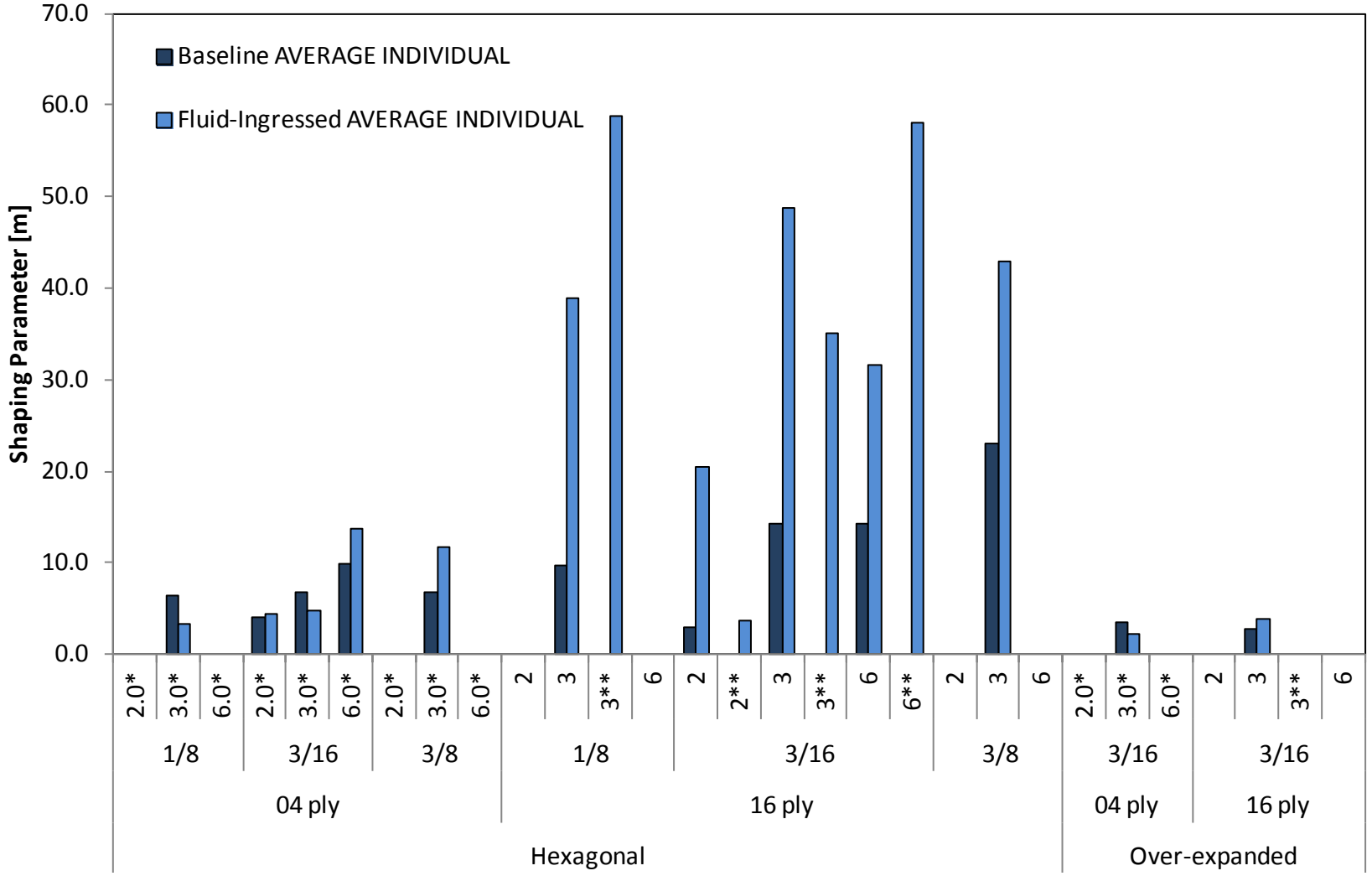

Figure 22. Master summary of average individual shaping parameter, *m*

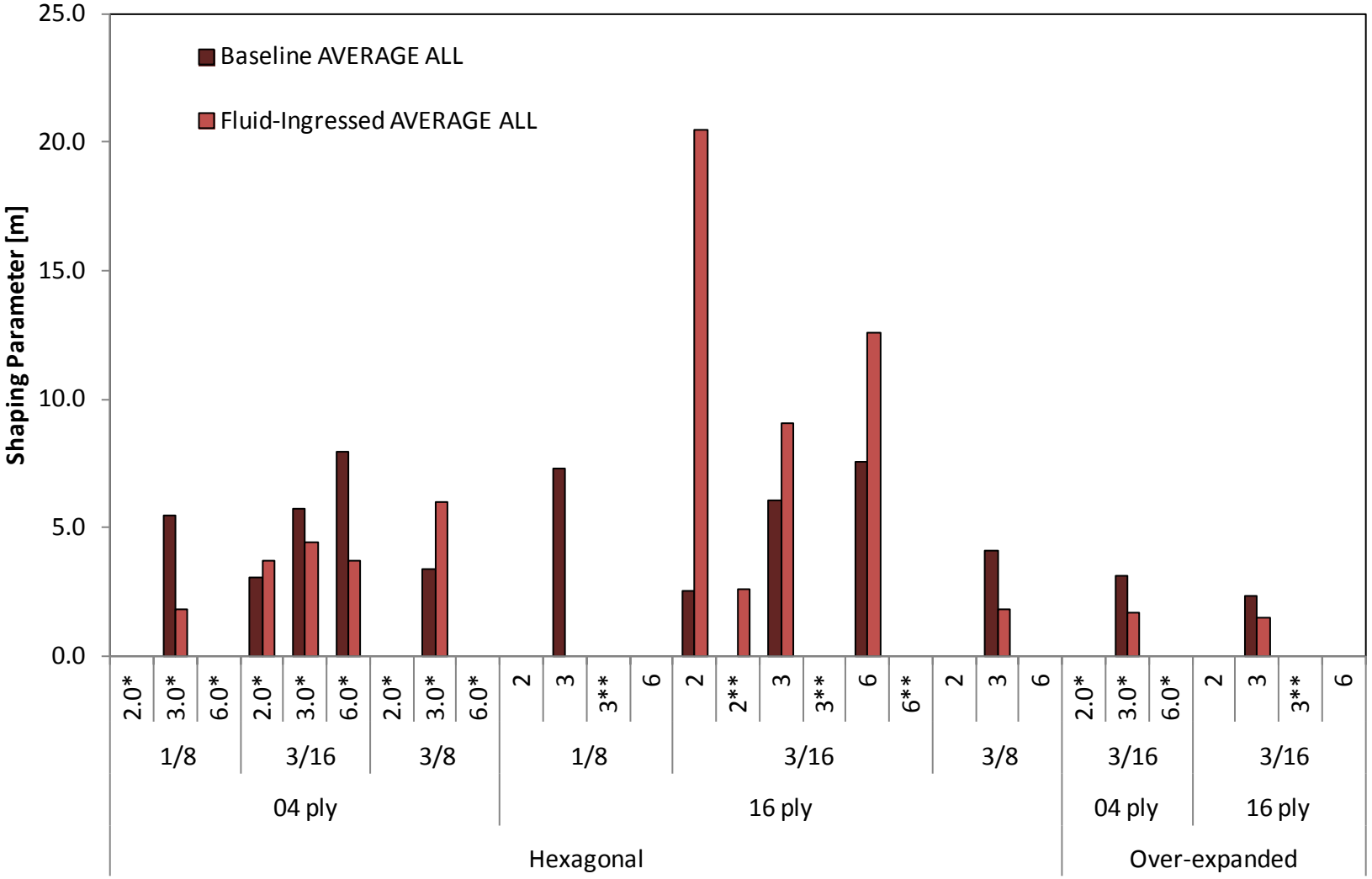

Figure 23. Master summary of average all shaping parameter, *m*

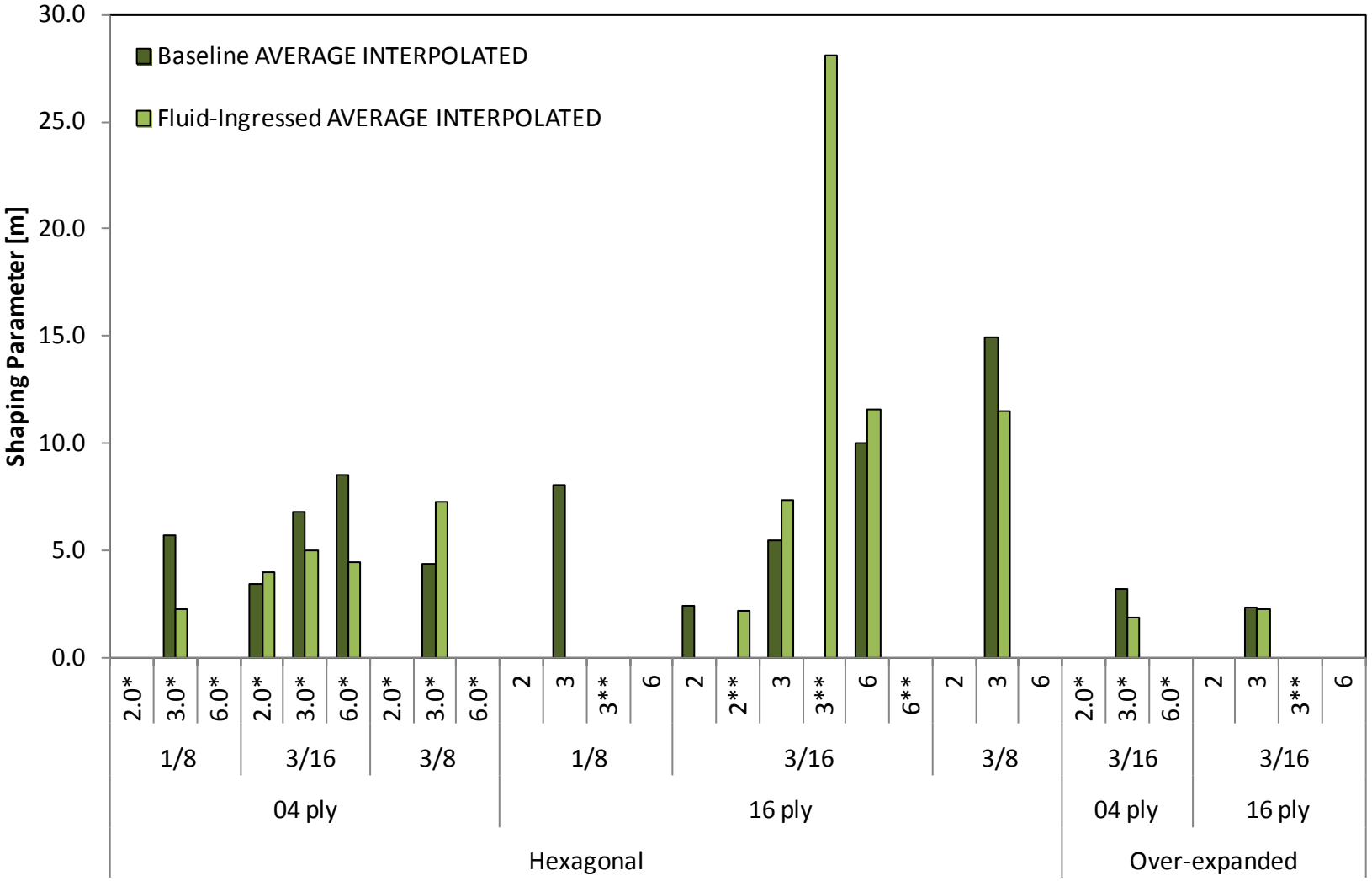

Figure 24. Master summary of average interpolated shaping parameter, *m*

Though the master summary tables and charts show a comparison of the shaping parameter, *m*, the effects of the aforementioned variables are coupled across different variables and require detailed data analysis for determining the impact of each variable. This section discusses, in detail, the impact of the following sandwich parameters on the shaping parameter, *m*:

- Core type
- Cell size
- Core density
- Environmental conditioning

The failure modes for each specimen are included.

3.1 EFFECTS OF CORE TYPE

Figure 25 shows the effects of fluid ingression on the average shaping parameter of 4-ply specimens. The HX had a higher shaping parameter, *m*, than the OX, regardless of environmental conditioning. However, the hexagonal specimens indicated higher data scatter than over-expanded specimens, possibly due to a change in the failure modes as the crack propagated. Figure 26 shows similar observations for the 16-ply specimens. Once more, the HX had a larger shaping parameter, *m*, than the OX, and this was true for both environmental conditions. The fluid-ingressed specimens were significantly different. However, the COV for the ingressed HX made it hard to reach a conclusion.

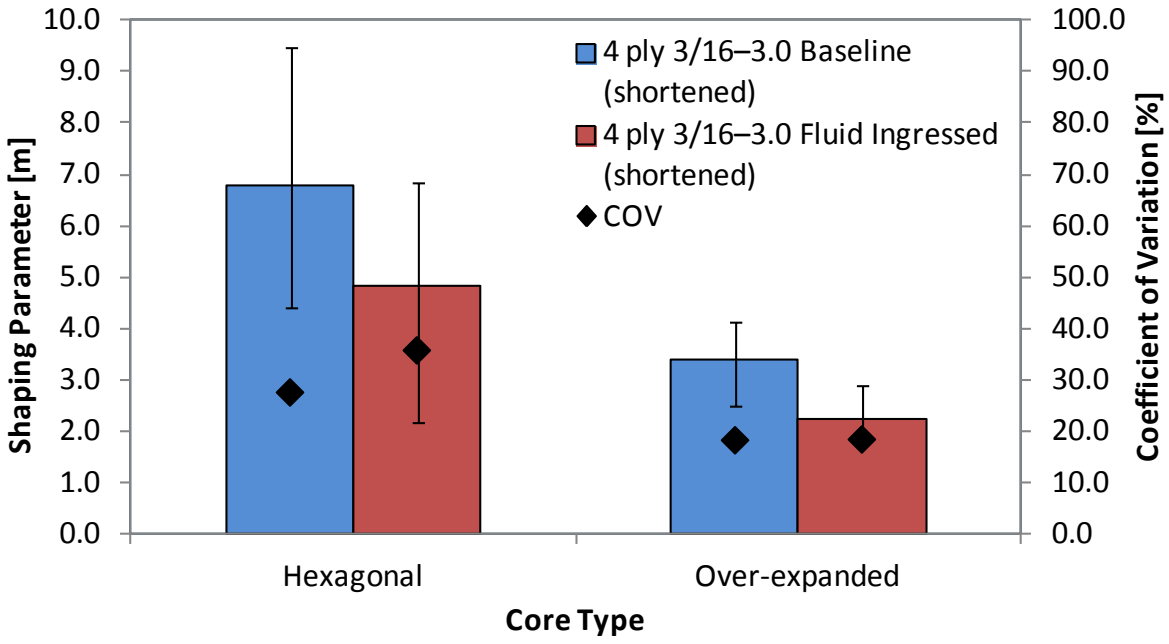

Figure 25. Effects of core type with respect to environmental conditioning (4-ply)

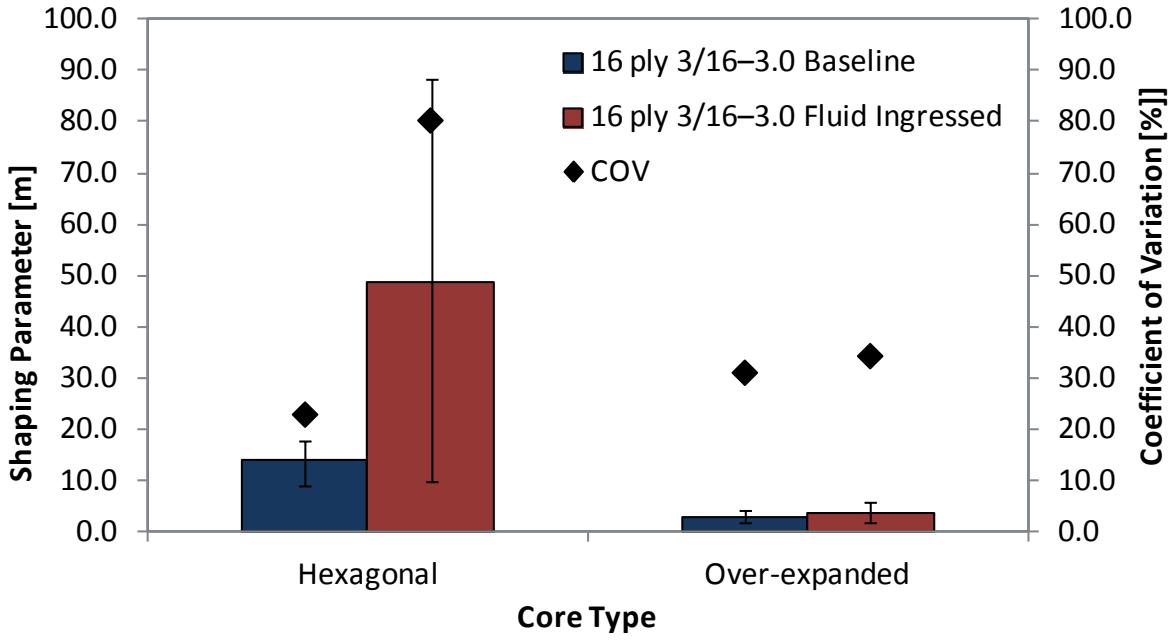

Figure 26. Effects of core type with respect to environmental conditioning (16-ply)

3.2 EFFECTS OF CELL SIZE

Figure 27 shows the effects of cell size on the average shaping parameter of 4-ply specimens. As can be seen in this figure, the cell size had no significant impact on the shaping parameter. Cell size played a large role in fluid-ingressed specimens with the 3/8″ cell size because the shaping parameter, *m*, increased substantially for the 4-ply specimens. The comparison of *m* for cell size against baseline specimens indicated mixed results for fluid-ingressed specimens. This could be because of the ratio of fillet size to cell size, core softening, and adhesive degradation due to environmental conditions with respect to cell size, or it could be due to failure mode as a response to cell size. Furthermore, as cell size changes, paper thickness within the core also varies. This could have a significant impact on the shaping parameter, *m*, but further analyses and studies must be conducted to quantify the effects.

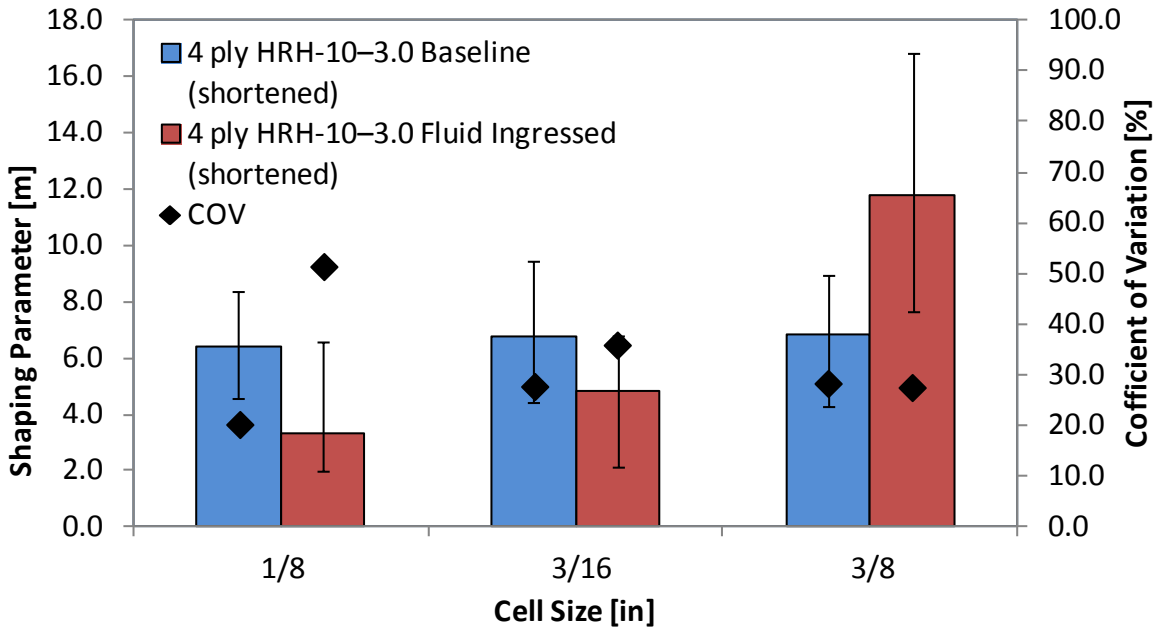

Figure 27. Effects of cell size with respect to environmental conditioning (4-ply)

Figure 28 shows the effects of cell size on the average shaping parameter of 16-ply specimens. The baseline specimens showed an increase in shaping parameter, *m*, with respect to cell size, whereas the fluid-ingressed specimens indicated an increase between 1/8″ and 3/16″, which then leveled off or slightly fell as the cell size approached 3/8″. This could be due to the coupling effects of facesheet thickness and environmental conditions or it could be an anomaly due to higher data scatter.

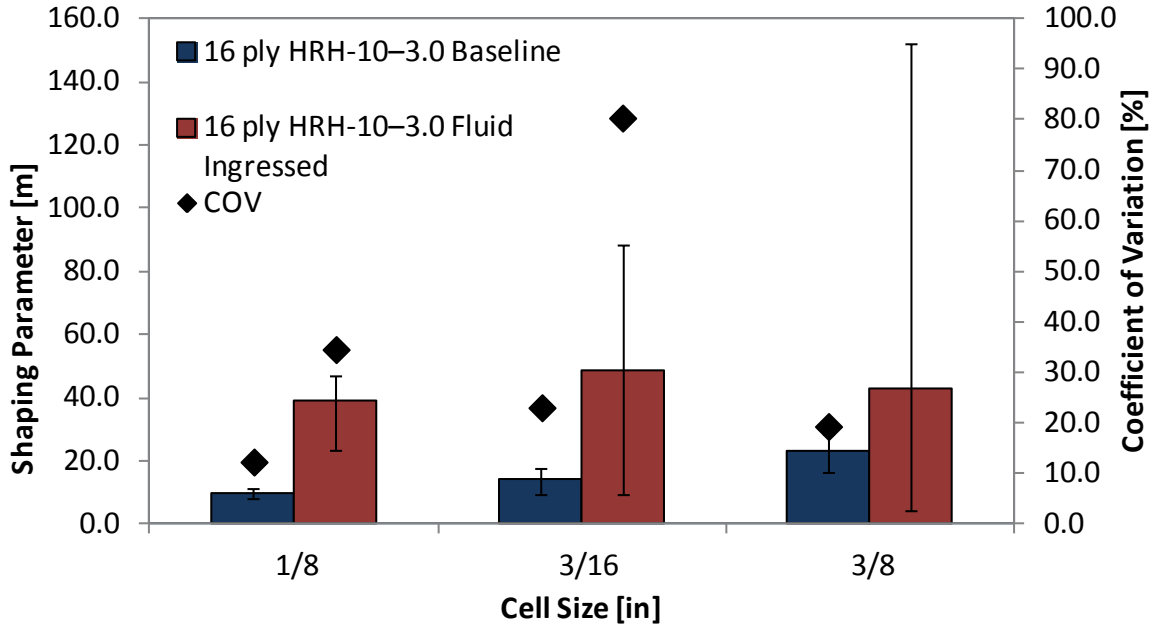

Figure 28. Effects of cell size with respect to environmental conditioning (16-ply)

3.3 EFFECTS OF CORE DENSITY

Figure 29 shows the effects of core density on the average shaping parameter of 4-ply specimens. The shaping parameter increased as the core density increased, regardless of environmental condition. Figure 30 shows the effects of core density on the average shaping parameter of 16-ply specimens. The results indicate that the shaping parameter increased between 2 and 3 lb per cubic foot, but leveled off or fell as the cell density approached 6 lb per cubic foot in both environmental conditions. This was possibly due to the coupling effects of facesheet thickness and environmental conditions. In addition, the adhesive fillets artificially increased the size of the cell walls, altering the significance of core density. As the core density changed, so did the paper thickness within the core, which significantly altered the impact of cell density. Future analysis is needed to establish the significance of paper thickness.

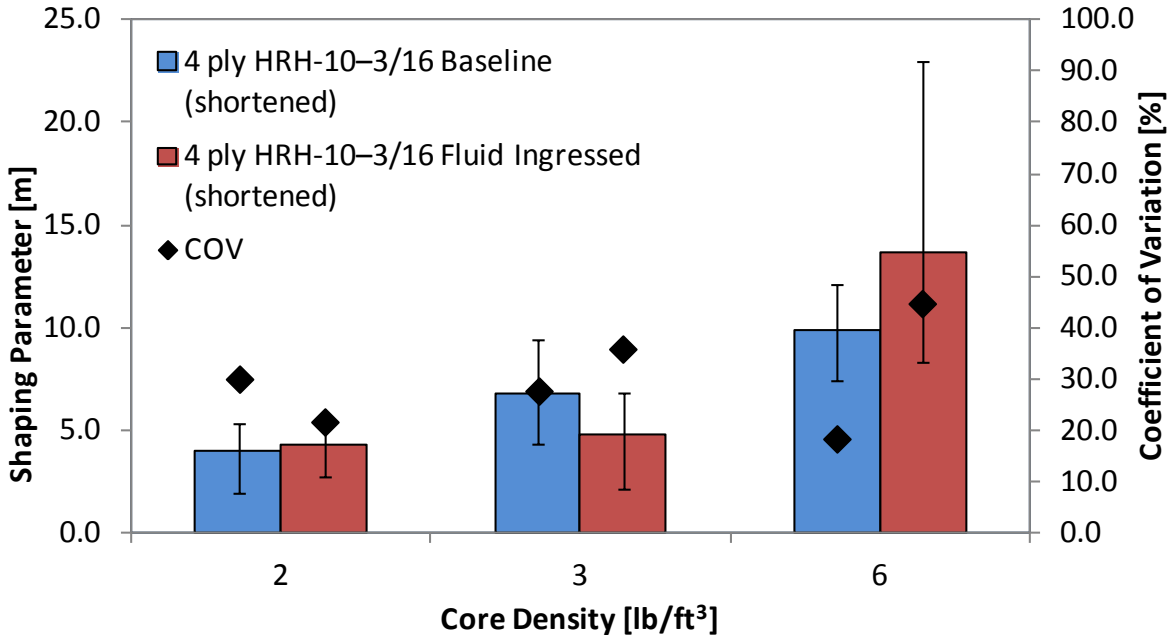

Figure 29. Effects of core density with respect to environmental conditioning (4-ply)

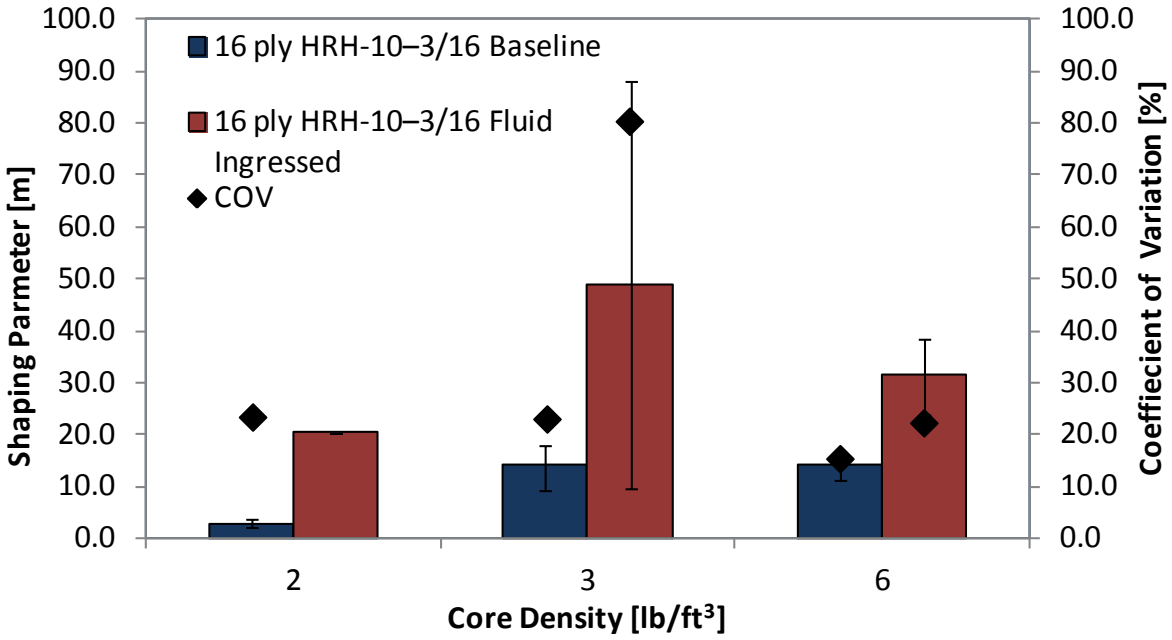

Figure 30. Effects of core density with respect to environmental conditioning (16-ply)

3.4 EFFECTS OF ENVIRONMENTAL CONDITIONING

Environmentally conditioned specimens in an acidic Skydrol-water solution affected material stiffness and failure modes, which in turn affected the shaping parameter, *m*. Generally, test data for fluid-ingressed specimens indicated significant data scatter compared to baseline specimens.

Figures 31–33 show the effects of fluid-ingression on the shaping parameter of 4-ply specimens with respect to core type, cell size, and core density, respectively. The shaping parameter, *m*, of fluid-ingressed 4-ply specimens was lower than baseline specimens, regardless of core type. When considering cell size, the shaping parameter, *m*, decreased for both 1/8″ and 3/16″ fluid-ingressed specimens, but increased for the 3/8″ specimens. Finally, when investigating the effects of core density within 4-ply specimens, no clear relationship could be established because the 2-pcf specimens indicated no change between environmental conditions, the 3-pcf specimens indicated a decrease in the shaping parameter, *m*, and the 6-pcf specimens indicated an increase in the shaping parameter, *m*.

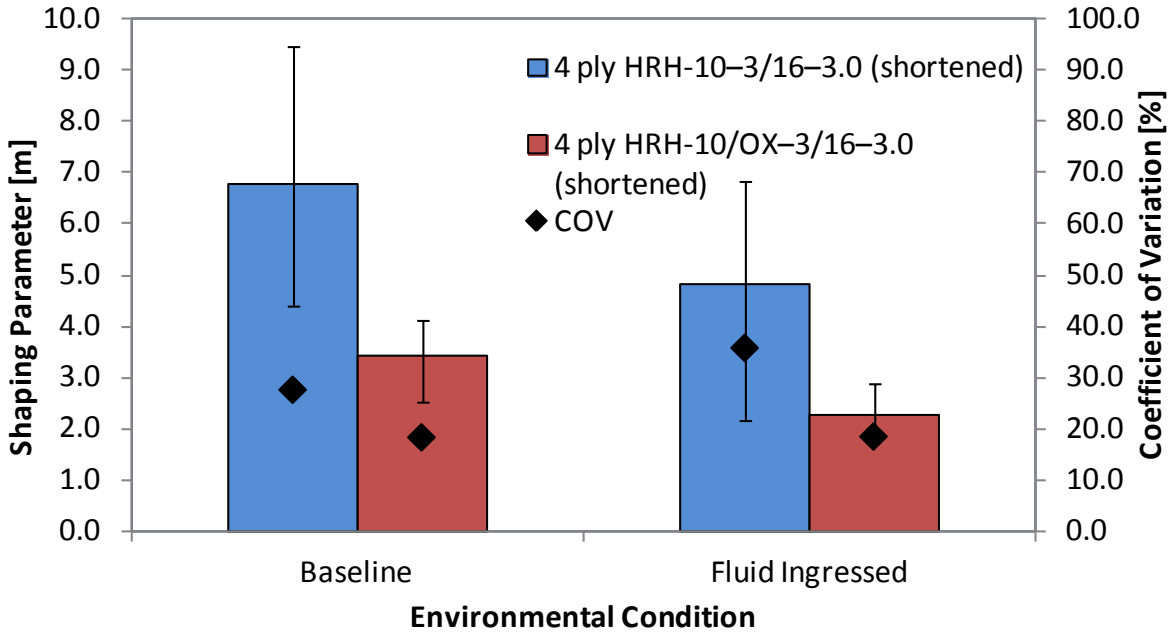

Figure 31. Effects of environmental conditioning with respect to core type (4-ply)

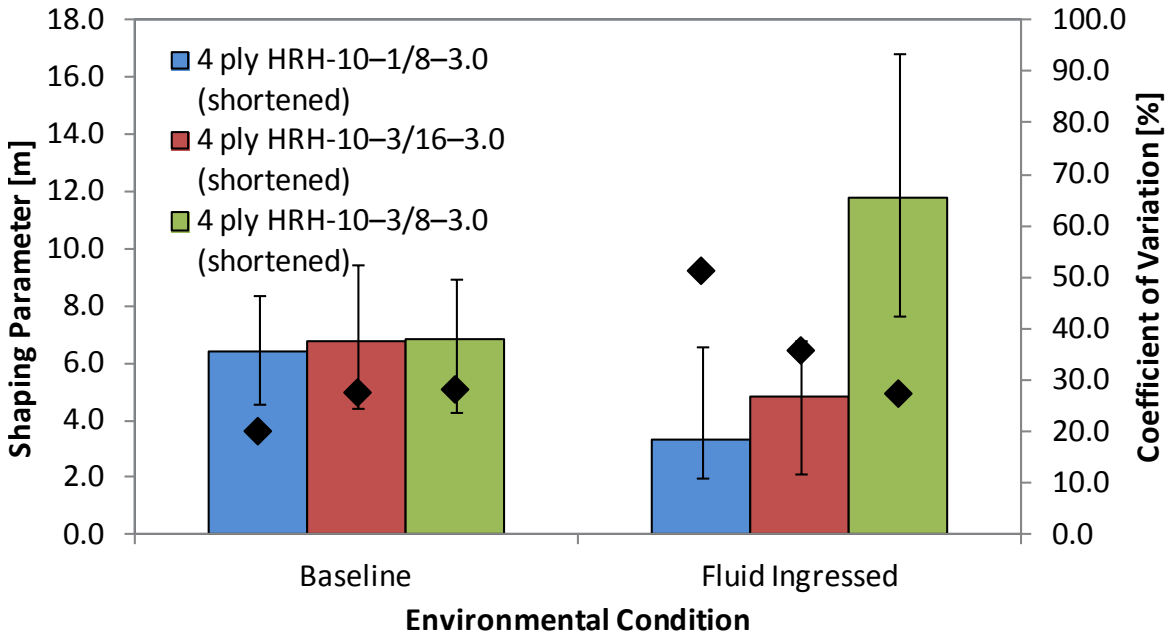

Figure 32. Effects of environmental conditioning with respect to cell size (4-ply)

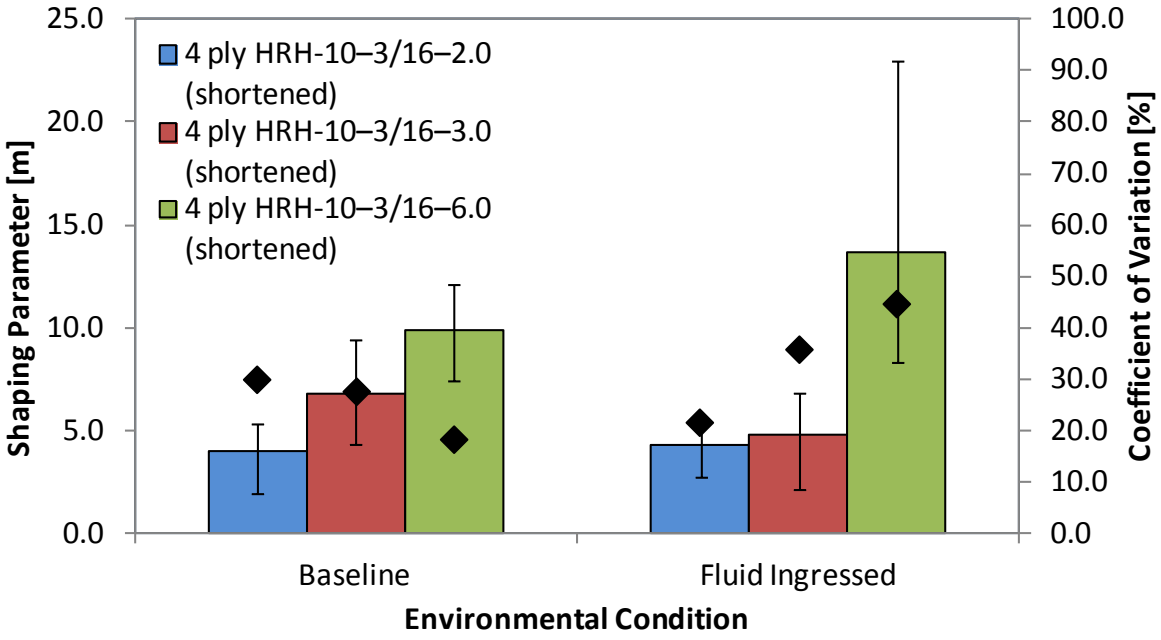

Figure 33. Effects of environmental conditioning with respect to core density (4-ply)

Figures 34–36 show the results for 16-ply specimens with respect to core type, cell size, and core density, respectively. With respect to cell size and core density, the shaping parameter *m* of fluid-ingressed specimens is higher than corresponding baseline specimens, increasing significantly for the smaller cell sizes and core densities, and only modestly for the larger cell sizes and core densities. However, because of high scatter (COV > 40), these results should be used with caution. Figure 37 shows a comparison of crack growth data for 16-ply baseline and fluid-ingressed specimens. As can be seen in figure 37, the higher-shaping parameter *m* of fluid-ingressed specimens indicates faster crack growth rate.

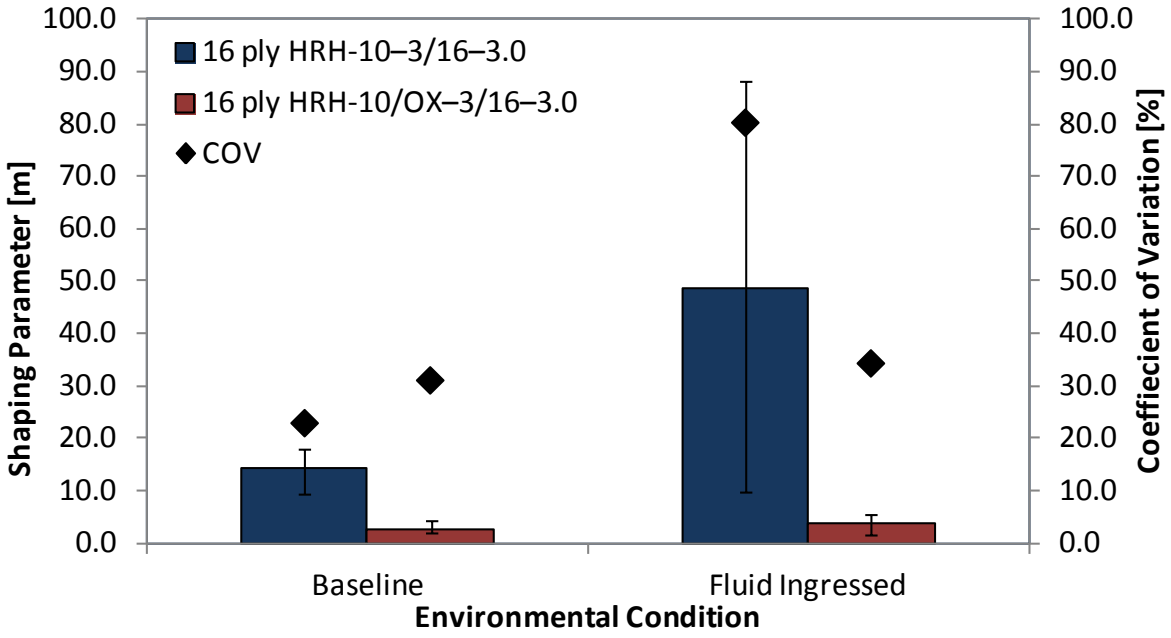

Figure 34. Effects of environmental conditioning with respect to core type (16-ply)

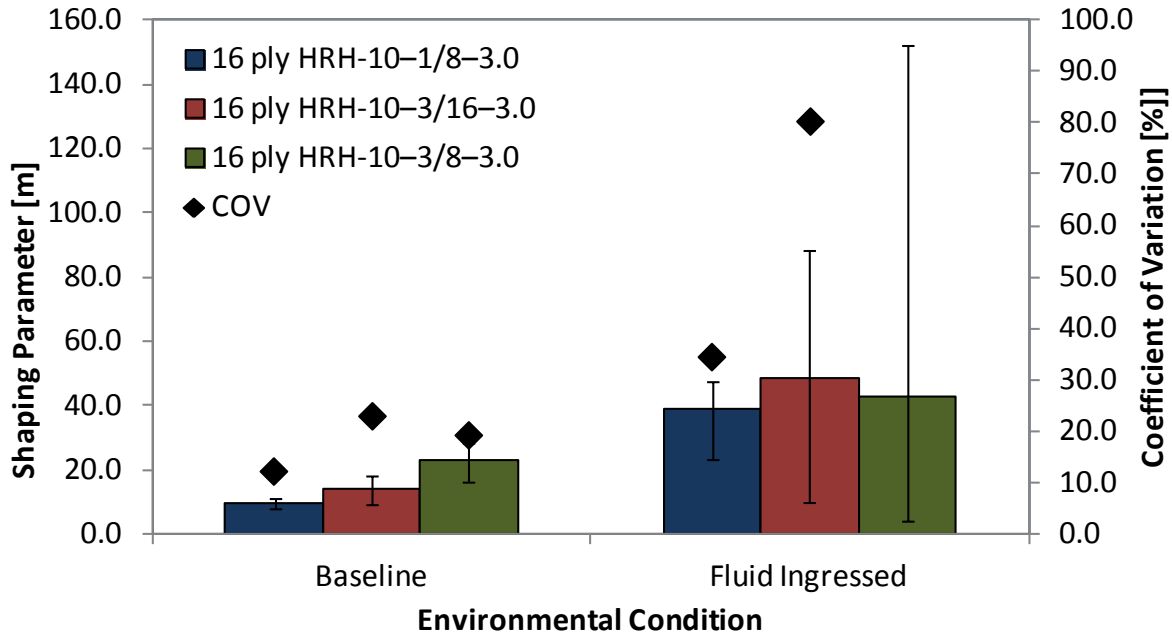

Figure 35. Effects of environmental conditioning with respect to cell size (16-ply)

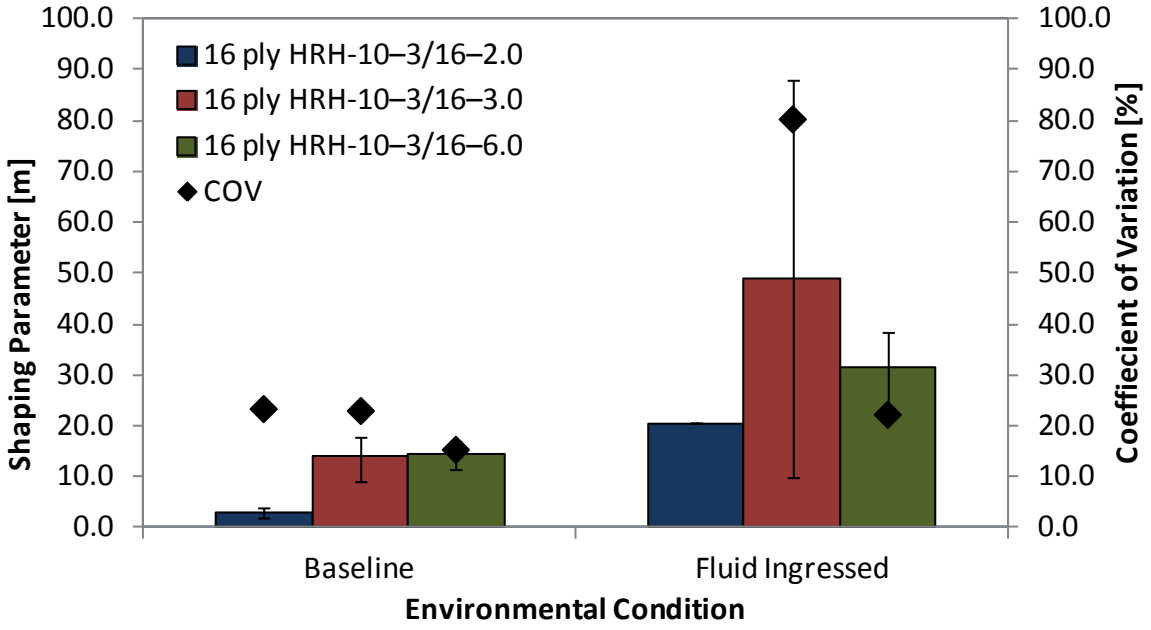

Figure 36. Effects of environmental conditioning with respect to core density (16-ply)

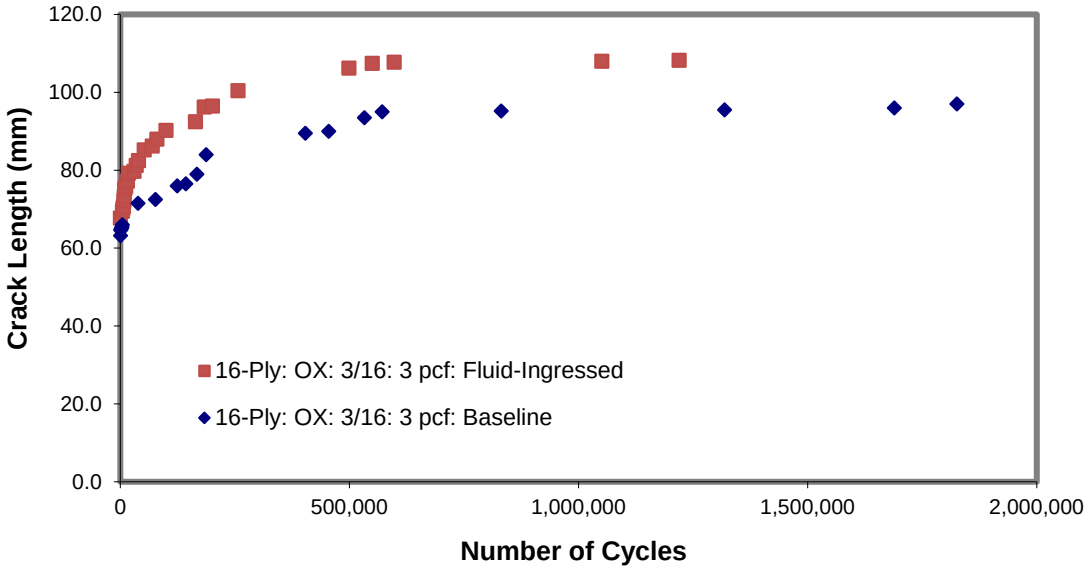

Figure 37. Comparison of crack growth in baseline and fluid-ingressed specimens

3.5 SUMMARY OF FAILURE MODES FOR SCB SANDWICH TEST SPECIMENS

Failure mode played a significant role in propagating fracture toughness and influenced the shaping parameter, *m*. A detailed analysis of failure modes helps distinguish the behavior of the fatigue growth da/dn curves. Failure modes are shown in figures 38–53. On completion of the fatigue tests, SCD specimens were cut open so that both fracture surfaces could be inspected for change in failure modes. Note that the prescribed crack tip occurs at the far-left edge, with the resulting crack propagation moving to the right.

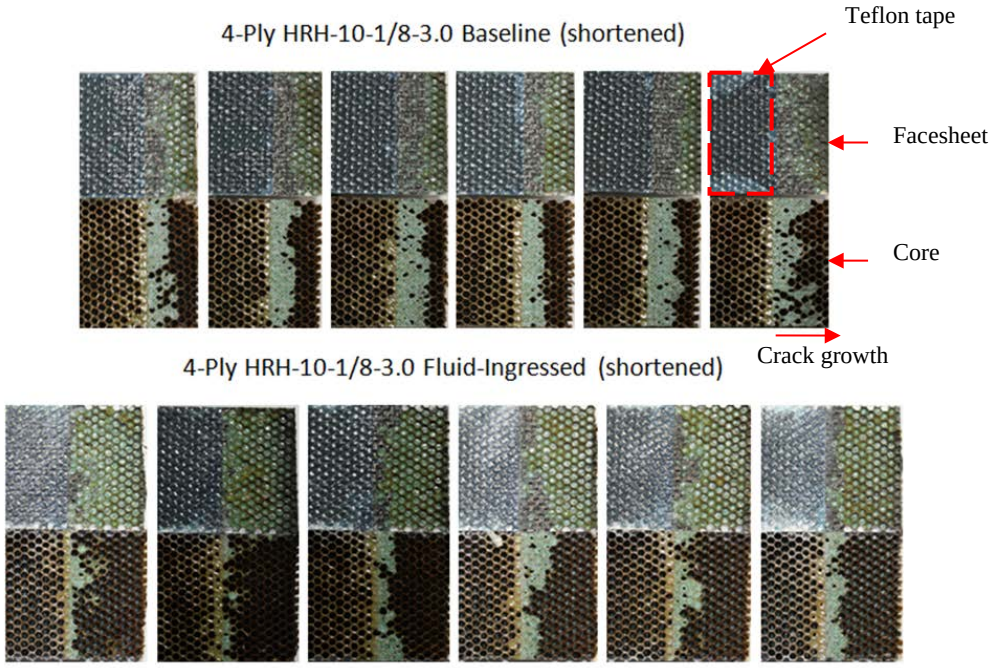

Figure 38. Failure modes of HRH-10–1/8–3.0 thin specimens (4-ply)

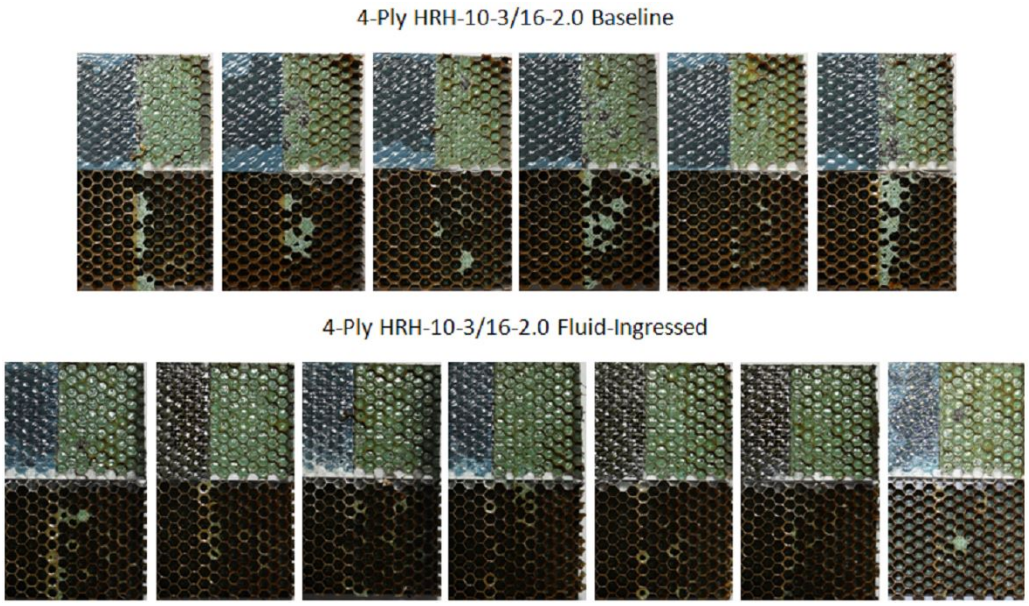

Figure 39. Failure modes of HRH-10–3/16–2.0 thin specimens (4-ply)

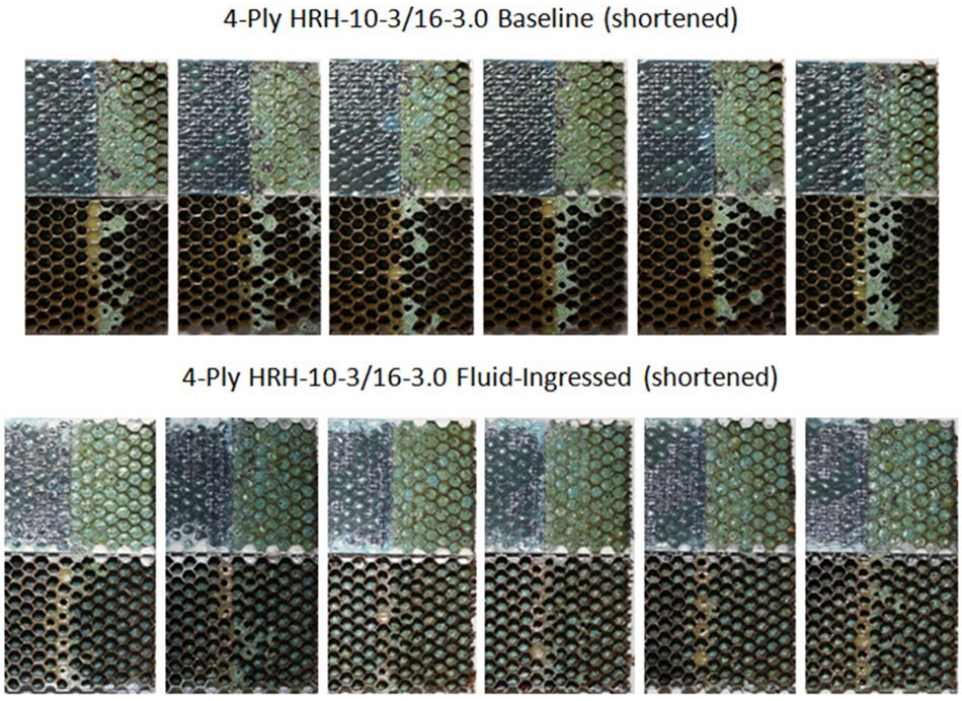

Figure 40. Failure modes of HRH-10–3/16–3.0 thin specimens (4-ply)

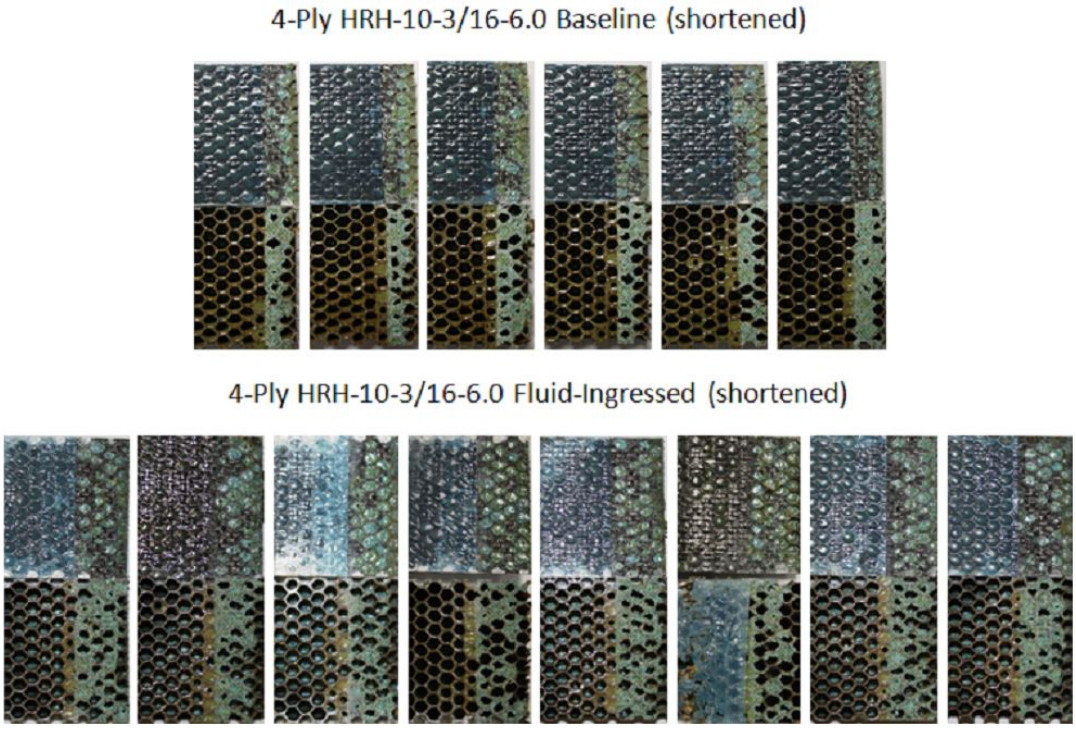

Figure 41. Failure modes of HRH-10–3/16–6.0 thin specimens (4-ply)

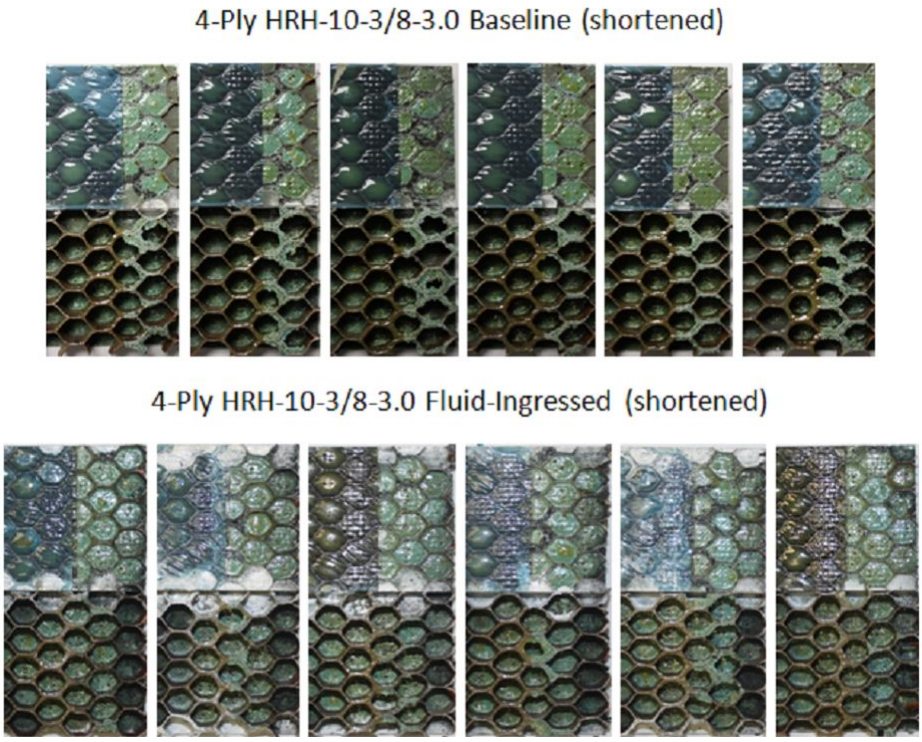

Figure 42. Failure modes of HRH-10–3/8–3.0 thin specimens (4-ply)

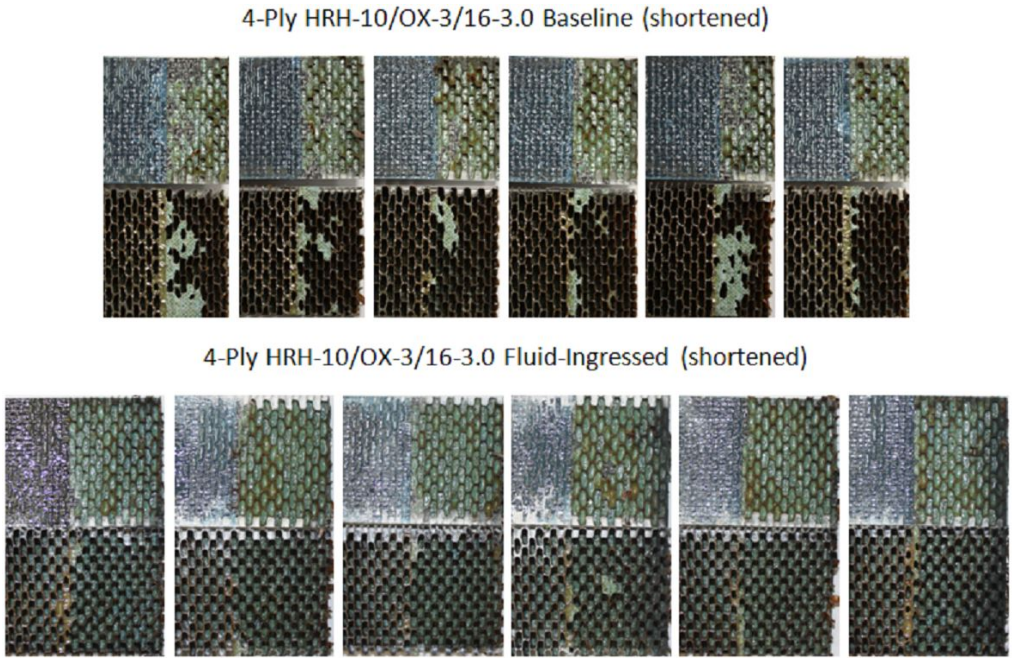

Figure 43. Failure modes of HRH-10/OX–3/16–3.0 thin specimens (4-ply)

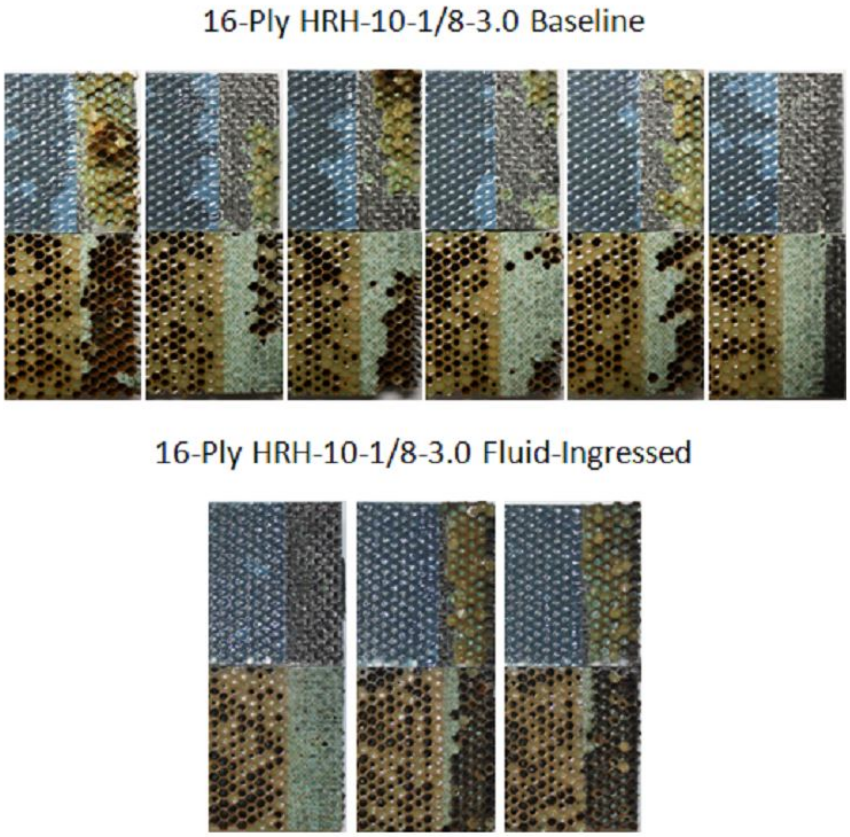

Figure 44. Failure modes of HRH-10–1/8–3.0 thick specimens (16-ply)

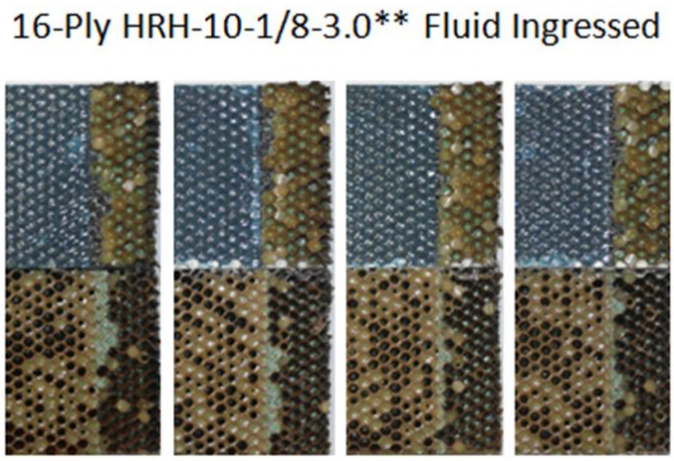

Figure 45. Failure modes of HRH-10–1/8–3.0 thick specimens (16-ply)**

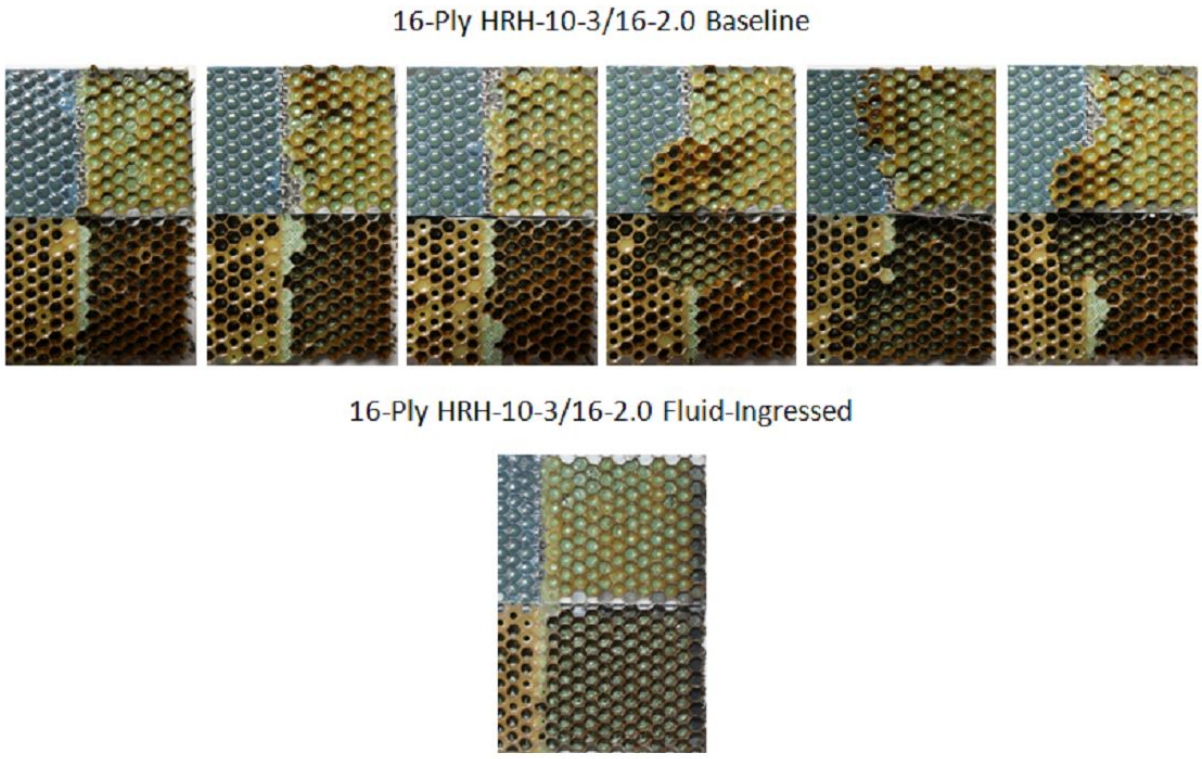

Figure 46. Failure modes of HRH-10–3/16–2.0 thick specimens (16-ply)

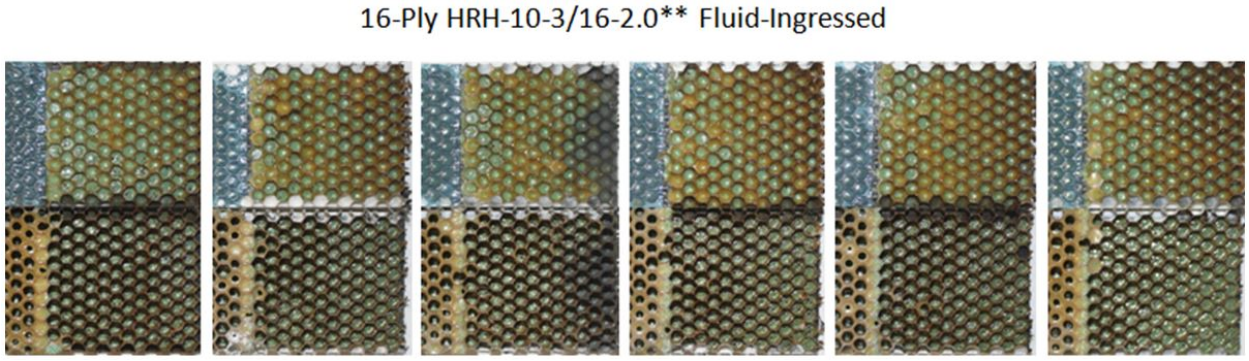

Figure 47. Failure modes of HRH-10–3/16–2.0 thick specimens (16-ply)**

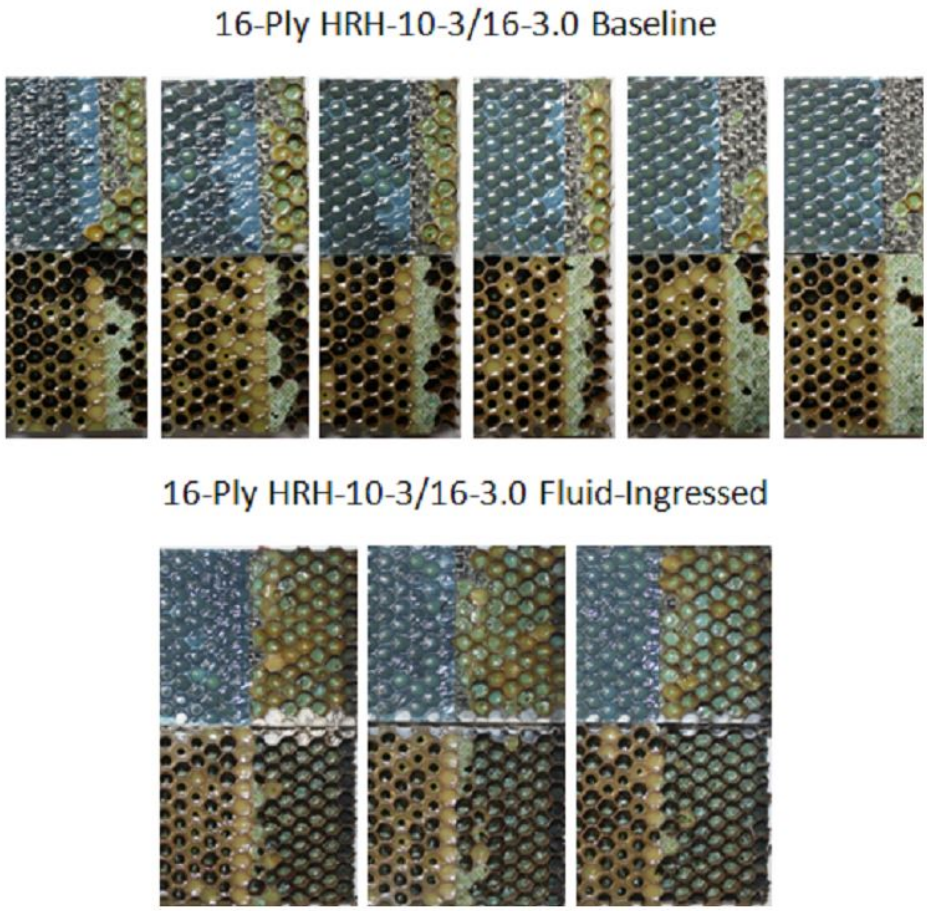

Figure 48. Failure modes of HRH-10–3/16–3.0 thick specimens (16-ply)

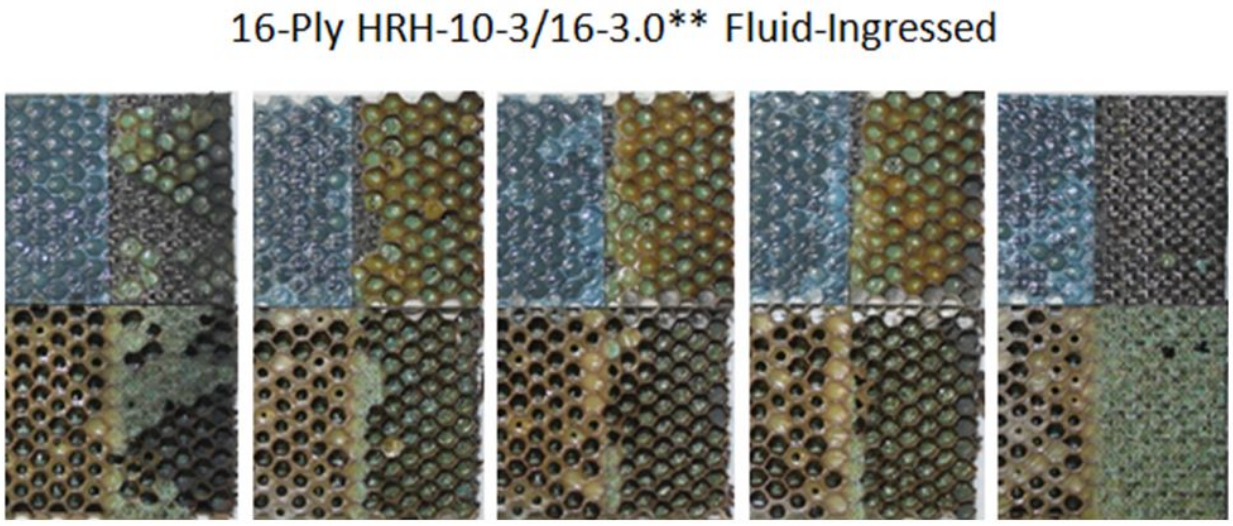

Figure 49. Failure modes of HRH-10–3/16–3.0 thick specimens (16-ply)**

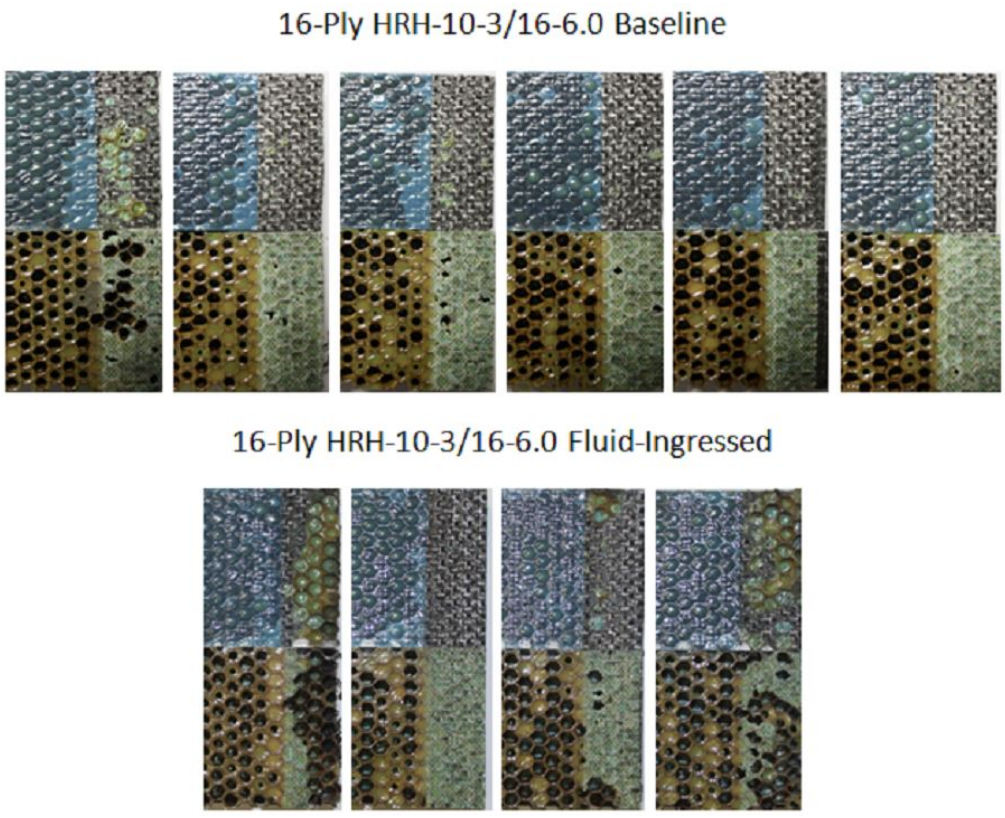

Figure 50. Failure modes of HRH-10–3/16–6.0 thick specimens (16-ply)

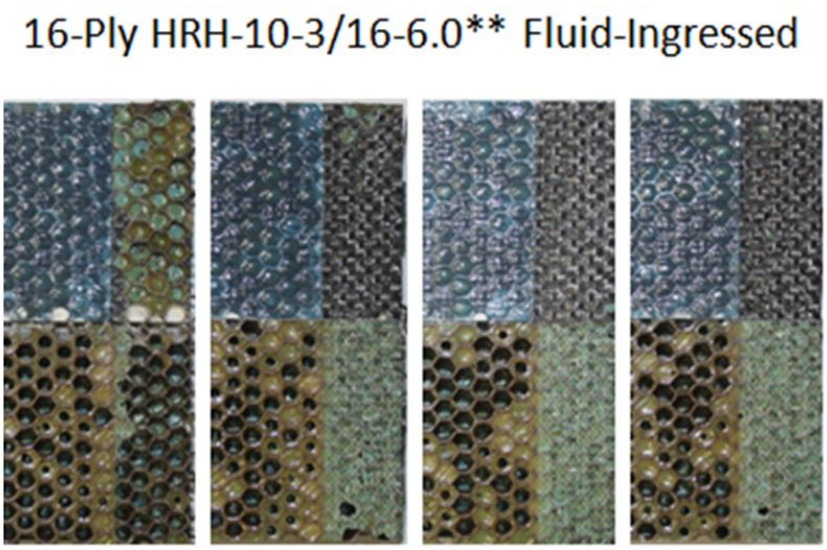

Figure 51. Failure modes of HRH-10–3/16–6.0 thick specimens (16-ply)**

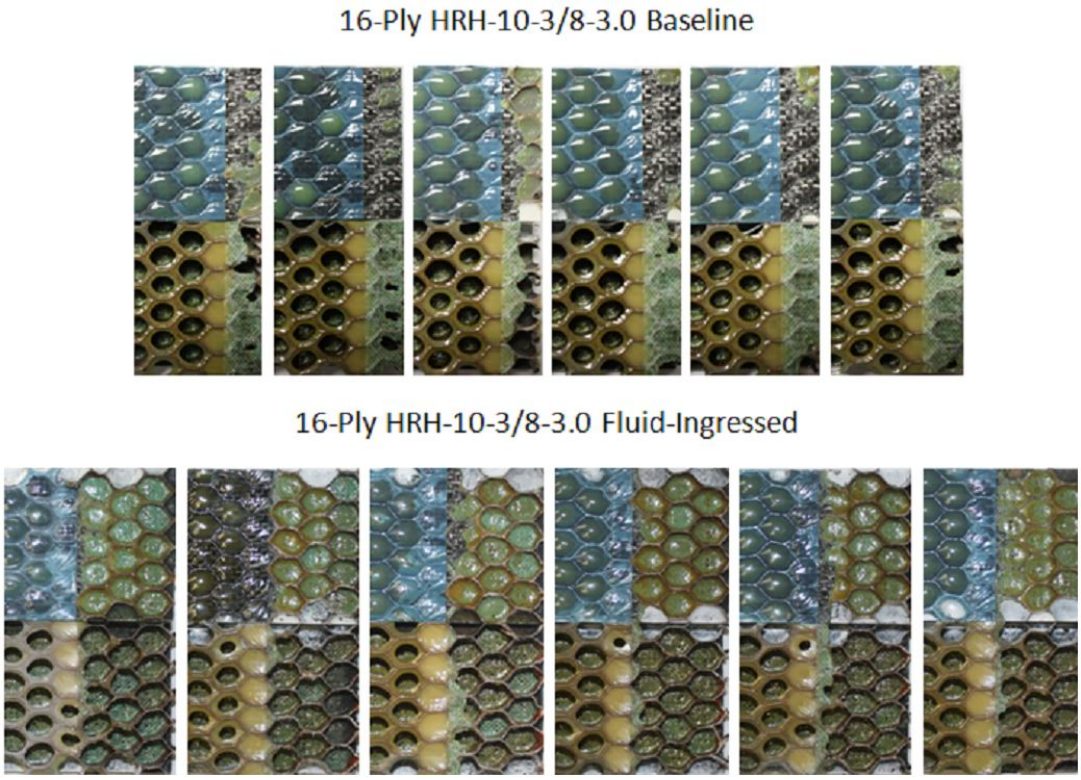

Figure 52. Failure modes of HRH-10–3/8–3.0 thick specimens (16-ply)

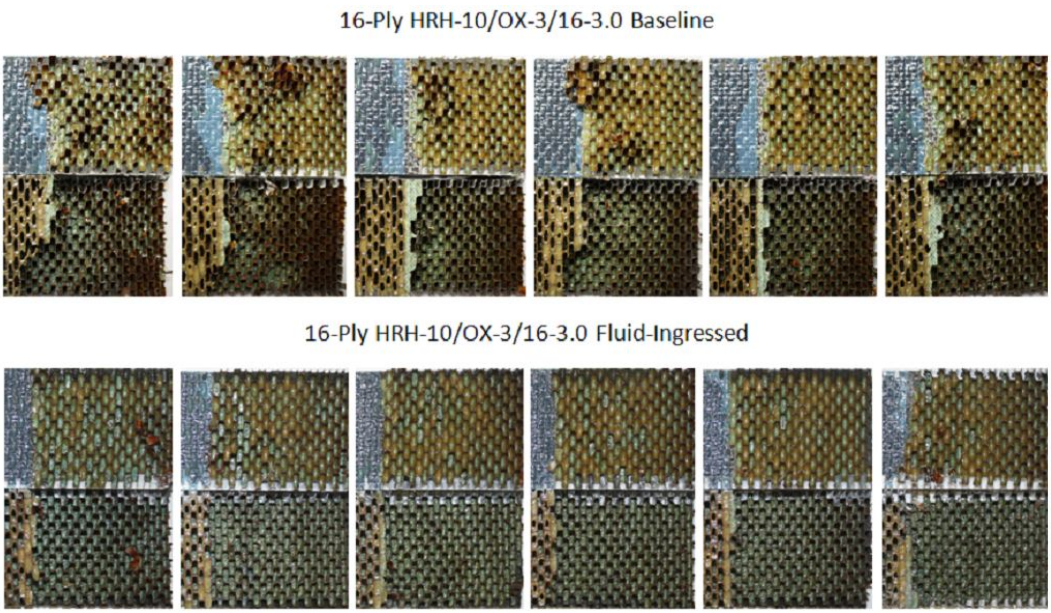

Figure 53. Failure modes of HRH-10/OX–3/16–3.0 thick specimens (16-ply)

4. CONCLUSIONS AND RECOMMENDATIONS

A research program was conducted on the effects of various configurations and fluid ingression on fracture toughness of the composite sandwich structures in fatigue. The SCB specimens were found to be the most suitable for determining the Mode I shaping parameter, *m*, of composite sandwich specimens. The SCB test fixture with a traveling stage prevented mixed-mode mechanics and kinking. This contributed to significant data scatter observed in the test data. The immaturity of the test procedure and variation in the initial flaw could also have contributed to the data scatter. Note that the SCB test configuration did not directly relate to the damage growth phenomenon in a sandwich structure because the realistic damage was often a mixed-mode fracture, but it provided a set of comparative data for identifying the effects of different core parameters on Mode I damage growth. In addition, these data will be used in analytical models for predicting the growth phenomenon. This research will be expanded to larger and more realistic specimen configurations representative of aircraft structures under GAG cycles.

This report discussed the impact of several key sandwich parameters on the shaping parameter, *m*: (1) core type, (2) cell size, (3) core density, and (4) environmental conditioning. It is important to note that several other variables can contribute to the crack growth rate, such as ribbon direction, fabrication technique, and prescribed crack location with respect to cell walls, etc. Therefore, the discussion and conclusions here are solely based on the test results in this report. When comparing the data in this report, the following must also be considered:

- Difference in initial crack length
- Data scatter
- Difference in minimum/maximum fatigue displacements
- Change in failure modes as the crack propagates

- Generally, small shaping parameter indicates higher fracture resistance or low crack growth rate

It was found that the HX had a larger shaping parameter, *m*, than the OX. In addition, the failure modes between the two core types varied significantly.

Cell size played a role in determining the shaping parameter, *m*. In addition, cell fillets and paper thickness may have also contributed to how cell size influenced the shaping parameter, *m*. Among 4-ply baseline specimens, the shaping parameter was level, with a decrease in the larger cell size, and fluid-ingressed specimens experienced an increasing shaping parameter. The shaping parameter in 16-ply specimens did not change for different cores.

Core density had an impact in determining the shaping parameter, *m*, but as stated previously, some of this could have been due to the fillets and how they artificially thicken cell walls and, potentially, paper thickness. Both 4-ply and 16-ply baseline specimens had an increasing shaping parameter, and the fluid-ingressed specimens also increased between the smaller densities and decreased among the larger densities.

Fluid ingression using an acidic Skydrol-water mixture had a significant impact on the shaping parameter, *m*. Though a weakened bondline was expected because of Skydrol ingression at an elevated temperature, crack-tip softening and plasticization increased the fracture toughness and, because of moisture absorption and the weakened adhesive, played a key role in damage growth. For the 4-ply specimens, the baseline data typically had a larger shaping parameter, *m*, indicating a higher fracture resistance than fluid-ingressed specimens. For the 16-ply specimens, the opposite relationship was observed. However, the fluid-ingressed test data had very high scatter; therefore, the results should be used with caution.

As shown in the detailed failure analysis explained in this report, the progressive failure modes often changed as the crack propagated. Changes in failure mode could have substantially impacted data scatter.

5. REFERENCES.

1. Seneviratne, W., Tomblin, J., and Gunawardana, S., "Experimental Fracture Mechanics for Adhesive Joint Design," *International Conference on Computational & Experimental Engineering and Sciences* (ICCES), Vol. 4, No. 2, 2007, pp. 81–86.

2. Anderson, T.L., *Fracture Mechanics: Fundamentals and Applications*, 2nd edition, CRC Press, pp. 12–15 and 34–40, 1995.

3. Smith, B. L., "Mechanics of Damage Tolerance: Residual Strength, Fracture Crack Propagation and Damage Tolerance Evaluation," Class Note Packet, Wichita State University,2010, pp. 13–18 and 280–295.

4. Aviles, F, and Carlsson, L. A., "Analysis of the Sandwich DCB Specimen for Debond Characterization," *Engineering Fracture Mechanics*, Vol. 75, 2008, pp. 153–168.

5. Li, X., and Carlsson, L. A., "Elastic Foundation Analysis of Tilted Sandwich Debond (TSD) Specimen," *Journal of Sandwich Structures and Materials*, Vol. 2, 2000, pp. 3–32.

6. Shivakumar, K., Chen, H., and Smith, S. A., "An Evaluation of Data Reduction Methods for Opening Mode Fracture Toughness of Sandwich Panels," *Journal of Sandwich Structures and Materials*, Vol. 7, 2005, pp. 77–90.

7. Seneviratne, W., and Tomblin, J., "Damage Growth in Fluid-Ingressed Sandwich Structures," *1st Technical Workshop for Safety Management Initiative for Sandwich Disbond Growth*, Hampton, Virginia, March 23–24, 2011.

8. Cantwell, W. J., and Davies, P., "A Test Technique for Assessing Core-Skin Adhesion in Composite Sandwich Structures," *Journal of Material Science Letters*, Vol. 13, No. 3, 1994, pp. 203–205.

9. Cantwell, W. J., and Davies, P., "A Study of Skin-Core Adhesion in Glass Fiber Reinforced Sandwich Materials," *Applied Composite Materials*, Vol. 3, No. 6, 1996, pp. 407–420.

10. Ratcliffe, J.G., "Sizing Single Cantilever Beam Specimens for Characterizing Facesheet/Core Peel Debonding in Sandwich Structure," NASA/TP-2010-216169, Hampton, Virginia, January, 2010.

APPENDIX A—SKYDROL®/WATER FLUID-INGRESSION PROCEDURE

The adhesive used to bond the facesheet to the core can break down when exposed to certain chemicals, such as phosphoric acid. Given enough time, when water and hydraulic fluid are combined, a byproduct of weak phosphoric acid can be produced. Because of the amount of hydraulic fluid and water on aircraft, it is vital to determine their effect on sandwich composites that have been ingressed in this volatile amalgam.

Before fluid ingression can begin, it is paramount to create a mixture with an acceptable amount of acidity. To produce a viable solution, water and Skydrol® are mixed in a 50:50 ratio, placed in an elevated temperature of 160°F, agitated for 2 weeks, and then placed at room temperature. The elevated temperature acts as a catalyst and accelerates the production of phosphoric acid. The solution is now at a pH of approximately 3–4, and the specimens can be conditioned. The acidity of these solutions for the entire duration can be seen in figure A-1.

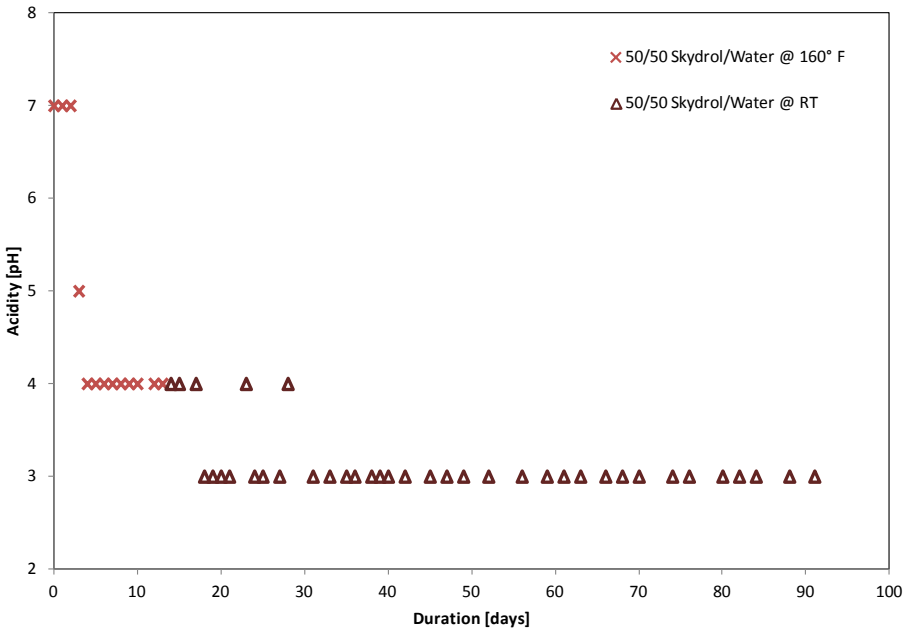

Figure A-1. Sample acidity plot showing solution kept at constant temperature of 160°F for 14 days and then at room temperature

Fluid-ingressed specimens were conditioned for 45 days and then immediately tested. The length of conditioning was determined empirically.

A.1 PROCEDURE

A.1.1 SCOPE

The scope for the Skydrol/water fluid-ingression procedure is as follows:

- This test procedure covers the proper methodology for creating a Skydrol and water amalgam. The resulting mixture should become a mild acid and is typically used to degrade adhesives.
- The temperature shall be measured in degrees Fahrenheit (F), and acidity shall be measured in pH, both regarded as standard.
- This test procedure does not address all safety and health concerns, if any, associated with the use of this test procedure. The user(s) of this standard must establish appropriate safety and health procedures and determine the applicable regulations associated with such concerns.

A.1.2 APPLICABLE STUDIES

Skydrol-water round robin testing was performed in the National Institute for Aviation Research at Wichita State University.

A.1.3 SIGNIFICANCE OF USE

Both Skydrol and water can be found within an aircraft—Skydrol as a hydraulic oil and water from condensation—and, when mixed, they produce a mild acid that can erode adhesives within sandwich materials and bonded joints. This test method provides a consistent and repeatable approach for producing an acidic mixture composed of Skydrol and water.

A.1.4 APPARATUS

The apparatus is as follows:

- Conditioning camber capable of maintaining 160°F ± 5°F.
- Airtight container that is both acid resistant and temperature rated.
- Litmus paper that is capable of attaining a solution acidity of 1–9 pH.

A.1.5 TEST SPECIMEN

The test specimen is a solution consisting of 50% Skydrol and 50% tap water by volume.

A.1.6 EXPERIMENTAL PROCEDURE

The experimental procedure is as follows:

- Mix the needed amount of 50% Skydrol and 50% water solution in an airtight container.
- Place the container inside the conditioning camber at 160°F for 14 days, mixing thoroughly once a day.
- Remove the container from the conditioning camber and let sit at room temperature until cooled.
- Ensure the solution is now at a pH of 3–4.

A.1.7 DATA REDUCTION

Litmus paper is used for monitoring acidity.

APPENDIX B—FATIGUE RESULTS FOR THIN FACESHEET (4-PLY) AND HRH-10 HEXAGONAL CORES TESTED AS SINGLE-CANTILEVER BEAMS

Note that 4-ply material systems were tested with one prescribed crack length. The baseline and fluid-ingressed specimens were all tested with a 1″ prescribed crack.

B.1 HRH–10–1/8–3.0 DATA

B.1.1 HRH-10–1/8–3.0 BASELINE DATA (1.0″ PRESCRIBED CRACK—SHORTENED)

Table B-1. Test summary for HRH-10–1/8–3.0 baseline (1″ prescribed crack—shortened)

Specimen	Shaping Parameter [m] English or SI	Shaping Parameter [B] English	Shaping Parameter [B] SI	Failure Mode
SDT-04-HX-1.8-3-BL-SLX-1 (shortened)	6.362	8.859E-06	1.203E-18	First three rows a mix of A and PO, then C
SDT-04-HX-1.8-3-BL-SLX-2 (shortened)	6.044	3.722E-06	2.614E-18	First three rows primarily A with several cells in PO, then C
SDT-04-HX-1.8-3-BL-SLX-3 (shortened)	5.829	2.848E-06	6.060E-18	First three rows a mix of A and PO, then C
SDT-04-HX-1.8-3-BL-SLX-4 (shortened)	8.399	5.924E-06	2.166E-23	First three rows primarily A with several cells in PO, then C
SDT-04-HX-1.8-3-BL-SLX-5 (shortened)	4.556	3.755E-06	5.824E-15	First three rows a mix of A and PO, then C
SDT-04-HX-1.8-3-BL-SL1-7 (shortened)	7.146	2.114E-06	5.000E-21	First three rows primarily PO with several cells in A, then C, with several cells in A and PO
AVERAGE (individual)	6.389	4.537E-06	9.723E-16	
STANDARD DEVIATION	1.297	2.474E-06	2.377E-15	
COEFFICIENT OF VARIATION [%]	20.295	54.526	244.451	
AVERAGE (all)	5.483	3.429E-06	4.359E-17	
AVERAGE (interpolated)	5.678	3.364E-06	1.561E-17	

A = adhesive interface disbond failure; PO = adhesive pullout failure; C = tensile core failure

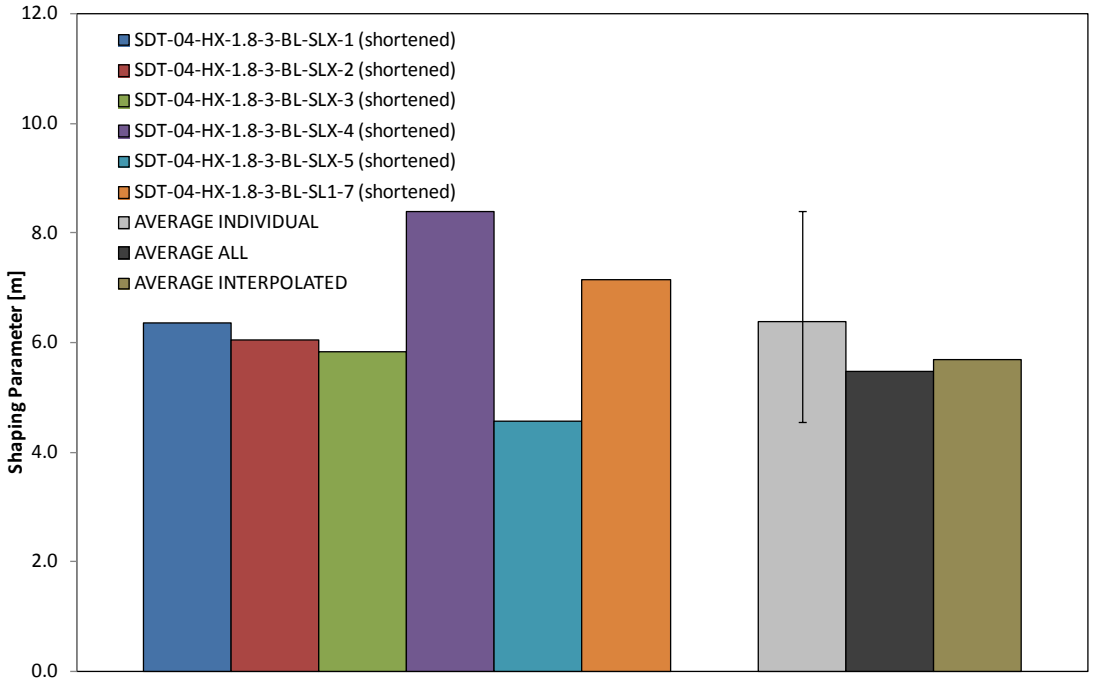

Figure B-1. Shaping parameter (*m*) for HRH-10–1/8–3.0 baseline (1″ prescribed crack—shortened)

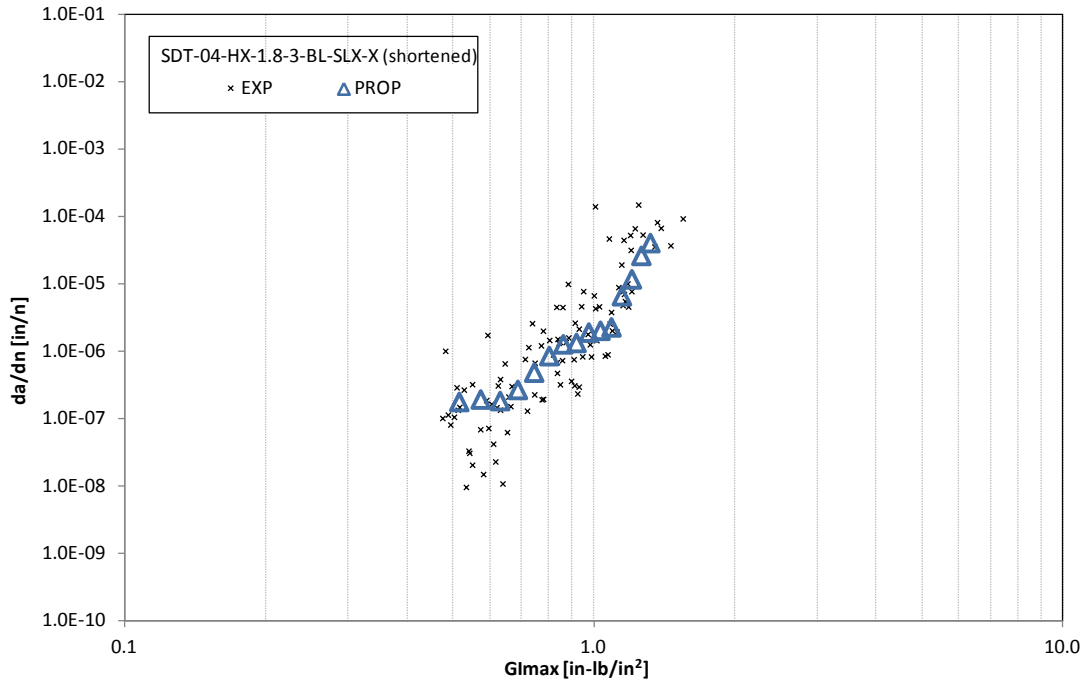

Figure B-2. Fatigue growth da/dn curve for HRH-10–1/8–3.0 baseline (1″ prescribed crack—shortened)

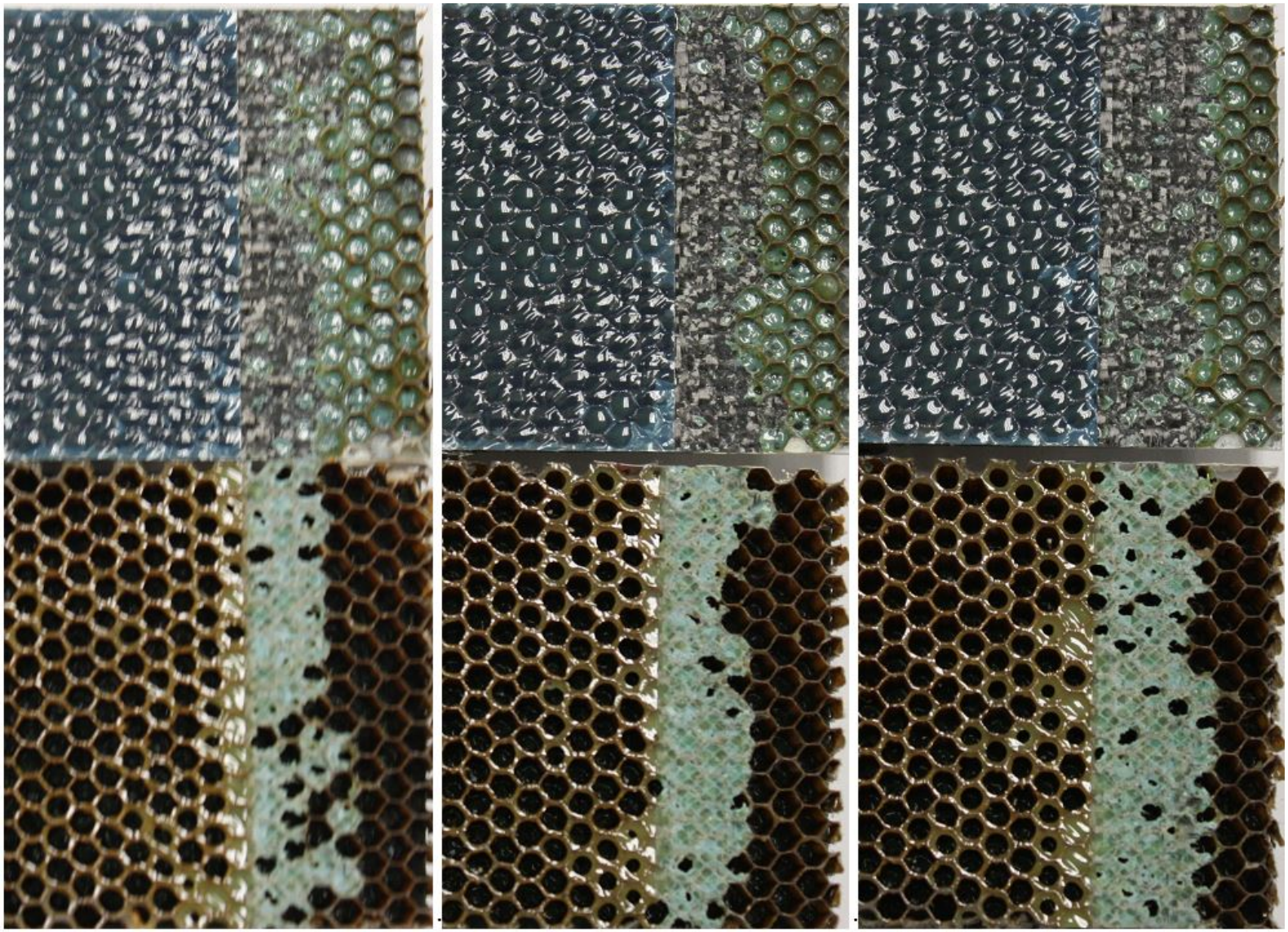

Figure B-3. Failure mode for SDT-04-HX-1.8-3-BL-SLX-X (shortened) #1, #2, and #3

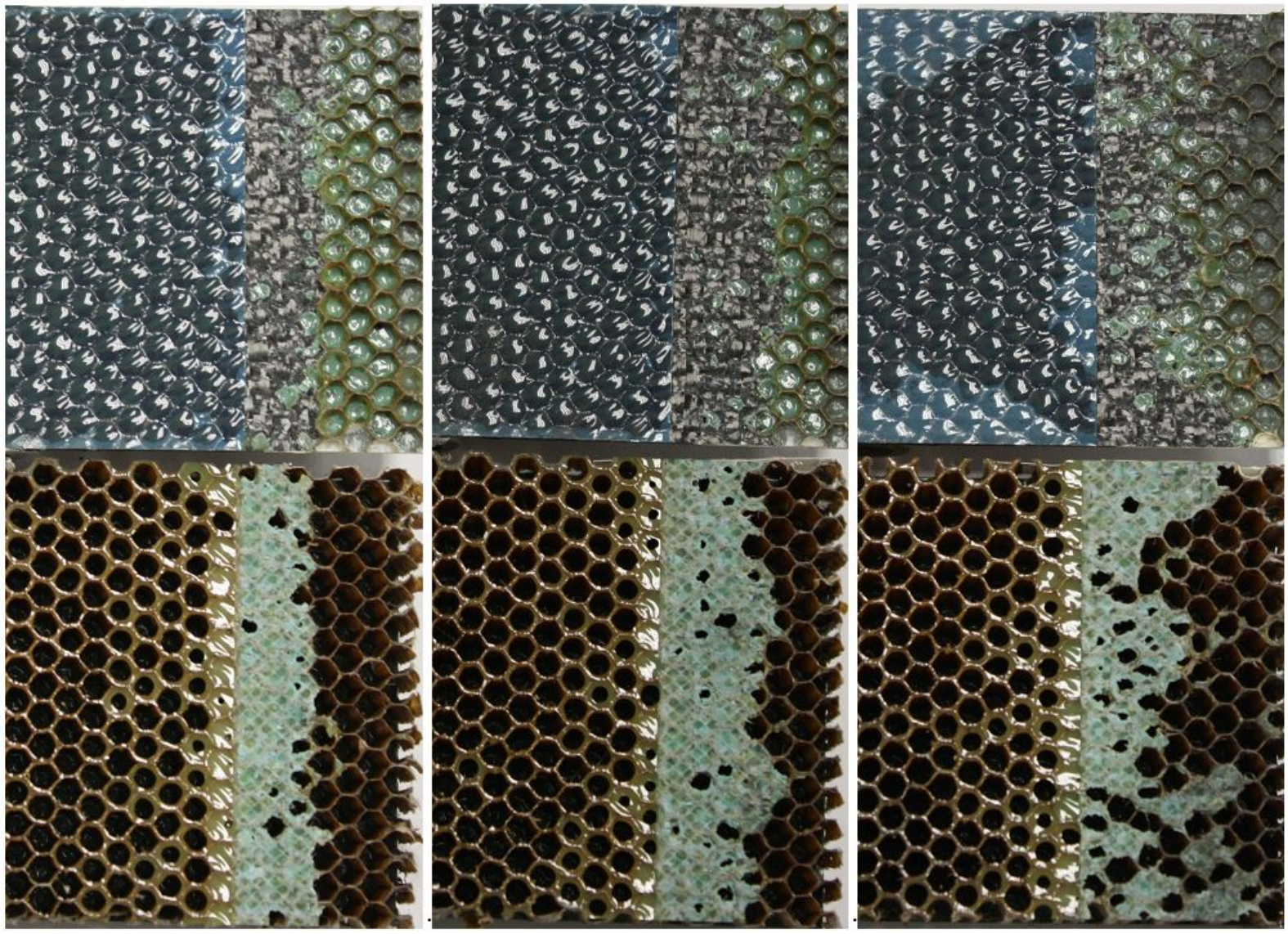

Figure B-4. Failure mode for SDT-04-HX-1.8-3-BL-SLX-X (shortened) #4, #5, and #7

B.1.2 HRH-10–1/8–3.0 FLUID-INGRESSED DATA (1″ PRESCRIBED CRACK—SHORTENED)

Table B-2. Test summary for HRH-10–1/8–3.0 fluid ingressed (1″ prescribed crack—shortened)

Specimen	Shaping Parameter [m] English or SI	Shaping Parameter [B] English	Shaping Parameter [B] SI	Failure Mode
SDT-04-HX-1.8-3-FI-SLX-1 (shortened)	2.583	4.146E-06	1.687E-10	Initially A transitioning into PO, then C with a pocket of A and PO
SDT-04-HX-1.8-3-FI-SLX-2 (shortened)	3.570	3.429E-06	8.526E-13	First row a mix of A and C with a few cells in PO, then C
SDT-04-HX-1.8-3-FI-SLX-3 (shortened)	2.822	4.155E-09	5.103E-71	First three rows primarily in A with several cells in C, then C
SDT-04-HX-1.8-3-FI-SLX-4 (shortened)	2.243	1.447E-10	1.749E-59	First two rows primarily in A with several cells in PO and a few cells in C, then split between A and C, then C
SDT-04-HX-1.8-3-FI-SLX-5 (shortened)	6.577	1.194E-06	5.330E-20	First row primarily A with a few cells in C; second row a mix of PO and C, then C with a pocket of A
SDT-04-HX-1.8-3-FI-SLX-6 (shortened)	1.989	7.389E-11	4.595E-54	First three rows primarily in A with a few cells in PO and C, then C
AVERAGE (individual)	3.297	1.462E-06	2.827E-11	
STANDARD DEVIATION	1.697	1.873E-06	6.882E-11	
COEFFICIENT OF VARIATION [%]	51.450	128.114	243.474	
AVERAGE (all)	1.859	1.085E-06	1.862E-09	
AVERAGE (interpolated)	2.286	1.015E-06	1.918E-10	

A = adhesive interface disbond failure; PO = adhesive pullout failure; C = tensile core failure

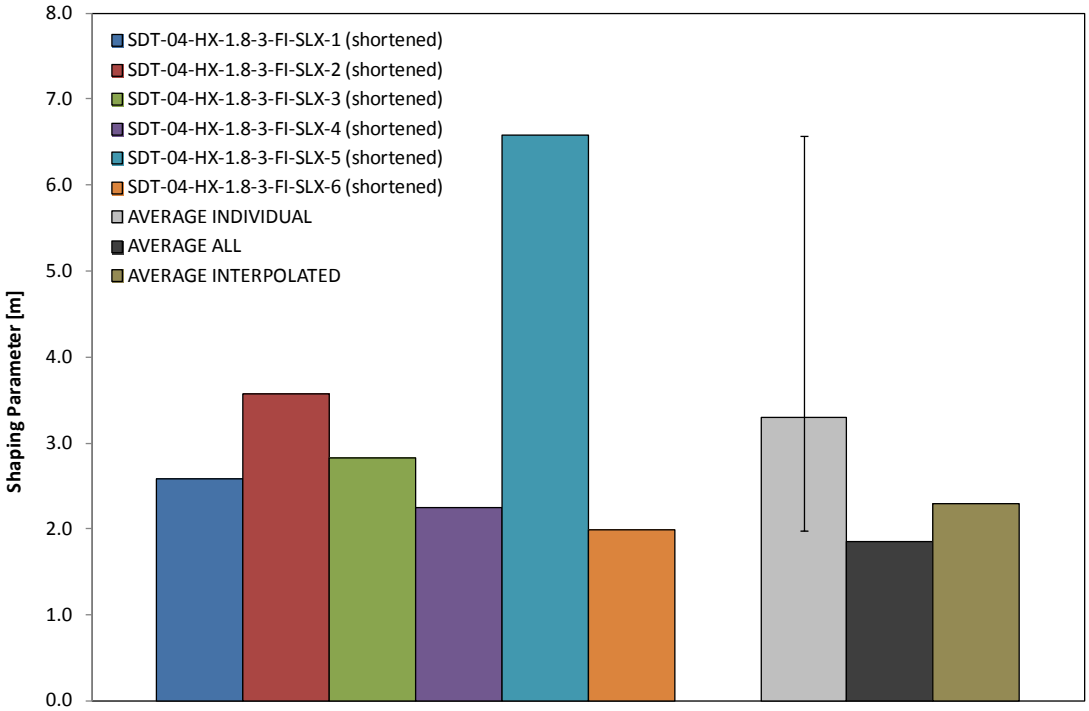

Figure B-5. Shaping parameter (*m*) for HRH-10–1/8–3.0 fluid ingressed (1″ prescribed crack—shortened)

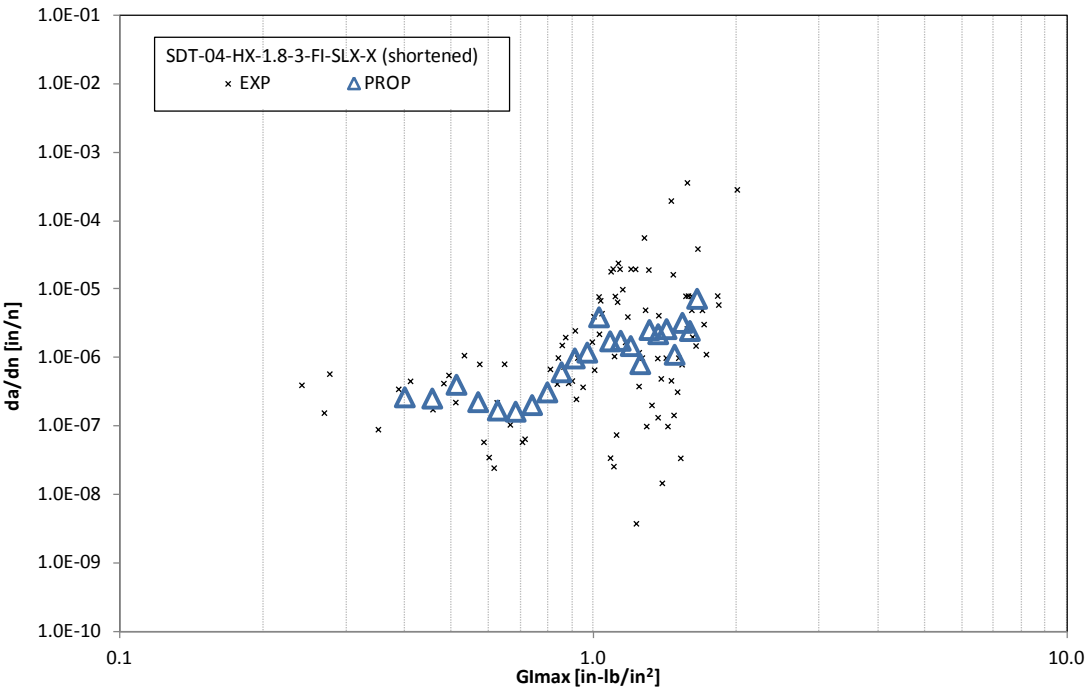

Figure B-6. Fatigue growth da/dn curve for HRH-10–1/8–3.0 fluid ingressed (1″ prescribed crack—shortened)

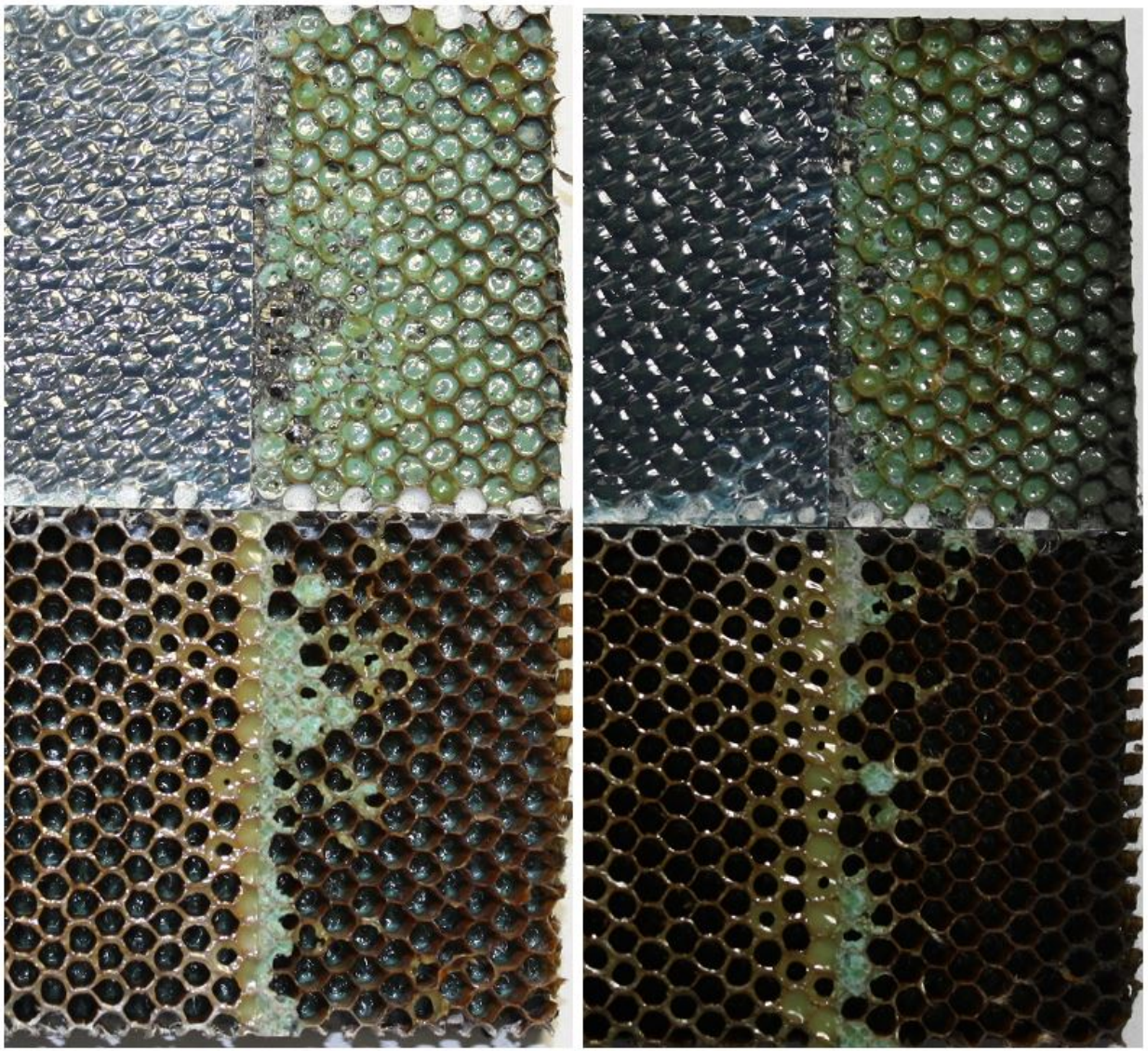

Figure B-7. Failure mode for SDT-04-HX-1.8-3-FI-SLX-X (shortened) #1 and #2

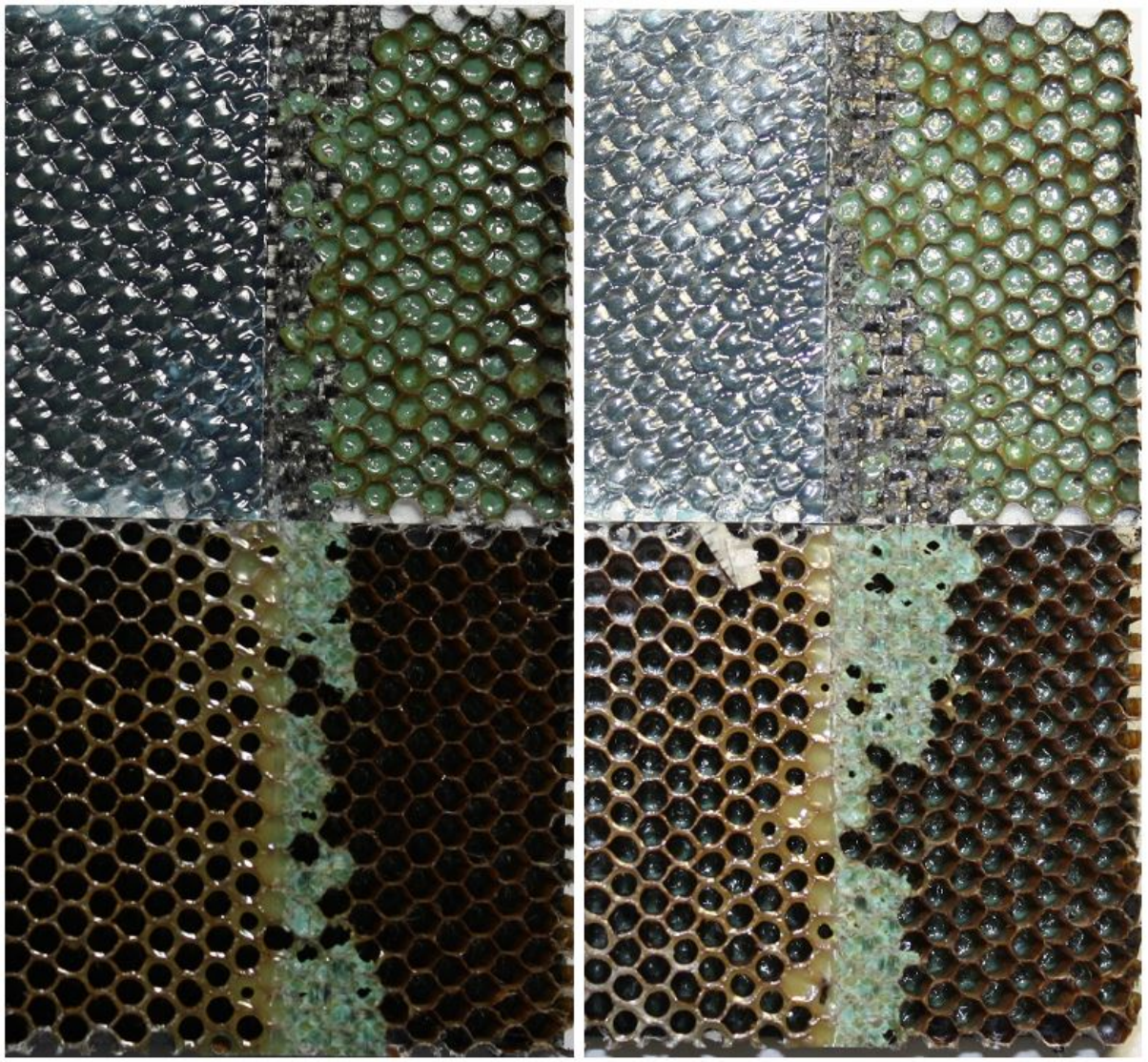

Figure B-8. Failure mode for SDT-04-HX-1.8-3-FI-SLX-X (shortened) #3 and #4

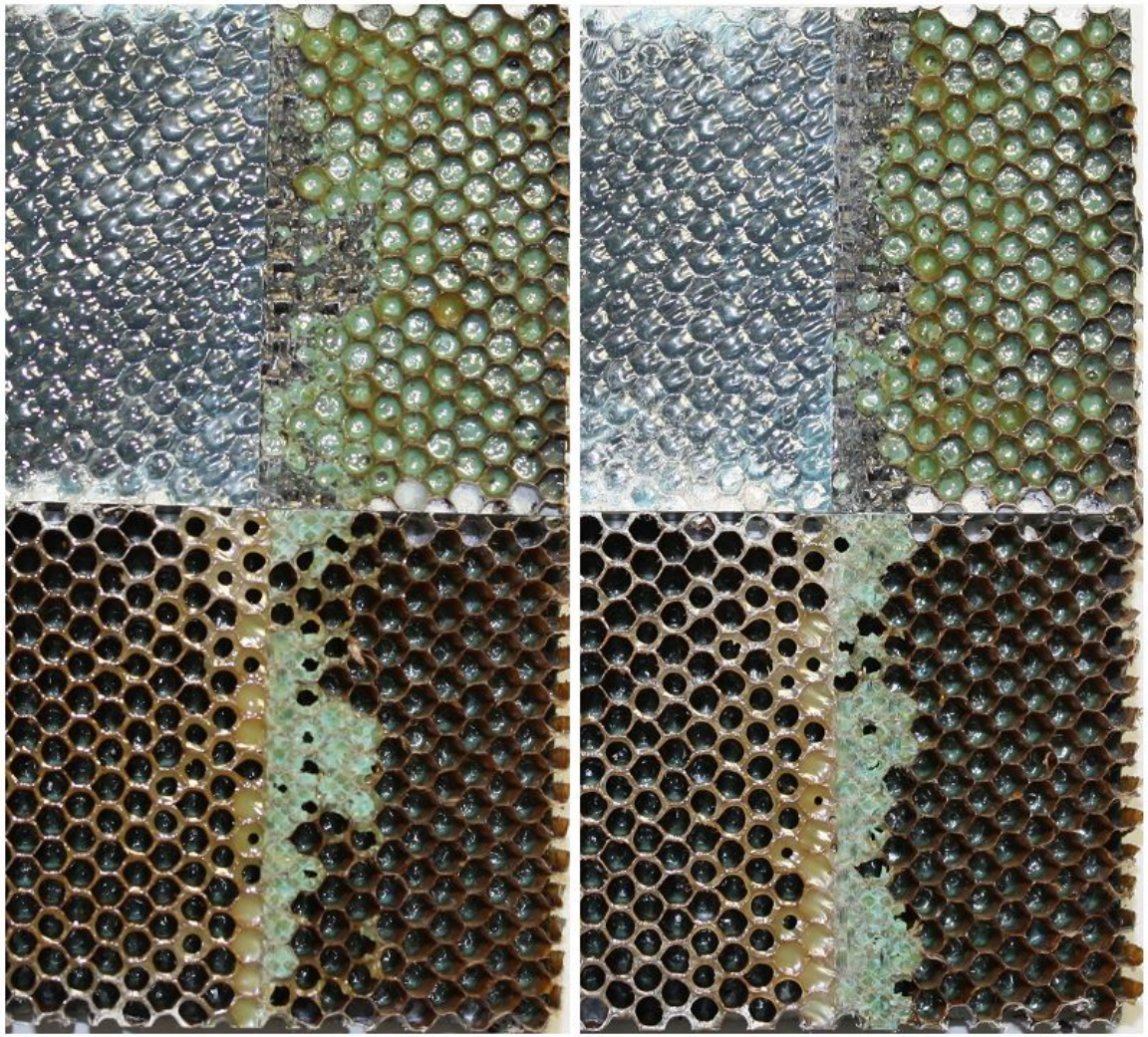

Figure B-9. Failure mode for SDT-04-HX-1.8-3-FI-SLX-X (shortened) #5 and #6

B.2 HRH-10–3/16–2.0 DATA

B.2.1 HRH-10–3/16–2.0 BASELINE DATA (1″ PRESCRIBED CRACK—SHORTENED)

Table B-3. Test summary for HRH-10–3/16–2.0 baseline (1″ prescribed crack—shortened)

Specimen	Shaping Parameter [m] English or SI	Shaping Parameter [B] English	Shaping Parameter [B] SI	Failure Mode
SDT-04-HX-3.16-2-BL-SLX-1 (shortened)	1.935	1.213E-05	1.407E-08	Initially a mix of A with a couple cells in PO, then C
SDT-04-HX-3.16-2-BL-SLX-2 (shortened)	5.171	3.095E-05	1.978E-15	Initially a mix of A and C, then C with a pocket of PO with a cell in A
SDT-04-HX-3.16-2-BL-SLX-3 (shortened)	3.770	2.669E-05	2.363E-12	Primarily in C with a couple cells in PO and a cell in A
SDT-04-HX-3.16-2-BL-SLX-4 (shortened)	4.013	1.969E-05	4.963E-13	Initially a PO with a cell in A and C then C, with a pocket of PO with a cell in A
SDT-04-HX-3.16-2-BL-SLX-5 (shortened)	5.337	2.770E-05	5.203E-16	Primarily in C with a few cells in PO
SDT-04-HX-3.16-2-BL-SLX-8 (shortened)	4.128	4.840E-06	6.737E-14	Initially PO, transitioning to a mix of PO and A, then C with a few cells in PO
AVERAGE (individual)	4.059	2.033E-05	2.345E-09	
STANDARD DEVIATION	1.222	1.015E-05	5.744E-09	
COEFFICIENT OF VARIATION [%]	30.116	49.925	244.888	
AVERAGE (all)	3.045	1.285E-05	4.820E-11	
AVERAGE (interpolated)	3.441	1.306E-05	1.931E-11	

A = adhesive interface disbond failure; PO = adhesive pullout failure; C = tensile core failure

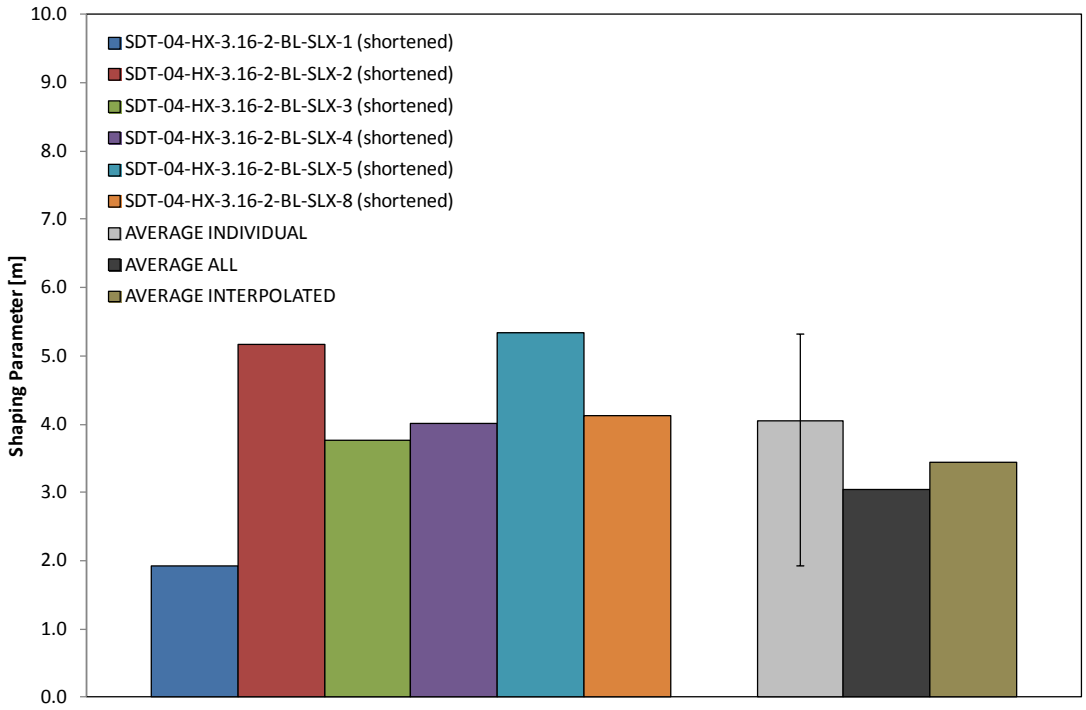

Figure B-10. Shaping parameter (*m*) for HRH-10–3/16–2.0 baseline (1″ prescribed crack—shortened)

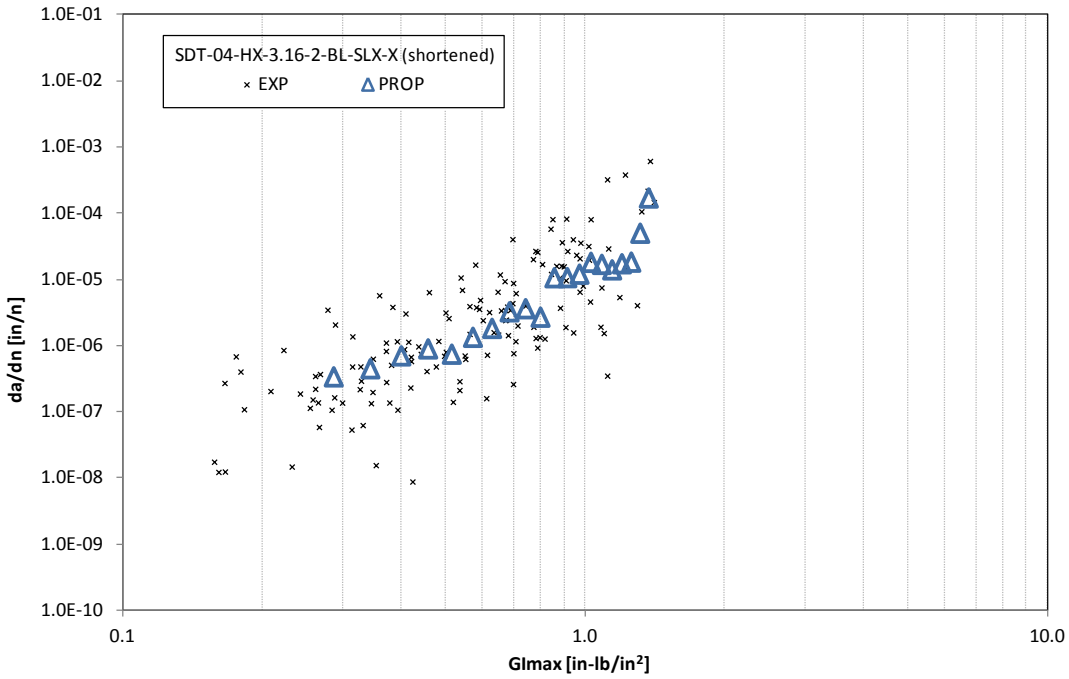

Figure B-11. Fatigue growth da/dn curve for HRH-10–3/16–2.0 baseline (1″ prescribed crack—shortened)

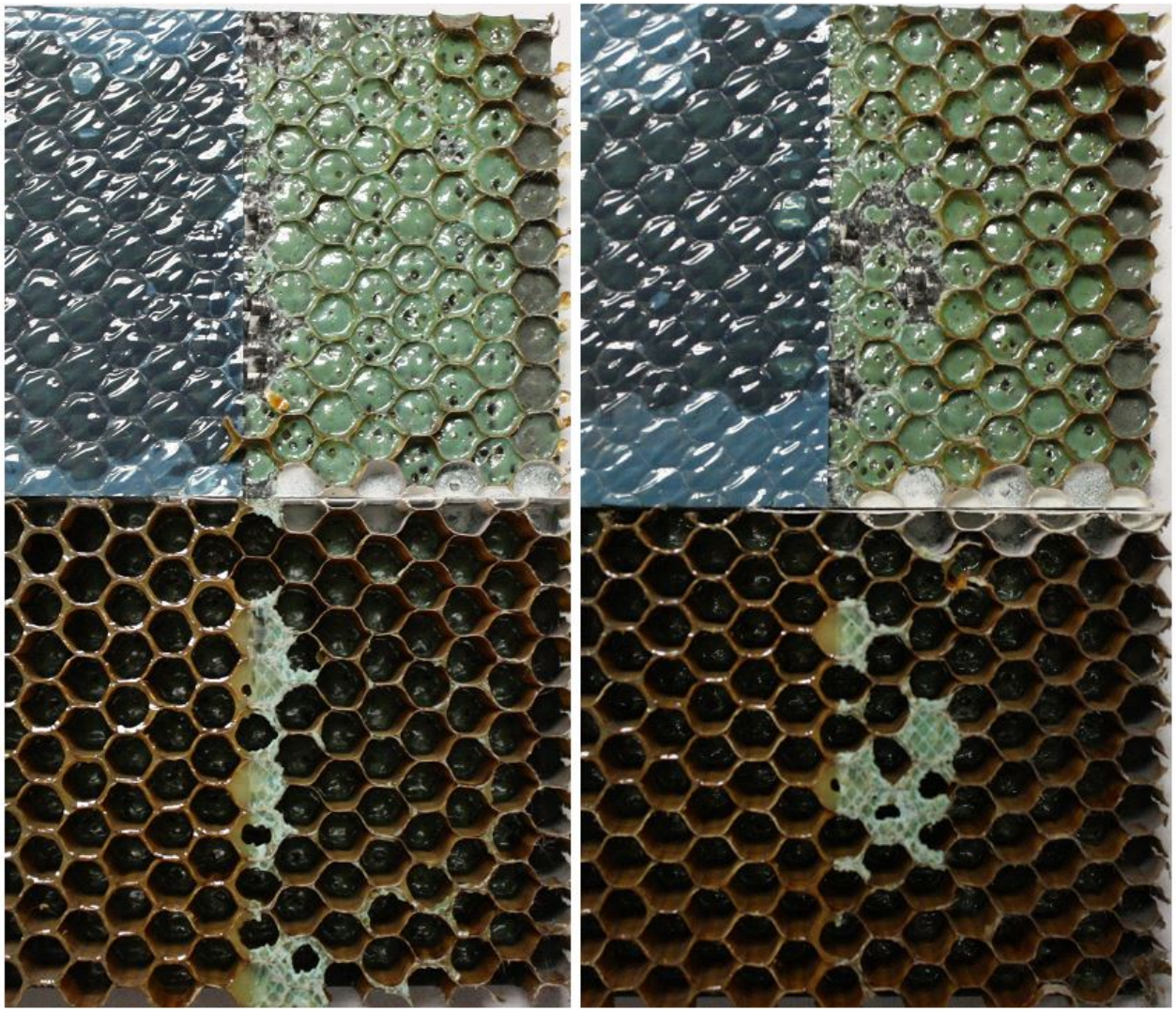

Figure B-12. Failure mode for SDT-04-HX-3.16-2-BL-SLX-X (shortened) #1 and #2

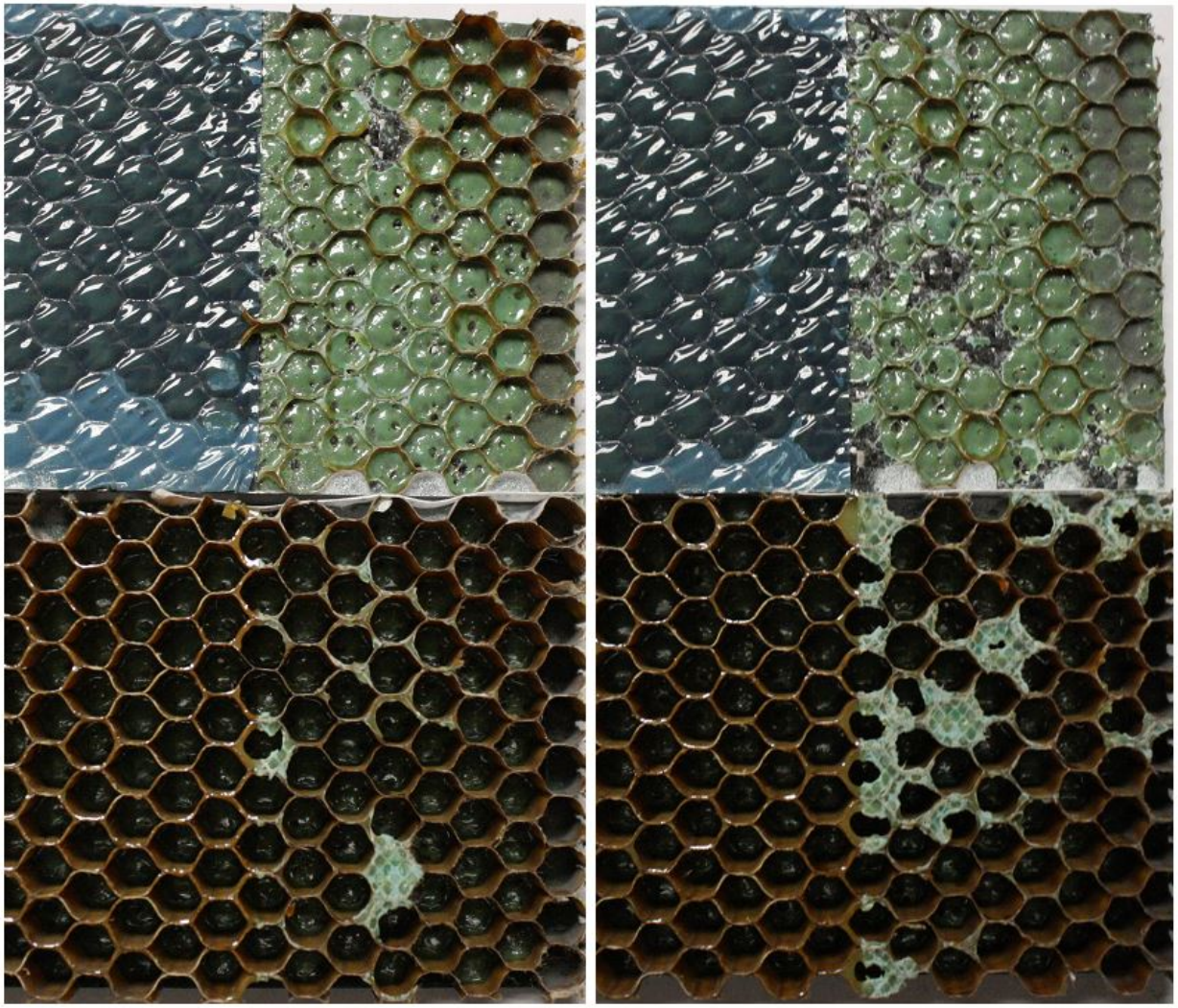

Figure B-13. Failure mode for SDT-04-HX-3.16-2-BL-SLX-X (shortened) #3 and #4

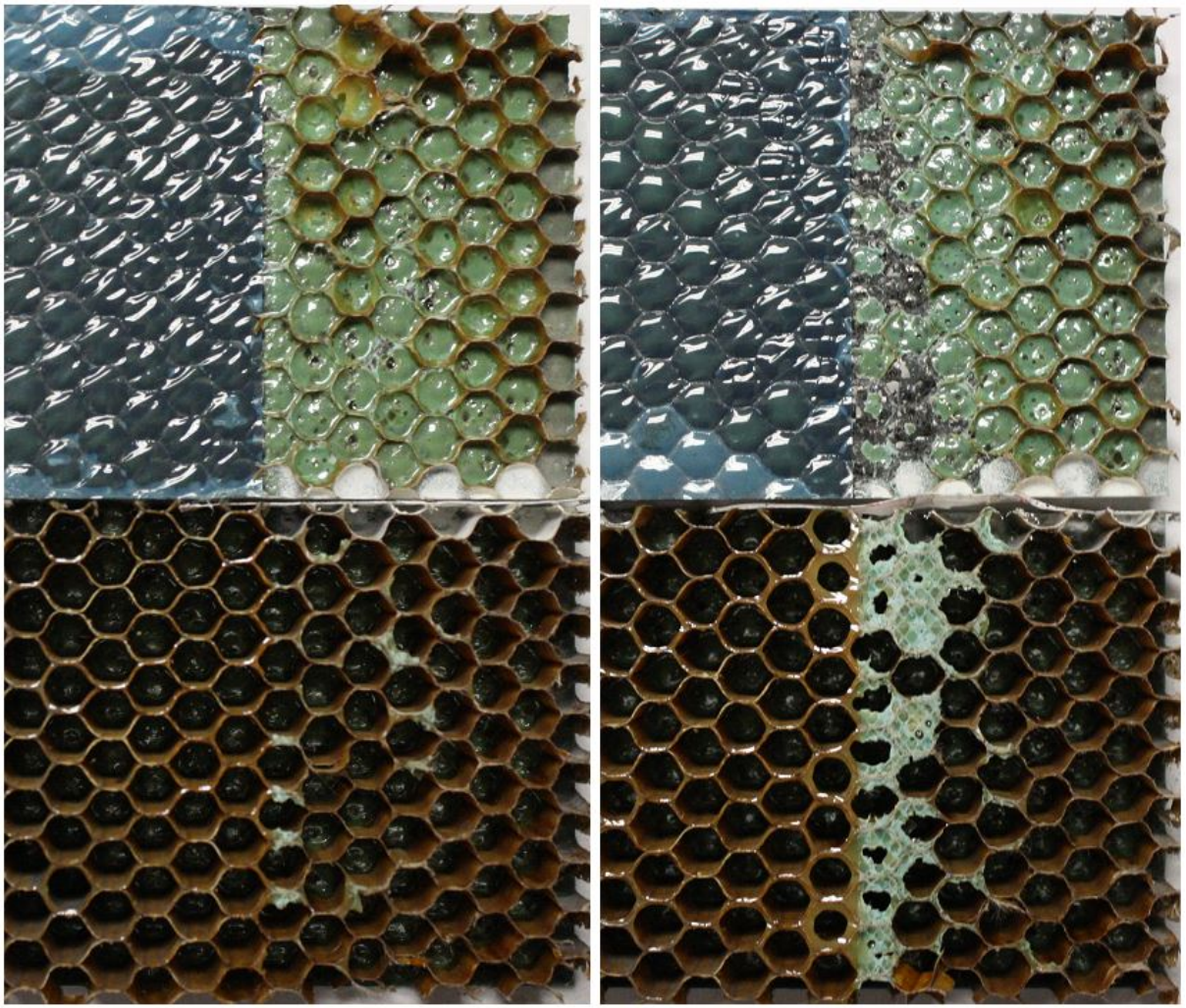

Figure B-14. Failure mode for SDT-04-HX-3.16-2-BL-SLX-X (shortened) #5 and #8

B.2.2 HRH-10–3/16–2.0 FLUID-INGRESSED DATA (1″ PRESCRIBED CRACK—SHORTENED)

Table B-4. Test summary for HRH-10–3/16–2.0 fluid ingressed (1″ prescribed crack—shortened)

Specimen	Shaping Parameter [m] English or SI	Shaping Parameter [B] English	Shaping Parameter [B] SI	Failure Mode
SDT-04-HX-3.16-2-FI-SLX-1 (shortened)	3.474	3.549E-05	1.448E-11	Primarily C with occasional cells in PO
SDT-04-HX-3.16-2-FI-SLX-2 (shortened)	4.169	2.548E-04	2.870E-12	Primarily C with occasional cells in PO
SDT-04-HX-3.16-2-FI-SLX-3 (shortened)	2.748	2.053E-05	3.570E-10	Primarily C with occasional cells in PO
SDT-04-HX-3.16-2-FI-SLX-4 (shortened)	4.650	3.514E-05	3.310E-14	Primarily C with occasional cells in PO
SDT-04-HX-3.16-2-FI-SLX-5 (shortened)	5.111	6.814E-05	5.932E-15	Primarily C with occasional cells in PO
SDT-04-HX-3.16-2-FI-SLX-6 (shortened)	4.627	7.188E-05	7.604E-14	Primarily C with occasional cells in PO
SDT-04-HX-3.16-2-FI-SLX-7 (shortened)	5.446	5.278E-05	8.113E-16	Primarily C with occasional cells in PO
AVERAGE (individual)	4.318	7.696E-05	5.350E-11	
STANDARD DEVIATION	0.940	8.059E-05	1.339E-10	
COEFFICIENT OF VARIATION [%]	21.778	104.707	250.376	
AVERAGE (all)	3.704	4.164E-05	5.190E-12	
AVERAGE (interpolated)	4.026	5.024E-05	1.187E-12	

C = tensile core failure; PO = adhesive pullout failure

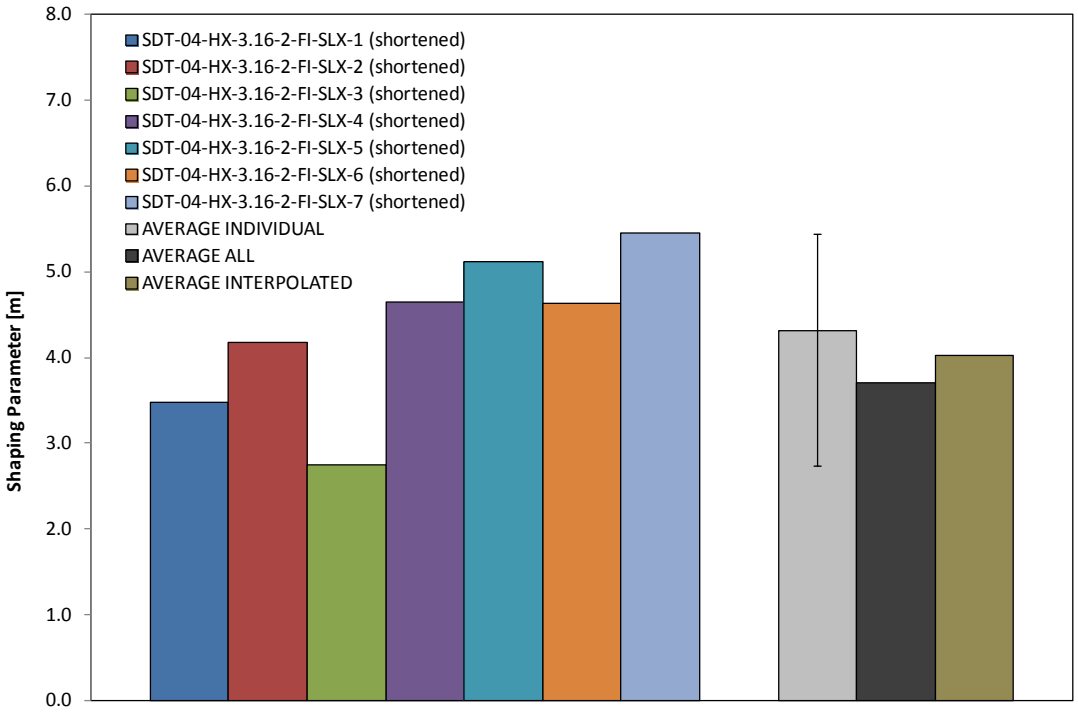

Figure B-15. Shaping parameter (*m*) for HRH-10–3/16–2.0 fluid ingressed (1″ prescribed crack—shortened)

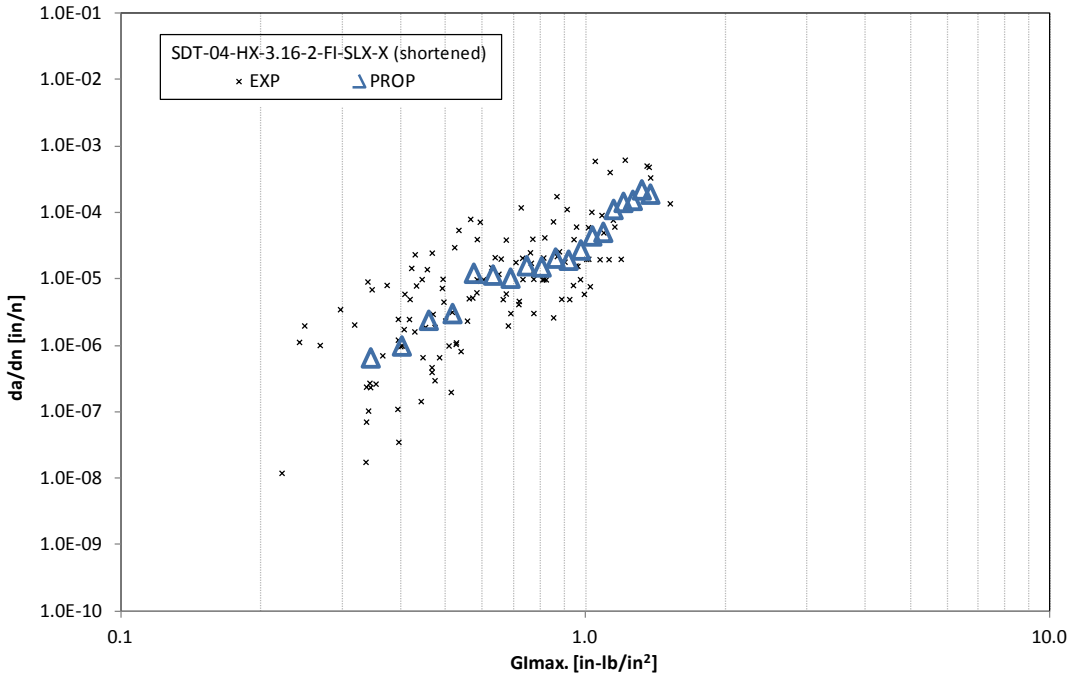

Figure B-16. Fatigue growth da/dn curve for HRH-10–3/16–2.0 fluid ingressed (1″ prescribed crack—shortened)

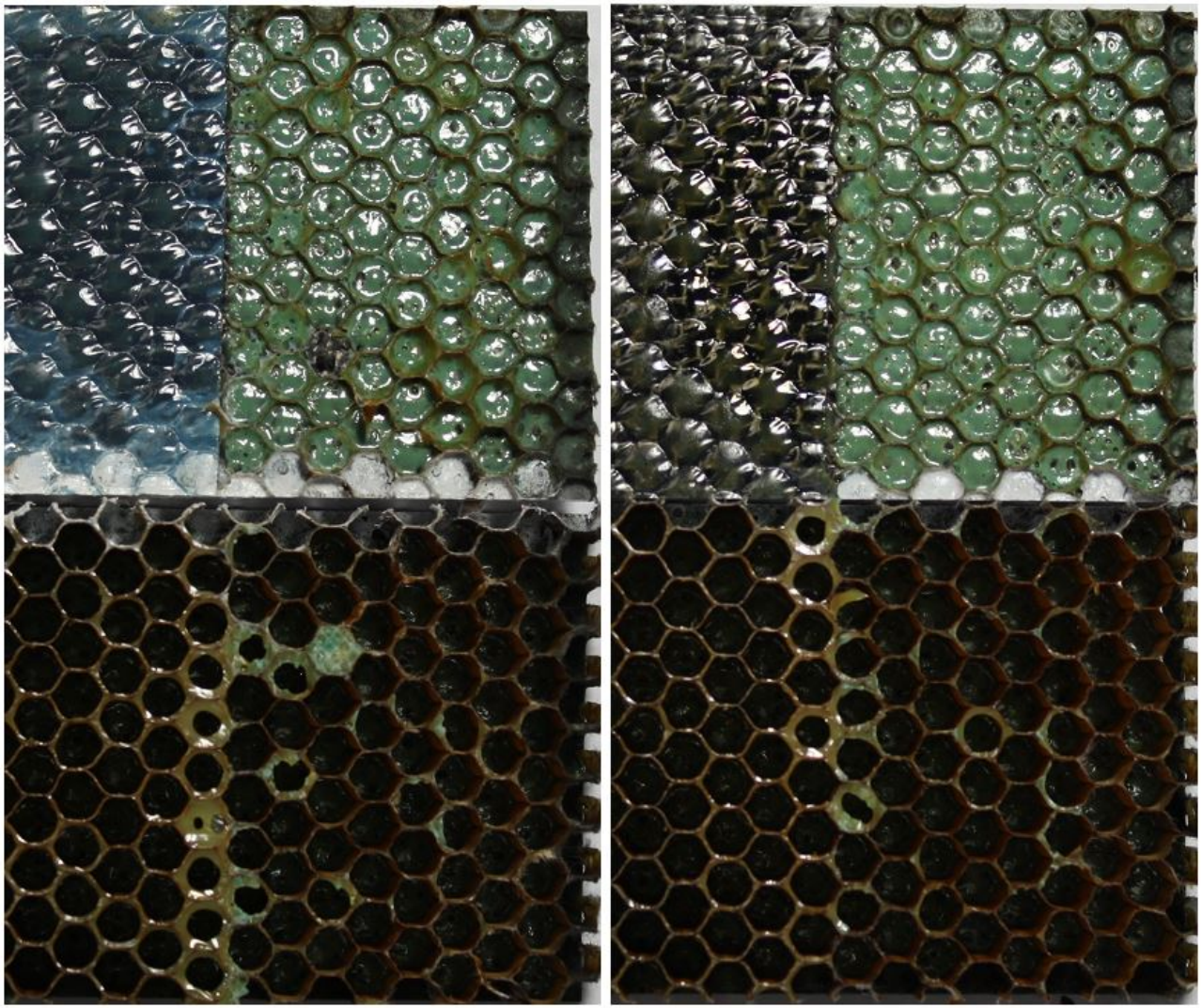

Figure B-17. Failure mode for SDT-04-HX-3.16-2-FI-SLX-X (shortened) #1 and #2

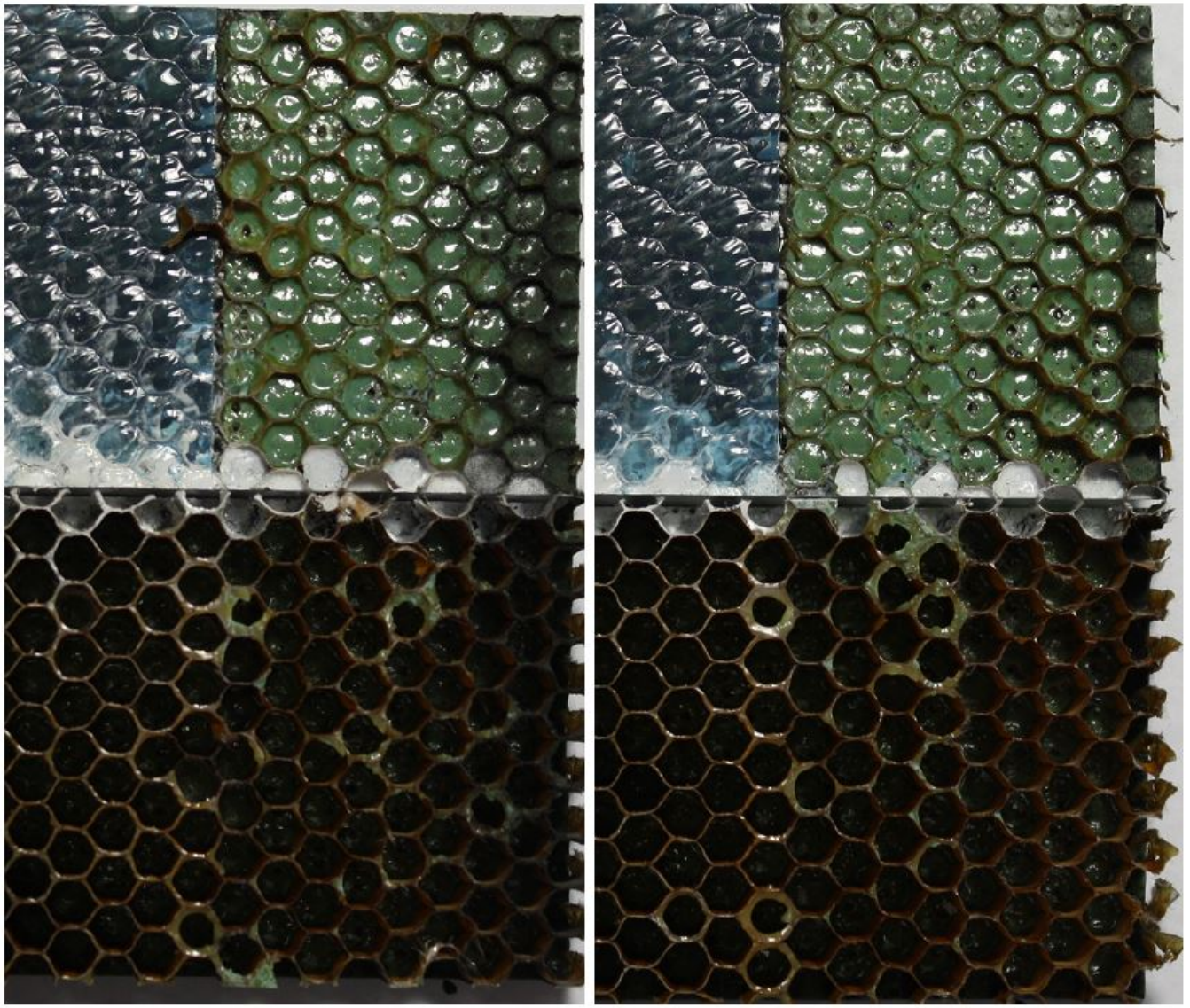

Figure B-18. Failure mode for SDT-04-HX-3.16-2-FI-SLX-X (shortened) #3 and #4

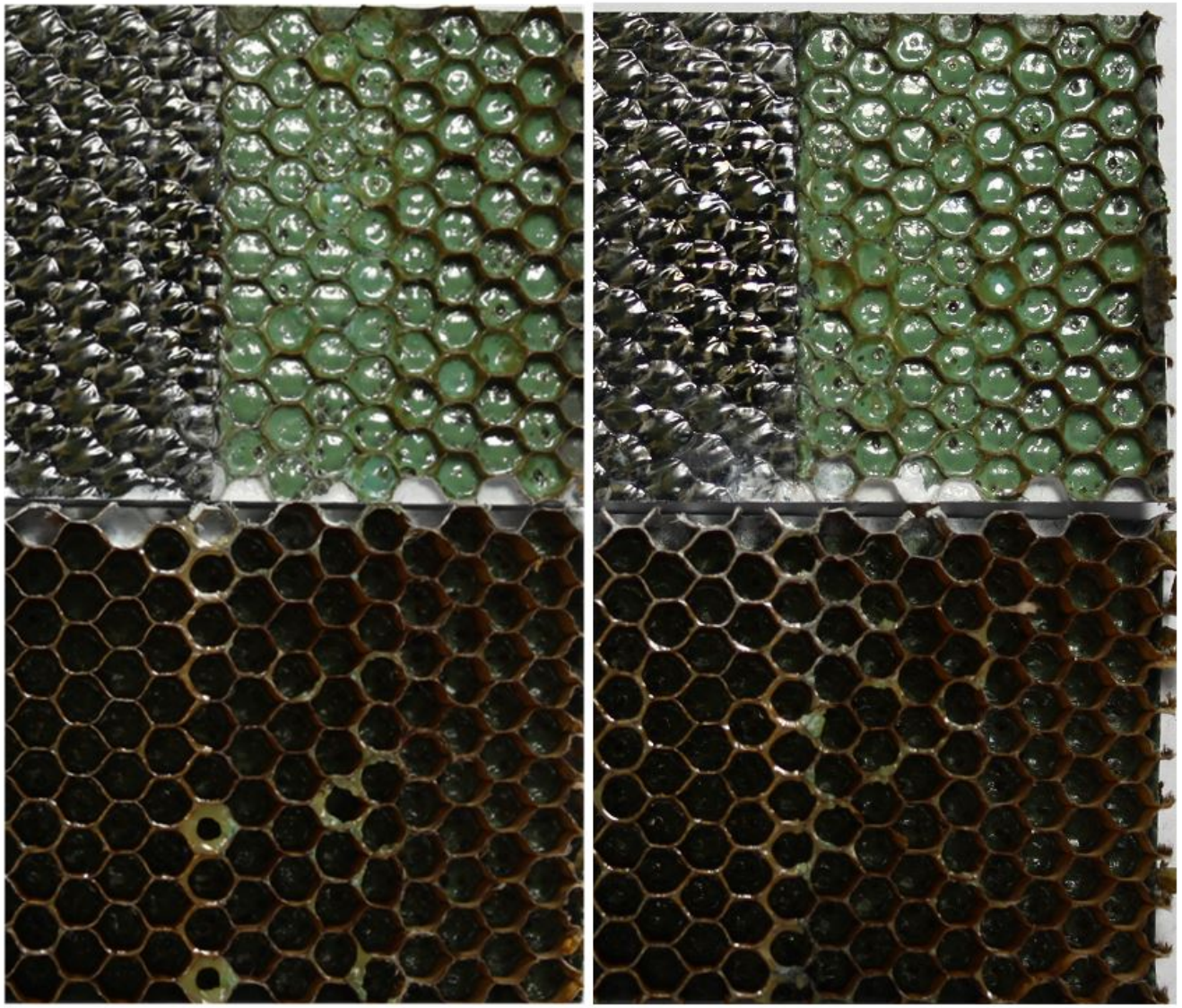

Figure B-19. Failure mode for SDT-04-HX-3.16-2-FI-SLX-X (shortened) #5 and #6

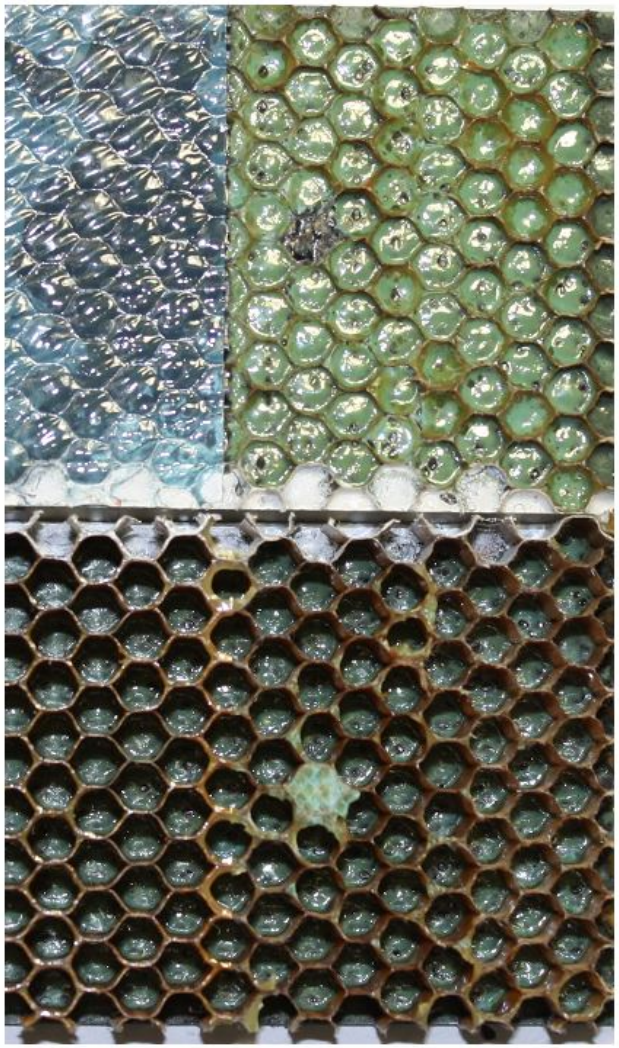

Figure B-20. Failure mode for SDT-04-HX-3.16-2-FI-SLX-X (shortened) #7

B.3 HRH-10–3/16–3.0 DATA

B.3.1 HRH-10–3/16–3.0 BASELINE DATA (1″PRESCRIBED CRACK—SHORTENED)

Table B-5. Test Summary for HRH-10–3/16–3.0 Baseline (1″ Prescribed Crack—Shortened)

Specimen	Shaping Parameter [m] English or SI	Shaping Parameter [B] English	Shaping Parameter [B] SI	Failure Mode
SDT-04-HX-3.16-3-BL-SLX-1 (shortened)	4.401	4.507E-06	1.537E-14	First three rows primarily in PO with a couple of cells in A, then C
SDT-04-HX-3.16-3-BL-SLX-2 (shortened)	8.530	2.884E-05	5.353E-23	First two rows primarily PO with a couple of cells in A, then C, with a few cells in PO
SDT-04-HX-3.16-3-BL-SLX-3 (shortened)	9.483	5.436E-05	7.367E-25	First two rows primarily PO with a couple cells in A, then C
SDT-04-HX-3.16-3-BL-SLX-5 (shortened)	6.346	1.856E-05	2.742E-18	First two rows in PO with a couple cells in A and C, then C
SDT-04-HX-3.16-3-BL-SLX-6 (shortened)	5.788	1.912E-05	5.006E-17	First two rows in PO with a cell in A and a couple of cells in C, then C with a few cells in PO and a small pocket of A
SDT-04-HX-3.16-3-BL-SLX-8 (shortened)	6.074	8.080E-06	4.847E-18	First two rows in PO with a couple cells in A, then C
AVERAGE (individual)	6.770	2.225E-05	2.572E-15	
STANDARD DEVIATION	1.881	1.796E-05	6.271E-15	
COEFFICIENT OF VARIATION [%]	27.791	80.755	243.852	
AVERAGE (all)	5.767	1.088E-05	3.187E-17	
AVERAGE (interpolated)	6.833	1.681E-05	2.006E-19	

PO = adhesive pullout failure; A = adhesive interface disbond failure; C = tensile core failure

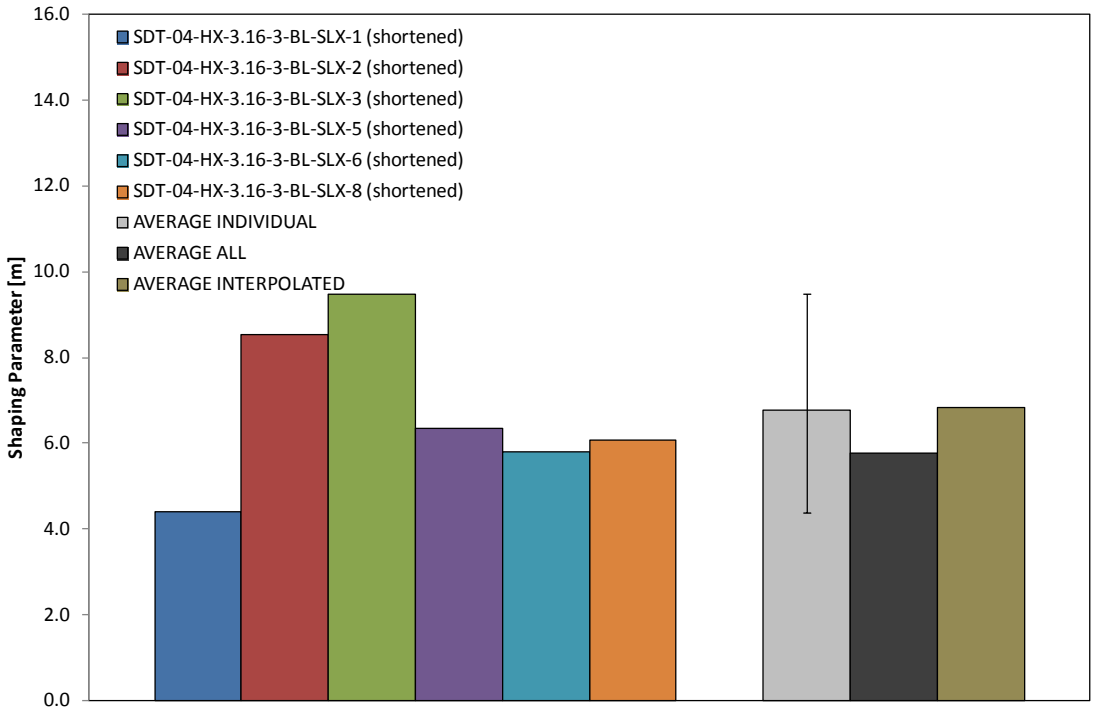

Figure B-21. Shaping parameter (*m*) for HRH-10–3/16–3.0 baseline (1″ prescribed crack—shortened)

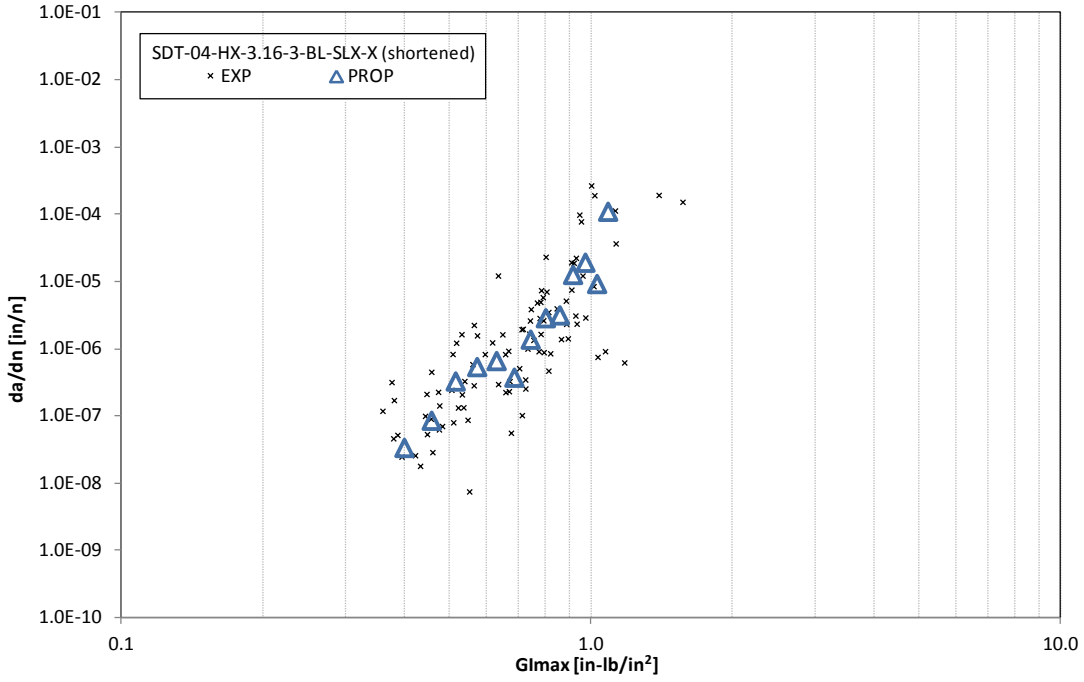

Figure B-22. Fatigue growth da/dn curve for HRH-10–3/16–3.0 baseline (1″ prescribed crack—shortened)

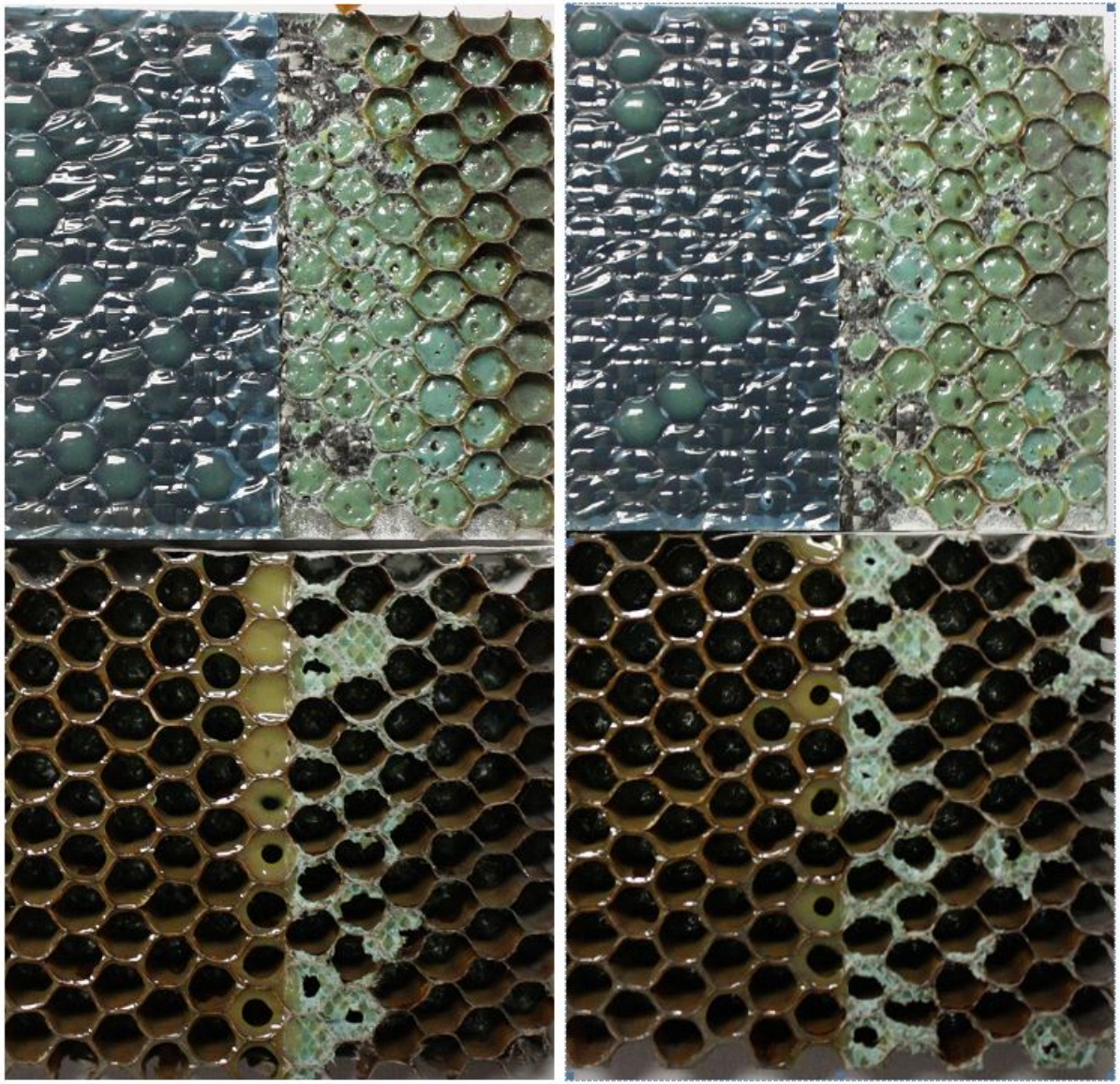

Figure B-23. Failure mode for SDT-04-HX-3.16-3-BL-SLX-X (shortened) #1 and #2

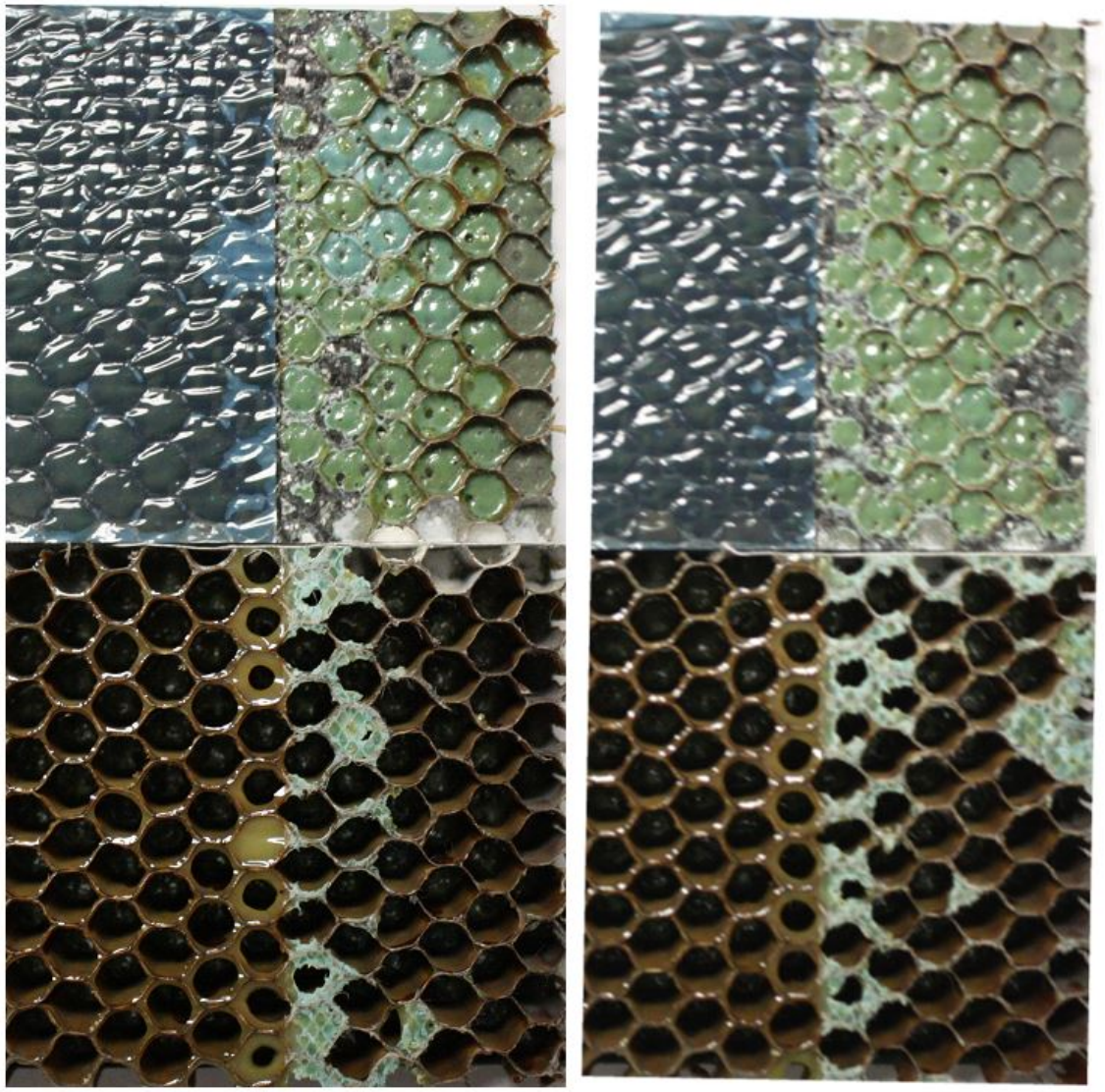

Figure B-24. Failure mode for SDT-04-HX-3.16-3-BL-SLX-X (shortened) #3 and #4

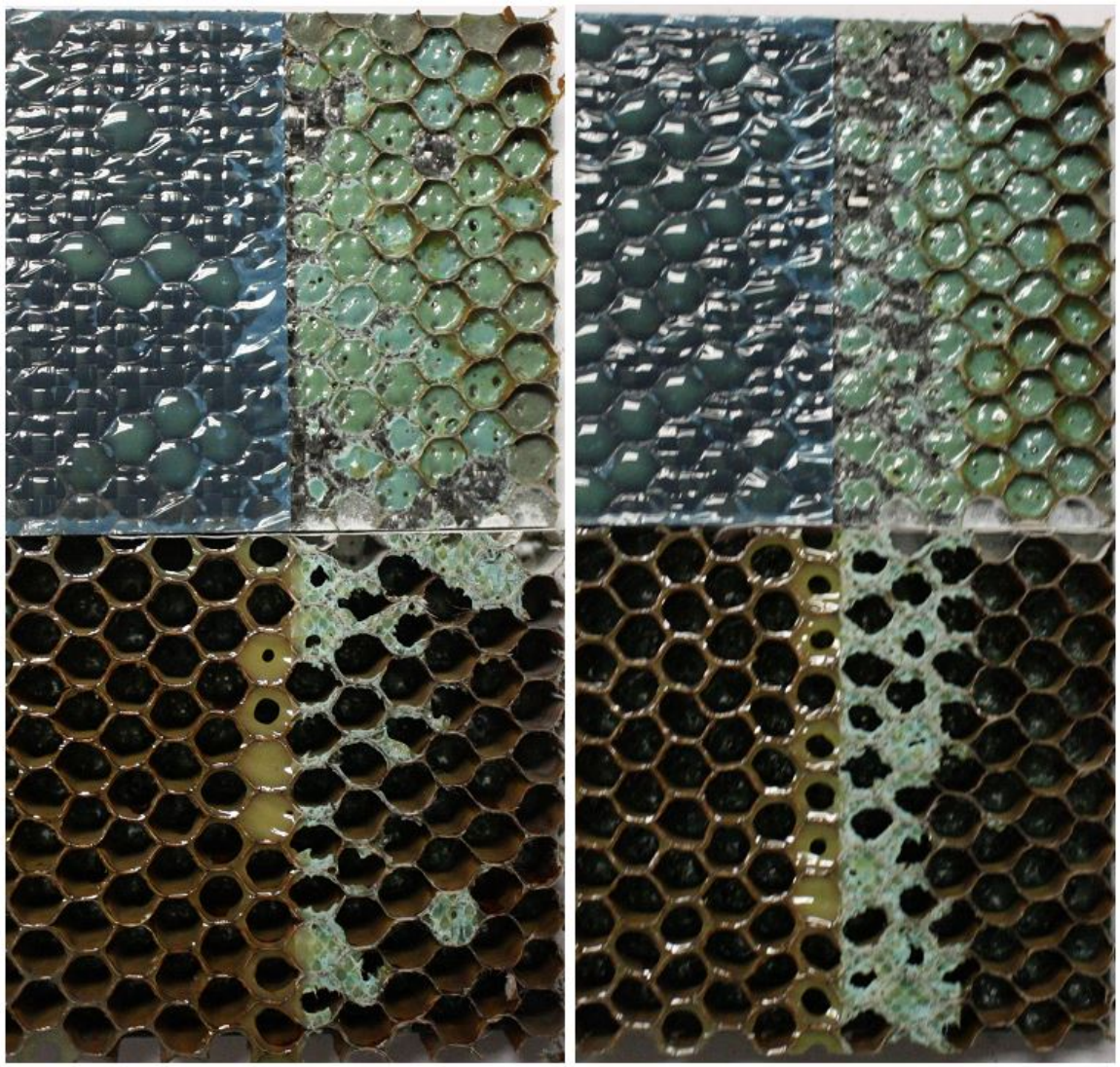

Figure B-25. Failure mode for SDT-04-HX-3.16-3-BL-SLX-X (shortened) #5 and #8

B.3.2 HRH-10–3/16–3.0 FLUID-INGRESSED DATA (1.0″ PRESCRIBED CRACK—SHORTENED)

Table B-6. Test summary for HRH-10–3/16–3.0 fluid ingressed (1″ prescribed crack—shortened)

Specimen	Shaping Parameter [m] English or SI	Shaping Parameter [B] English	Shaping Parameter [B] SI	Failure Mode
SDT-04-HX-3.16-3-FI-SLX-1 (shortened)	3.392	5.844E-06	3.657E-12	Primarily C with occasional cells in PO
SDT-04-HX-3.16-3-FI-SLX-2 (shortened)	5.414	2.057E-05	3.734E-16	Primarily C with occasional cells in PO
SDT-04-HX-3.16-3-FI-SLX-4 (shortened)	6.825	6.260E-05	7.778E-19	Primarily C with occasional cells in PO
SDT-04-HX-3.16-3-FI-SLX-5 (shortened)	2.165	2.518E-05	8.880E-09	Primarily C with occasional cells in PO
SDT-04-HX-3.16-3-FI-SLX-6 (shortened)	6.047	3.118E-05	2.149E-17	Primarily C with occasional cells in PO
SDT-04-HX-3.16-3-FI-SLX-7 (shortened)	5.093	3.566E-05	3.399E-15	Primarily C with occasional cells in PO
AVERAGE (individual)	4.823	3.017E-05	1.481E-09	
STANDARD DEVIATION	1.734	1.893E-05	3.625E-09	
COEFFICIENT OF VARIATION [%]	35.964	62.741	244.828	
AVERAGE (all)	4.447	1.831E-05	4.915E-14	
AVERAGE (interpolated)	5.000	2.363E-05	3.653E-15	

C = tensile core failure; PO = adhesive pullout failure

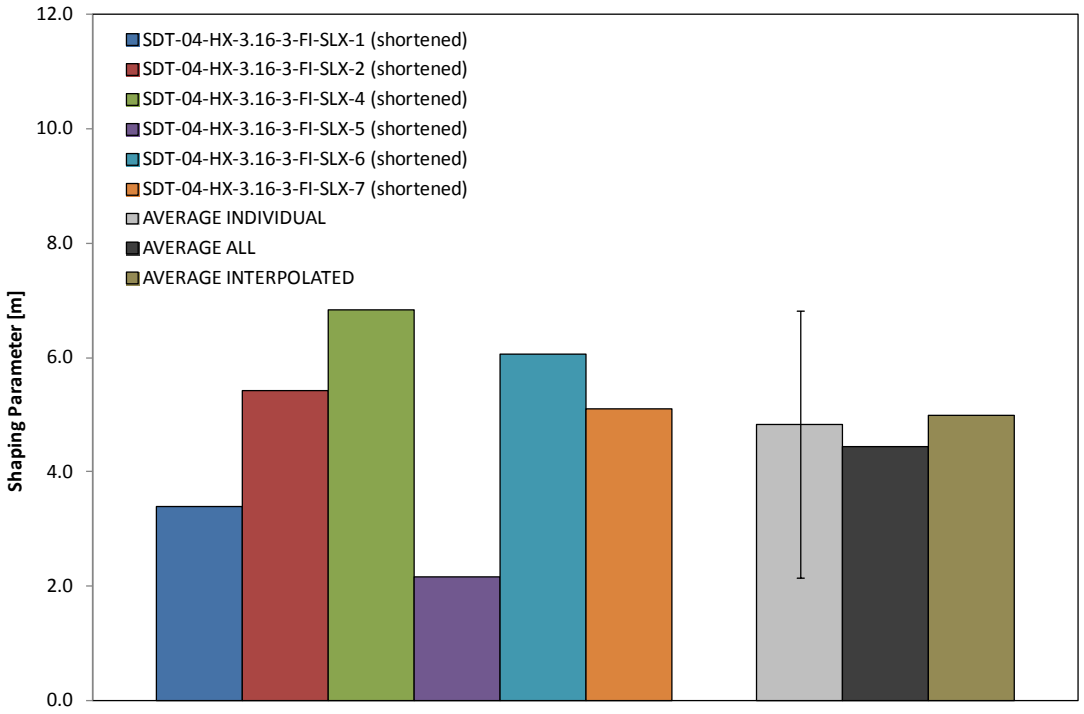

Figure B-26. Shaping parameter (*m*) for HRH-10–3/16–3.0 fluid ingressed (1″ prescribed crack—shortened)

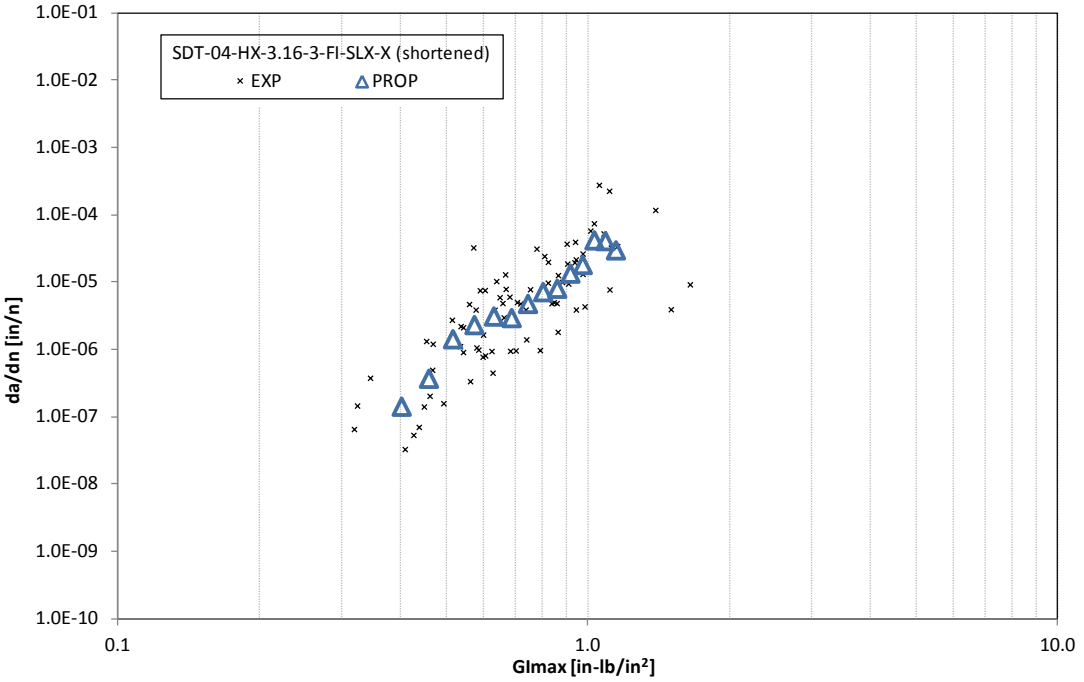

Figure B-27. Fatigue growth da/dn curve for HRH-10–3/16–3.0 fluid ingressed (1″ prescribed crack—shortened)

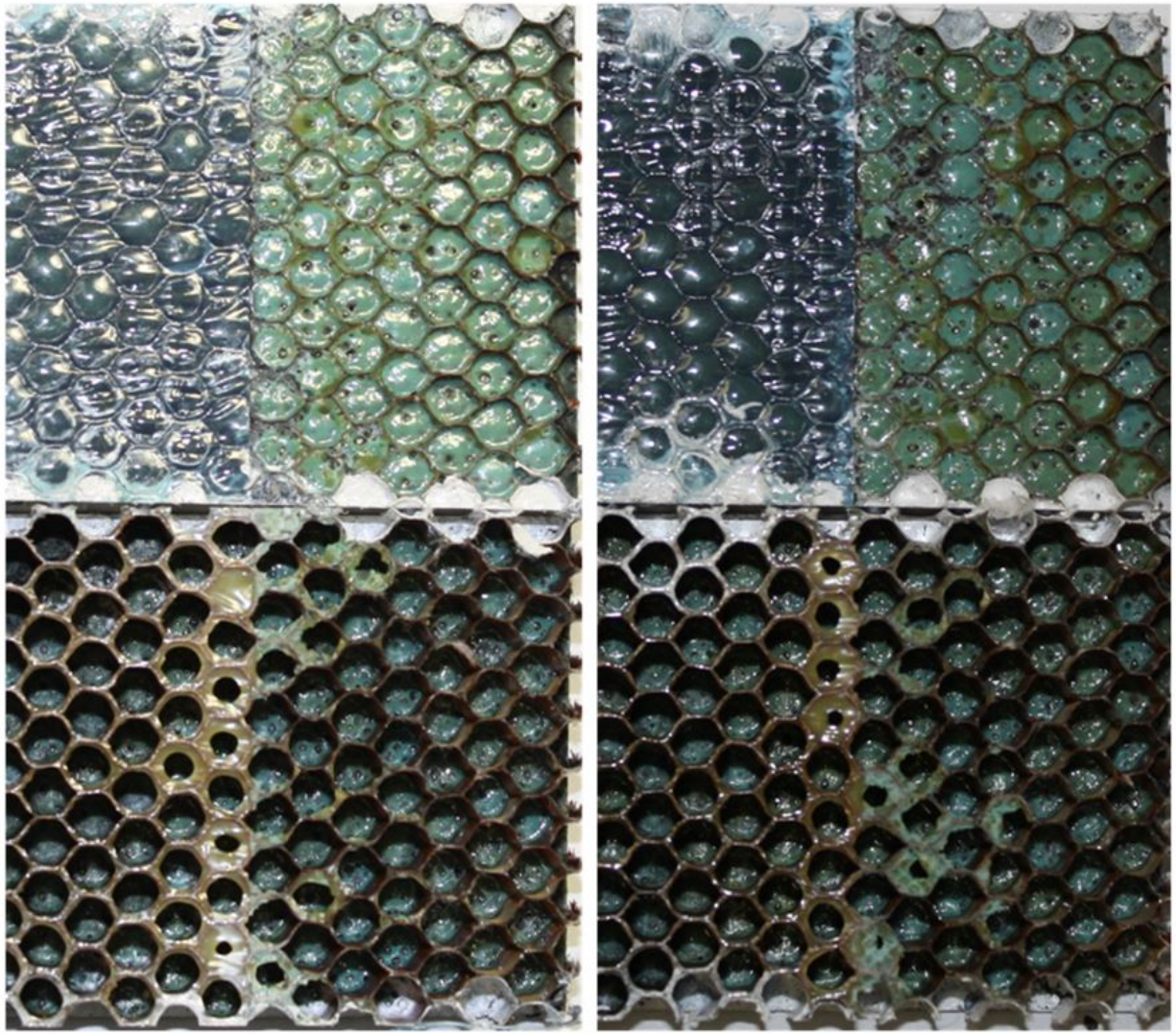

Figure B-28. Failure mode for SDT-04-HX-3.16-3-FI-SLX-X (shortened) #1 and #2

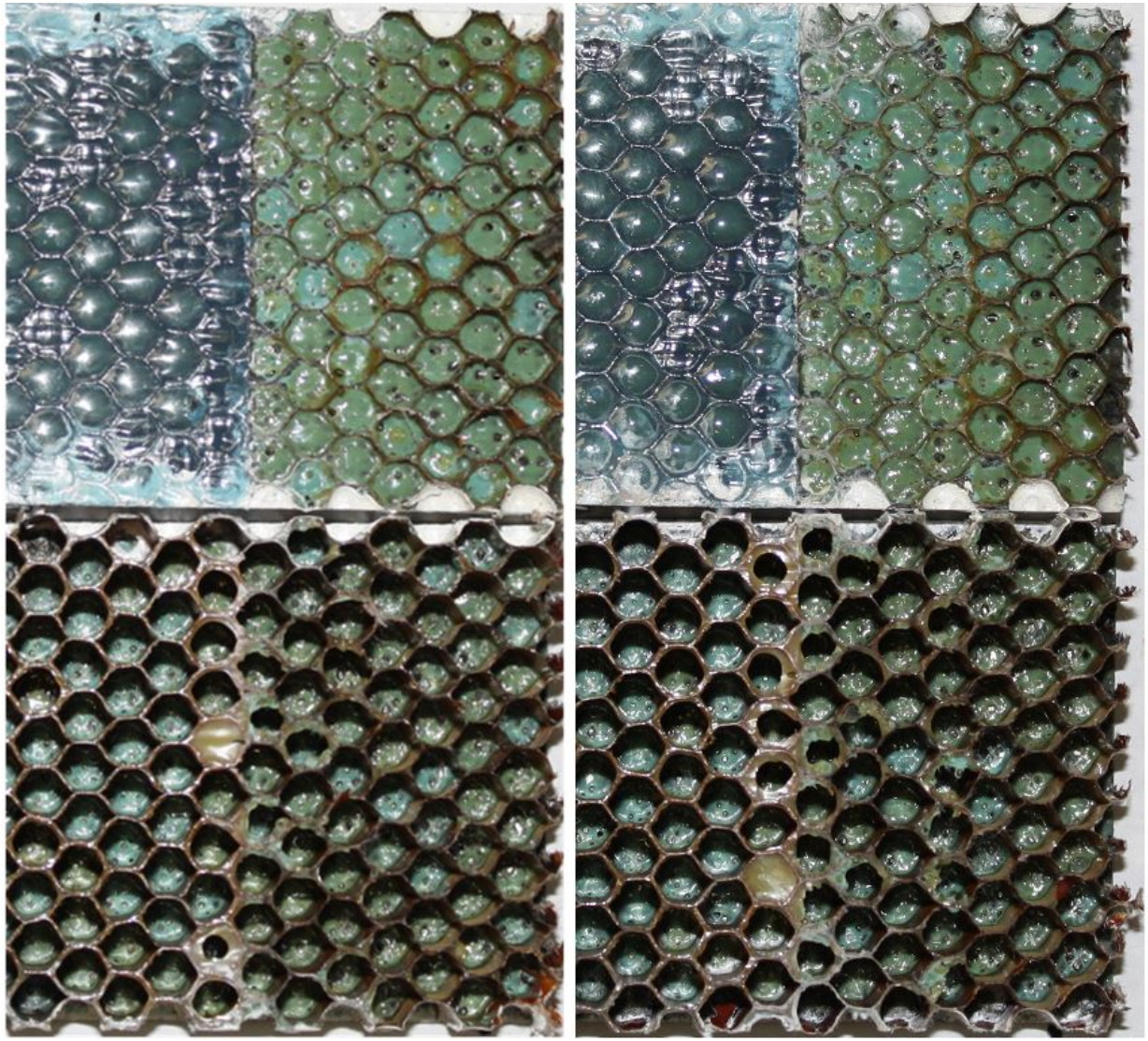

Figure B-29. Failure mode for SDT-04-HX-3.16-3-FI-SLX-X (shortened) #4 and #5

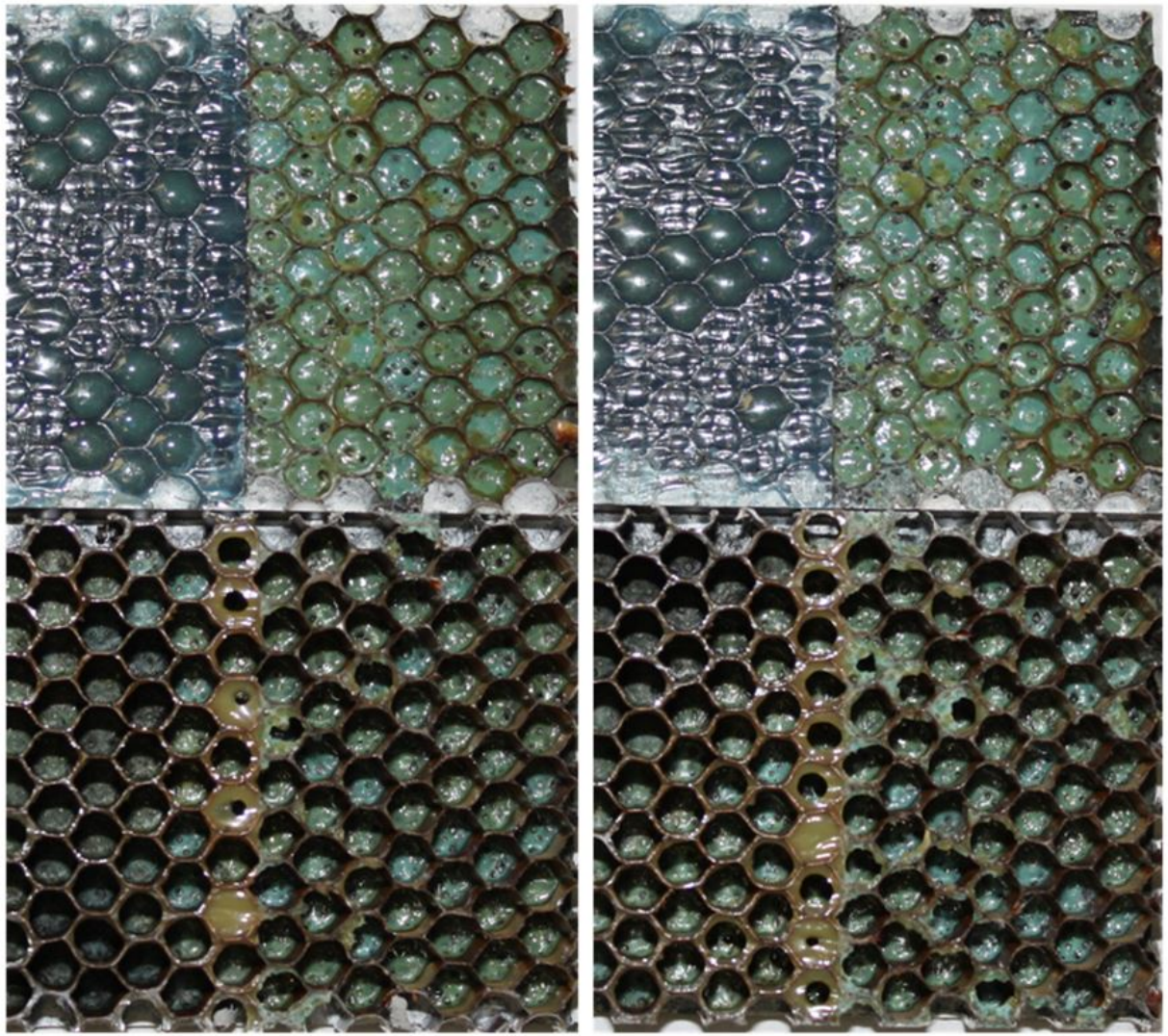

Figure B-30. Failure mode for SDT-04-HX-3.16-3-FI-SLX-X (shortened) #6 and #7

B.4 HRH-10–3/16–6.0 DATA

B.4.1 HRH-10–3/16–6.0 BASELINE DATA (1″ PRESCRIBED CRACK—SHORTENED)

Table B-7. Test summary for HRH-10–3/16–6.0 baseline (1″ prescribed crack—shortened)

Specimen	Shaping Parameter [m] English or SI	Shaping Parameter [B] English	Shaping Parameter [B] SI	Failure Mode
SDT-04-HX-3.16-6-BL-SLX-1 (shortened)	11.220	5.810E-05	9.970E-29	First row a mix of A and PO, then PO with a couple of cells in A
SDT-04-HX-3.16-6-BL-SLX-2 (shortened)	12.109	2.600E-05	4.523E-31	Primarily PO with a few cells in A
SDT-04-HX-3.16-6-BL-SLX-3 (shortened)	7.936	2.614E-06	1.044E-22	Primarily PO with a few cells in A
SDT-04-HX-3.16-6-BL-SLX-4 (shortened)	10.071	2.009E-05	1.303E-26	Primarily PO with a few cells in A
SDT-04-HX-3.16-6-BL-SLX-5 (shortened)	10.524	2.253E-05	1.407E-27	First row a mix of A and PO, then PO with a couple of cells in A
SDT-04-HX-3.16-6-BL-SLX-8 (shortened)	7.488	2.814E-06	1.140E-21	First row A with a couple of cells in PO, then a mix of A and PO
AVERAGE (individual)	9.891	2.203E-05	2.073E-22	
STANDARD DEVIATION	1.828	2.033E-05	4.586E-22	
COEFFICIENT OF VARIATION [%]	18.486	92.317	221.195	
AVERAGE (all)	7.934	7.140E-06	2.882E-22	
AVERAGE (interpolated)	8.528	8.227E-06	1.544E-23	

A = adhesive interface disbond failure; PO = adhesive pullout failure

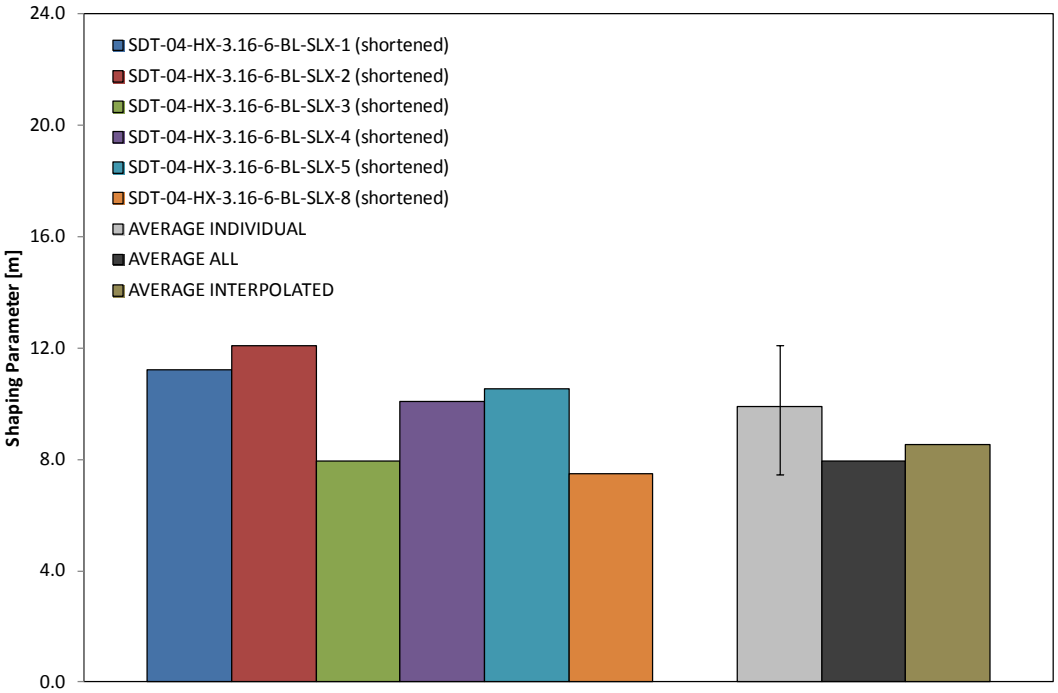

Figure B-31. Shaping parameter (*m*) for HRH-10–3/16–6.0 baseline (1″ prescribed crack—shortened)

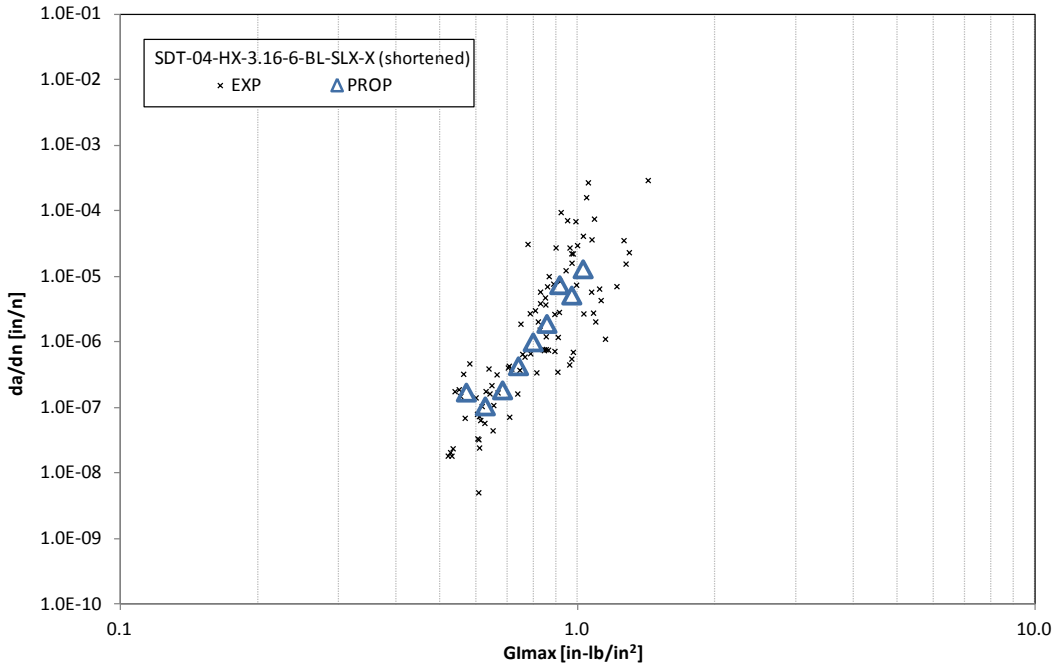

Figure B-32. Fatigue growth da/dn curve for HRH-10–3/16–6.0 baseline (1″ prescribed crack—shortened)

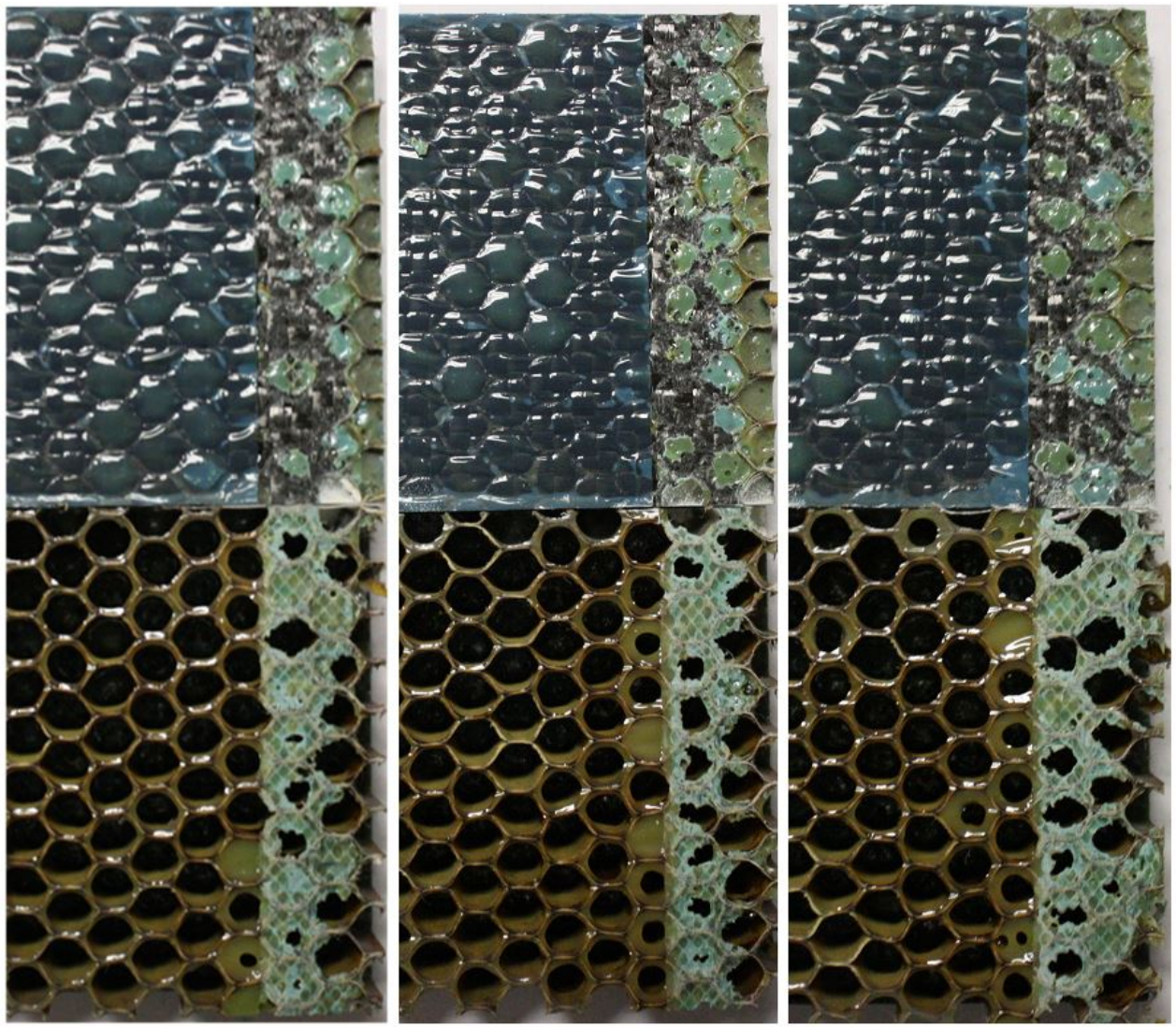

Figure B-33. Failure mode for SDT-04-HX-3.16-6-BL-SLX-X (shortened) #1, #2, and #3

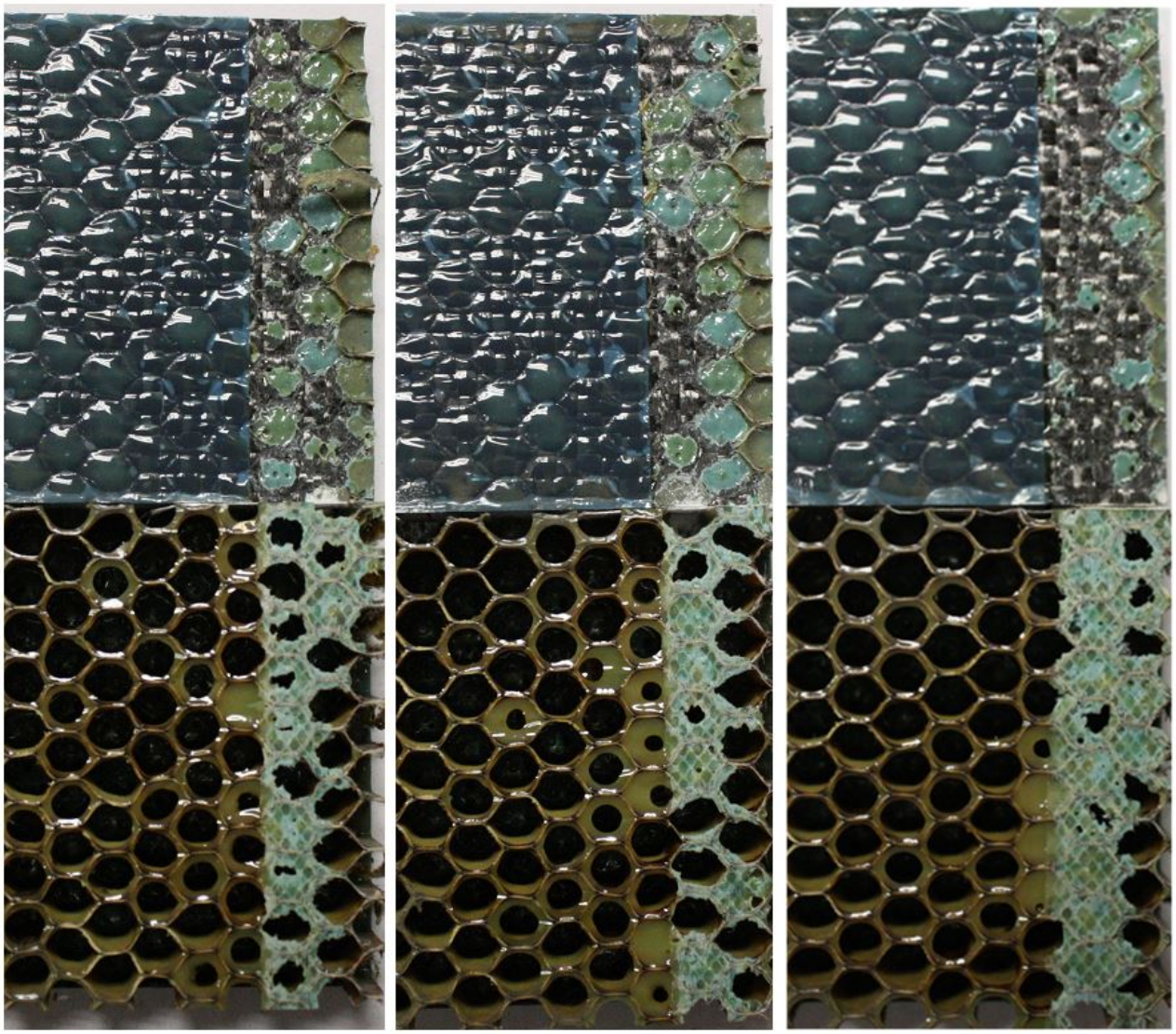

Figure B-34. Failure mode for SDT-04-HX-3.16-6-BL-SLX-X (shortened) #4, #5, and #8

B.4.2 HRH-10–3/16–6.0 FLUID-INGRESSED DATA (1″ PRESCRIBED CRACK—SHORTENED)

Table B-8. Test summary for HRH-10–3/16–6.0 fluid ingressed (1.0″ prescribed crack—shortened)

Specimen	Shaping Parameter [m] English or SI	Shaping Parameter [B] English	Shaping Parameter [B] SI	Failure Mode
SDT-04-HX-3.16-6-FI-SLX-1 (shortened)	9.080	3.399E-06	3.678E-25	Primarily PO with several cells in A
SDT-04-HX-3.16-6-FI-SLX-2 (shortened)	9.550	1.865E-06	1.788E-26	First two rows a mix of A and PO, then PO with a couple of cells in A
SDT-04-HX-3.16-6-FI-SLX-3 (shortened)	8.298	2.954E-05	1.817E-22	Primarily PO with several cells in A
SDT-04-HX-3.16-6-FI-SLX-4 (shortened)	14.855	2.446E-07	2.941E-39	Primarily PO with a few cells in A
SDT-04-HX-3.16-6-FI-SLX-5 (shortened)	13.309	1.258E-03	4.434E-32	Primarily PO with several cells in A
SDT-04-HX-3.16-6-FI-SLX-6 (shortened)	8.522	6.090E-07	1.179E-24	Primarily PO with a few cells in A
SDT-04-HX-3.16-6-FI-SLX-7 (shortened)	23.000	2.770E-09	1.766E-59	First row a mix of A and PO, then PO with a couple of cells in A
SDT-04-HX-3.16-6-FI-SLX-8 (shortened)	22.620	2.510E-08	1.163E-57	First row a mix of A and PO, then PO with a few cells in A
AVERAGE (individual)	13.654	1.617E-04	2.291E-23	
STANDARD DEVIATION	6.119	4.432E-04	6.416E-23	
COEFFICIENT OF VARIATION [%]	44.813	273.998	280.088	
AVERAGE (all)	3.733	1.198E-06	1.288E-13	
AVERAGE (interpolated)	4.434	1.612E-06	4.628E-15	

PO = adhesive pullout failure; A = Adhesive interface disbond failure

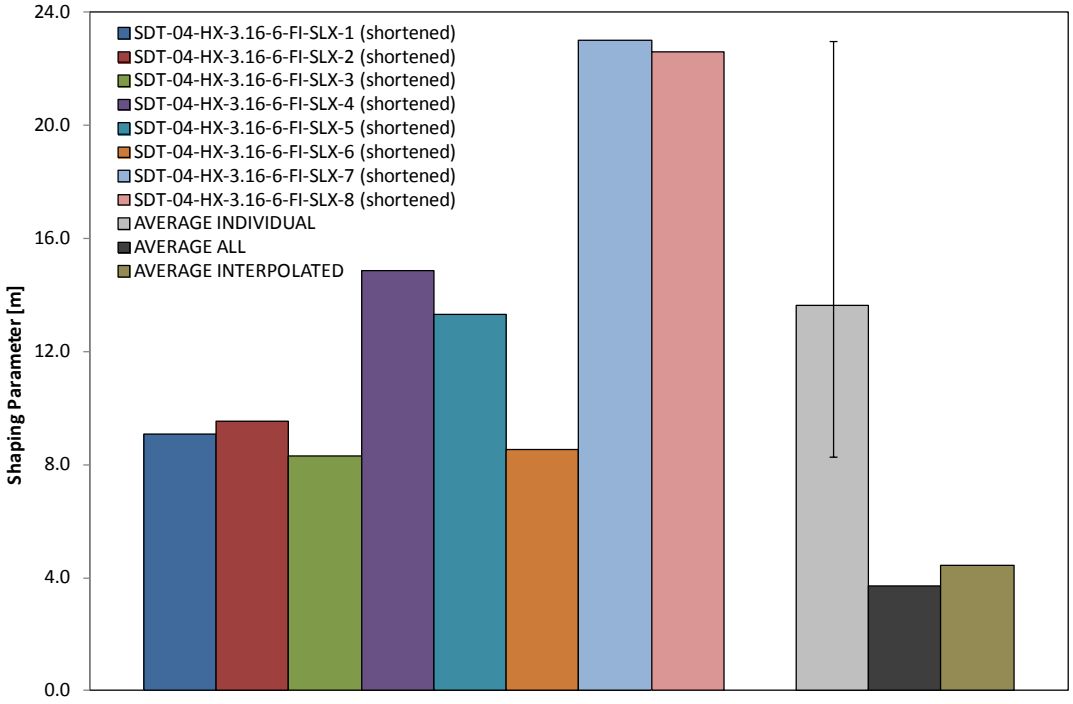

Figure B-35. Shaping parameter (*m*) for HRH-10–3/16–6.0 fluid ingressed (1″ prescribed crack—shortened)

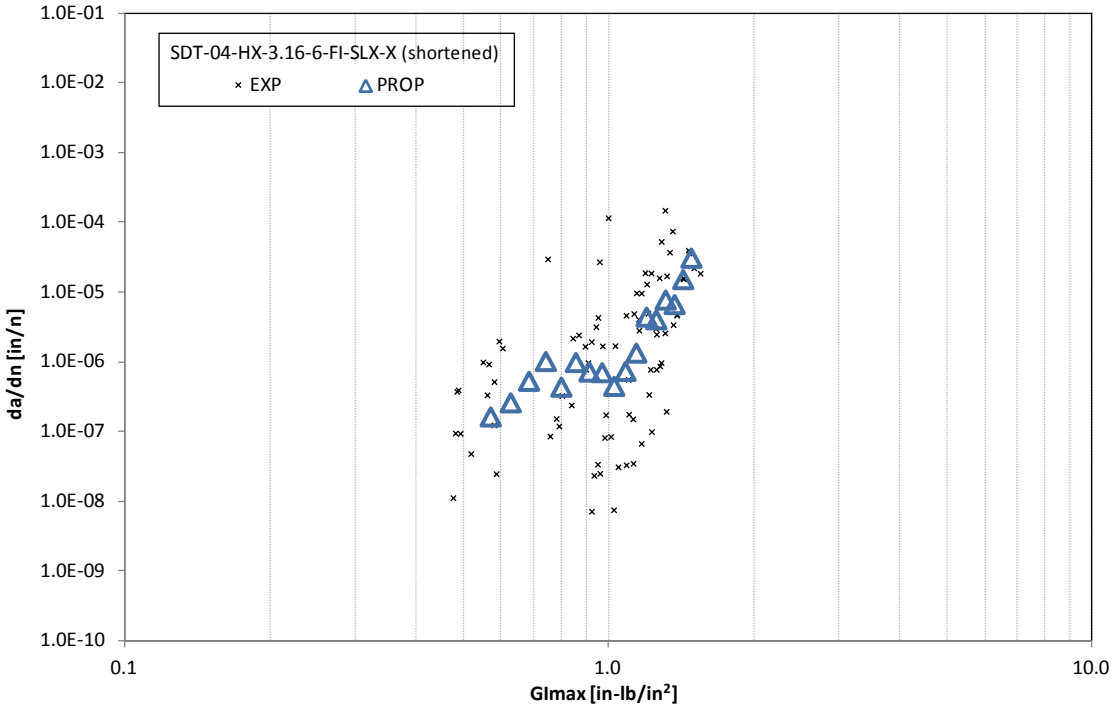

Figure B-36. Fatigue growth da/dn curve for HRH-10–3/16–6.0 fluid ingressed (1″ prescribed crack—shortened)

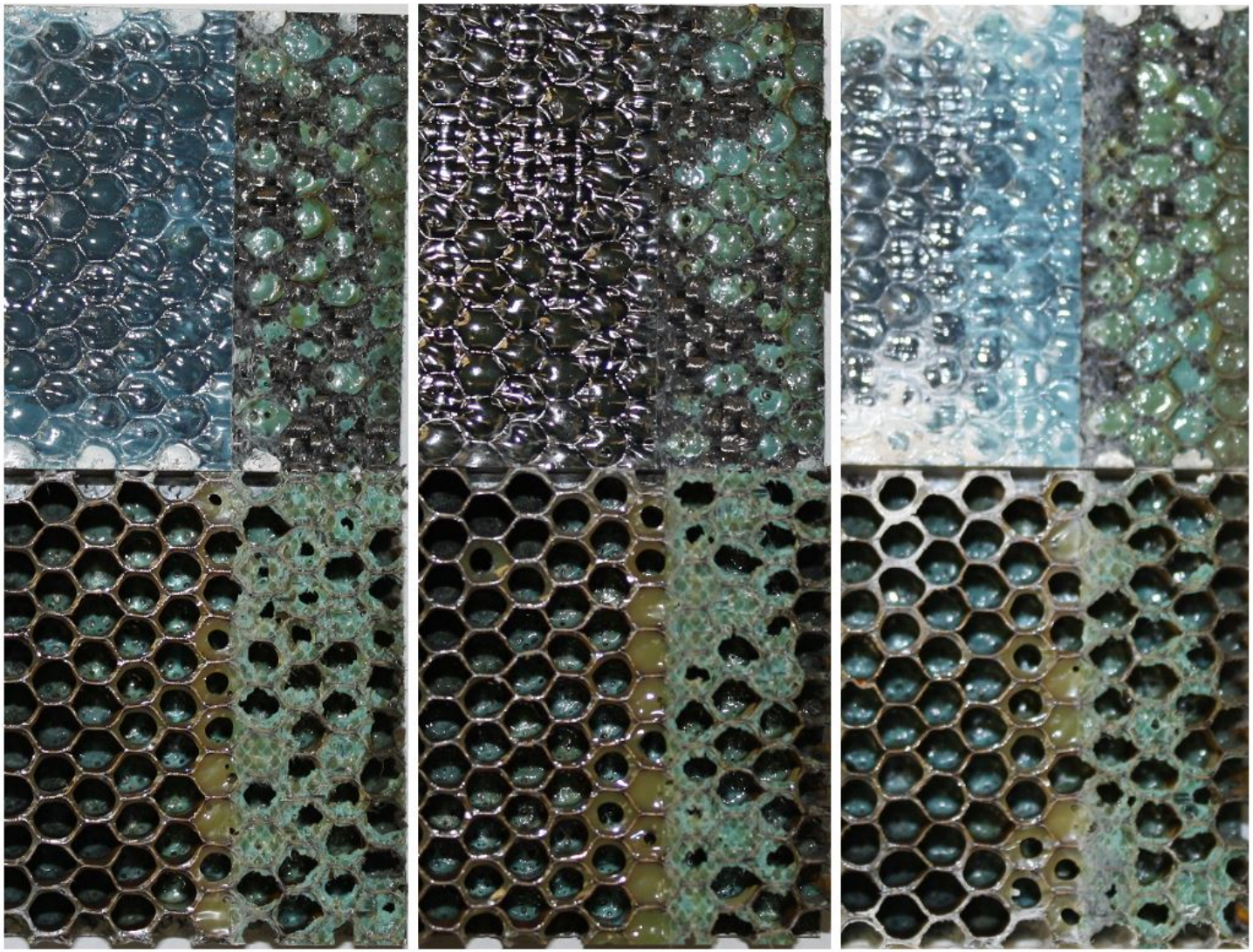

Figure B-37. Failure mode for SDT-04-HX-3.16-6-FI-SLX-X (shortened) #1,#2, and #3

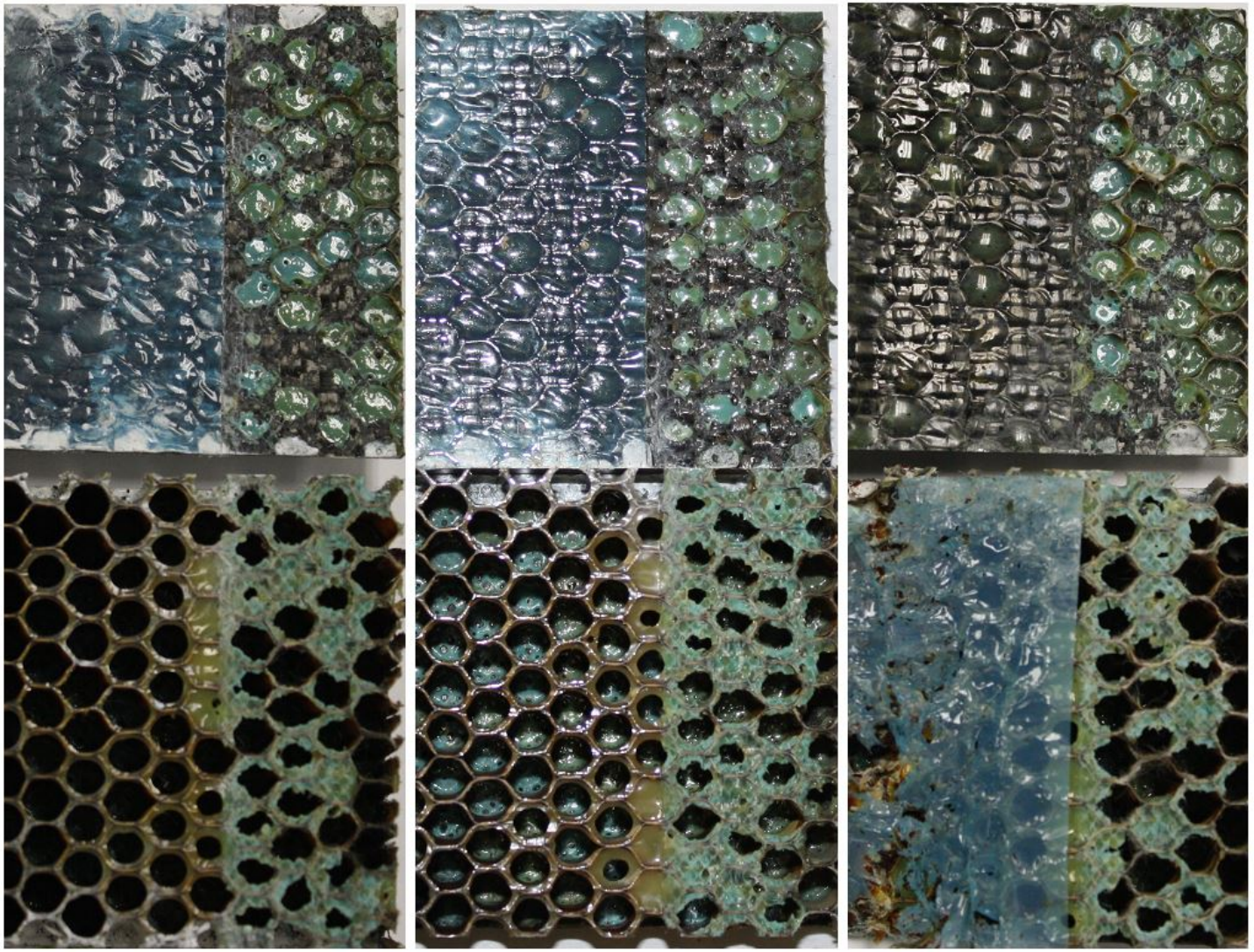

Figure B-38. Failure mode for SDT-04-HX-3.16-6-FI-SLX-X (shortened) #4, #5, and #6

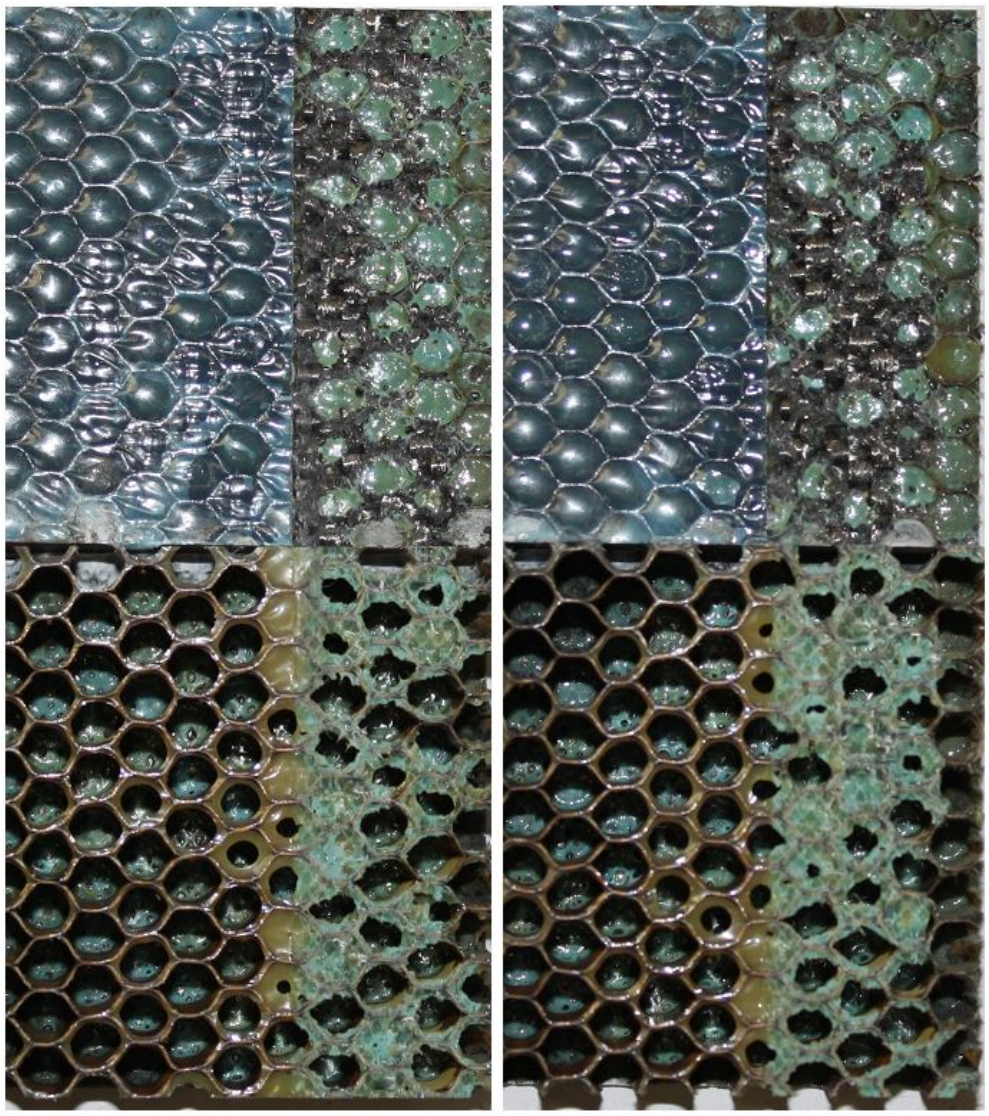

Figure B-39. Failure mode for SDT-04-HX-3.16-6-FI-SLX-X (shortened) #7 and #8

B.5 HRH-10–3/8–3.0 DATA

B.5.1 HRH-10–3/8–3.0 BASELINE DATA (1″ PRESCRIBED CRACK—SHORTENED)

Table B-9. Test summary for HRH-10–3/8–3.0 baseline (1″ prescribed crack—shortened)

Specimen	Shaping Parameter [m] English or SI	Shaping Parameter [B] English	Shaping Parameter [B] SI	Failure Mode
SDT-04-HX-3.8-3-BL-SLX-1 (shortened)	8.926	1.645E-05	3.959E-24	Primarily PO
SDT-04-HX-3.8-3-BL-SLX-2 (shortened)	5.220	5.254E-06	2.603E-16	Primarily PO
SDT-04-HX-3.8-3-BL-SLX-3 (shortened)	7.941	1.793E-06	6.973E-23	Primarily PO
SDT-04-HX-3.8-3-BL-SLX-4 (shortened)	5.889	5.754E-05	8.991E-17	Primarily PO
SDT-04-HX-3.8-3-BL-SLX-6 (shortened)	4.320	5.717E-05	2.955E-13	Primarily PO
SDT-04-HX-3.8-3-BL-SLX-8 (shortened)	8.670	8.439E-05	7.597E-23	Primarily PO
AVERAGE (individual)	6.828	3.710E-05	4.931E-14	
STANDARD DEVIATION	1.939	3.390E-05	1.206E-13	
COEFFICIENT OF VARIATION [%]	28.394	91.361	244.601	
AVERAGE (all)	3.399	4.496E-06	2.704E-12	
AVERAGE (interpolated)	4.419	9.039E-06	2.863E-14	

PO = adhesive pullout failure

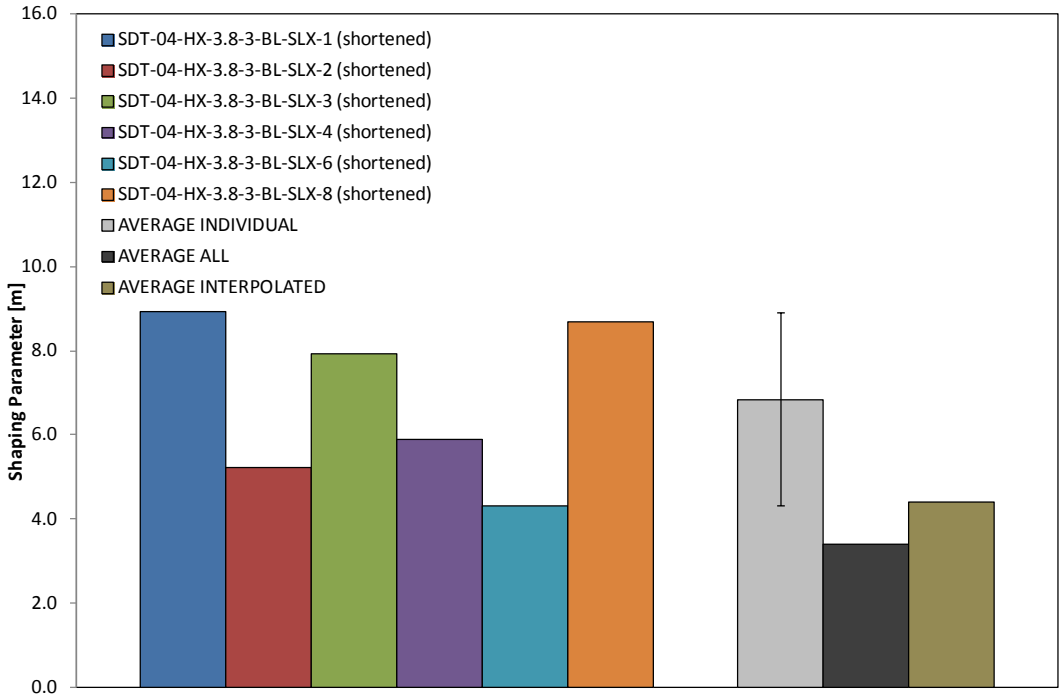

Figure B-40. Shaping parameter (*m*) for HRH-10–3/8–3.0 baseline (1″ prescribed crack—shortened)

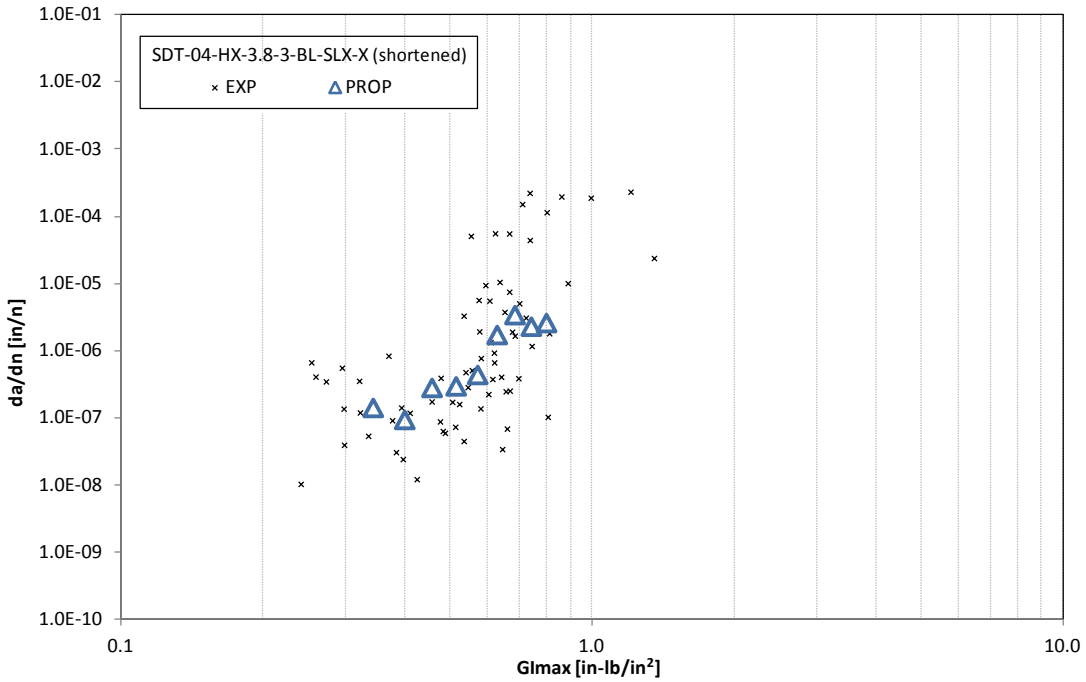

Figure B-41. Fatigue growth da/dn curve for HRH-10–3/8–3.0 baseline (1″ prescribed crack—shortened)

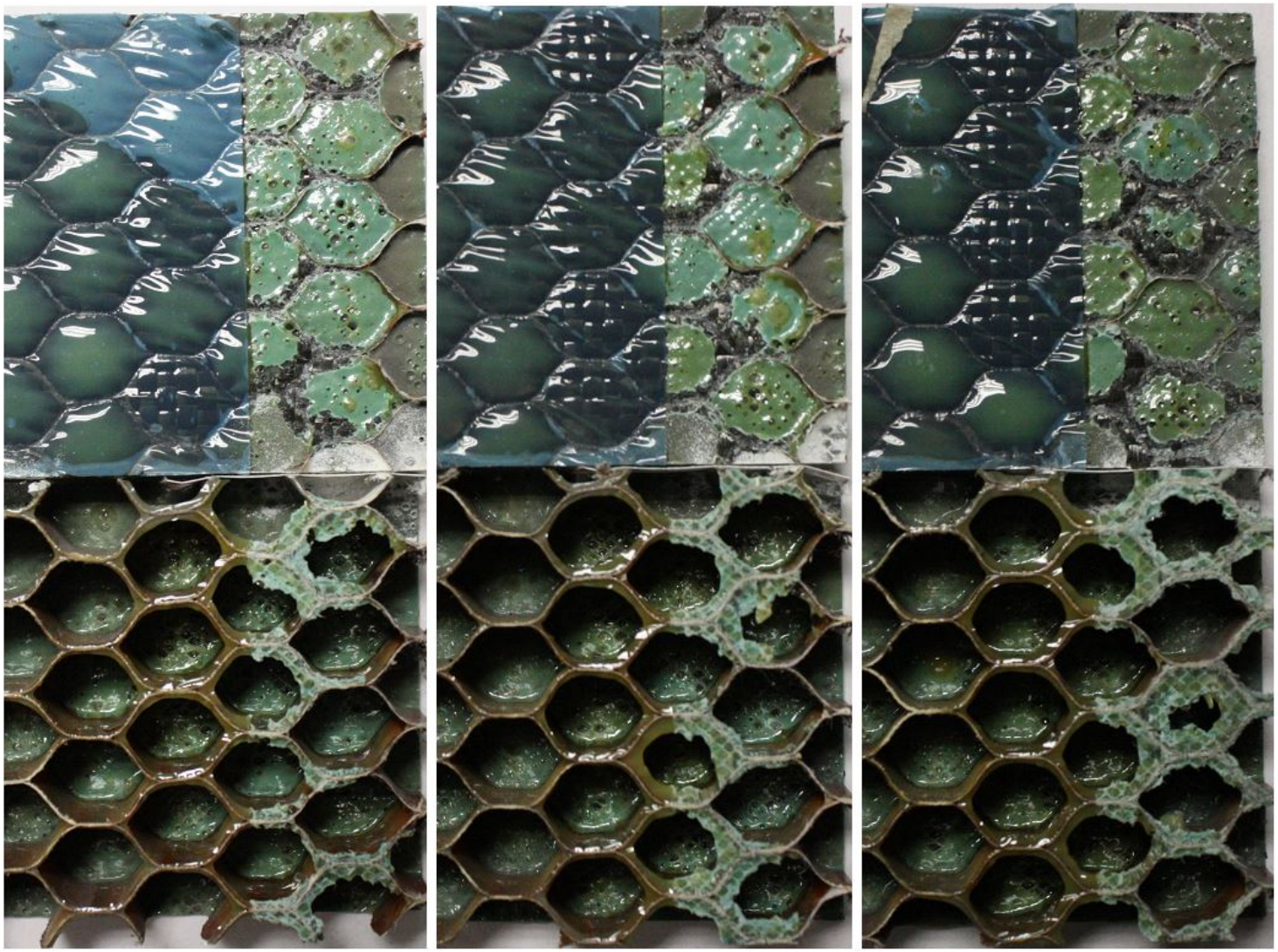

Figure B-42. Failure mode for SDT-04-HX-3.8-3-BL-SLX-X (shortened) #1, #2, and #3

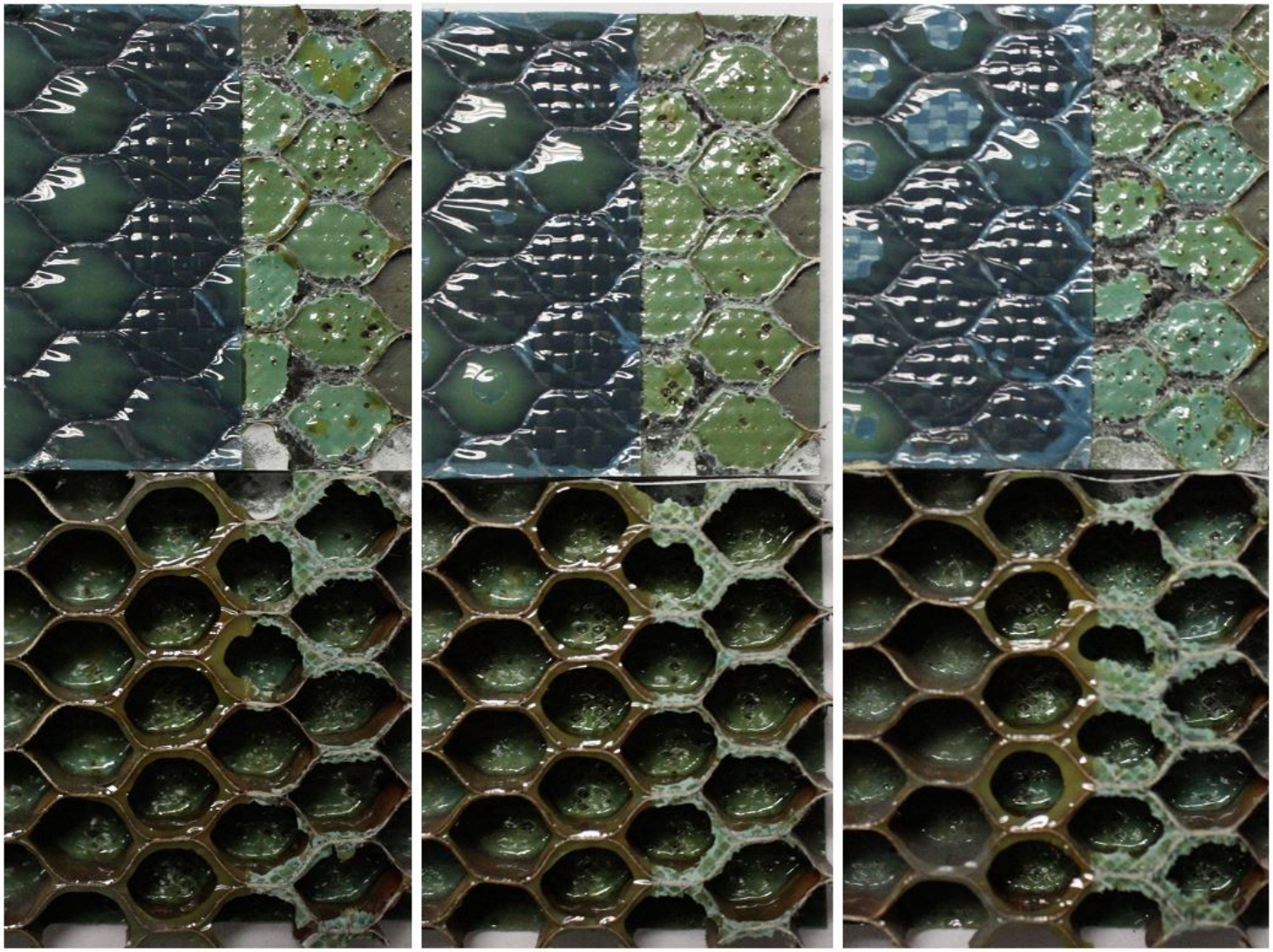

Figure B-43. Failure mode for SDT-04-HX-3.8-3-BL-SLX-X (shortened) #4, #6, and #8

B.5.2 HRH-10–3/8–3.0 FLUID-INGRESSED DATA (1.0″ PRESCRIBED CRACK—SHORTENED)

Table B-10. Test summary for HRH-10–3/8–3.0 fluid ingressed (1″ prescribed crack—shortened)

Specimen	Shaping Parameter [m] English or SI	Shaping Parameter [B] English	Shaping Parameter [B] SI	Failure Mode
SDT-04-HX-3.8-3-FI-SLX-1 (shortened)	12.699	2.238E-05	1.846E-32	Primarily C with a few cells in PO
SDT-04-HX-3.8-3-FI-SLX-2 (shortened)	9.854	1.339E-07	2.673E-28	A mix of PO and C, then C
SDT-04-HX-3.8-3-FI-SLX-3 (shortened)	13.432	4.984E-07	9.313E-36	A mix of PO and C, then C
SDT-04-HX-3.8-3-FI-SLX-4 (shortened)	10.099	6.735E-07	3.788E-28	A mix of PO and C, then C
SDT-04-HX-3.8-3-FI-SLX-5 (shortened)	7.677	3.253E-06	4.950E-22	Primarily PO then C
SDT-04-HX-3.8-3-FI-SLX-6 (shortened)	16.857	2.971E-05	1.150E-41	Primarily PO then C
AVERAGE (individual)	11.770	9.441E-06	8.251E-23	
STANDARD DEVIATION	3.247	1.311E-05	2.021E-22	
COEFFICIENT OF VARIATION [%]	27.589	138.907	244.949	
AVERAGE (all)	6.007	1.990E-06	1.692E-18	
AVERAGE (interpolated)	7.296	1.455E-06	1.588E-21	

C = tensile core failure; PO = adhesive pullout failure

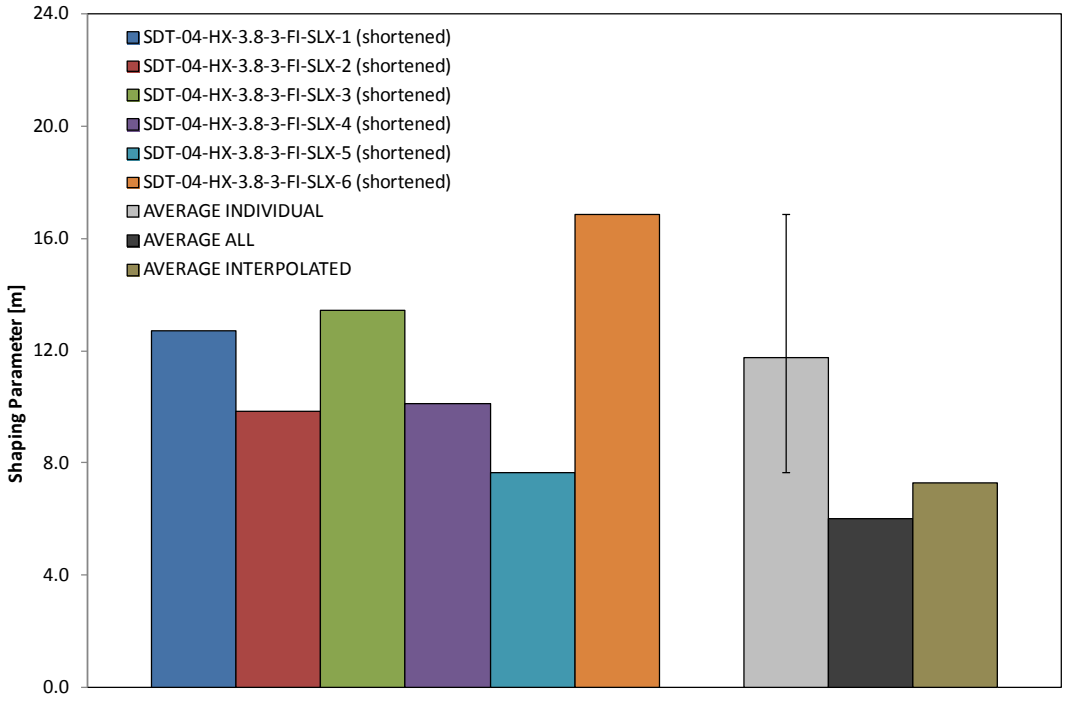

Figure B-44. Shaping parameter (*m*) for HRH-10–3/8–3.0 fluid ingressed (1″ prescribed crack—shortened)

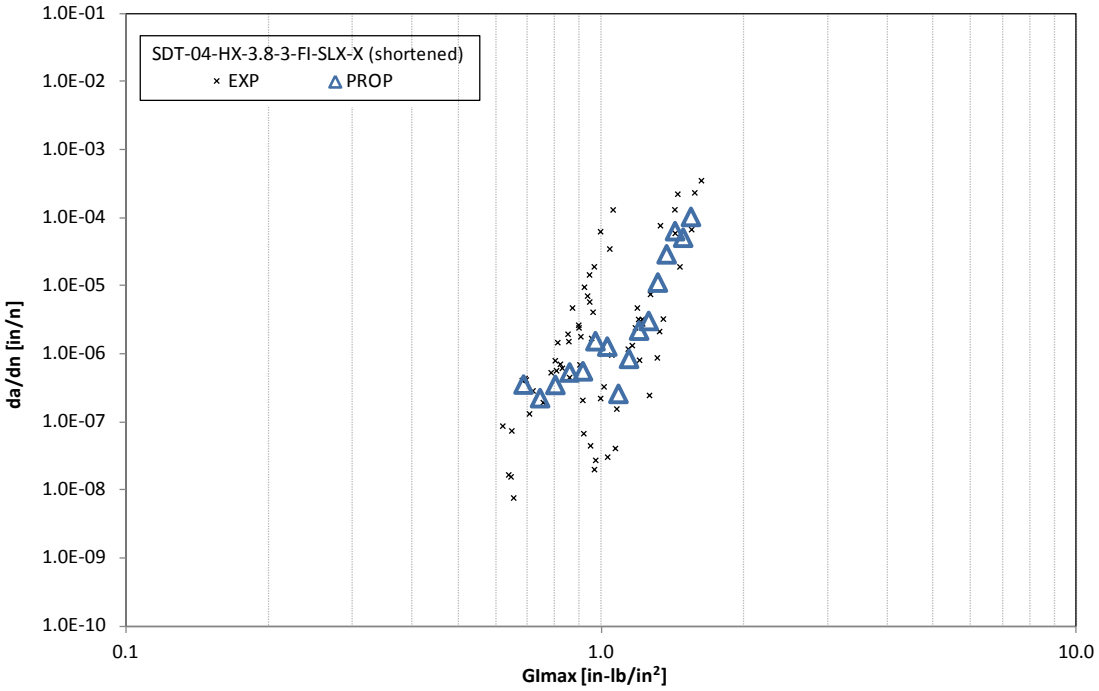

Figure B-45. Fatigue growth da/dn curve for HRH-10–3/8–3.0 fluid ingressed (1″ prescribed crack—shortened)

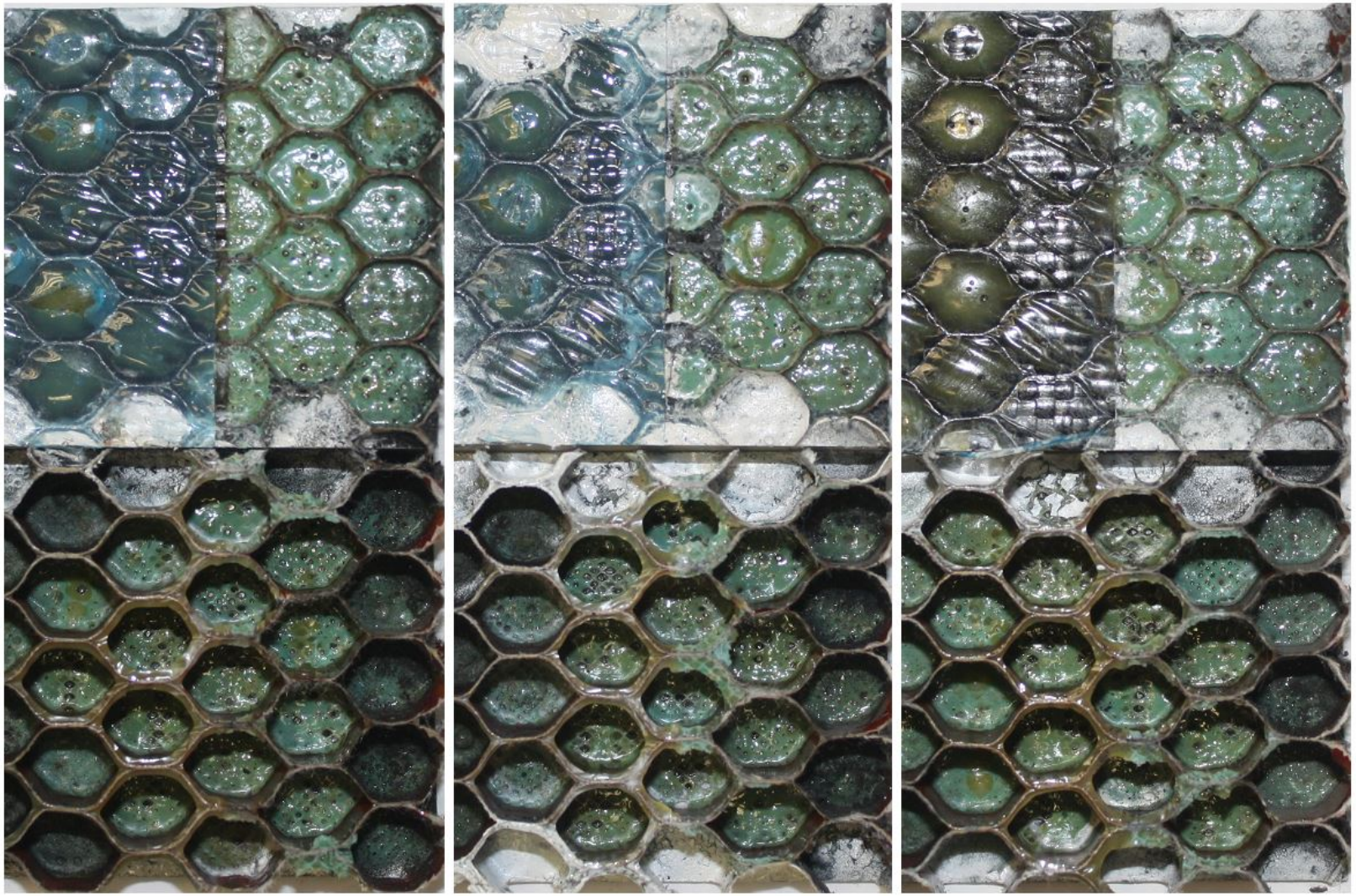

Figure B-46. Failure mode for SDT-04-HX-3.8-3-FI-SLX-X (shortened) #1, #2, and #3

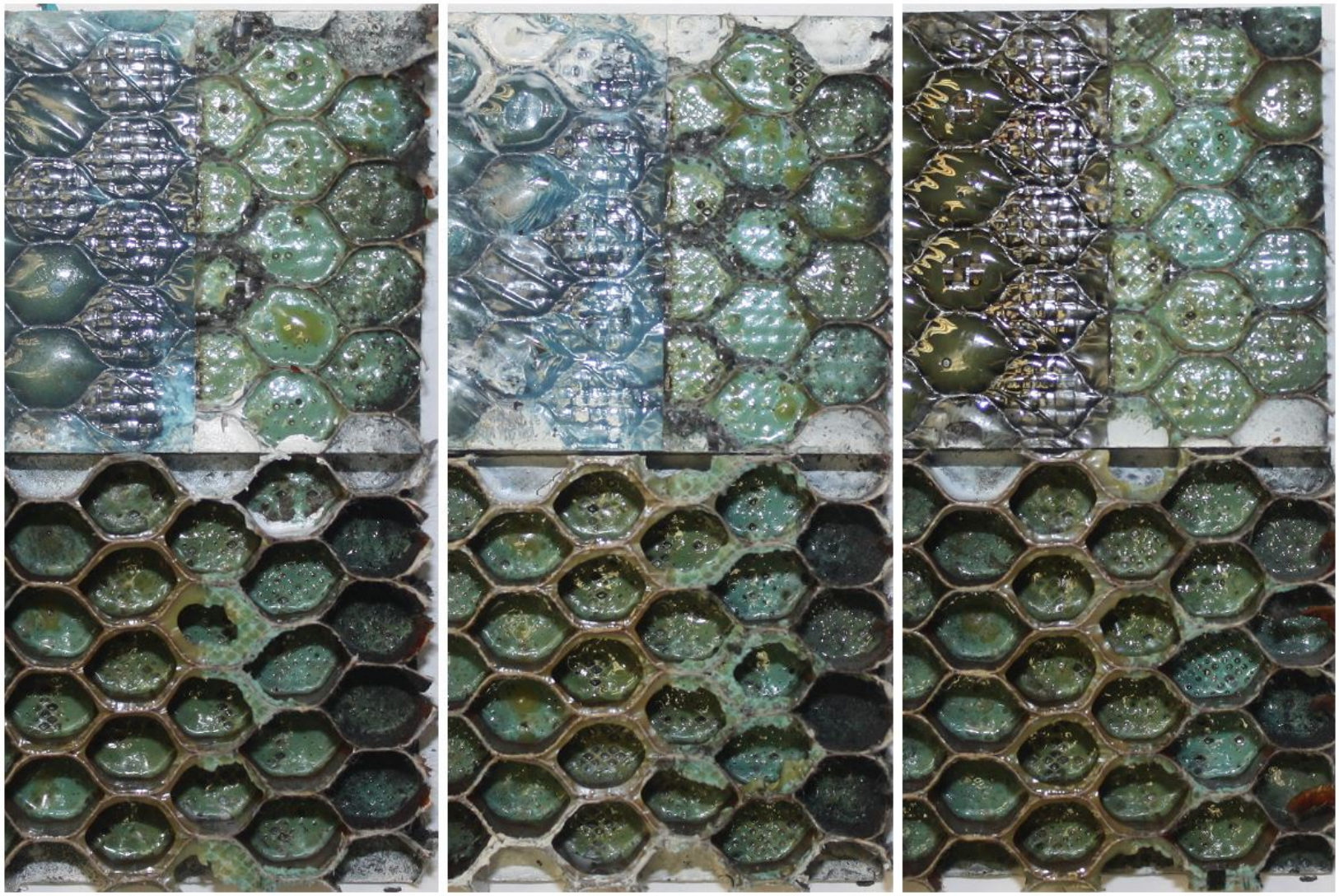

Figure B-47. Failure mode for SDT-04-HX-3.8-3-FI-SLX-X (shortened) #4, #5, and #6

APPENDIX C—STATIC RESULTS FOR THICK FACESHEET (16-PLY) AND HRH-10 HEXAGONAL CORES TESTED AS SINGLE-CANTILEVER BEAMS

Note that 16-ply material systems were tested with one prescribed crack length. The baseline and fluid-ingressed specimens were all tested with a 2.5″ prescribed crack.

C.1 HRH-10–1/8–3.0 DATA

C.1.1 HRH-10–1/8–3.0 BASELINE DATA (2.5″ PRESCRIBED CRACK)

Table C-1. Test summary for HRH-10–1/8–3.0 baseline (2.5″ prescribed crack)

Specimen	Shaping Parameter [m] English or SI	Shaping Parameter [B] English	Shaping Parameter [B] SI	Failure Mode
SDT-16-HX-1.8-3-BL-SLX-1	8.785	2.626E-05	1.304E-23	First row a mix of A and C, then C with a few cells in A
SDT-16-HX-1.8-3-BL-SLX-2	9.621	2.536E-06	1.679E-26	First three rows primarily A, then split between A and C
SDT-16-HX-1.8-3-BL-SLX-3	8.139	2.102E-06	2.943E-23	First two rows primarily A, then split between A and C
SDT-16-HX-1.8-3-BL-SLX-4	11.042	6.471E-06	2.786E-29	Primarily A with two pockets of C
SDT-16-HX-1.8-3-BL-SLX-5	9.671	9.551E-06	4.880E-26	First two rows primarily A, then a mix of A and C, then C
SDT-16-HX-1.8-3-BL-SLX-6	11.175	3.117E-06	6.761E-30	Primarily A with the two last rows in S
AVERAGE (individual)	9.739	8.339E-06	7.090E-24	
STANDARD DEVIATION	1.204	9.229E-06	1.212E-23	
COEFFICIENT OF VARIATION [%]	12.362	110.673	170.976	
AVERAGE (all)	7.297	3.806E-06	4.126E-21	
AVERAGE (interpolated)	8.039	3.744E-06	8.784E-23	

A = adhesive interface disbond failure; C = tensile core failure; S = interlaminar facesheet delamination failure

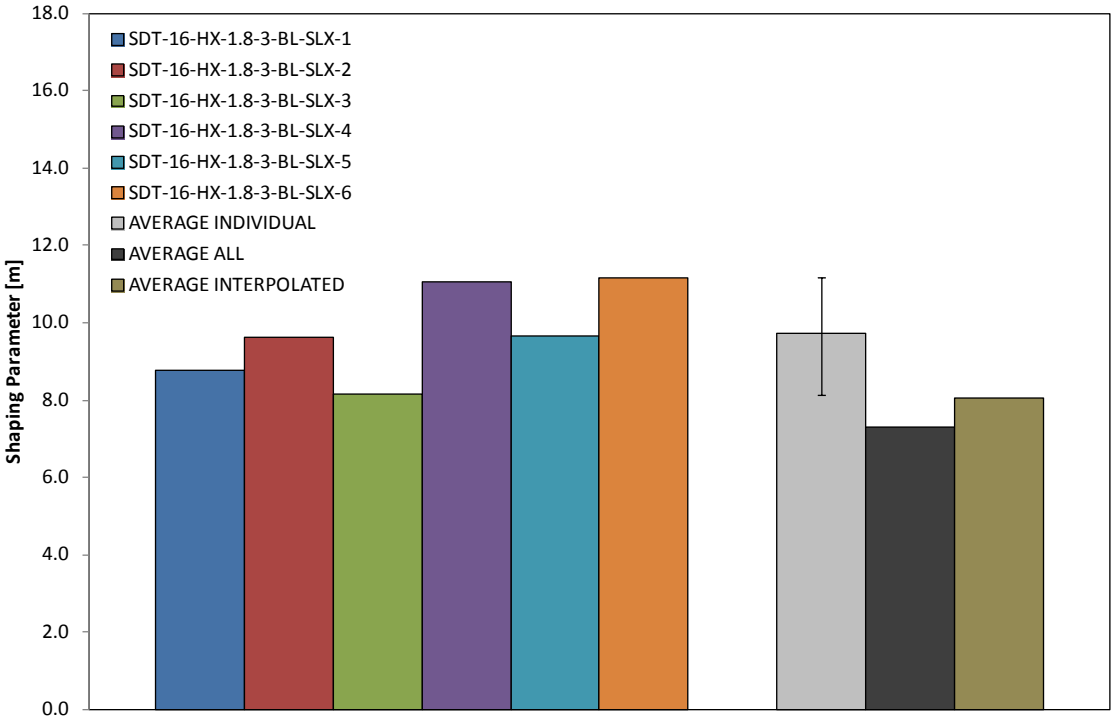

Figure C-1. Shaping parameter (*m*) for HRH-10–1/8–3.0 baseline (2.5″ prescribed crack)

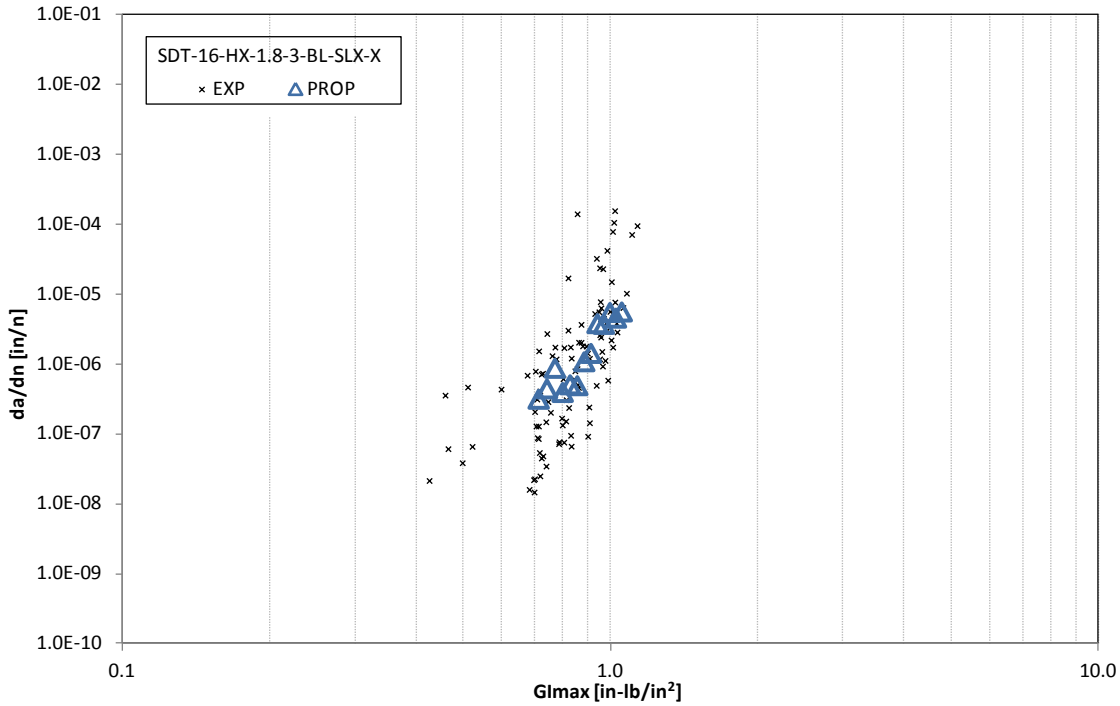

Figure C-2. Fatigue growth da/dn curve for HRH-10–1/8–3.0 baseline (2.5″ prescribed crack)

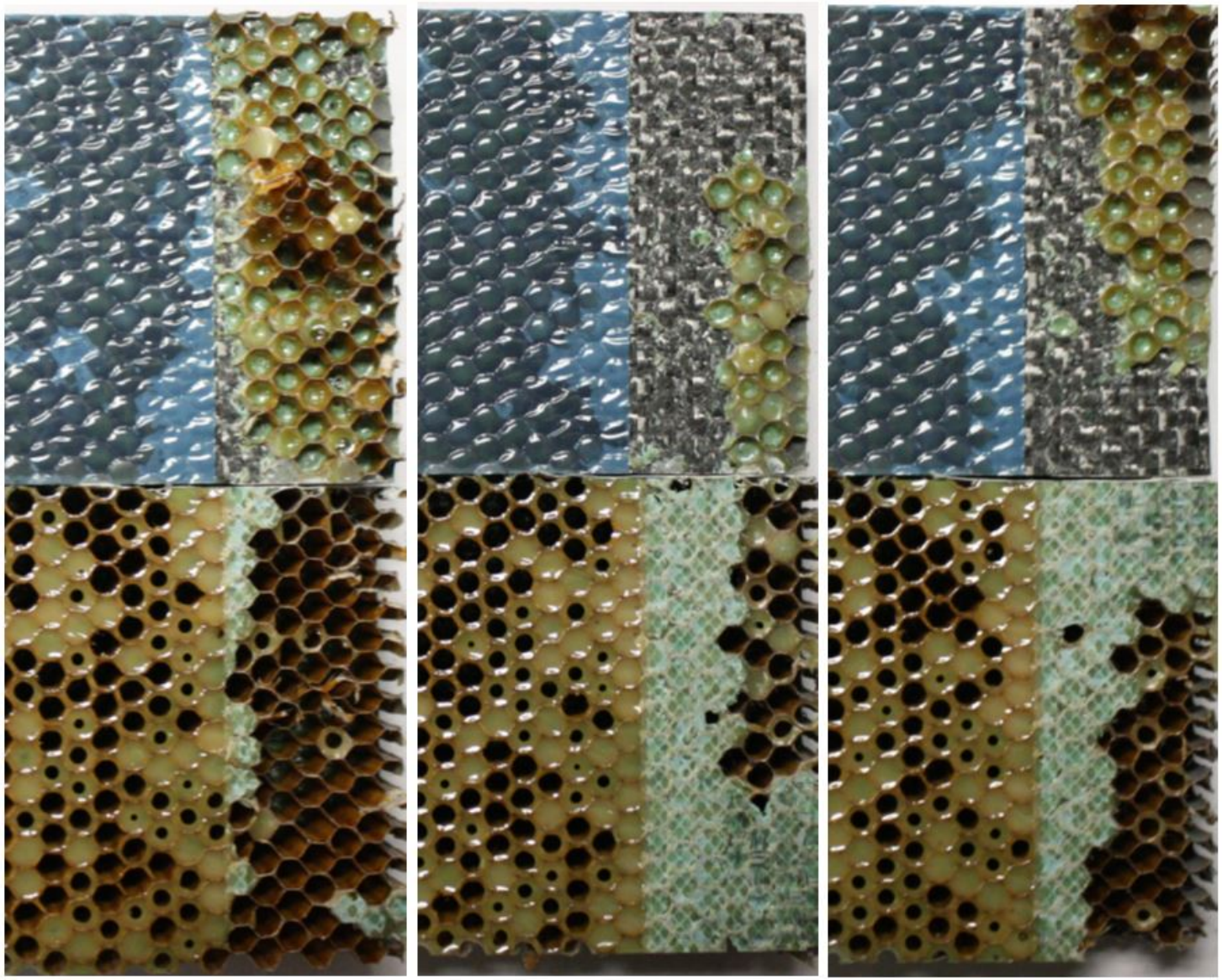

Figure C-3. Failure mode image for SDT-16-HX-1.8-3-BL-SLX-X #1, #2, and #3

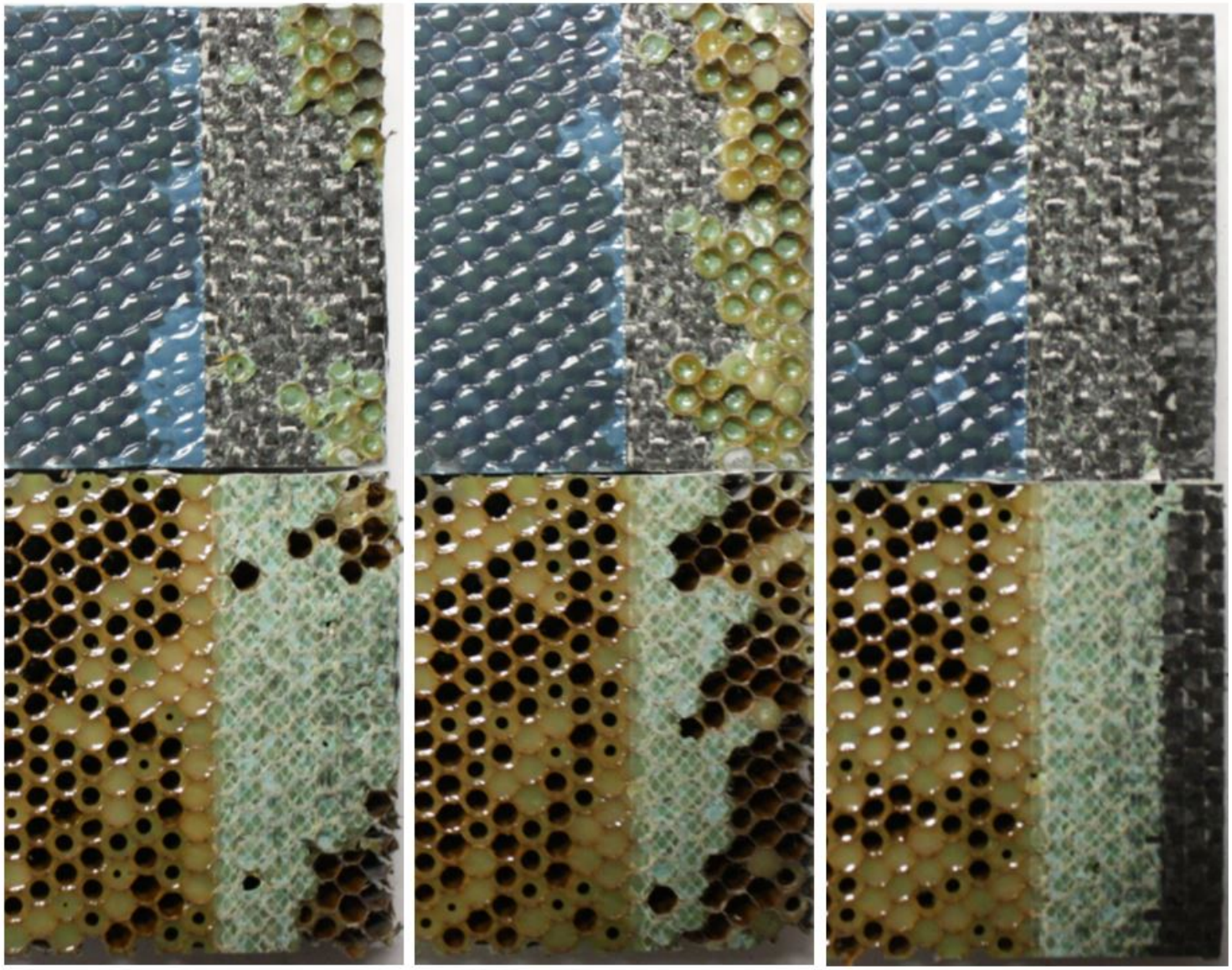

Figure C-4. Failure mode image for SDT-16-HX-1.8-3-BL-SLX-X #4, #5, and #6

C.1.2 HRH-10–1/8–3.0 FLUID-INGRESSED DATA (2.5″ PRESCRIBED CRACK)

Table C-2. Test summary for HRH-10–1/8–3.0 fluid ingressed (2.5″prescribed crack)

Specimen	Shaping Parameter [m] English or SI	Shaping Parameter [B] English	Shaping Parameter [B] SI	Failure Mode
SDT-16-HX-1.8-3-FI-SLX-6	23.333	8.486E-07	9.775E-58	Primarily A with a couple of cells in PO
SDT-16-HX-1.8-3-FI-SLX-7	47.305	3.453E-06	6.630E-111	First row primarily in A; second row split between A and C, then C
SDT-16-HX-1.8-3-FI-SLX-8	45.830	1.318E-14	5.515E-116	First row split between A and C, then C
AVERAGE (individual)	38.823	1.434E-06	3.258E-58	
STANDARD DEVIATION	13.435	1.799E-06	5.643E-58	
COEFFICIENT OF VARIATION [%]	34.605	125.489	173.205	
AVERAGE (all)	N/A	N/A	N/A	
AVERAGE (interpolated)	N/A	N/A	N/A	

A = adhesive interface disbond failure; PO = adhesive pullout failure; C = tensile core failure

Table C-3. Test summary for HRH-10–1/8–3.0 fluid ingressed (2.5″ prescribed crack)

Specimen	Shaping Parameter [m] English or SI	Shaping Parameter [B] English	Shaping Parameter [B] SI	Failure Mode
SDT-16-HX-1.8-3-FI-SLX-2**	6.420	1.504E+02	3.624E-141	First row split between A and C, then C
SDT-16-HX-1.8-3-FI-SLX-3**	102.860	1.105E+06	4.910E-224	First row split between A and C, then C
SDT-16-HX-1.8-3-FI-SLX-4**	153.800	2.051E+65	4.786E-279	First row primarily in A then C
SDT-16-HX-1.8-3-FI-SLX-5**	-28.124	6.656E-11	2.093E+54	First row primarily in A then C
AVERAGE** (individual)	58.739	5.127E+64	5.233E+53	
STANDARD DEVIATION	84.194	1.025E+65	1.047E+54	
COEFFICIENT OF VARIATION [%]	143.335	200.000	200.000	
AVERAGE** (all)	N/A	N/A	N/A	
AVERAGE** (interpolated)	N/A	N/A	N/A	

A = adhesive interface disbond failure; C = tensile core failure

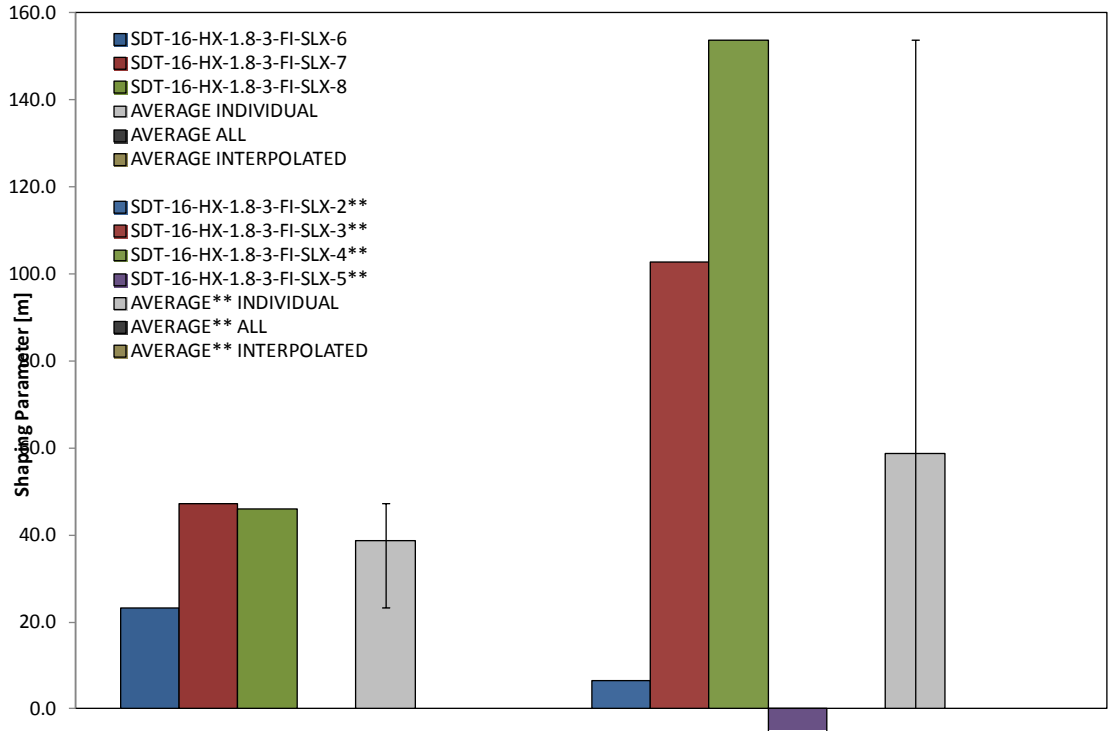

Figure C-5. Shaping parameter (*m*) for HRH-10–1/8–3.0 fluid ingressed (2.5″ prescribed crack)

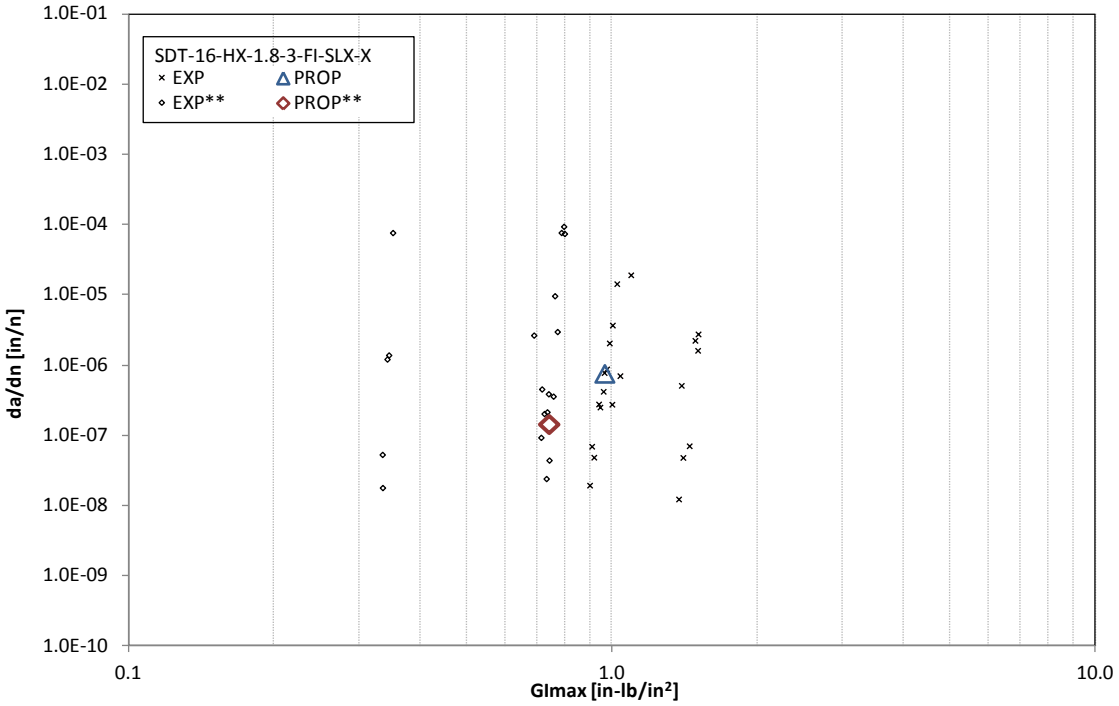

Figure C-6. Fatigue growth da/dn curve for HRH-10–1/8–3.0 fluid ingressed (2.5″ prescribed crack)

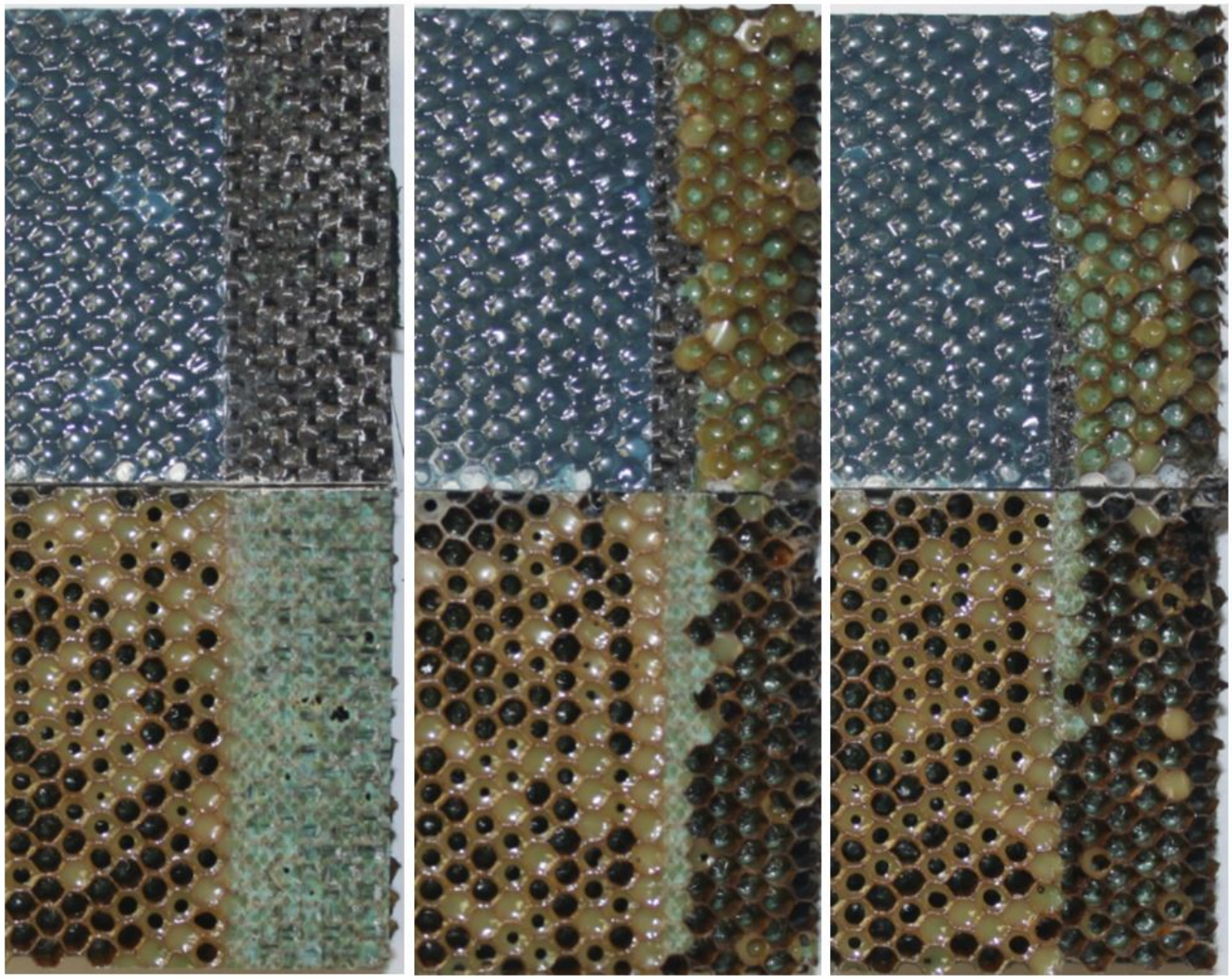

Figure C-7. Failure mode image for SDT-16-HX-1.8-3-FI-SLX-X #6, #7, and #8

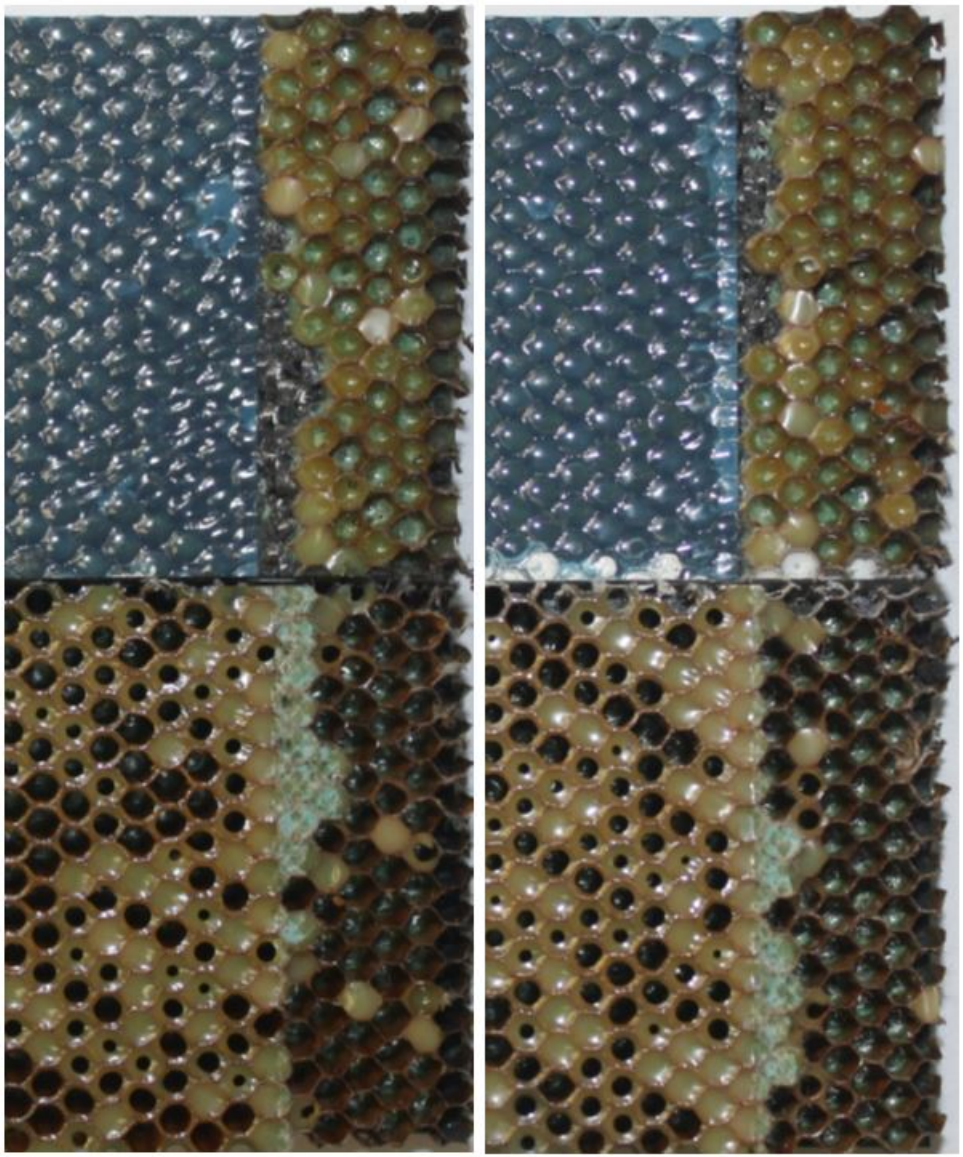

Figure C-8. Failure mode image for SDT-16-HX-1.8-3-FI-SLX-X #2 and #3****

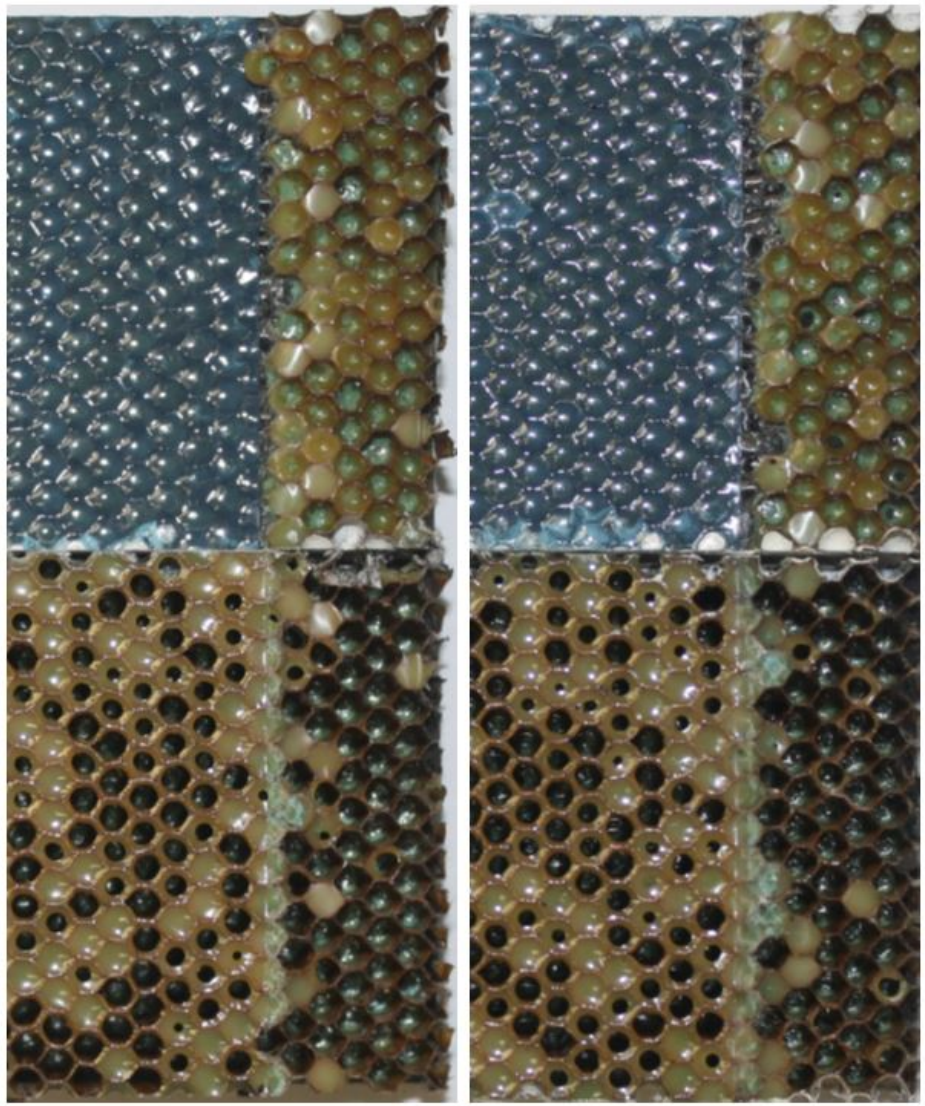

Figure C-9. Failure mode image for SDT-16-HX-1.8-3-FI-SLX-X #4 and #5****

C.2 HRH-10–3/16–2.0 DATA

C.2.1 HRH-10–3/16–2.0 BASELINE DATA (2.5″ PRESCRIBED CRACK)

Table C-4. Test summary for HRH-10–3/16–2.0 baseline (2.5″ prescribed crack)

Specimen	Shaping Parameter [m] English or SI	Shaping Parameter [B] English	Shaping Parameter [B] SI	Failure Mode
SDT-16-HX-3.16-2-BL-SLX-1	2.163	3.051E-06	1.088E-09	First row in A with a couple of cells in C, then C
SDT-16-HX-3.16-2-BL-SLX-2	2.480	2.167E-06	1.504E-10	First row in A with a cell in C, then C
SDT-16-HX-3.16-2-BL-SLX-3	2.250	2.611E-06	5.948E-10	First row in A with a couple of cells in C, then C
SDT-16-HX-3.16-2-BL-SLX-4	3.193	2.069E-06	3.615E-12	First row split between A and C, then C
SDT-16-HX-3.16-2-BL-SLX-5	3.038	2.541E-06	9.867E-12	First row split between A and C, then C
SDT-16-HX-3.16-2-BL-SLX-6	3.897	2.891E-06	1.327E-13	First row split between A and C, then C
AVERAGE (individual)	2.837	2.555E-06	3.078E-10	
STANDARD DEVIATION	0.666	3.871E-07	4.455E-10	
COEFFICIENT OF VARIATION [%]	23.475	15.152	144.711	
AVERAGE (all)	2.519	2.322E-06	1.320E-10	
AVERAGE (interpolated)	2.397	1.620E-06	1.726E-10	

A = adhesive interface disbond failure; C = tensile core failure

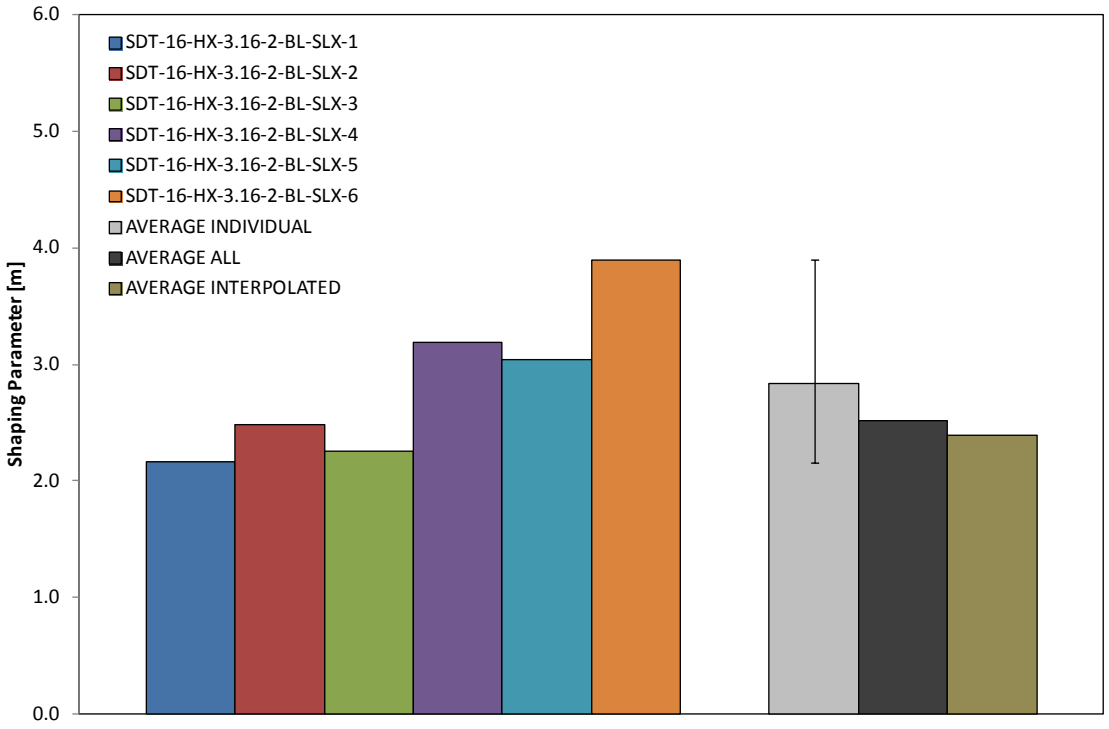

Figure C-10. Shaping parameter (*m*) for HRH-10–3/16–2.0 baseline (2.5″ prescribed crack)

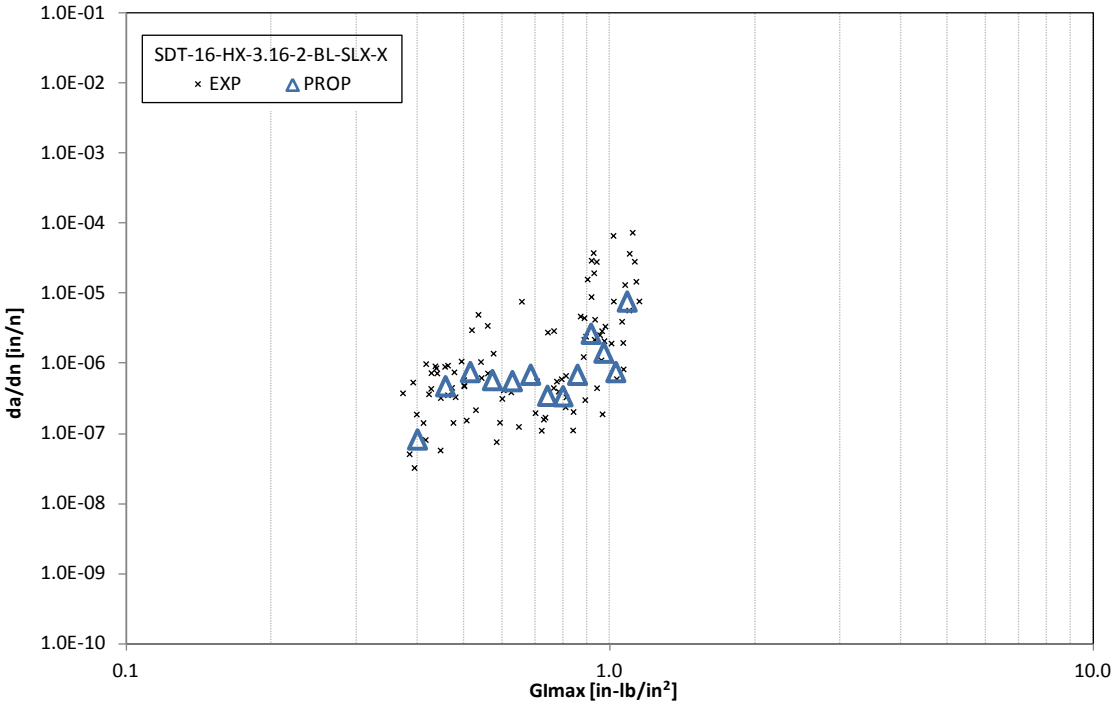

Figure C-11. Fatigue growth da/dn curve for HRH-10–3/16–2.0 baseline (2.5″ prescribed crack)

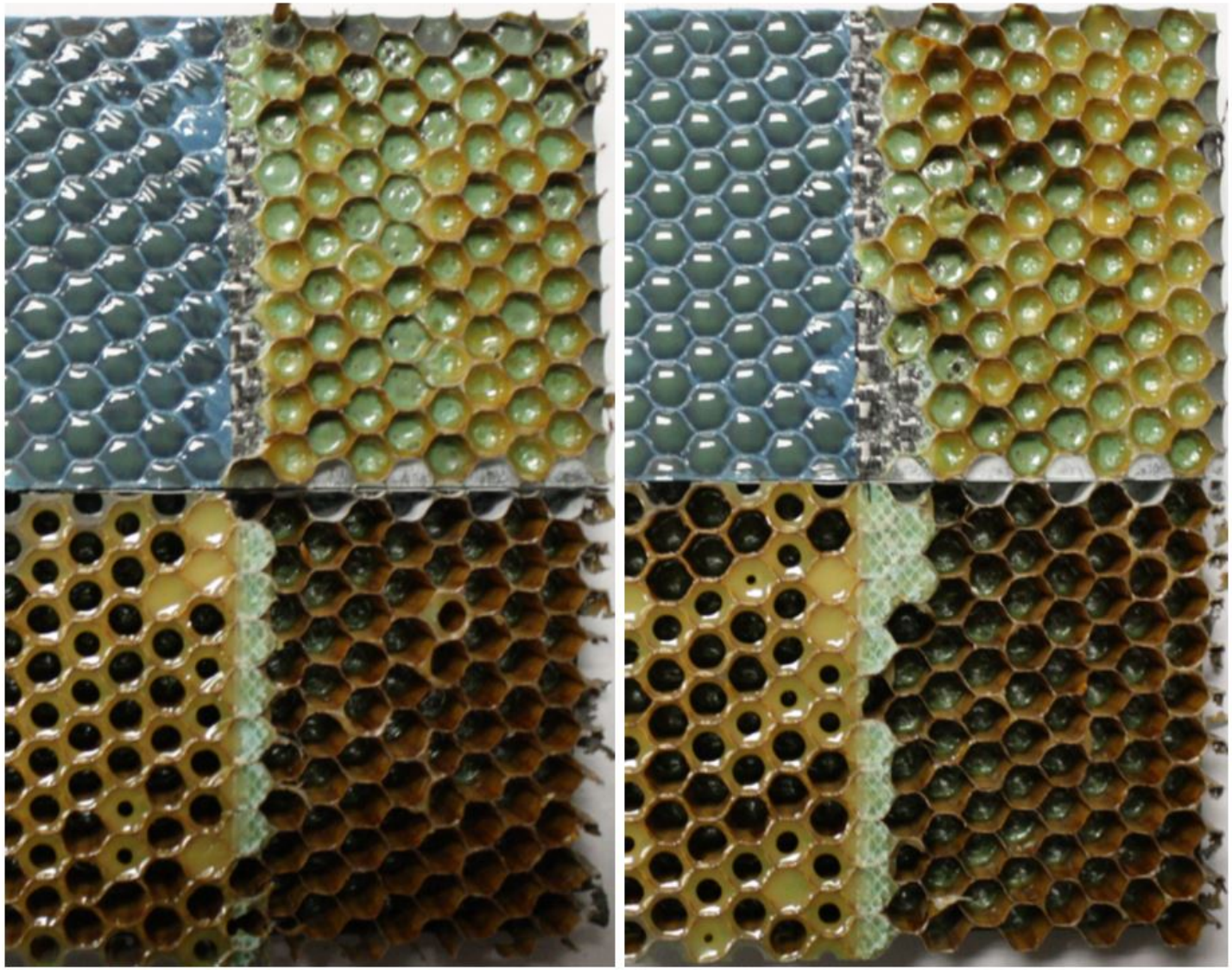

Figure C-12. Failure mode image for SDT-16-HX-3.16-2-BL-SLX-X #1 and #2

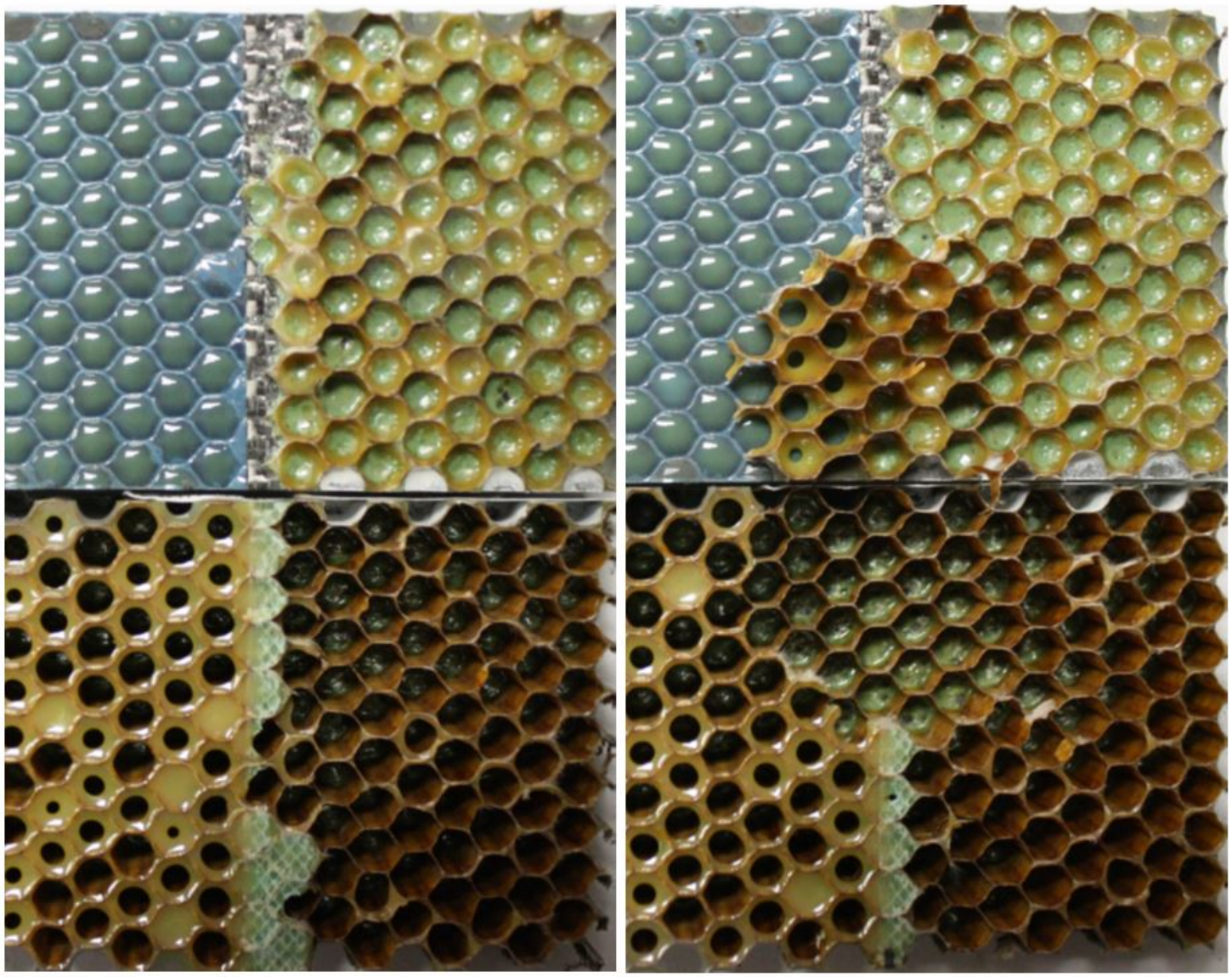

Figure C-13. Failure mode image for SDT-16-HX-3.16-2-BL-SLX-X #3 and #4

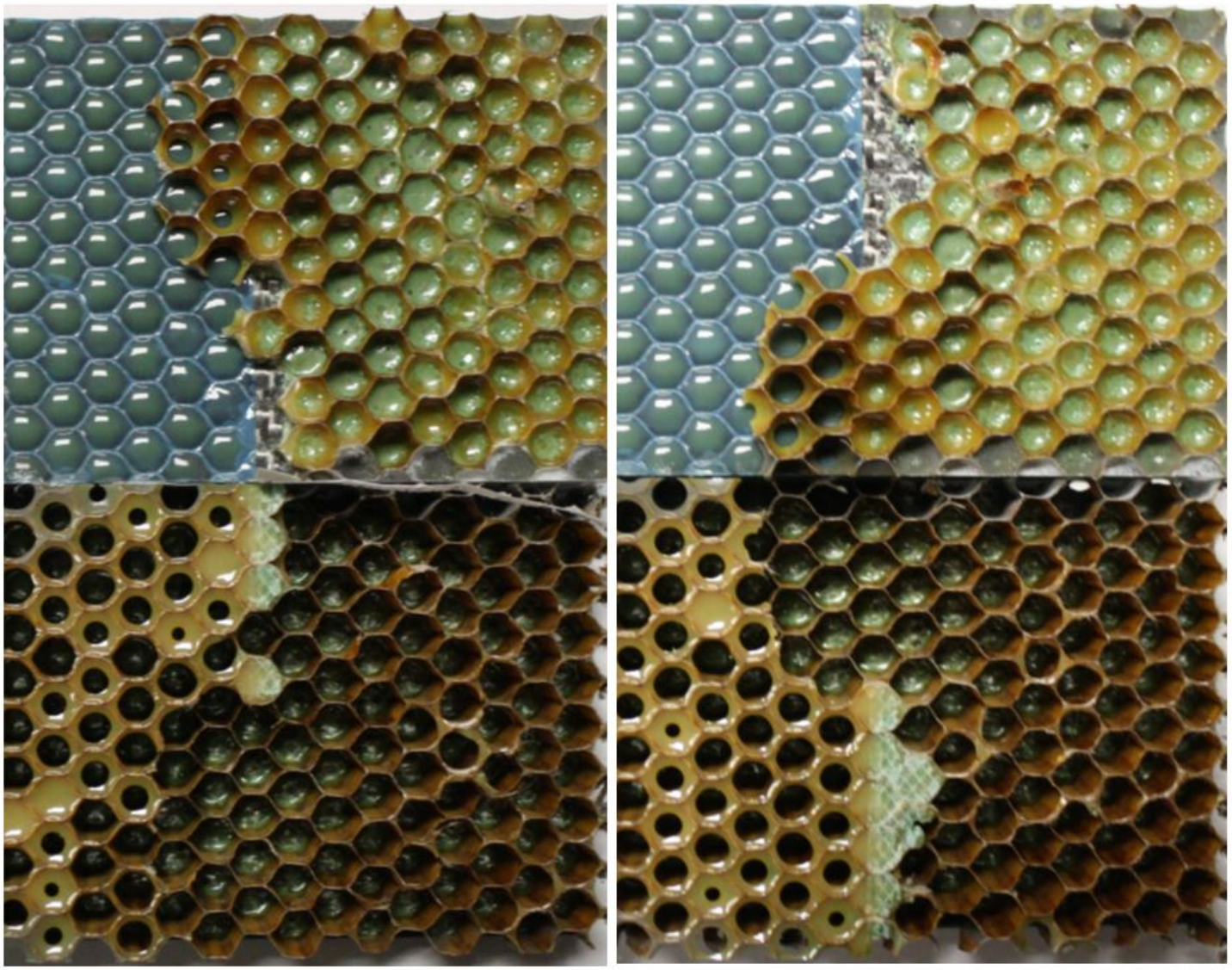

Figure C-14. Failure mode image for SDT-16-HX-3.16-2-BL-SLX-X #5 and #6

C.2.2 HRH-10–3/16–2.0 FLUID-INGRESSED DATA (2.5″ PRESCRIBED CRACK)

Table C-5. Test summary for HRH10–3/16–2.0 fluid ingressed (2.5″ prescribed crack)

Specimen	Shaping Parameter [m] English or SI	Shaping Parameter [B] English	Shaping Parameter [B] SI	Failure Mode
SDT-16-HX-3.16-2-FI-SLX-7	20.461	2.626E-05	8.375E-50	Primarily C
AVERAGE (individual)	20.461	2.626E-05	8.375E-50	
STANDARD DEVIATION	N/A	N/A	N/A	
COEFFICIENT OF VARIATION [%]	N/A	N/A	N/A	
AVERAGE (all)	20.461	2.626E-05	8.375E-50	
AVERAGE (interpolated)	N/A	N/A	N/A	

C = tensile core failure

Table C-6. Test summary for HRH-10–3/16–2.0 fluid ingressed (2.5″ prescribed crack)

Specimen	Shaping Parameter [m] English or SI	Shaping Parameter [B] English	Shaping Parameter [B] SI	Failure Mode
SDT-16-HX-3.16-2-FI-SLX-1**	2.828	4.943E-05	5.674E-10	Primarily C
SDT-16-HX-3.16-2-FI-SLX-3**	2.479	5.935E-06	4.133E-10	Primarily C
SDT-16-HX-3.16-2-FI-SLX-4**	4.507	5.240E-05	1.034E-13	Primarily C
SDT-16-HX-3.16-2-FI-SLX-5**	4.824	1.385E-05	5.315E-15	Primarily C
SDT-16-HX-3.16-2-FI-SLX-6**	3.343	2.110E-05	1.697E-11	Primarily C
AVERAGE** (individual)	3.596	2.854E-05	1.996E-10	
STANDARD DEVIATION	1.029	2.114E-05	2.711E-10	
COEFFICIENT OF VARIATION [%]	28.617	74.071	135.839	
AVERAGE** (all)	2.638	1.380E-05	4.228E-10	
AVERAGE** (interpolated)	2.213	9.908E-06	2.730E-09	

C = tensile core failure

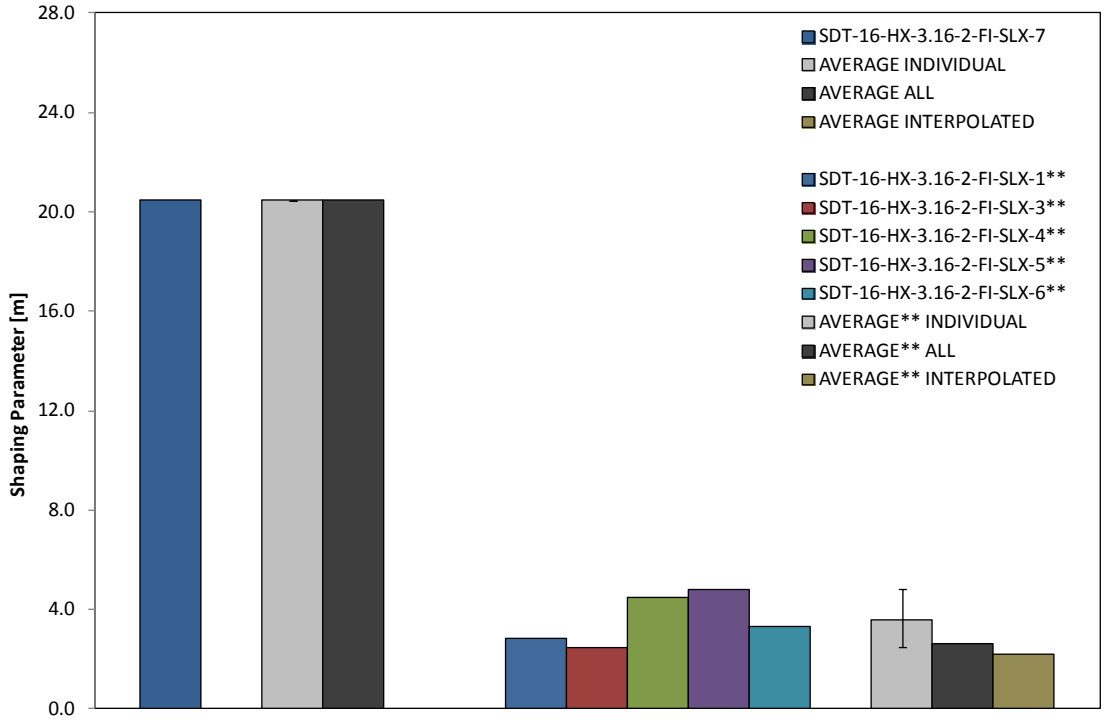

Figure C-15. Shaping parameter (*m*) for HRH-10–3/16–2.0 fluid-ingressed (2.5″ prescribed crack)

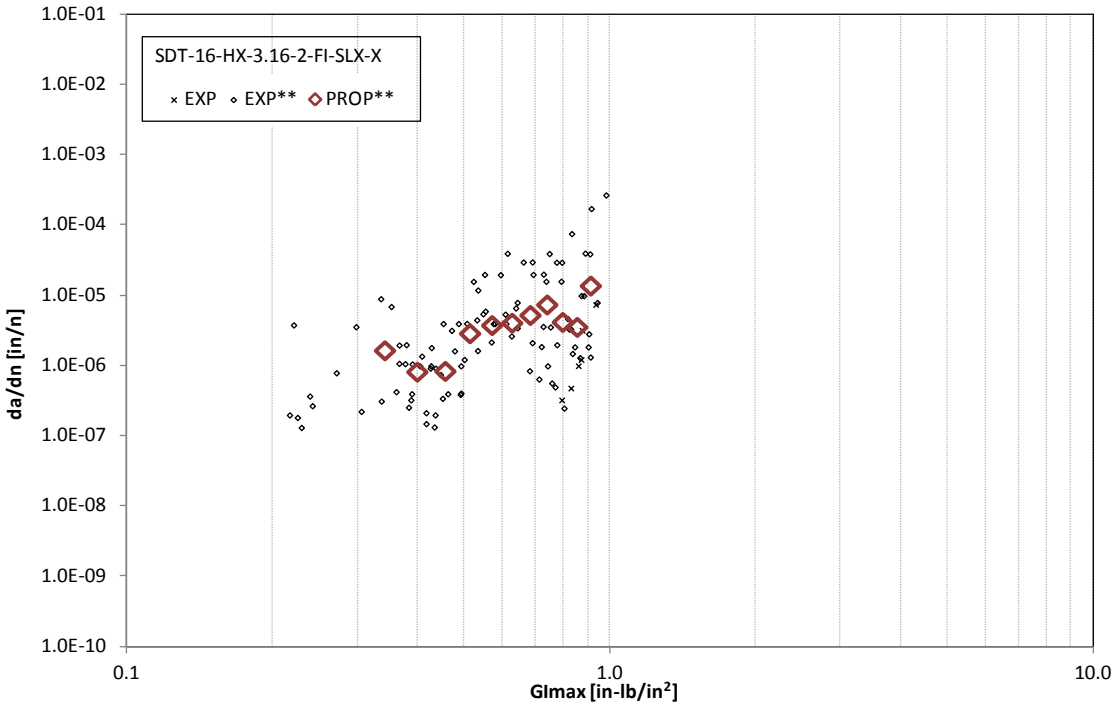

Figure C-16. Fatigue growth da/dn curve for HRH-10–3/16–2.0 fluid-ingressed (2.5″ prescribed crack)

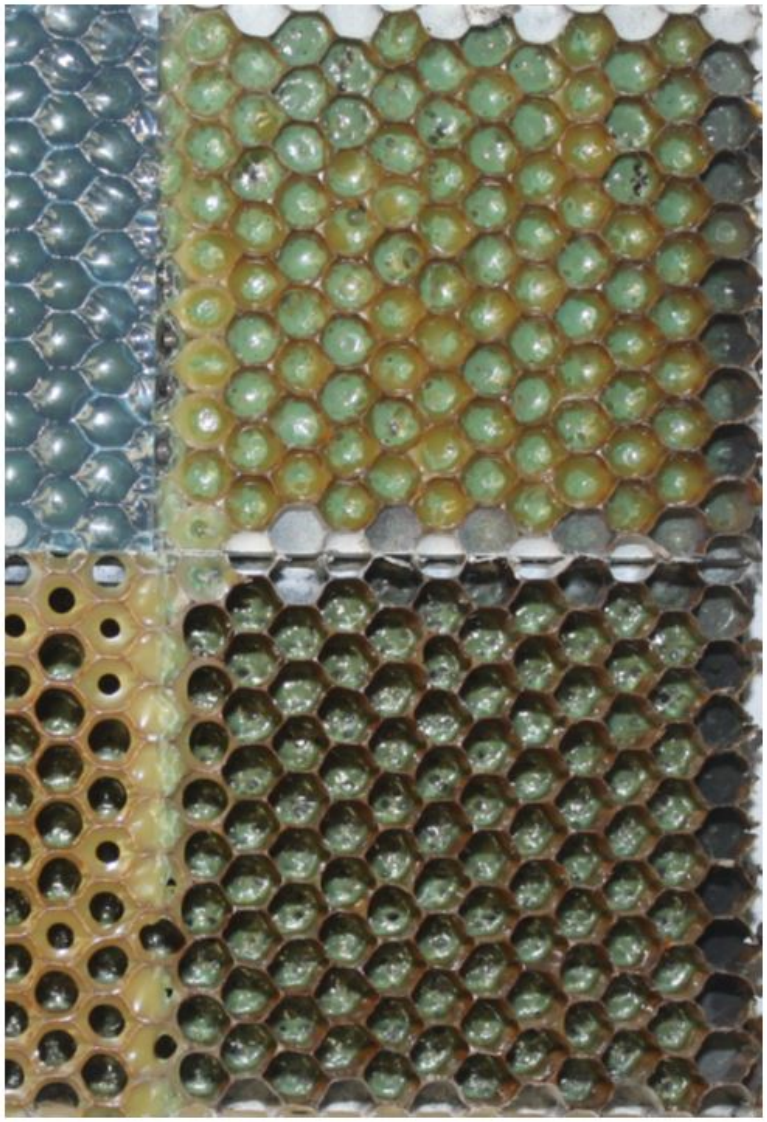

Figure C-17. Failure mode image for SDT-16-HX-3.16-2-FI-SLX-X #7

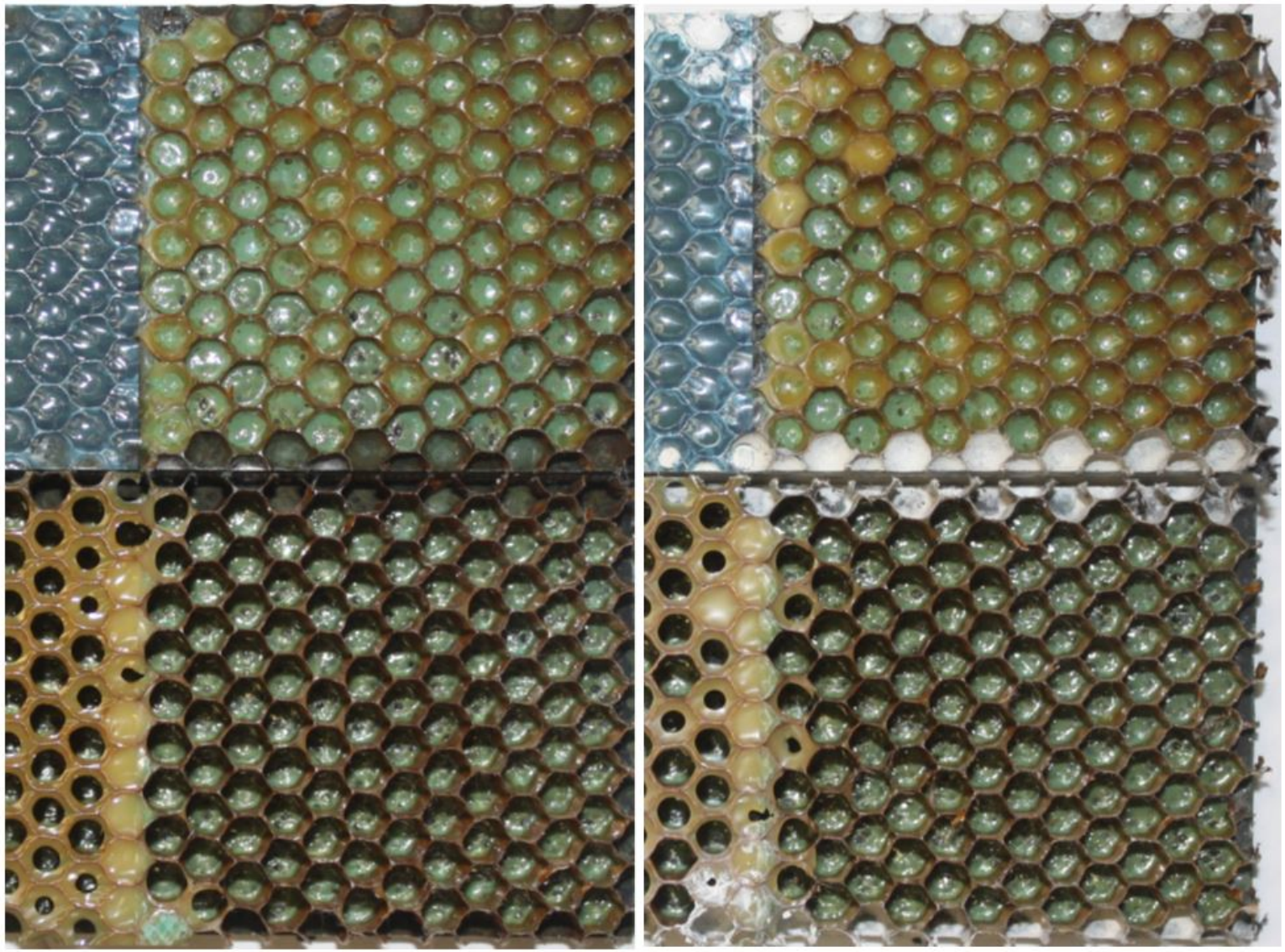

Figure C-18. Failure mode image for SDT-16-HX-3.16-2-FI-SLX-X #1 and #2****

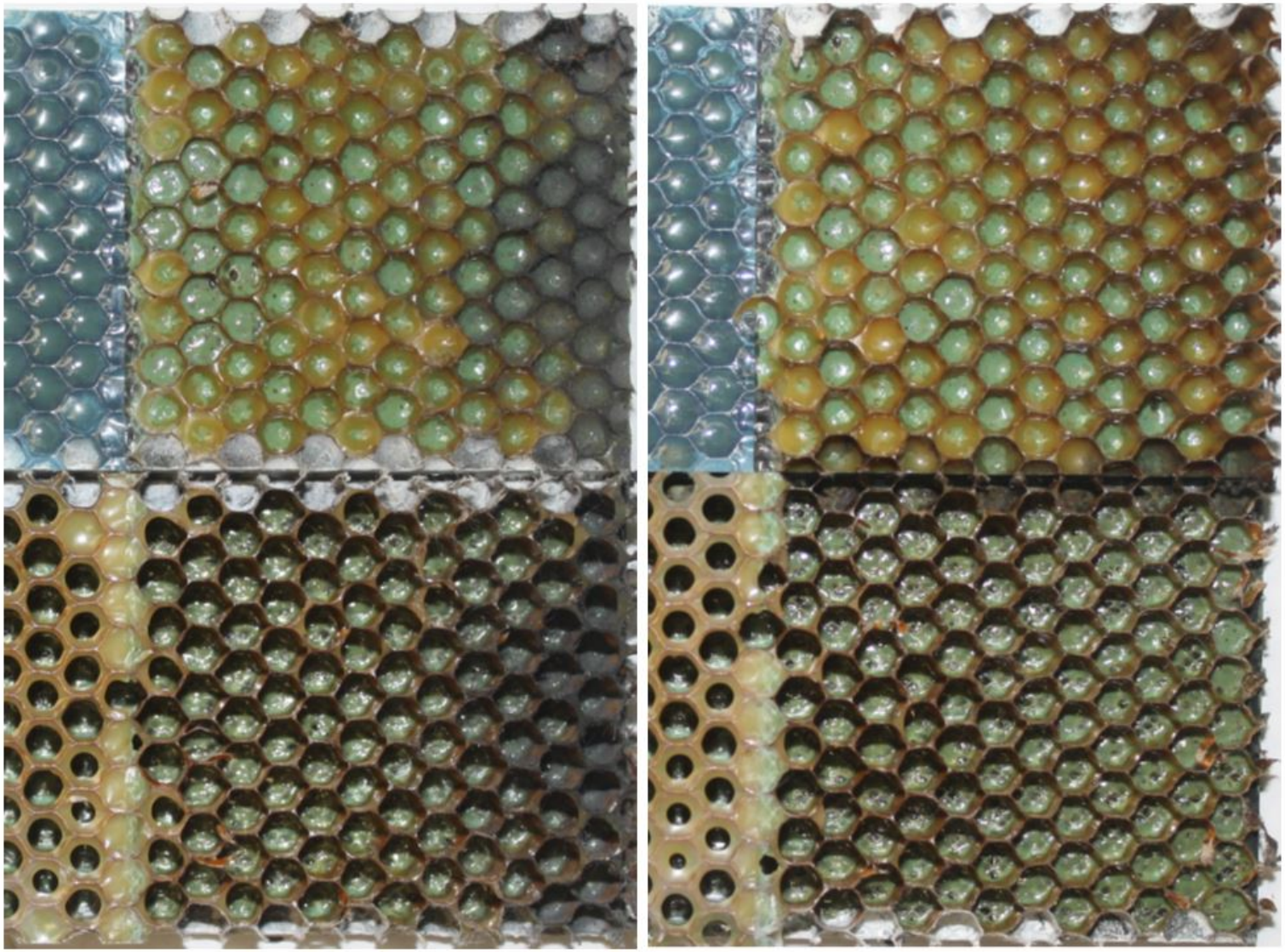

Figure C-19. Failure mode image for SDT-16-HX-3.16-2-FI-SLX-X #3 and #4****

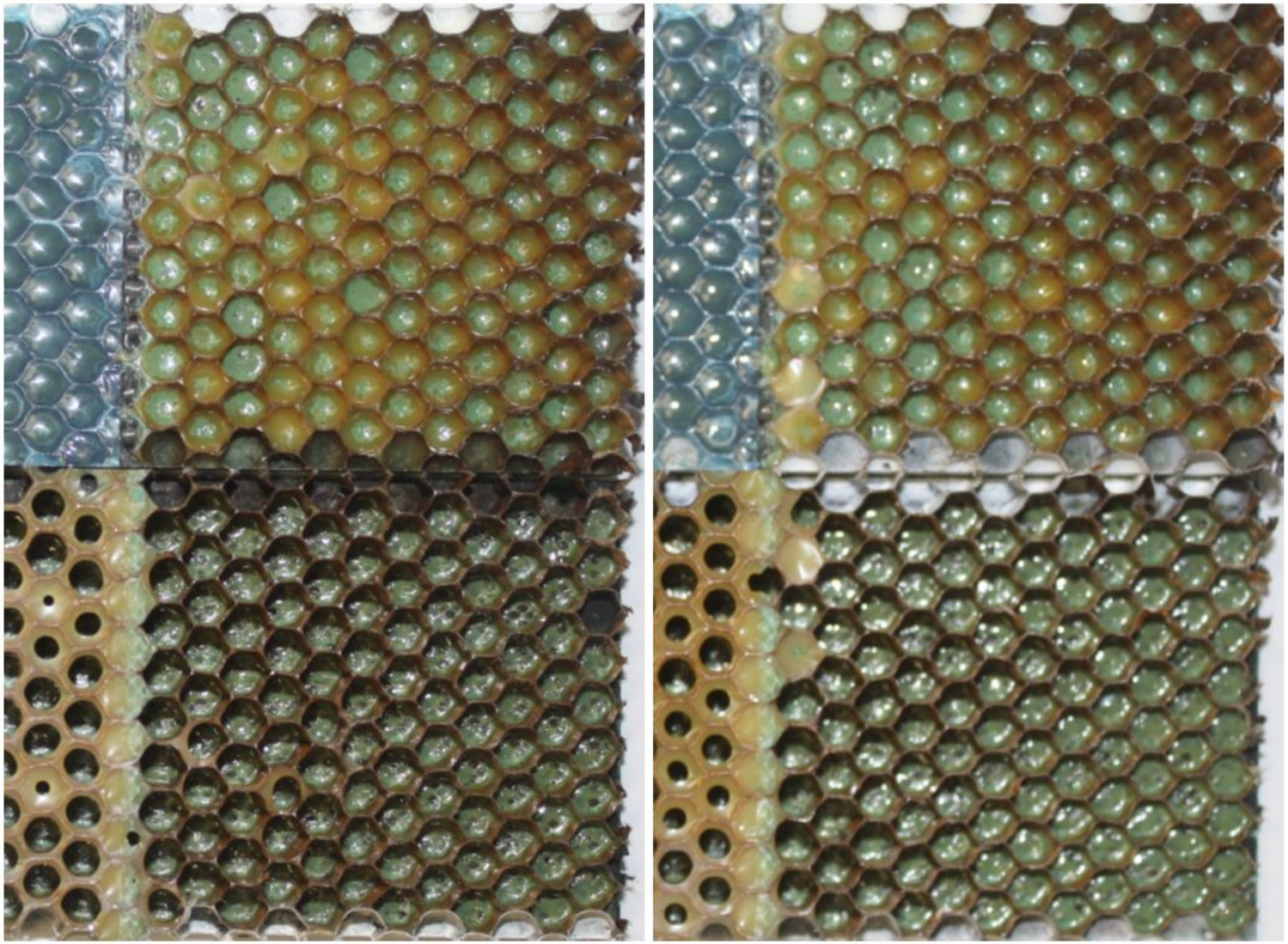

Figure C-20. Failure mode image for SDT-16-HX-3.16-2-FI-SLX-X #5 and #6****

C.3 HRH-10–3/16–3.0 DATA

C.3.1 HRH-10–3/16–3.0 BASELINE DATA (2.5″ PRESCRIBED CRACK)

Table C-7. Test summary for HRH-10–3/16–3.0 baseline (2.5″ prescribed crack)

Specimen	Shaping Parameter [m] English or SI	Shaping Parameter [B] English	Shaping Parameter [B] SI	Failure Mode
SDT-16-HX-3.16-3-BL-SLX-1	12.942	4.900E-07	1.152E-34	First row primarily in A with a few cells in C and a cell in PO, then C with a couple of cells in A
SDT-16-HX-3.16-3-BL-SLX-2	16.577	2.074E-05	3.409E-41	First row primarily in A with a couple of cells in C, then C with a cell in A
SDT-16-HX-3.16-3-BL-SLX-3	16.505	6.125E-07	1.465E-42	First row primarily in A with a couple of cells in C, then C with a few cells in A
SDT-16-HX-3.16-3-BL-SLX-4	12.285	3.563E-07	2.497E-33	First row in A, then a mix of A and C, then C
SDT-16-HX-3.16-3-BL-SLX-5	17.943	2.163E-05	3.070E-44	Primarily in A with a pocket of C
SDT-16-HX-3.16-3-BL-SLX-6	9.297	3.535E-06	1.248E-25	Primarily in A with a couple of cells in C
AVERAGE (individual)	14.258	7.894E-06	2.081E-26	
STANDARD DEVIATION	3.294	1.037E-05	5.096E-26	
COEFFICIENT OF VARIATION [%]	23.100	131.327	244.949	
AVERAGE (all)	6.044	1.196E-06	5.116E-17	
AVERAGE (interpolated)	5.516	1.065E-06	1.140E-17	

A = adhesive interface disbond failure; C = tensile core failure; PO = adhesive pullout failure

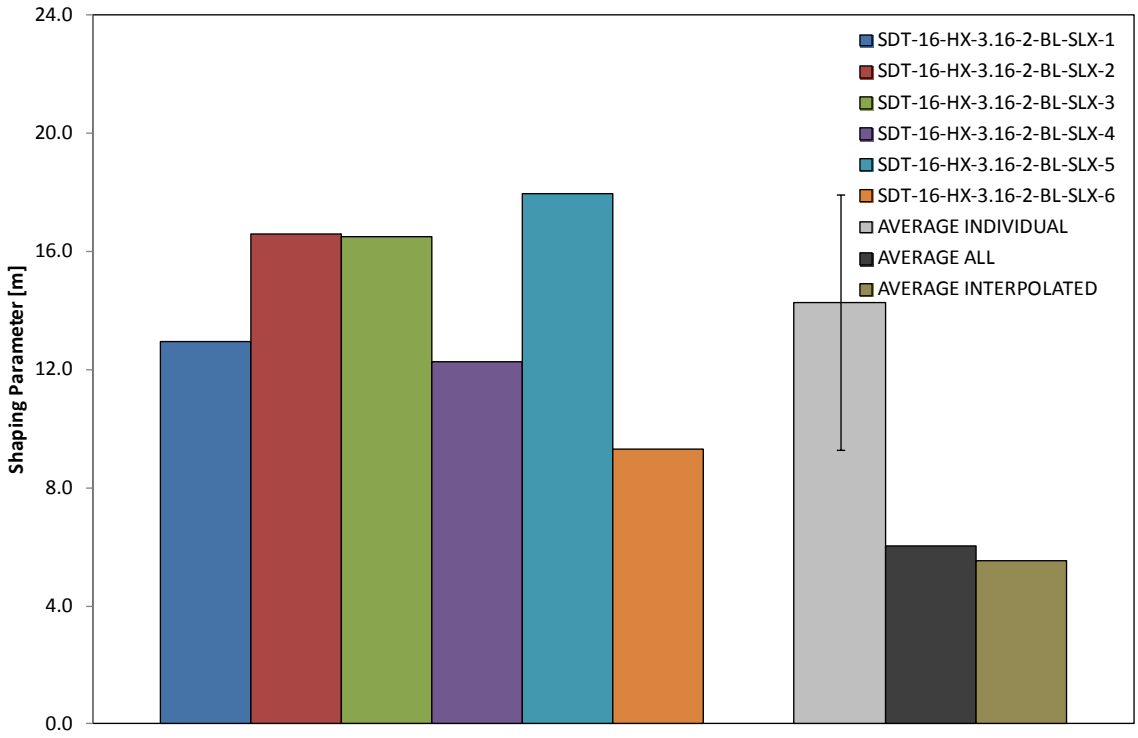

Figure C-21. Shaping parameter (*m*) for HRH-10–3/16–3.0 baseline (2.5″ prescribed crack)

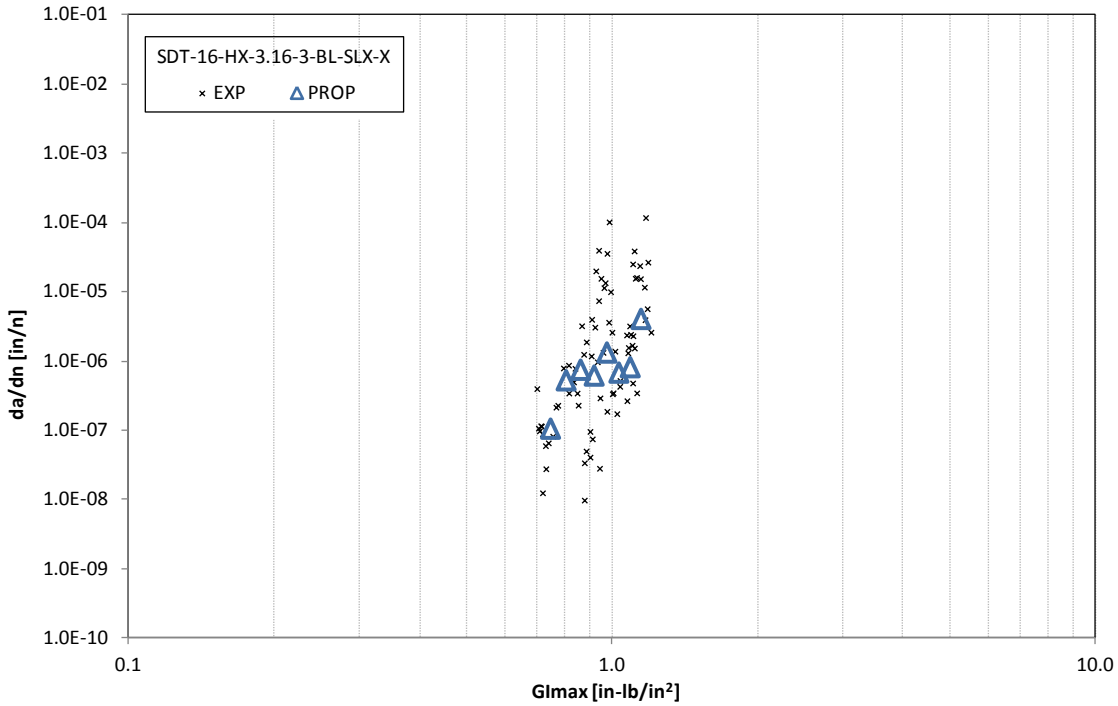

Figure C-22. Fatigue growth da/dn curve for HRH-10–3/16–3.0 baseline (2.5″ prescribed crack)

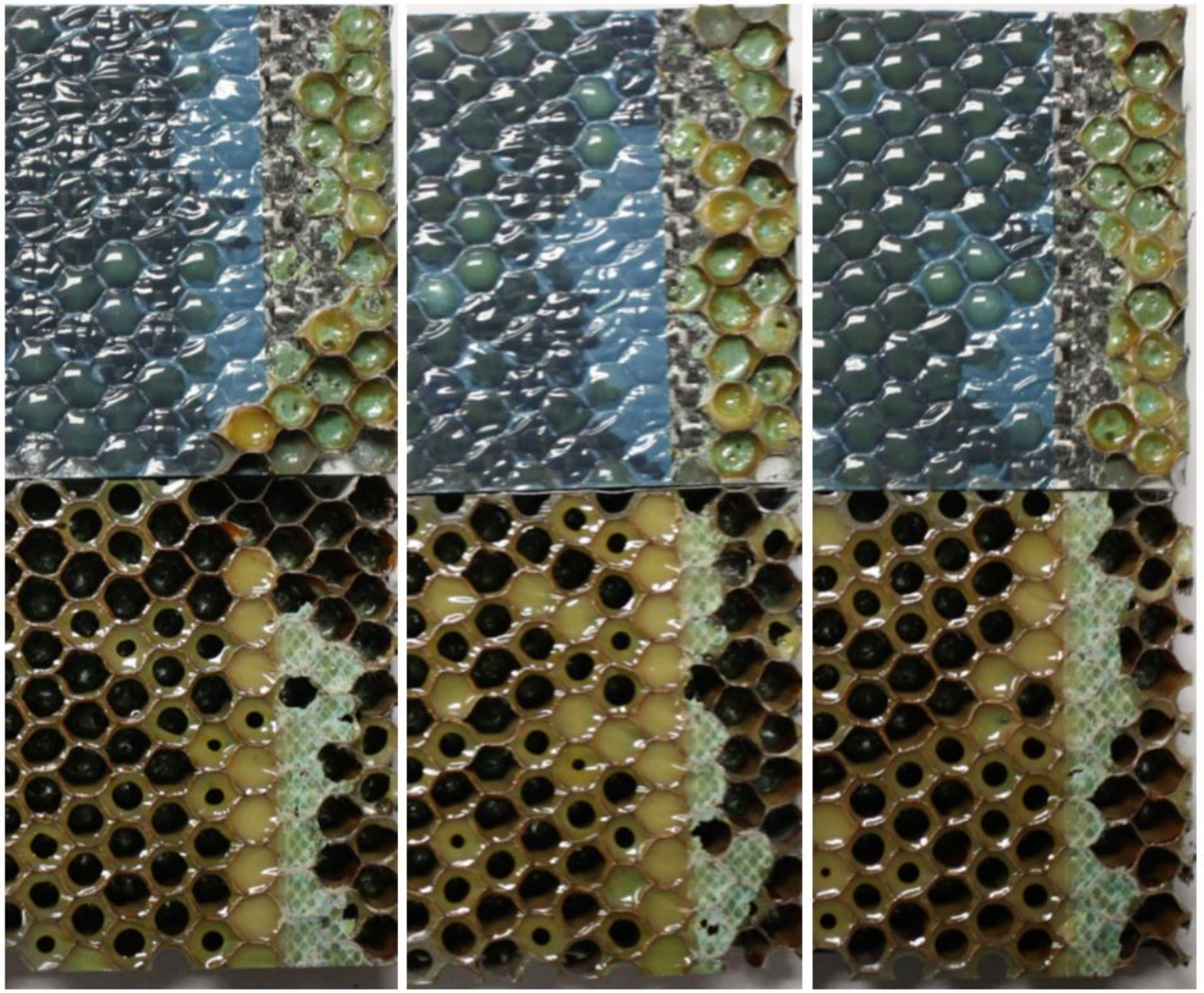

Figure C-23. Failure mode image for SDT-16-HX-3.16-3-BL-SLX-X #1, #2, and #3

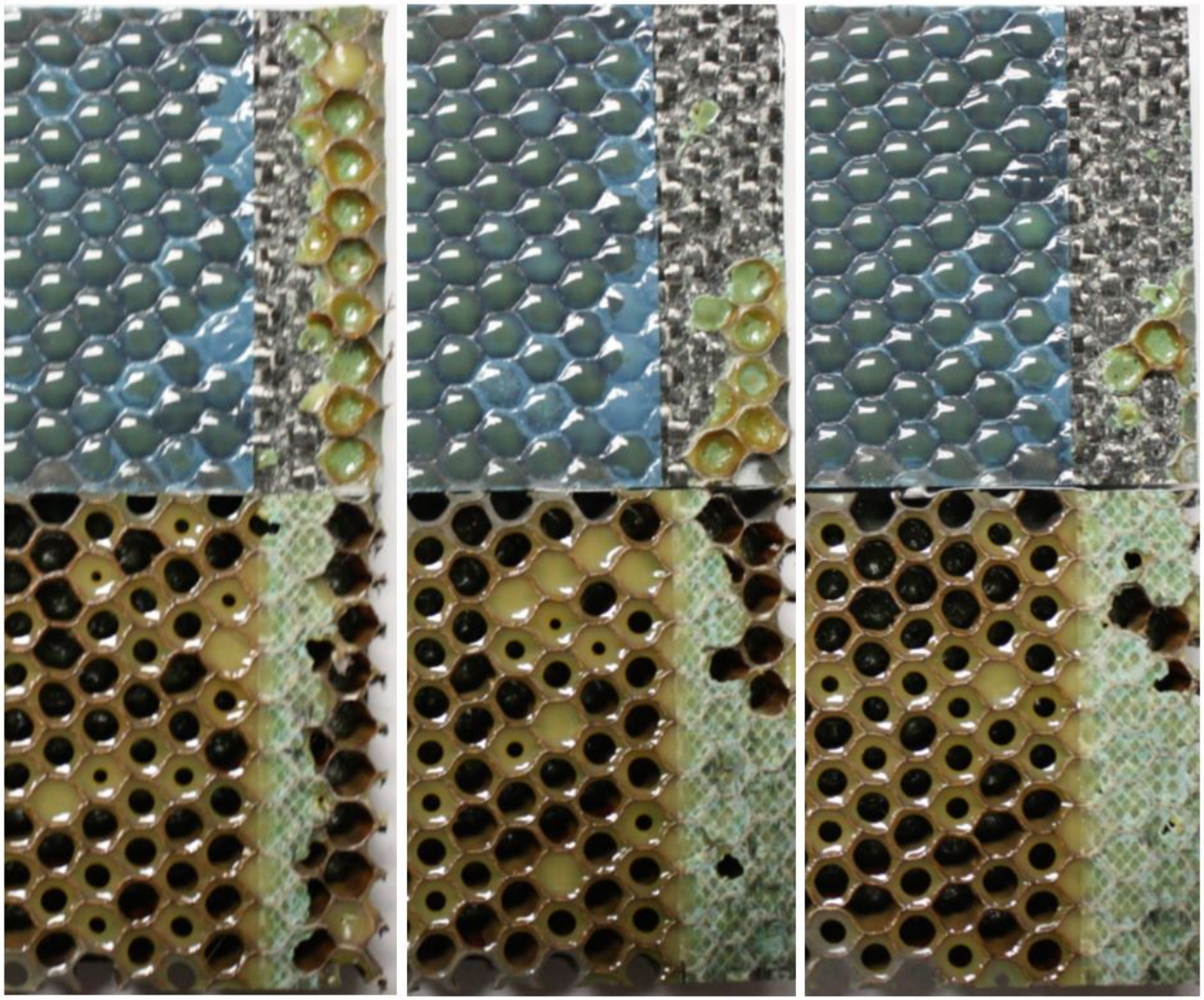

Figure C-24. Failure mode image for SDT-16-HX-3.16-3-BL-SLX-X #4, #5, and #6

C.3.2 HRH-10–3/16–3.0 FLUID-INGRESSED DATA (2.5″ PRESCRIBED CRACK)

Table C-8. Test summary for HRH-10–3/16–3.0 fluid ingressed (2.5″ prescribed crack)

Specimen	Shaping Parameter [m] English or SI	Shaping Parameter [B] English	Shaping Parameter [B] SI	Failure Mode
SDT-16-HX-3.16-3-FI-SLX-6	88.172	1.113E-06	4.465E-203	First row a mix of A, PO, and C, then C
SDT-16-HX-3.16-3-FI-SLX-7	9.773	1.047E-06	3.174E-27	First row a mix of A, PO, and C, then C
SDT-16-HX-3.16-3-FI-SLX-8	48.330	5.323E-04	5.219E-111	Primarily C with a cell in A
AVERAGE (individual)	48.758	1.782E-04	1.058E-27	
STANDARD DEVIATION	39.201	3.067E-04	1.832E-27	
COEFFICIENT OF VARIATION [%]	80.399	172.155	173.205	
AVERAGE (all)	9.068	1.585E-06	1.830E-25	
AVERAGE (interpolated)	7.396	8.004E-07	5.192E-22	

A = adhesive interface disbond failure; PO = adhesive pullout failure; C = tensile core failure

Table C-9. Test summary for HRH-10–3/16–3.0 fluid ingressed (2.5″ prescribed crack)

Specimen	Shaping Parameter [m] English or SI	Shaping Parameter [B] English	Shaping Parameter [B] SI	Failure Mode
SDT-16-HX-3.16-3-FI-SLX-1**	16.651	9.452E-04	1.061E-39	First three rows primarily A with a pocket of C, then a split between A and C
SDT-16-HX-3.16-3-FI-SLX-2**	66.826	1.115E-05	3.448E-154	First row primarily A, then C
SDT-16-HX-3.16-3-FI-SLX-3**	8.306	4.269E-07	2.518E-24	First row a mix of A and C, then C
SDT-16-HX-3.16-3-FI-SLX-4**	21.704	1.158E+03	6.020E-45	First row a mix of A, PO, and C, then C
SDT-16-HX-3.16-3-FI-SLX-5**	62.076	2.018E-10	2.832E-148	Primarily in A with a couple of cells in PO
AVERAGE** (individual)	35.113	2.316E+02	5.036E-25	
STANDARD DEVIATION	27.258	5.179E+02	1.126E-24	
COEFFICIENT OF VARIATION [%]	77.630	223.607	223.607	
AVERAGE** (all)	N/A	N/A	N/A	
AVERAGE** (interpolated)	28.134	1.586E-06	3.091E-68	

A = adhesive interface disbond failure; C = tensile core failure; PO = adhesive pullout failure

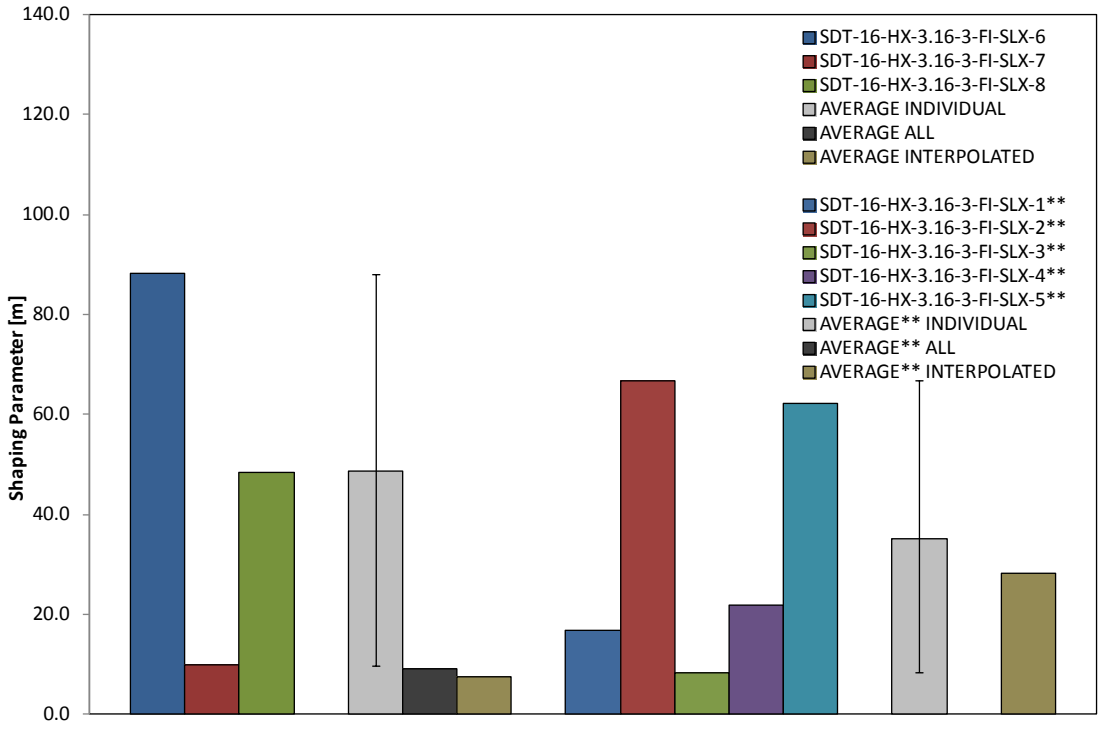

Figure C-25. Shaping parameter (*m*) for HRH-10–3/16–3.0 fluid ingressed (2.5″ prescribed crack)

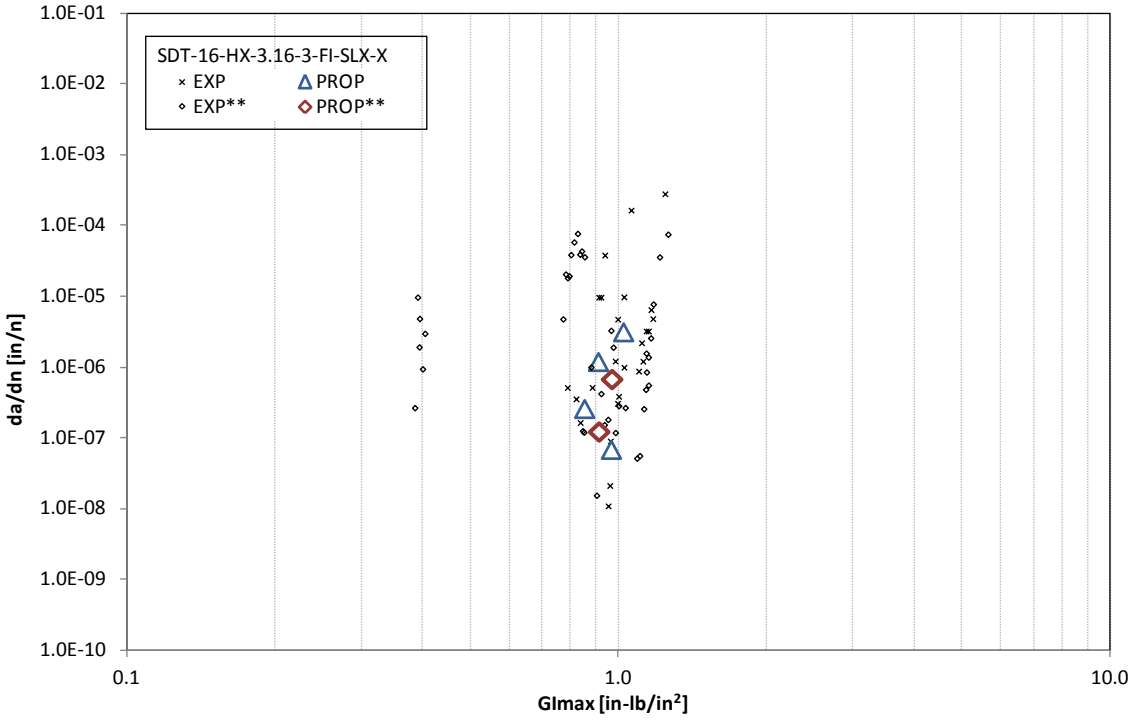

Figure C-26. Fatigue growth da/dn curve for HRH-10–3/16–3.0 fluid ingressed (2.5″prescribed crack)

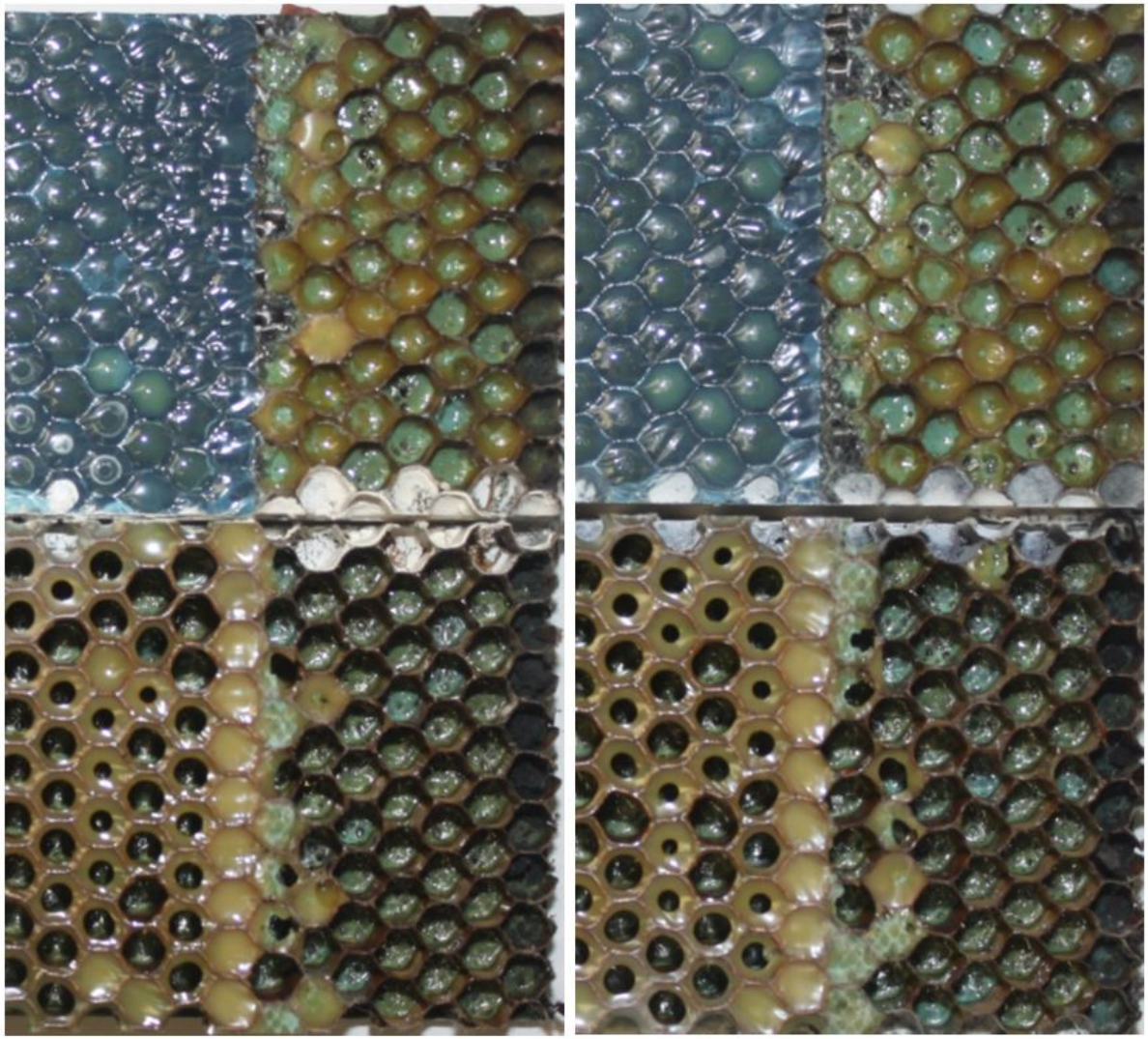

Figure C-27. Failure mode image for SDT-16-HX-3.16-3-FI-SLX-X #6 and #7

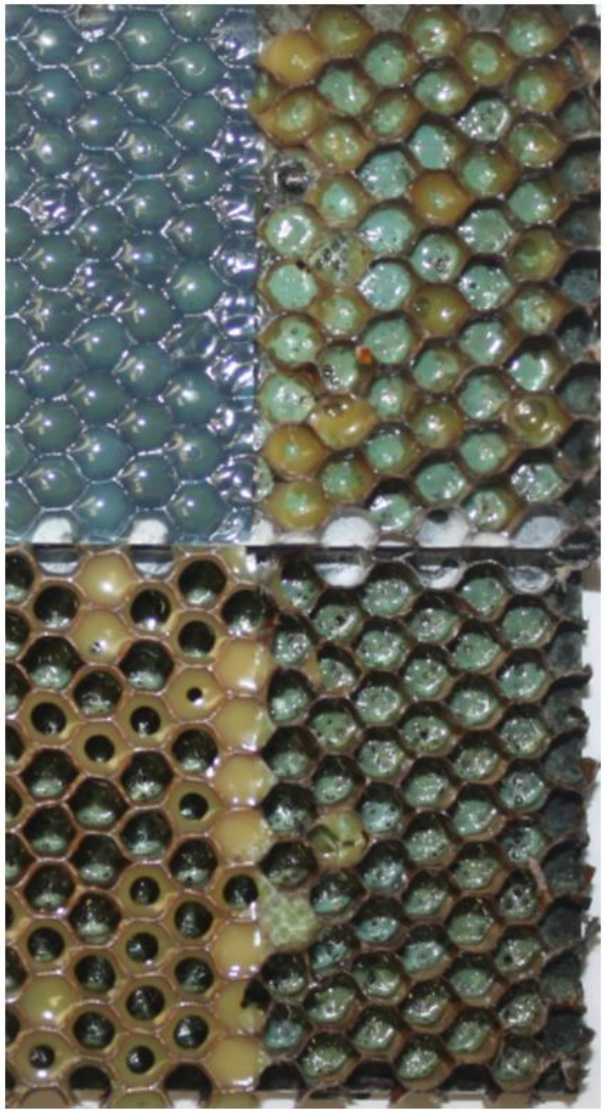

Figure C-28. Failure mode image for SDT-16-HX-3.16-3-FI-SLX-X #8

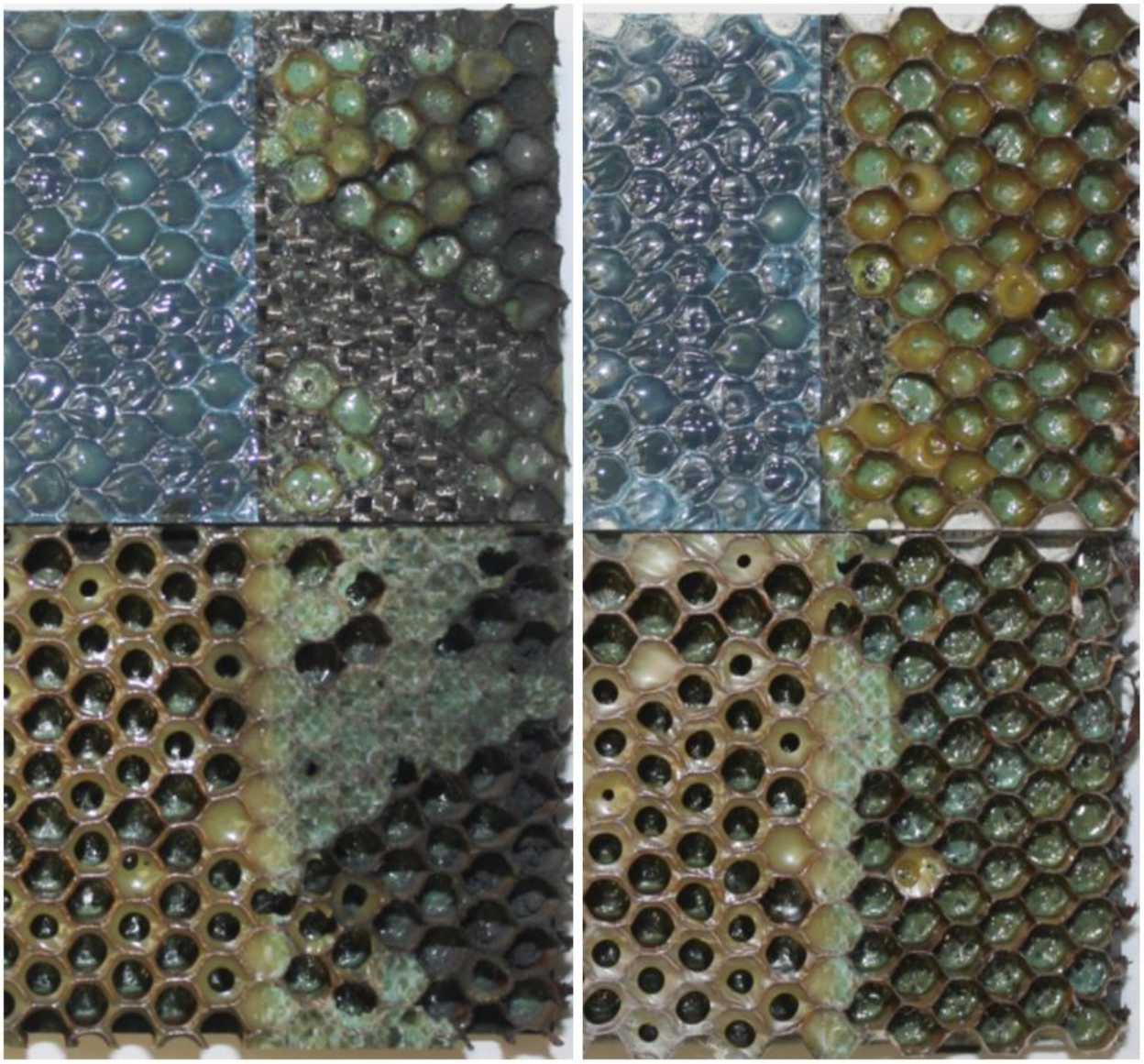

Figure C-29. Failure mode image for SDT-16-HX-3.16-3-FI-SLX-X #1 and #2****

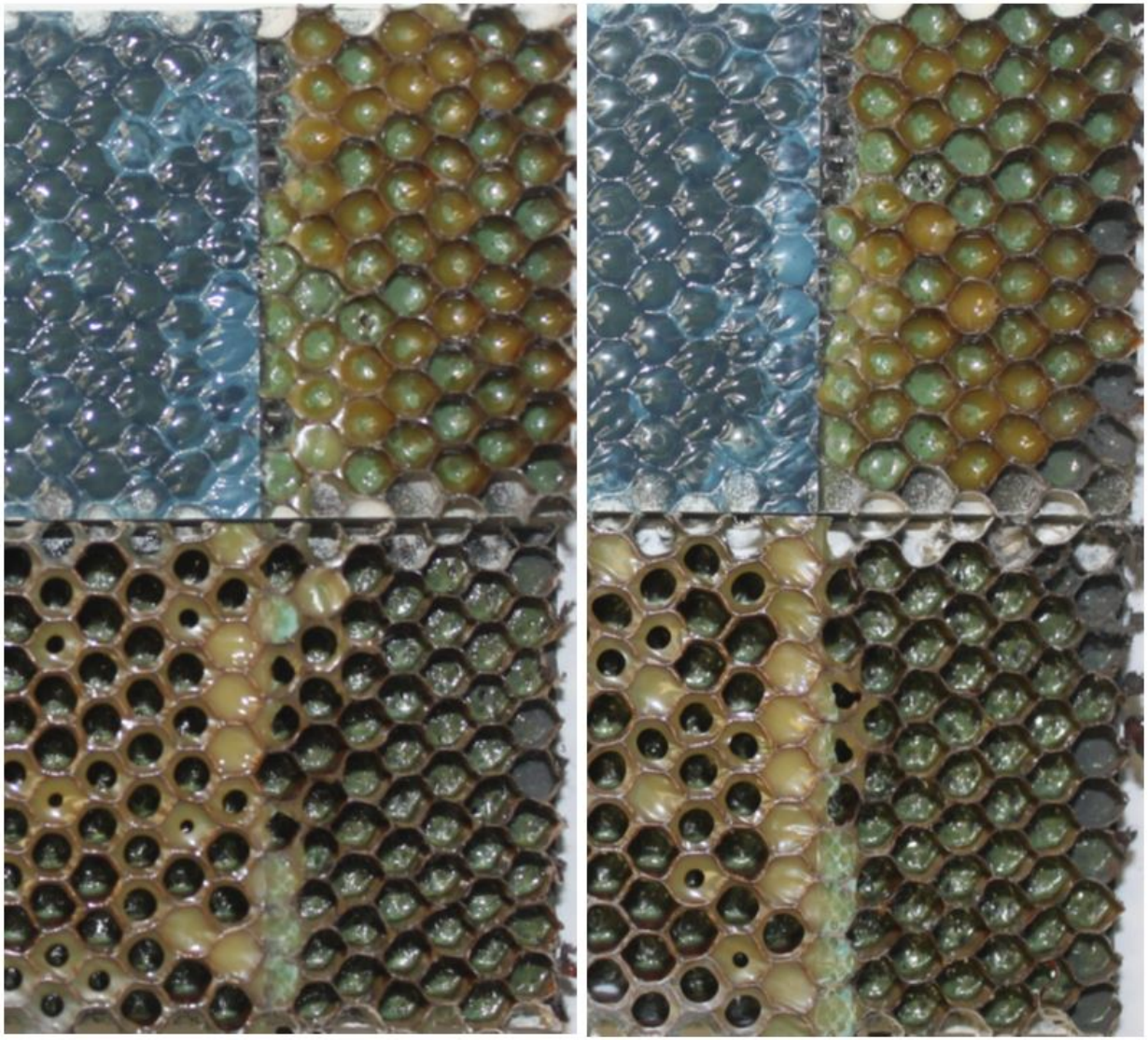

Figure C-30. Failure mode image for SDT-16-HX-3.16-3-FI-SLX-X #3 and #4****

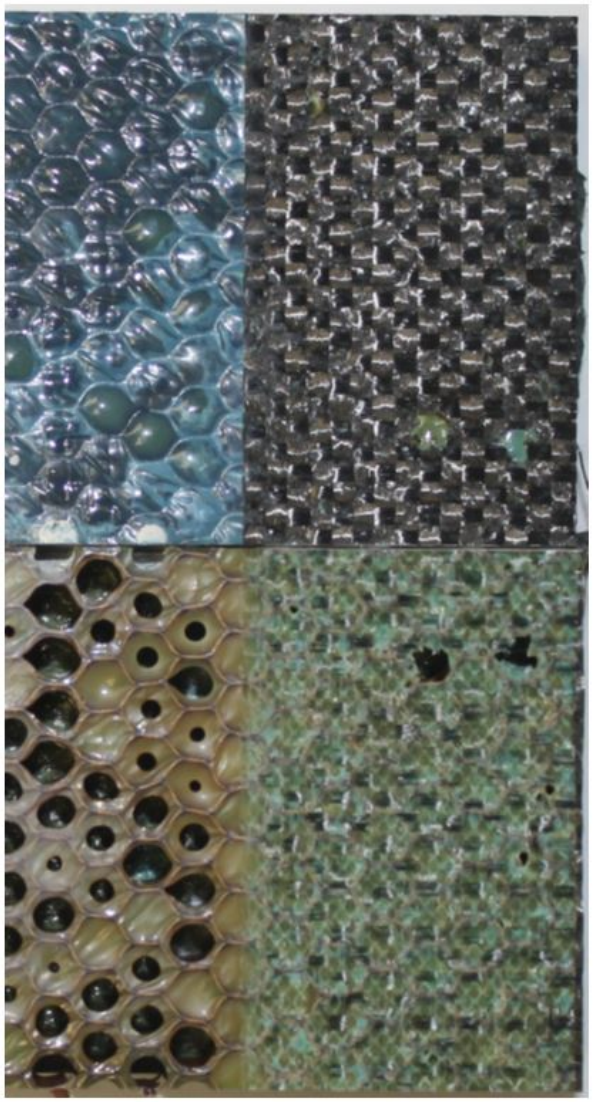

Figure C-31. Failure mode image for SDT-16-HX-3.16-3-FI-SLX-X #5**

C.4 HRH-10–3/16–6.0 DATA

C.4.1 HRH-10–3/16–6.0 BASELINE DATA (2.5″ PRESCRIBED CRACK)

Table C-10. Test summary for HRH-10–3/16–6.0 baseline (2.5″ prescribed crack)

Specimen	Shaping Parameter [m] English or SI	Shaping Parameter [B] English	Shaping Parameter [B] SI	Failure Mode
SDT-16-HX-3.16-6-BL-SLX-1	15.338	5.415E-07	5.370E-40	First three rows a mix of A and C with a couple of cells in PO, then A with a few cells in PO
SDT-16-HX-3.16-6-BL-SLX-2	14.304	6.802E-07	1.406E-37	Primarily in A with a couple of cells in PO
SDT-16-HX-3.16-6-BL-SLX-3	16.942	1.680E-08	4.204E-45	First row a mix of A and PO, then A with a cell in PO
SDT-16-HX-3.16-6-BL-SLX-4	15.813	2.963E-07	2.521E-41	Primarily in A with a couple of cells in PO
SDT-16-HX-3.16-6-BL-SLX-5	11.403	2.654E-06	1.772E-30	Primarily A with the last row in S
SDT-16-HX-3.16-6-BL-SLX-6	11.920	9.604E-07	4.425E-32	Primarily in A
AVERAGE (individual)	14.287	8.581E-07	3.027E-31	
STANDARD DEVIATION	2.209	9.370E-07	7.199E-31	
COEFFICIENT OF VARIATION [%]	15.463	109.187	237.859	
AVERAGE (all)	7.555	6.568E-07	1.875E-22	
AVERAGE (interpolated)	10.032	6.197E-07	4.921E-28	

A = adhesive interface disbond failure; C = tensile core failure; PO = adhesive pullout failure

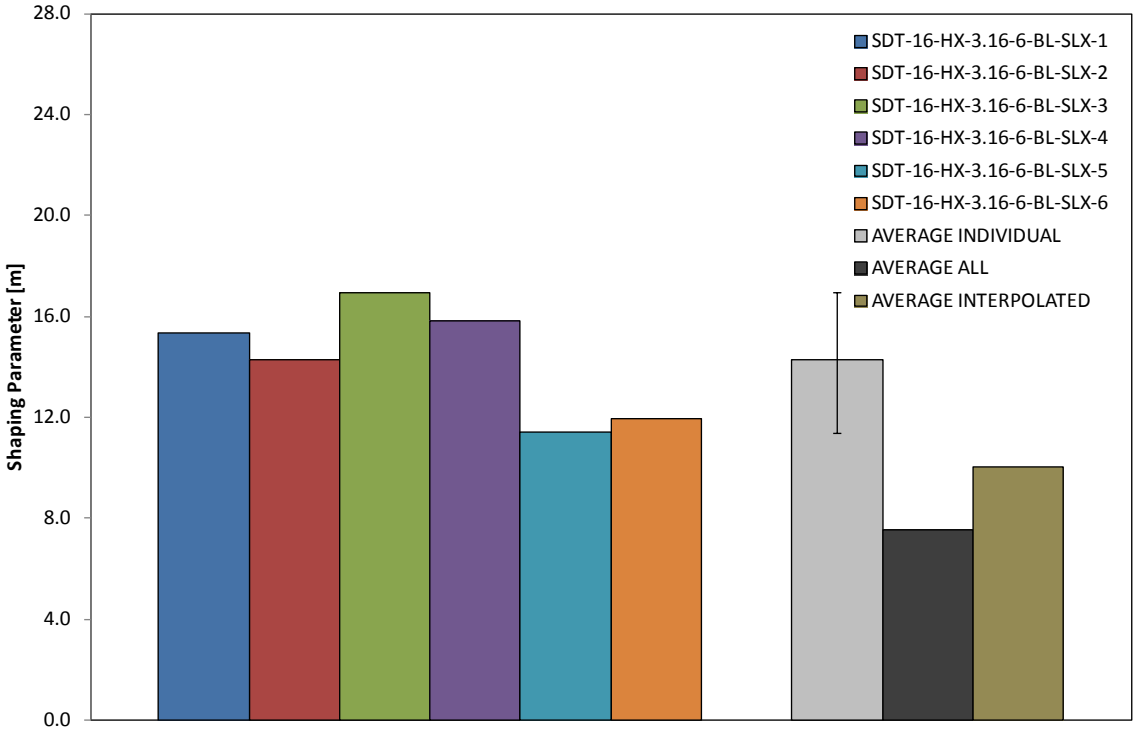

Figure C-32. Shaping parameter (*m*) for HRH-10–3/16–,6.0 baseline (2.5″ prescribed crack)

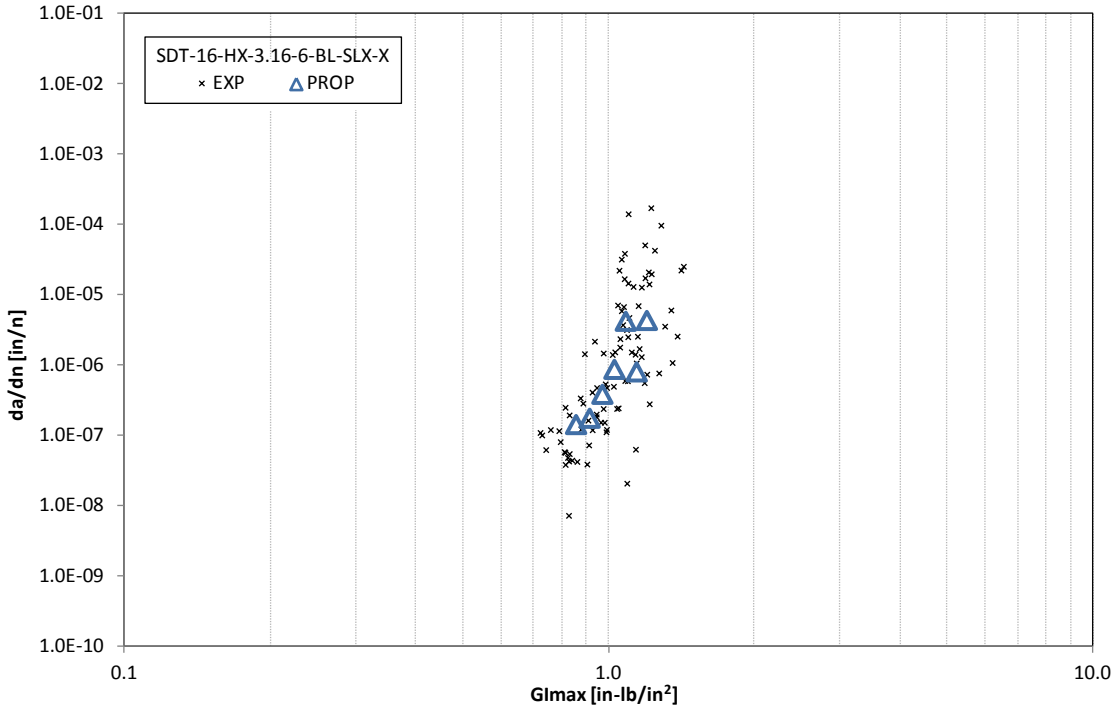

Figure C-33. Fatigue growth da/dn curve for HRH-10–3/16–6.0 baseline (2.5″ prescribed crack)

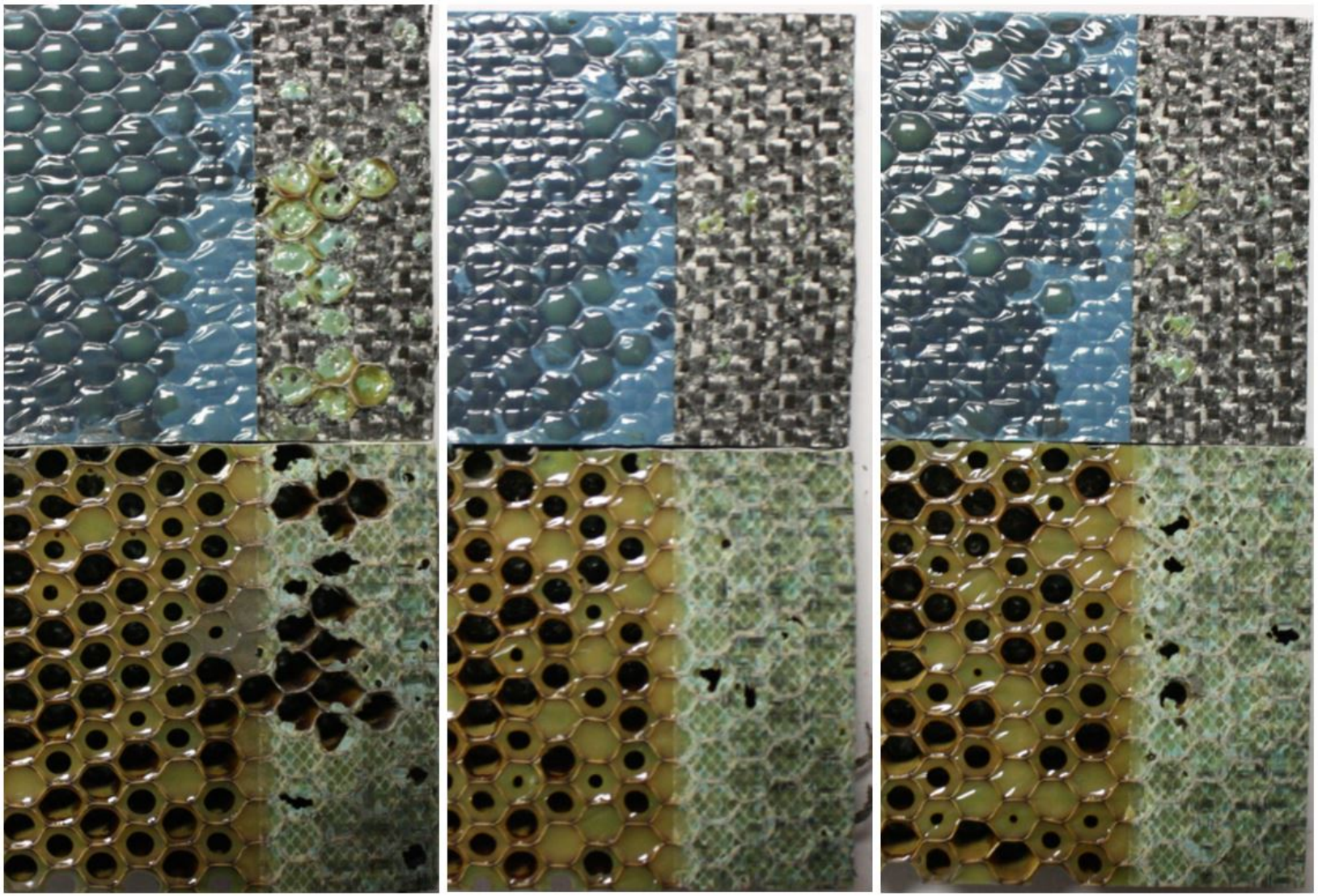

Figure C-34. Failure mode image for SDT-16-HX-3.16-6-BL-SLX-X #1, #2, and #3

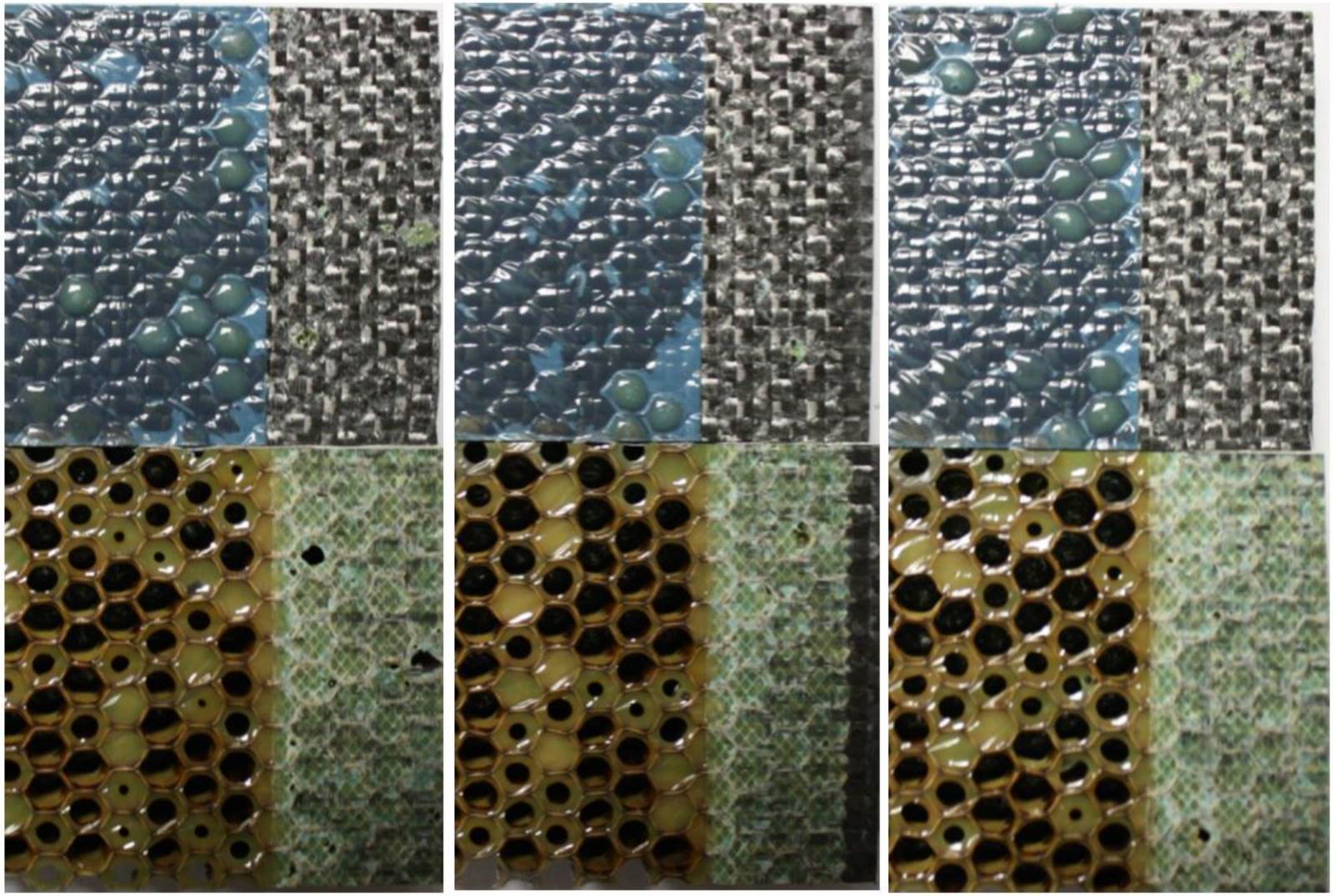

Figure C-35. Failure mode image for SDT-16-HX-3.16-6-BL-SLX-X #4, #5, and #6

C.4.2 HRH-10–3/16–6.0 FLUID-INGRESSED DATA (2.5″ PRESCRIBED CRACK)

Table C-11. Test summary for HRH-10–3/16–6.0 fluid ingressed (2.5″ prescribed crack)

Specimen	Shaping Parameter [m] English or SI	Shaping Parameter [B] English	Shaping Parameter [B] SI	Failure Mode
SDT-16-HX-3.16-6-FI-SLX-5	27.486	1.243E-07	6.909E-68	First two rows A with several cells in C, then C
SDT-16-HX-3.16-6-FI-SLX-6	38.536	9.278E-12	8.382E-97	Primarily A
SDT-16-HX-3.16-6-FI-SLX-7	36.450	7.949E-10	3.514E-90	Primarily A with a few cells in PO and a pocket of C
SDT-16-HX-3.16-6-FI-SLX-8	23.800	1.322E-09	1.397E-61	First three rows a mix of A and PO with a few cells in C, then split between A and C with a couple of cells in PO
AVERAGE (individual)	31.568	3.160E-08	3.492E-62	
STANDARD DEVIATION	7.057	6.178E-08	6.984E-62	
COEFFICIENT OF VARIATION [%]	22.354	195.521	200.000	
AVERAGE (all)	12.562	8.288E-08	1.390E-34	
AVERAGE (interpolated)	11.570	8.149E-08	2.299E-32	

A = adhesive interface disbond failure; C = tensile core failure; PO = adhesive pullout failure

Table C-12. Test summary for HRH-10–3/16–6.0 fluid ingressed (2.5″ prescribed crack)

Specimen	Shaping Parameter [m] English or SI	Shaping Parameter [B] English	Shaping Parameter [B] SI	Failure Mode
SDT-16-HX-3.16-6-FI-SLX-1**	43.033	2.992E-05	2.199E-100	First row split between A and C with a cell in PO, then C
SDT-16-HX-3.16-6-FI-SLX-2**	99.749	5.566E-22	2.390E-244	Primarily A with a cell in PO
SDT-16-HX-3.16-6-FI-SLX-3**	66.378	1.335E+08	4.190E-140	Primarily A
SDT-16-HX-3.16-6-FI-SLX-4**	23.486	3.016E-08	1.575E-59	Primarily A with a cell in PO
AVERAGE** (individual)	58.162	3.338E+07	3.937E-60	
STANDARD DEVIATION	32.804	6.676E+07	7.873E-60	
COEFFICIENT OF VARIATION [%]	56.401	200.000	200.000	
AVERAGE** (all)	N/A	N/A	N/A	
AVERAGE** (interpolated)	N/A	N/A	N/A	

A = adhesive interface disbond failure; C = tensile core failure; PO = adhesive pullout failure

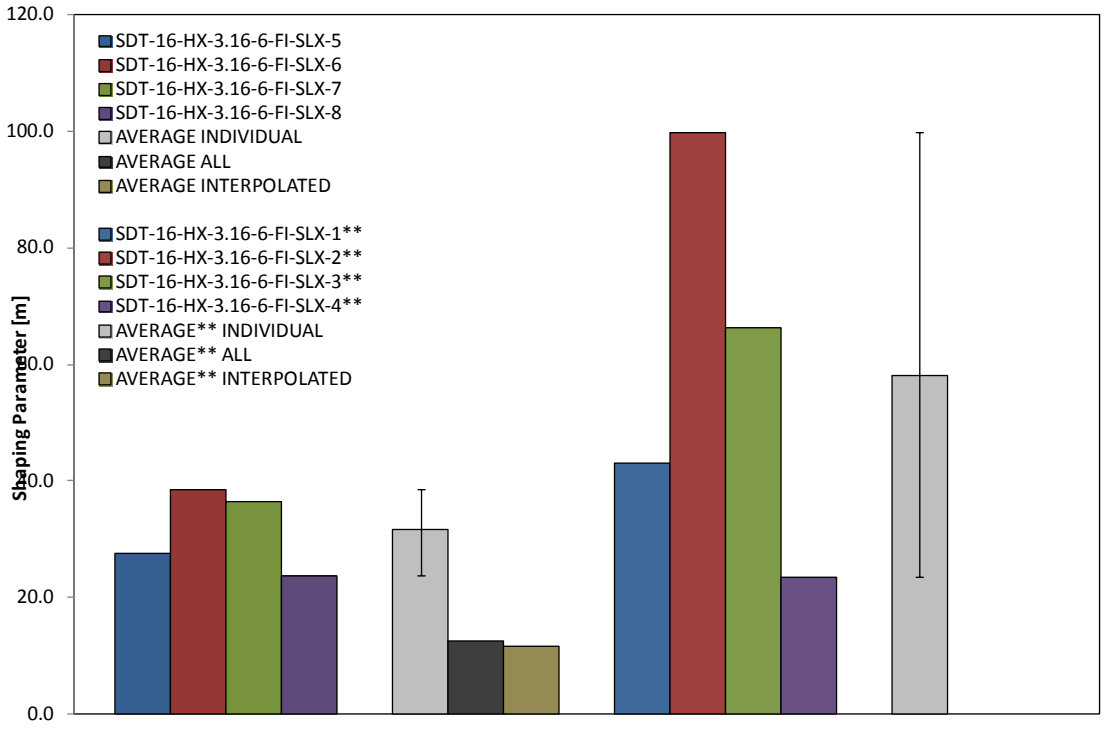

Figure C-36. Shaping parameter (*m*) for HRH-10–3/16–6.0 fluid ingressed (2.5″ prescribed crack)

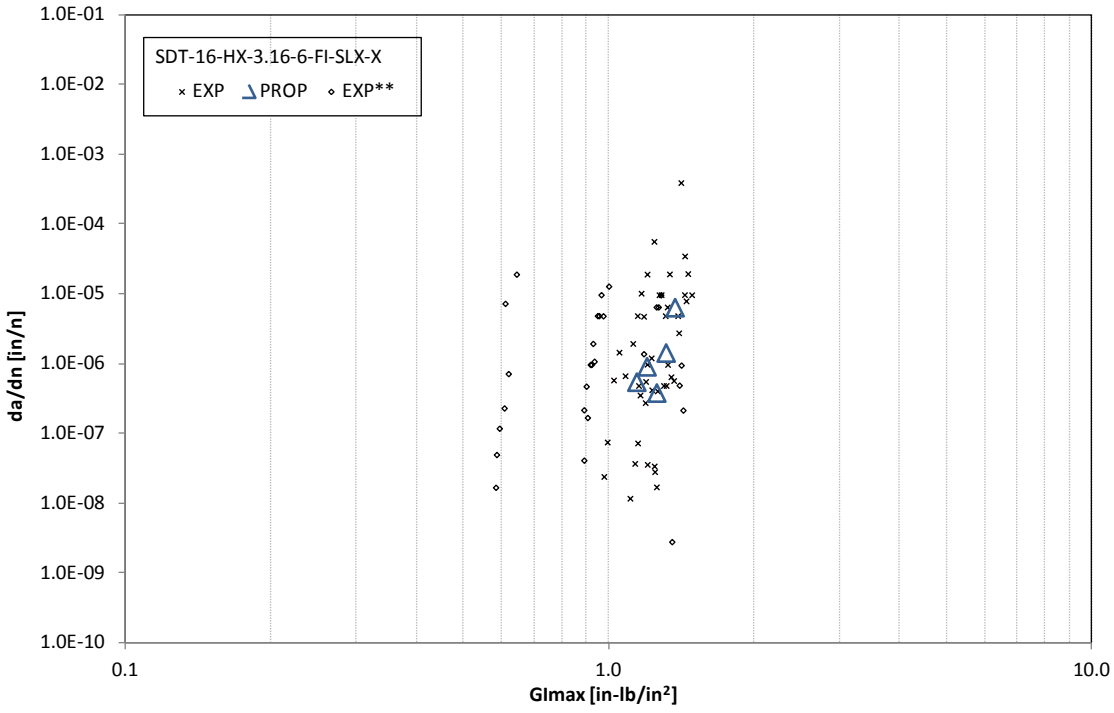

Figure C-37. Fatigue growth da/dn curve for HRH-10–3/16–6.0 fluid ingressed (2.5″ prescribed crack)

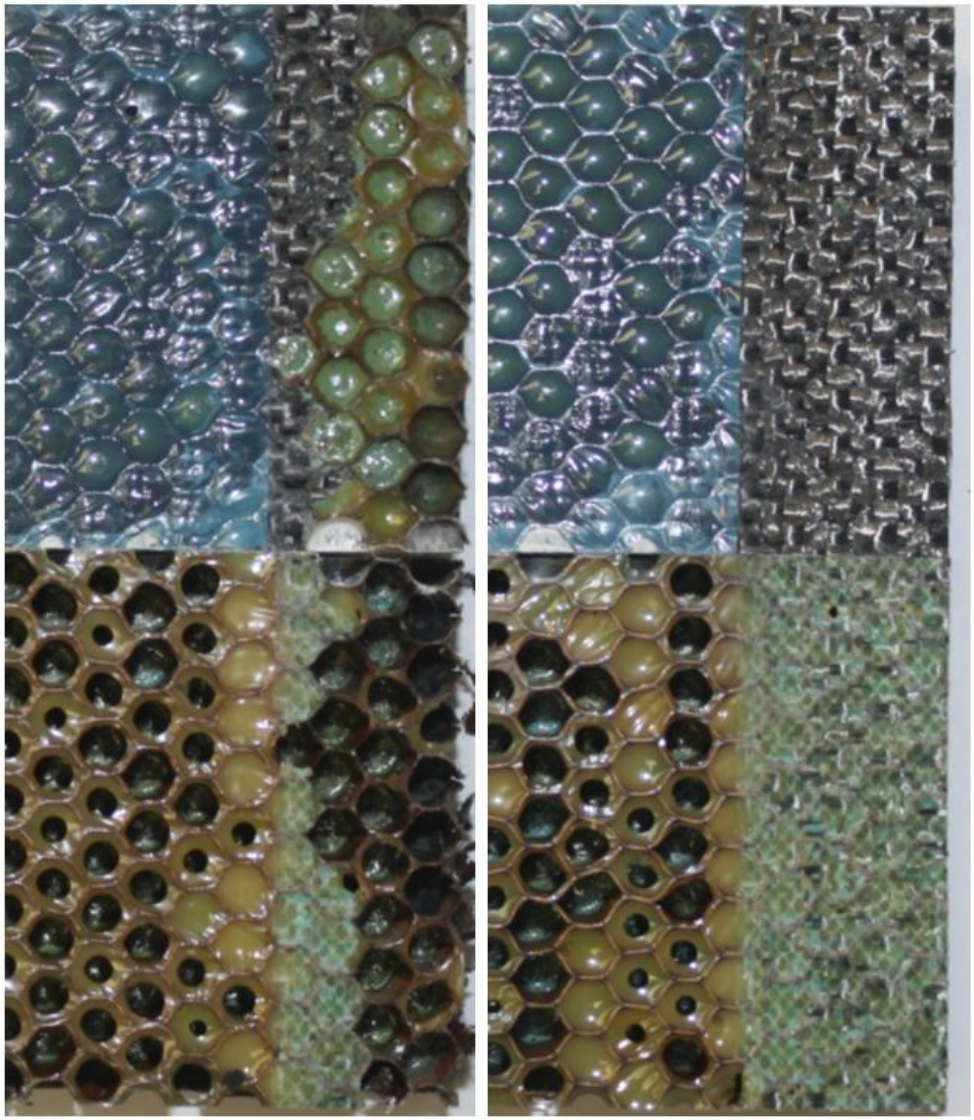

Figure C-38. Failure mode image for SDT-16-HX-3.16-6-FI-SLX-X #5 and #6

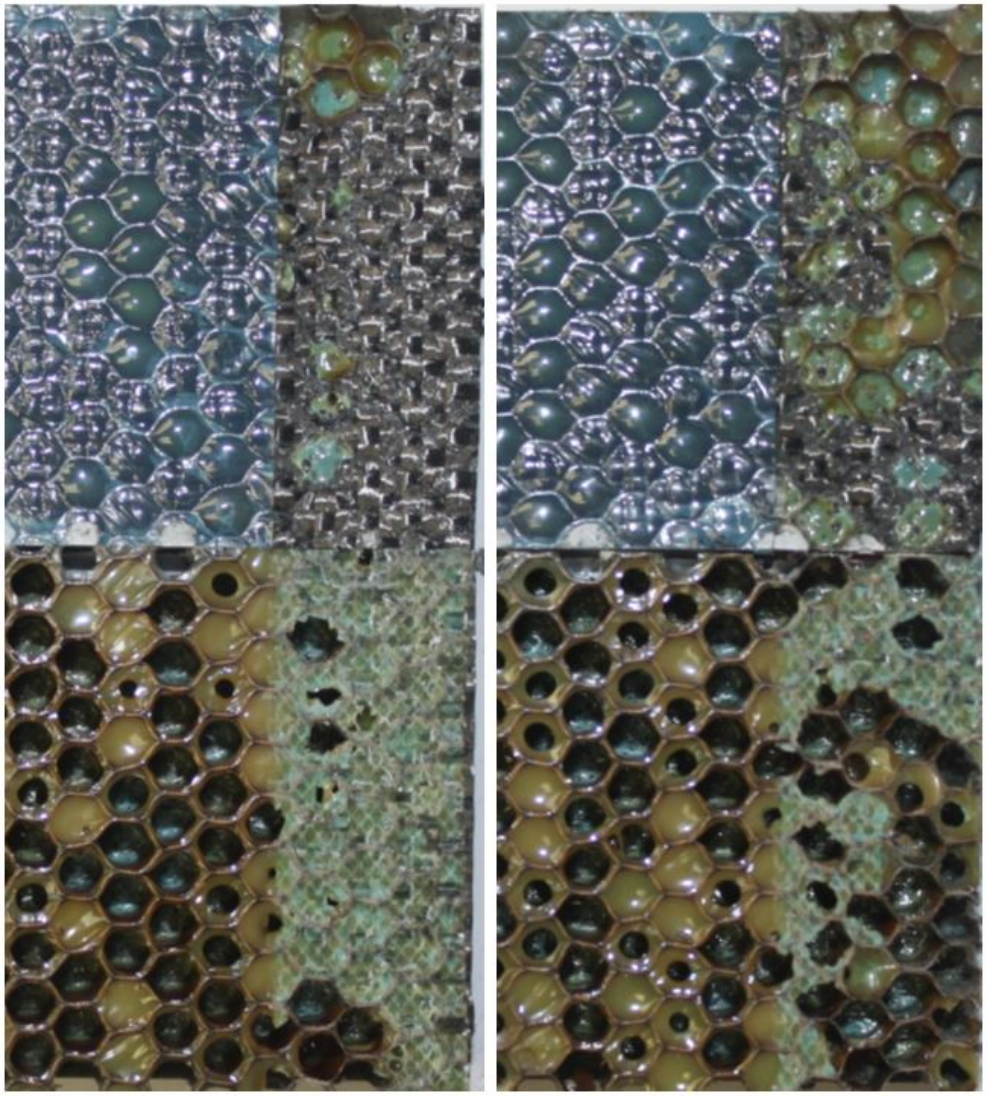

Figure C-39. Failure mode image for SDT-16-HX-3.16-6-FI-SLX-X #7 and #8

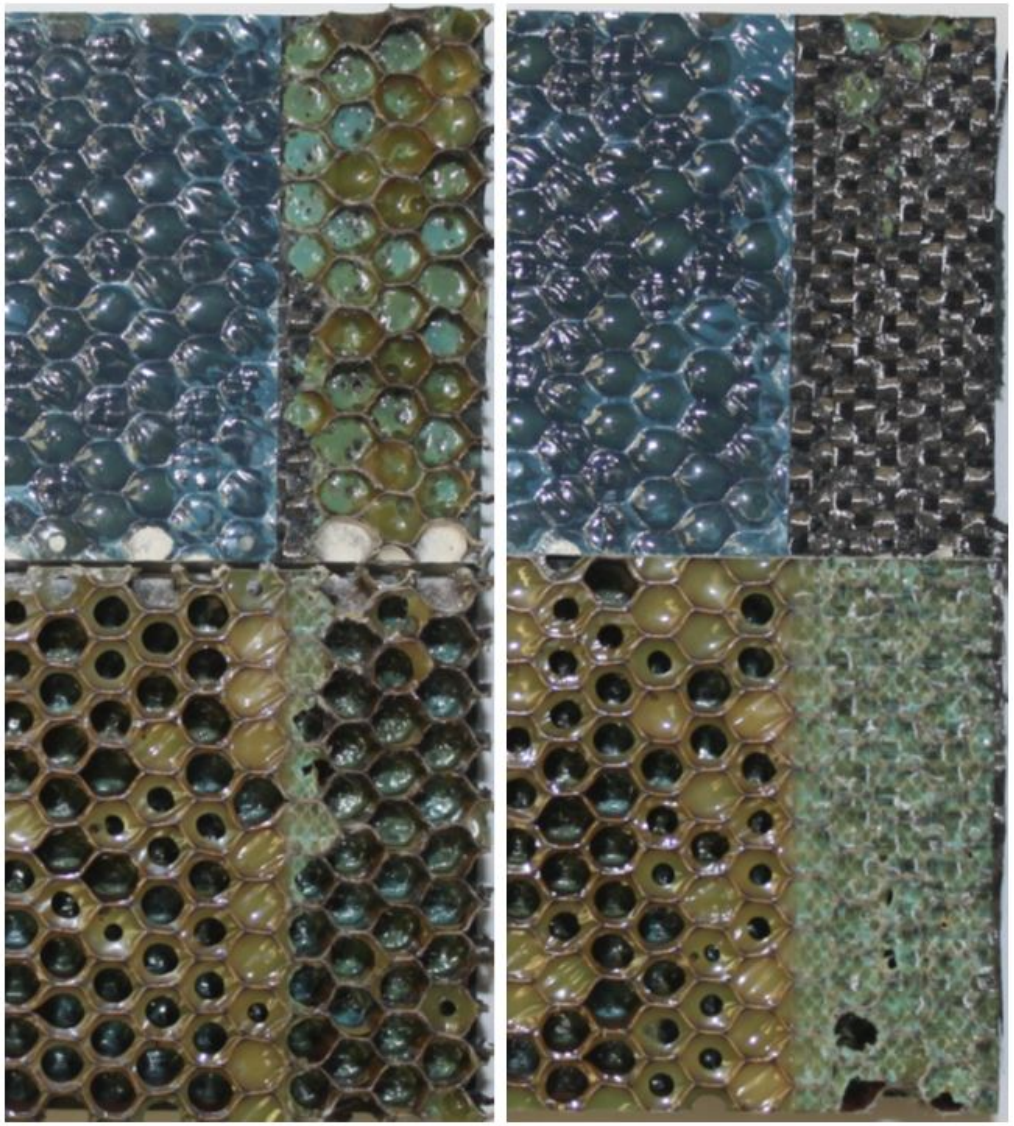

Figure C-40. Failure mode image for SDT-16-HX-3.16-6-FI-SLX-X #1 and #2****

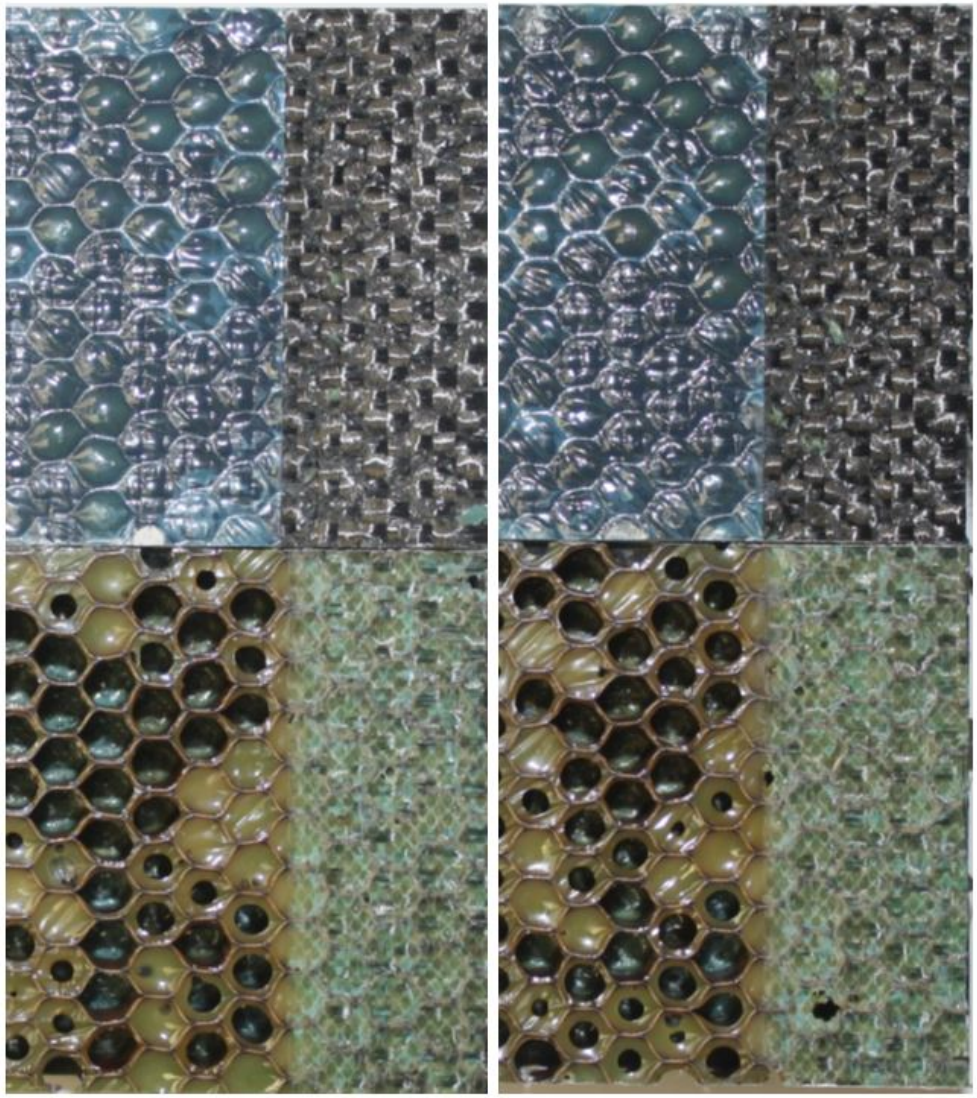

Figure C-41. Failure mode image for SDT-16-HX-3.16-6-FI-SLX-X #3 and #4****

C.5 HRH-10–3/8–3.0 DATA

C.5.1 HRH-10–3/8–3.0 BASELINE DATA (2.5″ PRESCRIBED CRACK)

Table C-13. Test summary for HRH-10–3/8–3.0 baseline (2.5″ prescribed crack)

Specimen	Shaping Parameter [m] English or SI	Shaping Parameter [B] English	Shaping Parameter [B] SI	Failure Mode
SDT-16-HX-3.8-3-BL-SLX-1	16.370	2.070E-07	9.911E-43	Mix of A and PO
SDT-16-HX-3.8-3-BL-SLX-2	22.753	7.018E-04	1.618E-53	Mix of A and PO
SDT-16-HX-3.8-3-BL-SLX-3	20.611	4.238E-03	6.215E-48	Initially A, transitioning into PO
SDT-16-HX-3.8-3-BL-SLX-4	22.762	8.248E-04	1.808E-53	Primarily A with a couple of cells in PO
SDT-16-HX-3.8-3-BL-SLX-5	28.451	2.776E-02	1.055E-64	Primarily A with a couple of cells in PO
SDT-16-HX-3.8-3-BL-SLX-6	27.541	3.739E-03	1.557E-63	Primarily A with a couple of cells in PO
AVERAGE (individual)	23.081	6.211E-03	1.652E-43	
STANDARD DEVIATION	4.474	1.070E-02	4.046E-43	
COEFFICIENT OF VARIATION [%]	19.383	172.273	244.947	
AVERAGE (all)	4.136	4.631E-06	6.193E-14	
AVERAGE (interpolated)	14.947	1.590E-04	1.188E-36	

A = adhesive interface disbond failure; PO = adhesive pullout failure

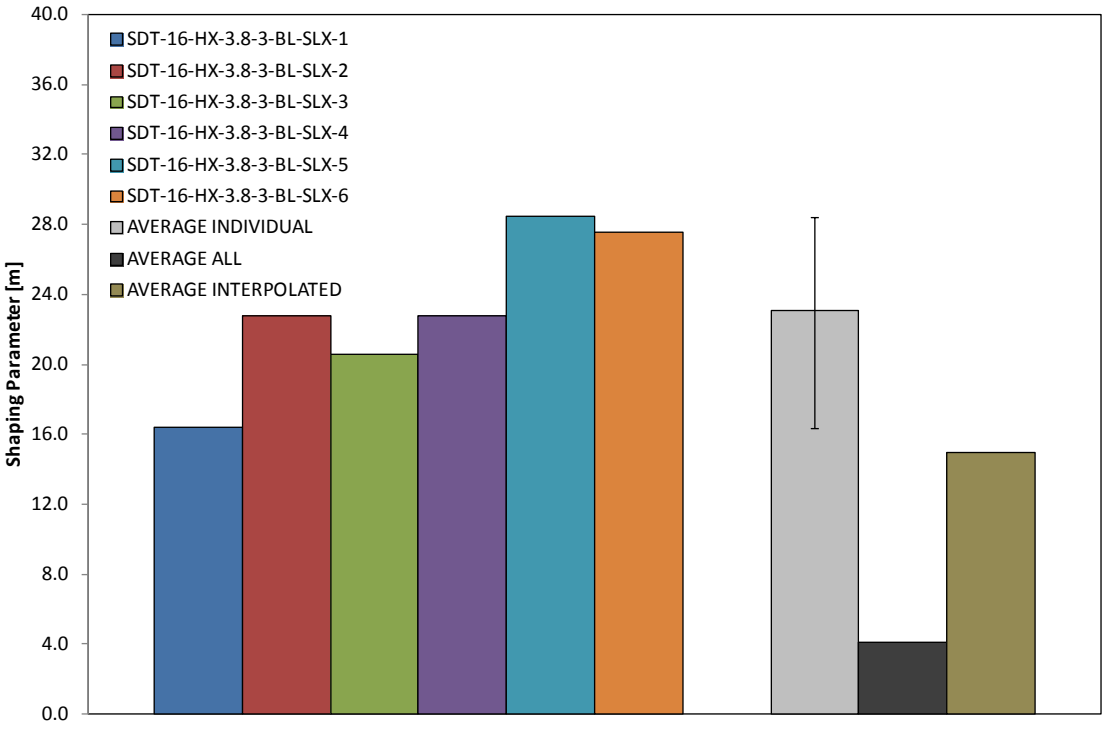

Figure C-42. Shaping parameter (*m*) for HRH-10–3/8–3.0 baseline (2.5″ prescribed crack)

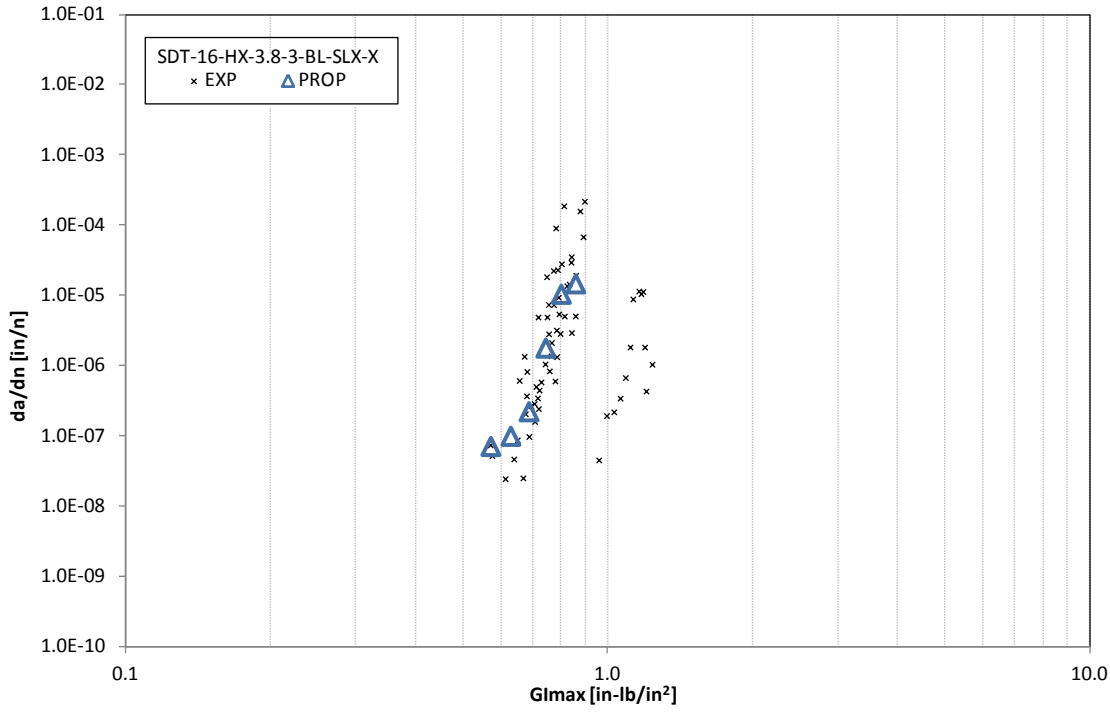

Figure C-43. Fatigue growth da/dn curve for HRH-10–3/8–3.0 baseline (2.5″ prescribed crack)

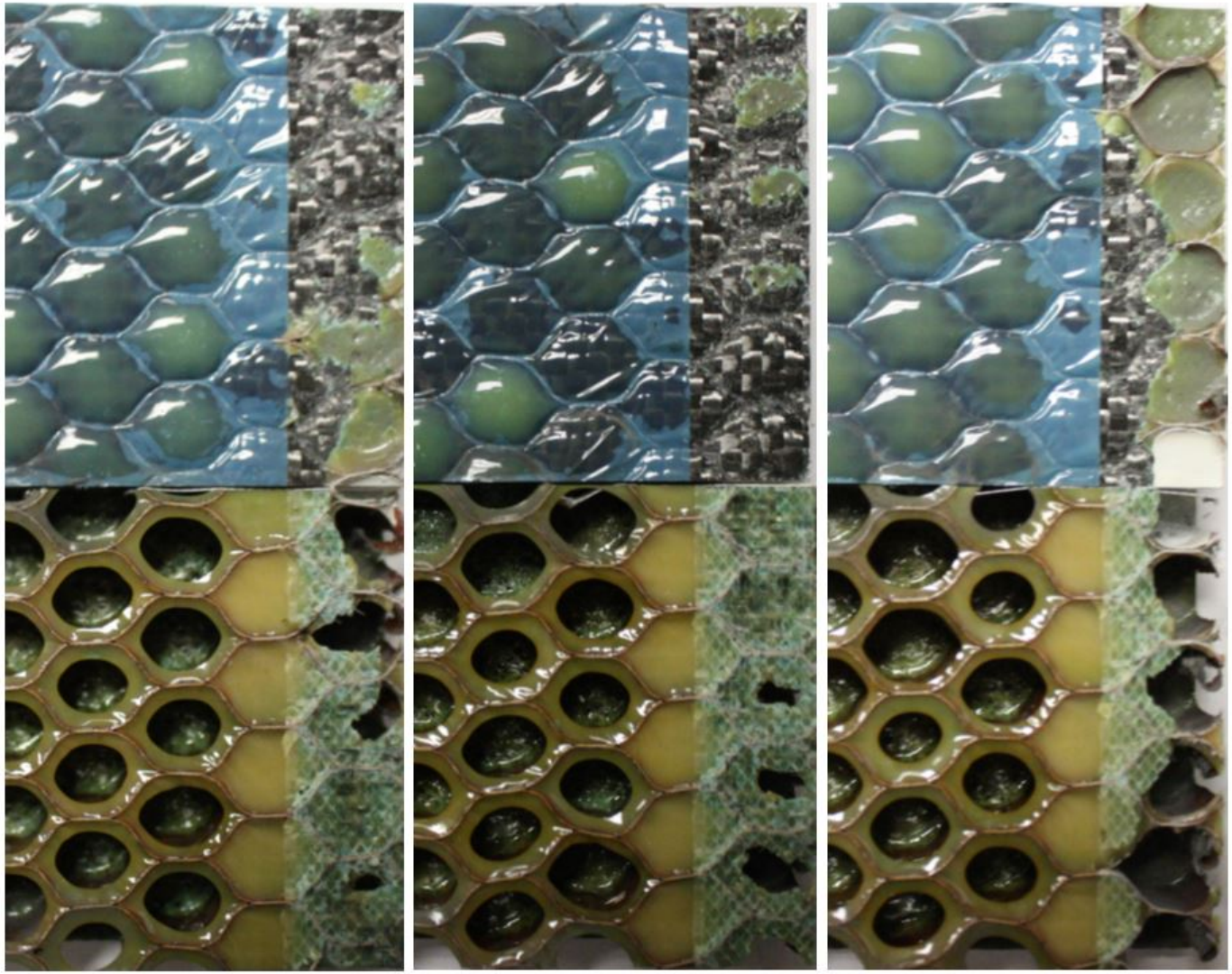

Figure C-44. Failure mode image for SDT-16-HX-3.8-3-BL-SLX-X #1, #2, and #3

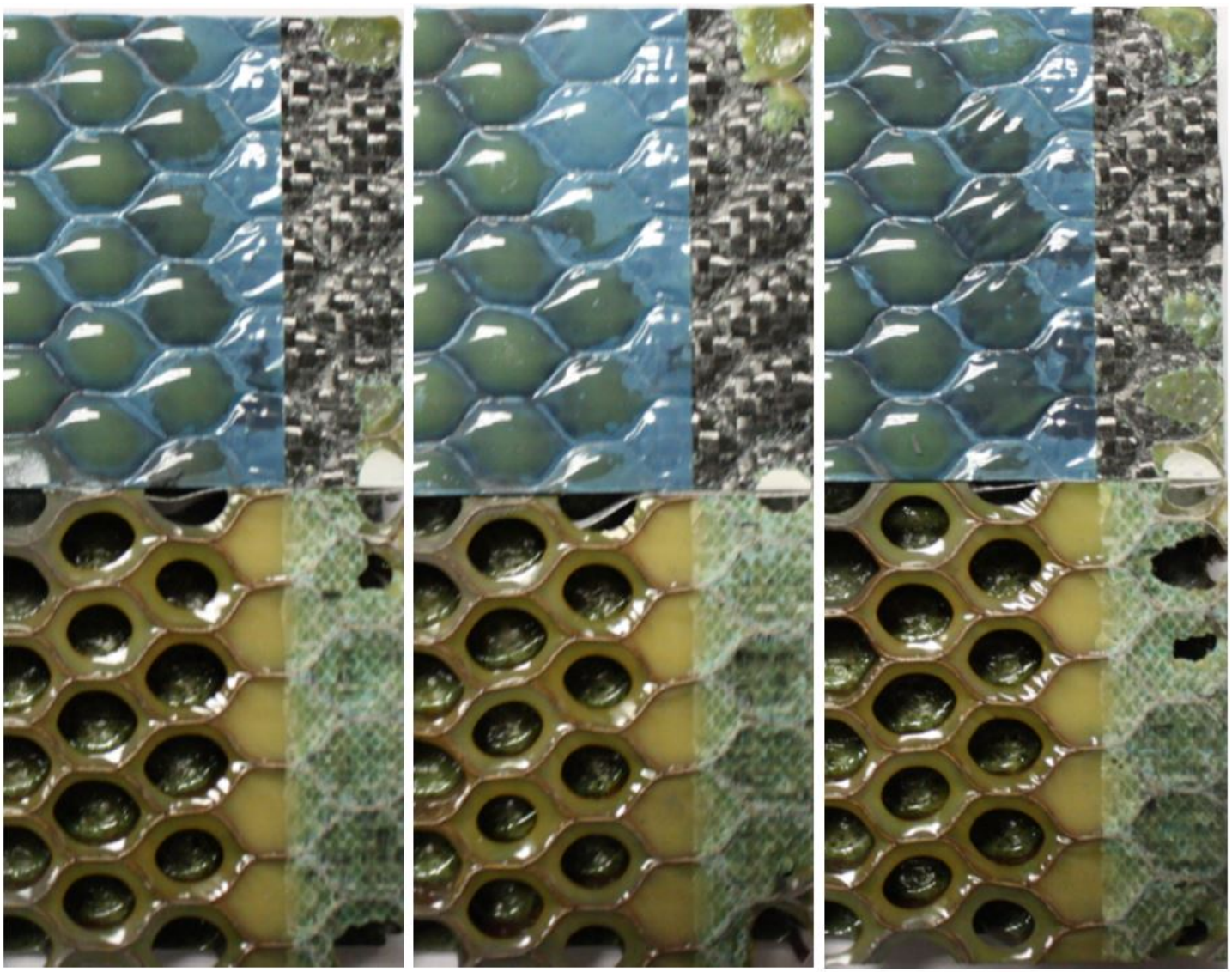

Figure C-45. Failure mode image for SDT-16-HX-3.8-3-BL-SLX-X #4, #5, and #6

C.5.2 HRH-10–3/8–3.0 FLUID-INGRESSED DATA (2.5″ PRESCRIBED CRACK)

Table C-14. Test summary for HRH-10–3/8–3.0 fluid ingressed (2.5″ prescribed crack)

Specimen	Shaping Parameter [m] English or SI	Shaping Parameter [B] English	Shaping Parameter [B] SI	Failure Mode
SDT-16-HX-3.8-3-FI-SLX-1	11.149	1.380E-05	3.412E-29	Front half of first row is A or PO, then C
SDT-16-HX-3.8-3-FI-SLX-2	60.461	1.748E-12	1.029E-146	Front half of first row is A or PO, then C
SDT-16-HX-3.8-3-FI-SLX-3	14.042	4.124E-06	3.300E-36	Front half of first row is A or PO, then C
SDT-16-HX-3.8-3-FI-SLX-4	152.130	2.109E+55	2.765E-285	Front half of first row is A or PO, then C
SDT-16-HX-3.8-3-FI-SLX-5	15.703	4.116E-07	6.185E-41	Front half of first row is A or PO, then C
SDT-16-HX-3.8-3-FI-SLX-6	4.173	2.422E-06	2.680E-14	Front half of first row is A or PO, then C
AVERAGE (individual)	42.943	3.515E+54	4.467E-15	
STANDARD DEVIATION	57.131	8.610E+54	1.094E-14	
COEFFICIENT OF VARIATION [%]	133.040	244.949	244.949	
AVERAGE (all)	1.803	2.138E-06	4.910E-09	
AVERAGE (interpolated)	11.481	1.209E-05	5.381E-30	

A = adhesive interface disbond failure; PO = adhesive pullout failure; C = tensile core failure

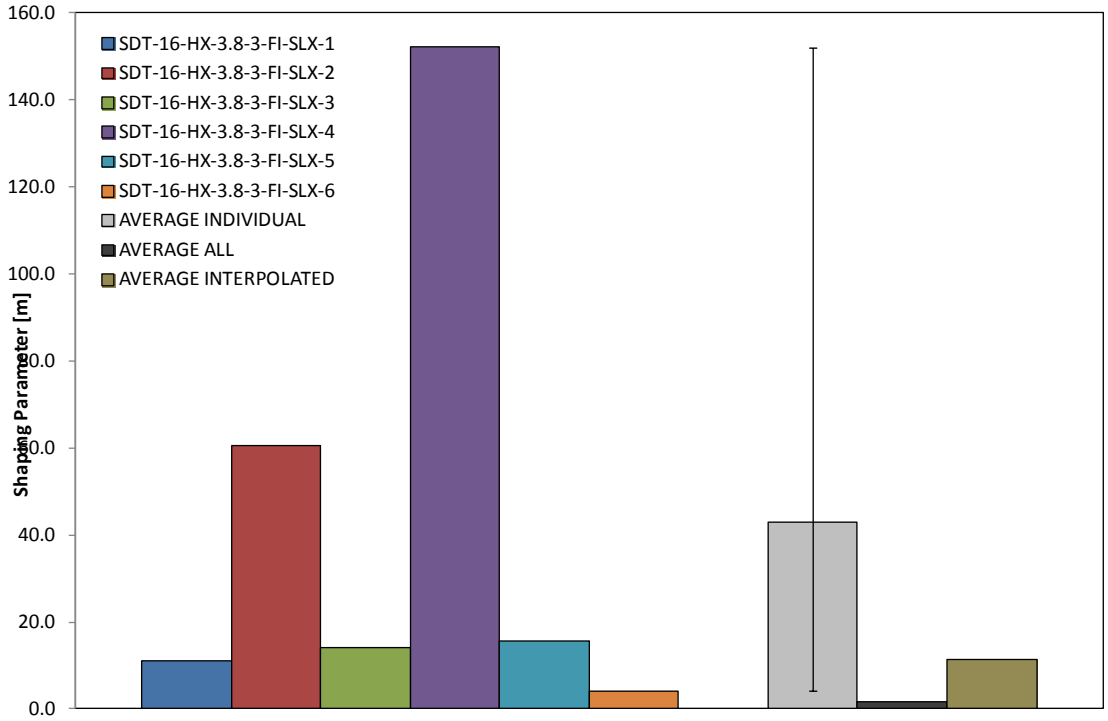

Figure C-46. Shaping parameter (*m*) for HRH-10–3/8–3.0 fluid ingressed (2.5″ prescribed crack)

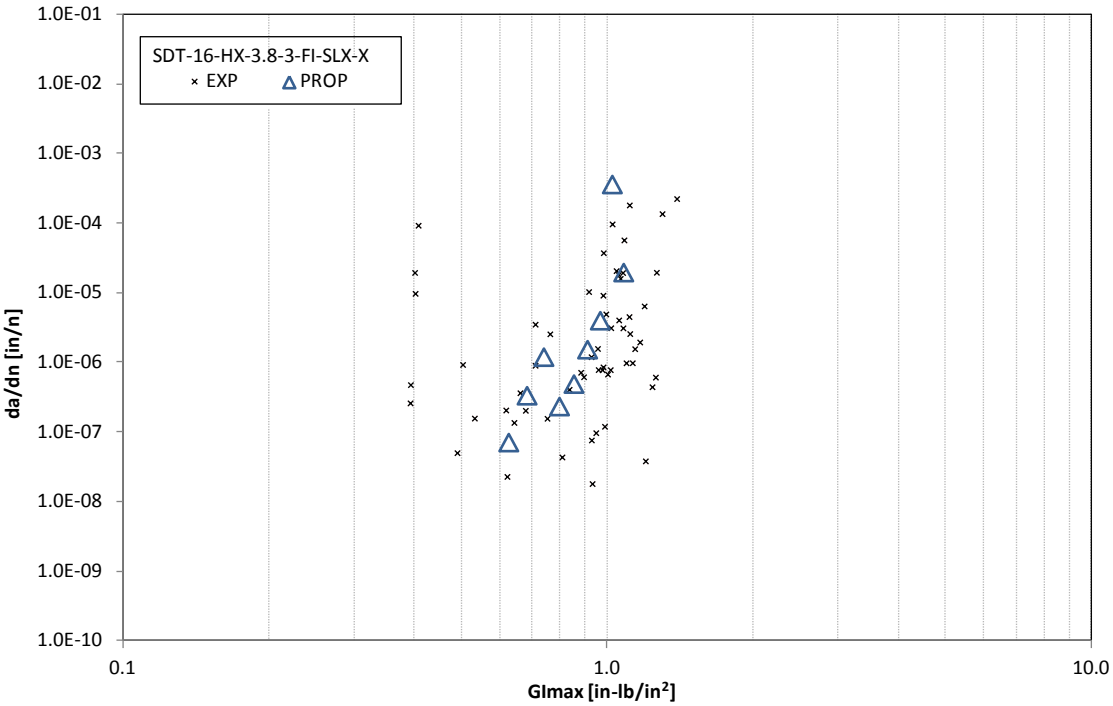

Figure C-47. Fatigue growth da/dn curve for HRH-10–3/8–3.0 fluid ingressed (2.5″ prescribed crack)

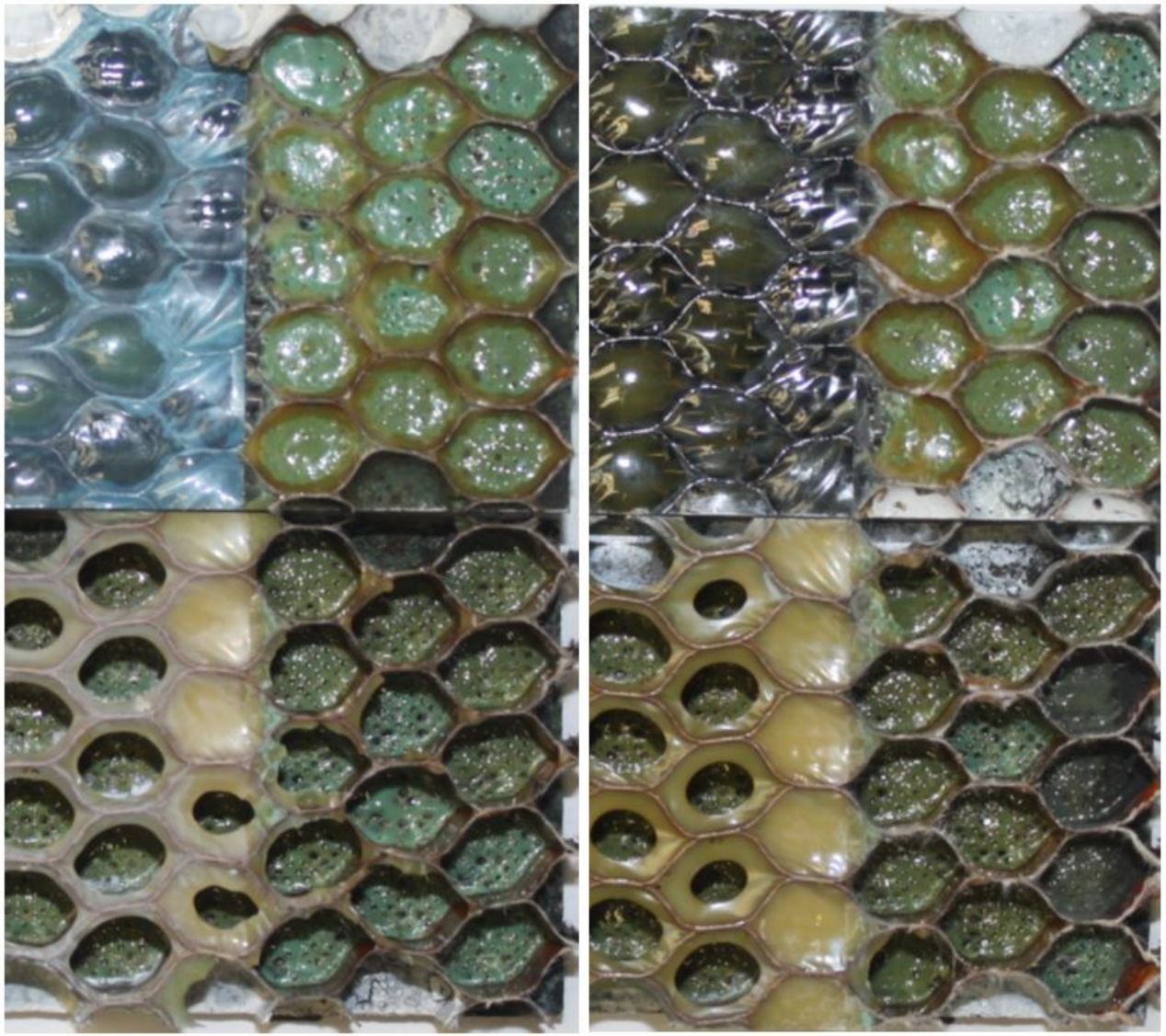

Figure C-48. Failure mode image for SDT-16-HX-3.8-3-FI-SLX-X #1 and #2

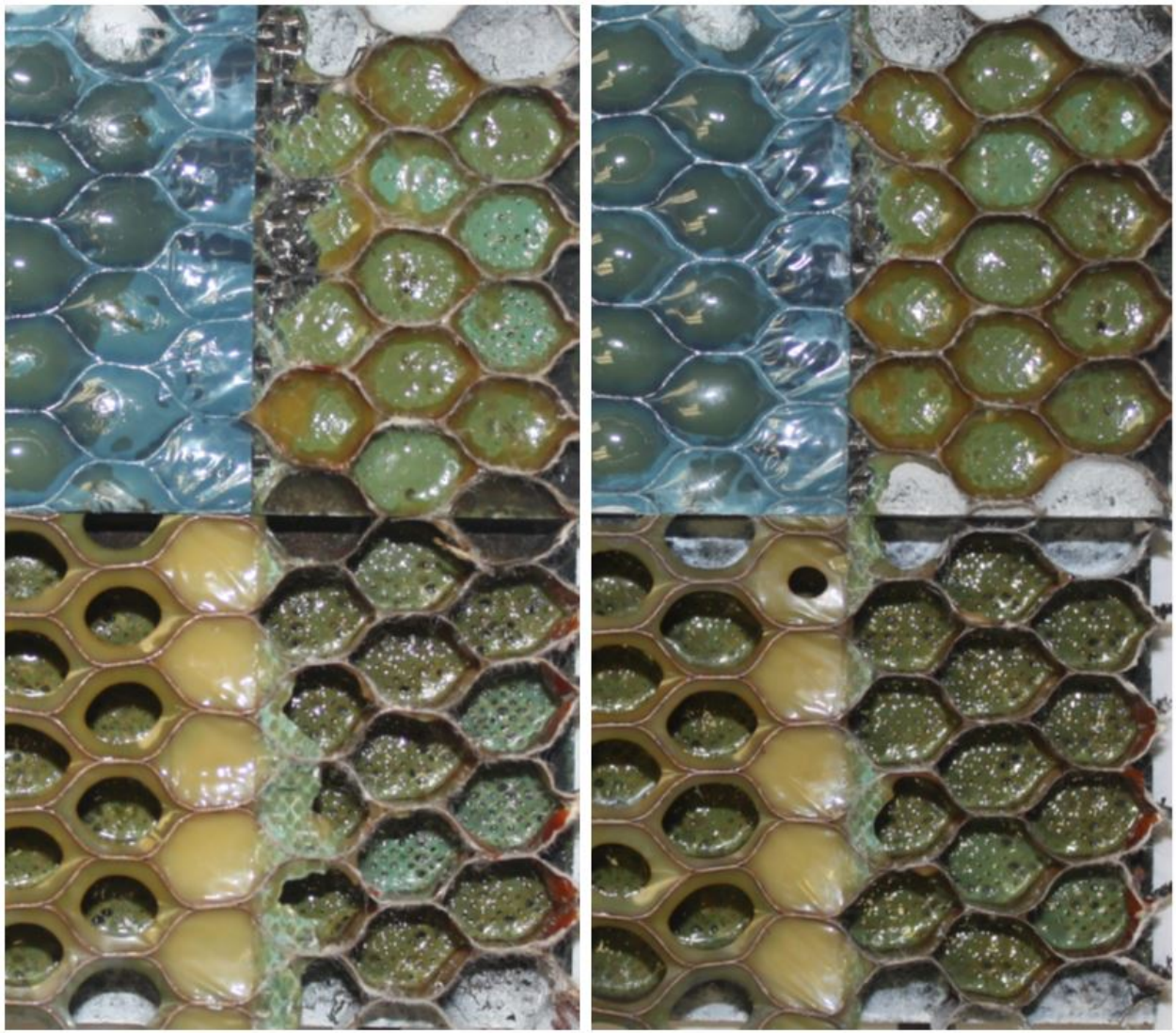

Figure C-49. Failure mode image for SDT-16-HX-3.8-3-FI-SLX-X #3 and #4

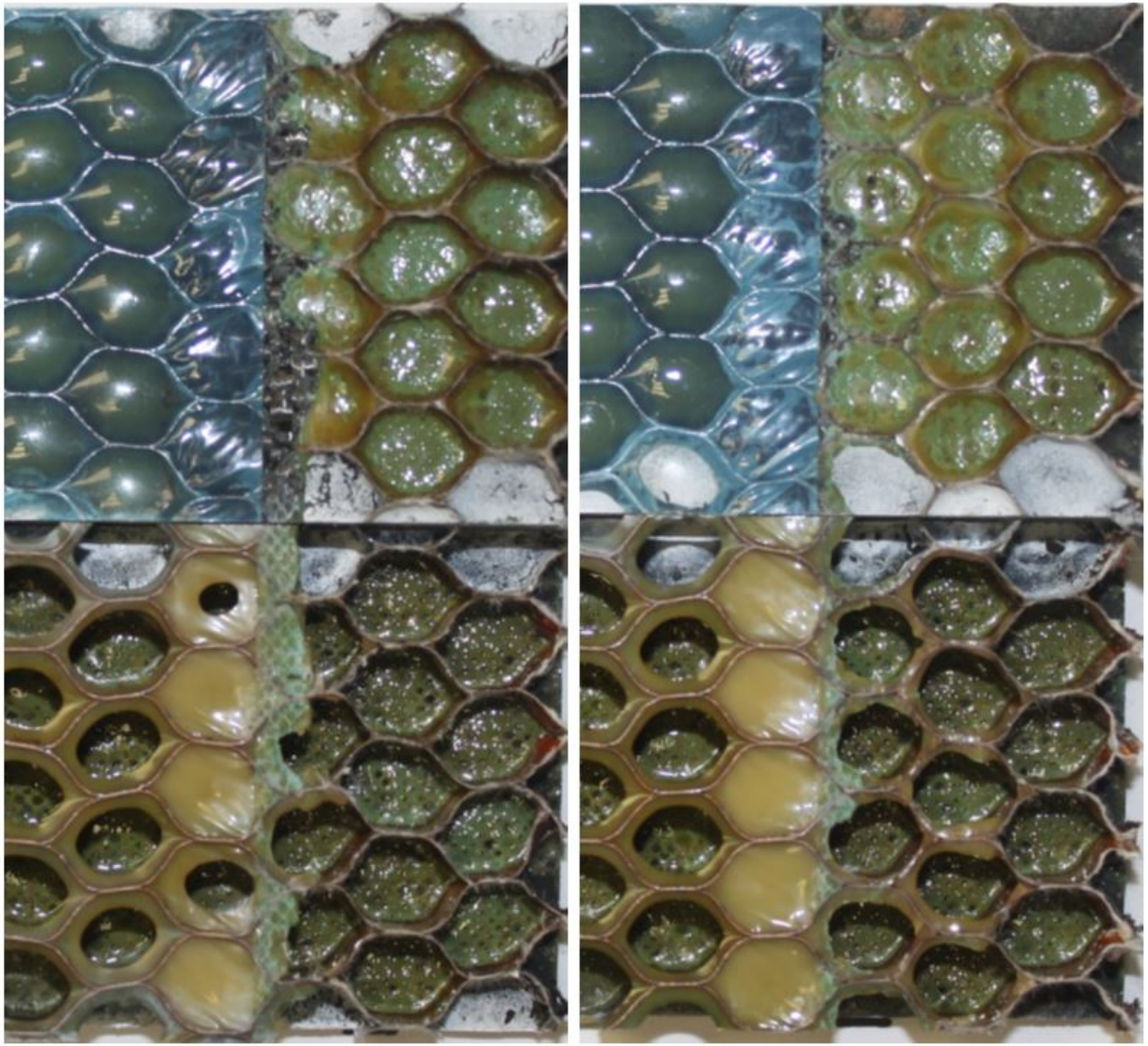

Figure C-50. Failure mode image for SDT-16-HX-3.8-3-FI-SLX-X #5 and #6

APPENDIX D—FATIGUE RESULTS FOR THIN FACESHEET (4-PLY) AND HRH-10 OVER-EXPANDED CORES TESTED AS SINGLE-CANTILEVER BEAMS

Note that 4-ply material systems were tested with one prescribed crack length. The baseline and fluid-ingressed specimens were all tested with a 1.0″ prescribed crack.

D.1 HRH-10/OX–3/16–3.0 DATA

D.1.1 HRH-10/OX–3/16–3.0 BASELINE DATA (1.0″ PRESCRIBED CRACK—SHORTENED)

Table D-1. Test summary for HRH-10/OX–3/16–3.0 baseline (1.0″ prescribed crack—shortened)

Specimen	Shaping Parameter [m] English or SI	Shaping Parameter [B] English	Shaping Parameter [B] SI	Failure Mode
SDT-04-OX-3.16-3-BL-SLX-2 (shortened)	4.142	3.626E-06	4.693E-14	First row in A with a few cells in PO, then a mix of A and C with a few cells in PO, then C
SDT-04-OX-3.16-3-BL-SLX-3 (shortened)	3.455	3.866E-06	1.747E-12	First row a mix of A and PO, then C, with a few cells in A
SDT-04-OX-3.16-3-BL-SLX-4 (shortened)	3.811	3.241E-06	2.328E-13	Primarily C with a pocket of A and a cell in PO
SDT-04-OX-3.16-3-BL-SLX-5 (shortened)	2.794	3.861E-06	5.284E-11	First row in C with a couple of cells in A, then C with a few cells in A and a cell in PO
SDT-04-OX-3.16-3-BL-SLX-6 (shortened)	3.729	1.583E-06	1.732E-13	First row half in A with a few cells in PO and a few cells in C, then primarily C with a large pocket of A and PO
SDT-04-OX-3.16-3-BL-SLX-8 (shortened)	2.512	4.288E-06	2.521E-10	First row a mix of PO and C, then C
AVERAGE (individual)	3.407	3.411E-06	5.119E-11	
STANDARD DEVIATION	0.630	9.589E-07	1.006E-10	
COEFFICIENT OF VARIATION [%]	18.497	28.113	196.566	
AVERAGE (all)	3.159	2.979E-06	6.198E-12	
AVERAGE (interpolated)	3.235	2.994E-06	4.209E-12	

A = adhesive interface disbond failure; PO = adhesive pullout failure; C = tensile core failure

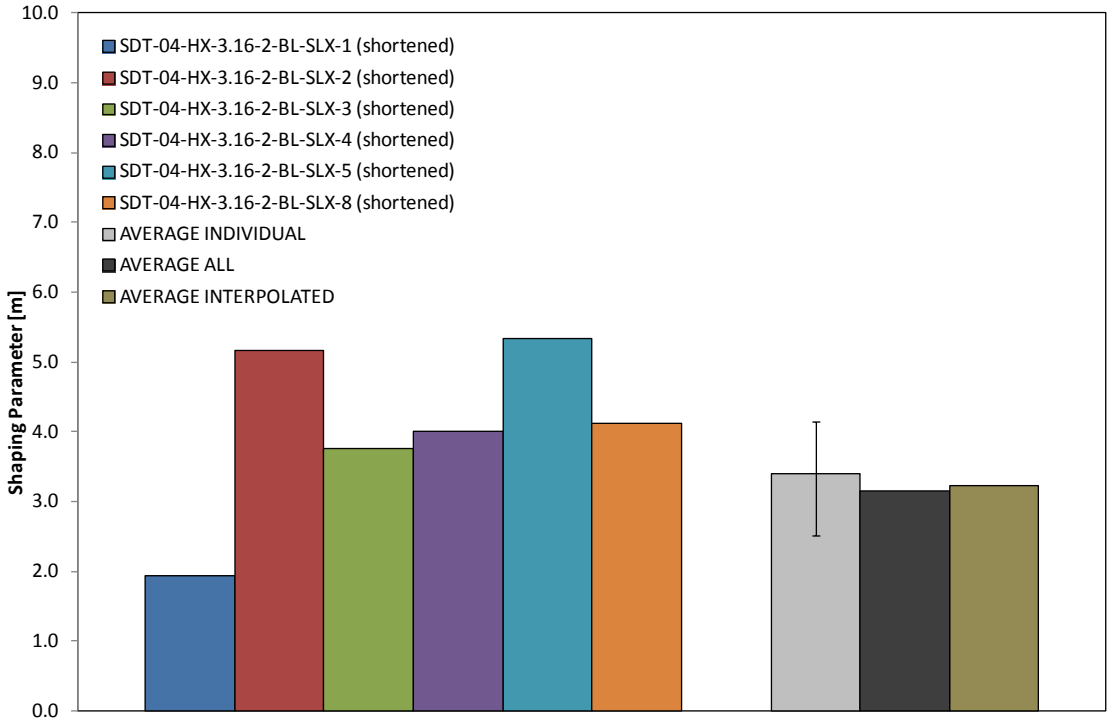

Figure D-1. Shaping parameter (*m*) for HRH-10/OX–3/16–3.0 baseline (1.0″ prescribed crack—shortened)

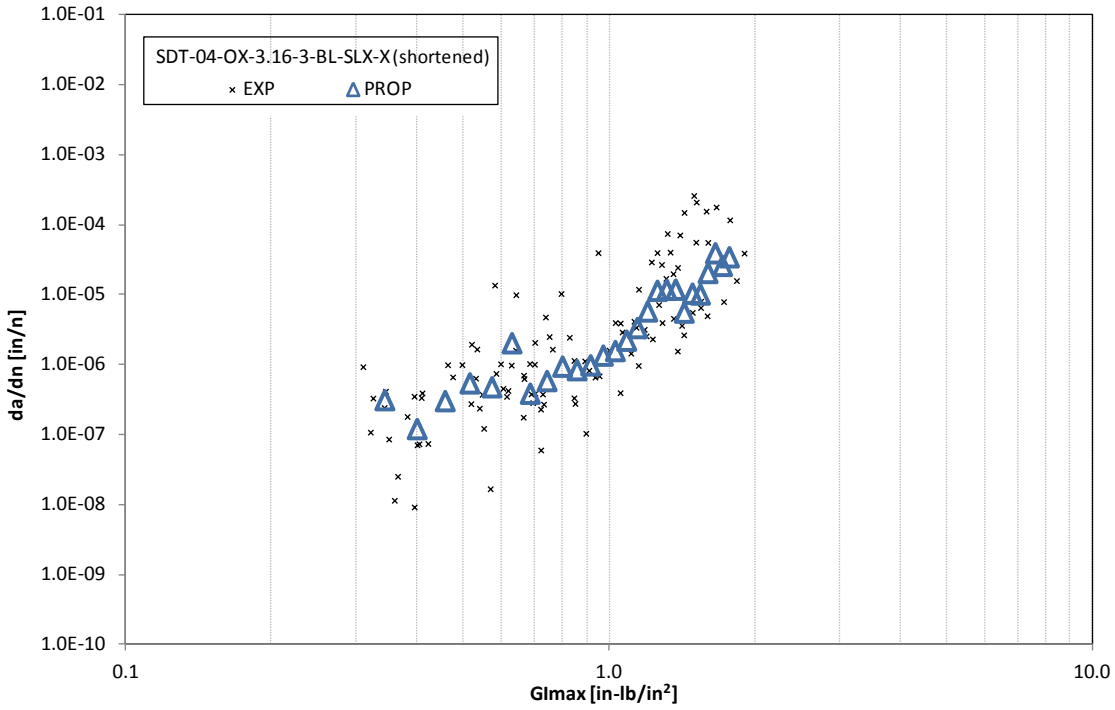

Figure D-2. Fatigue growth da/dn curve for HRH-10/OX–3/16–3.0 baseline (1.0″ prescribed crack—shortened)

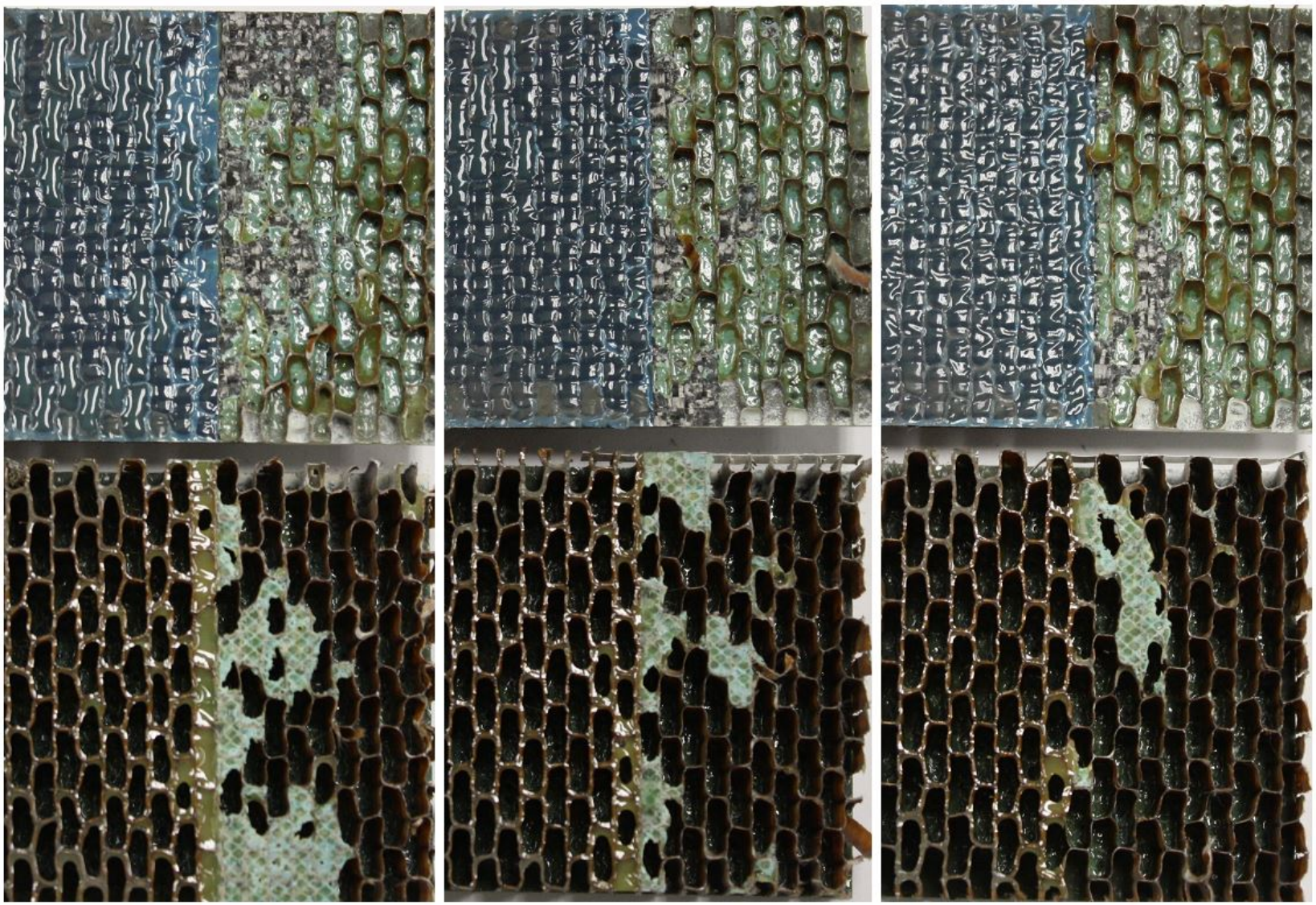

Figure D-3. Failure mode image of SDT-04-OX-13.16-3-BL-SLX-X (shortened) #2, #3, and #4

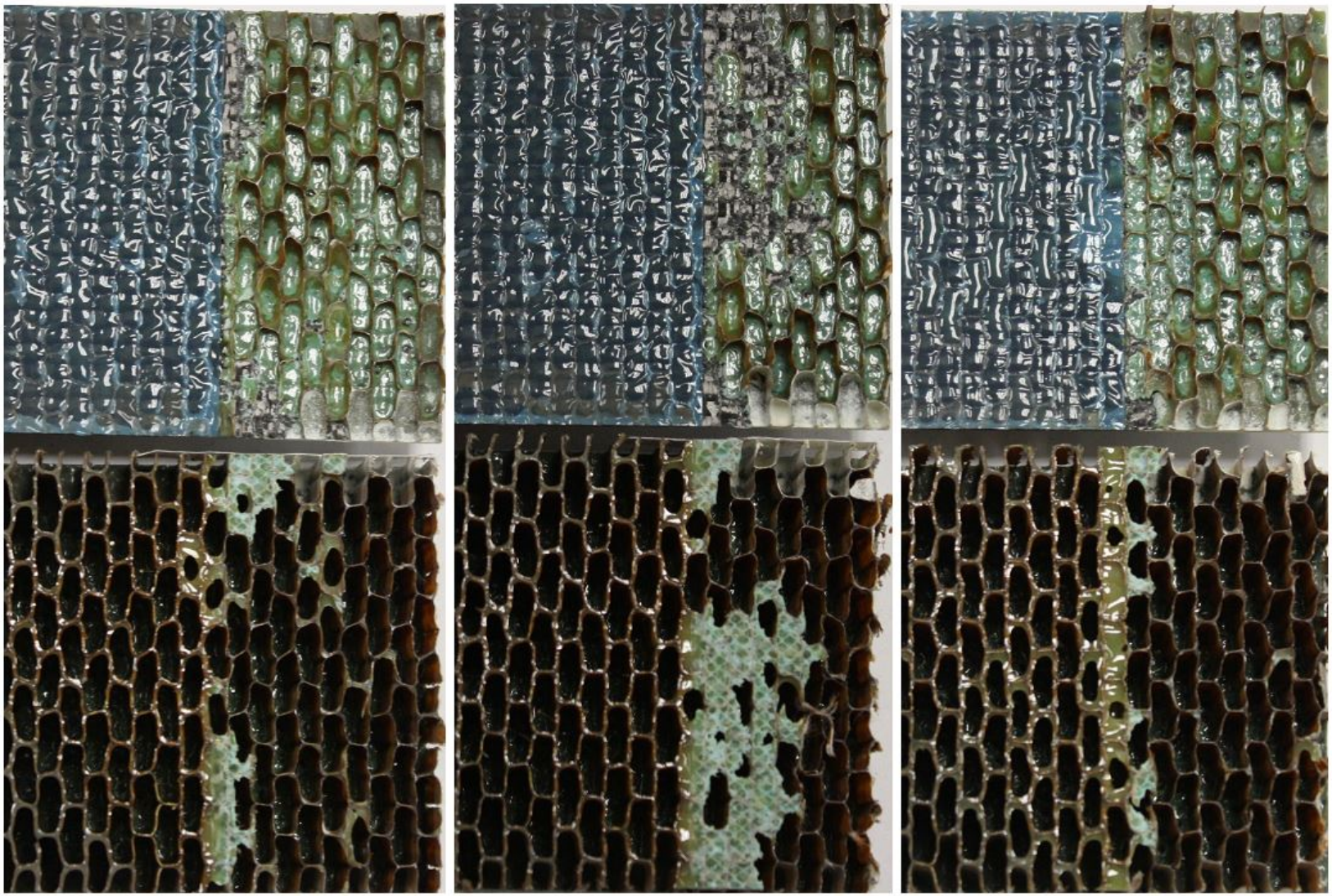

Figure D-4. Failure mode image of SDT-04-OX-13.16-3-BL-SLX-X (shortened) #5, #6, and #8

D.1.2 HRH-10/OX–3/16–3.0 FLUID-INGRESSED DATA (1.0″ PRESCRIBED CRACK—SHORTENED)

Table D-2. Test summary for HRH-10/OX–3/16–3.0 fluid ingressed (1.0″ prescribed crack—shortened)

Specimen	Shaping Parameter [m] English or SI	Shaping Parameter [B] English	Shaping Parameter [B] SI	Failure Mode
SDT-04-OX-3.16-3-FI-SLX-2 (shortened)	2.623	1.207E-05	4.010E-10	Primarily C with a couple of cells in A
SDT-04-OX-3.16-3-FI-SLX-3 (shortened)	1.868	1.530E-05	2.503E-08	Primarily C with a couple of cells in A
SDT-04-OX-3.16-3-FI-SLX-4 (shortened)	2.047	2.592E-05	1.683E-08	Primarily C with a couple of cells in A
SDT-04-OX-3.16-3-FI-SLX-5 (shortened)	2.888	1.574E-05	1.327E-10	Primarily C with a couple of cells in A
SDT-04-OX-3.16-3-FI-SLX-6 (shortened)	1.861	1.082E-05	1.836E-08	Primarily C with a couple of cells in A
SDT-04-OX-3.16-3-FI-SLX-7 (shortened)	2.238	4.871E-06	1.183E-09	Primarily C with a couple of cells in PO
AVERAGE (individual)	2.254	1.412E-05	1.032E-08	
STANDARD DEVIATION	0.421	6.983E-06	1.104E-08	
COEFFICIENT OF VARIATION [%]	18.656	49.455	106.917	
AVERAGE (all)	1.686	1.099E-05	4.601E-08	
AVERAGE (interpolated)	1.903	1.222E-05	1.670E-08	

C = tensile core failure; A = adhesive interface disbond failure; PO = adhesive pullout failure

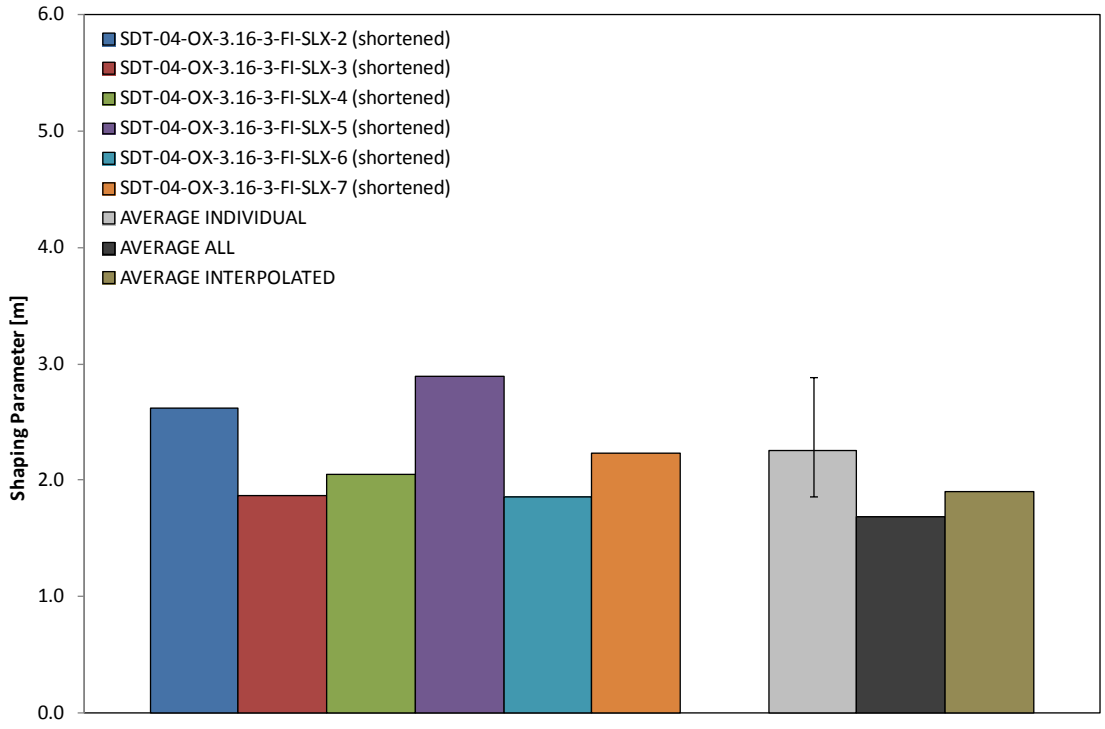

Figure D-5. Shaping parameter (*m*) for HRH-10/OX–3/16–3.0 fluid ingressed (1.0″ prescribed crack—shortened)

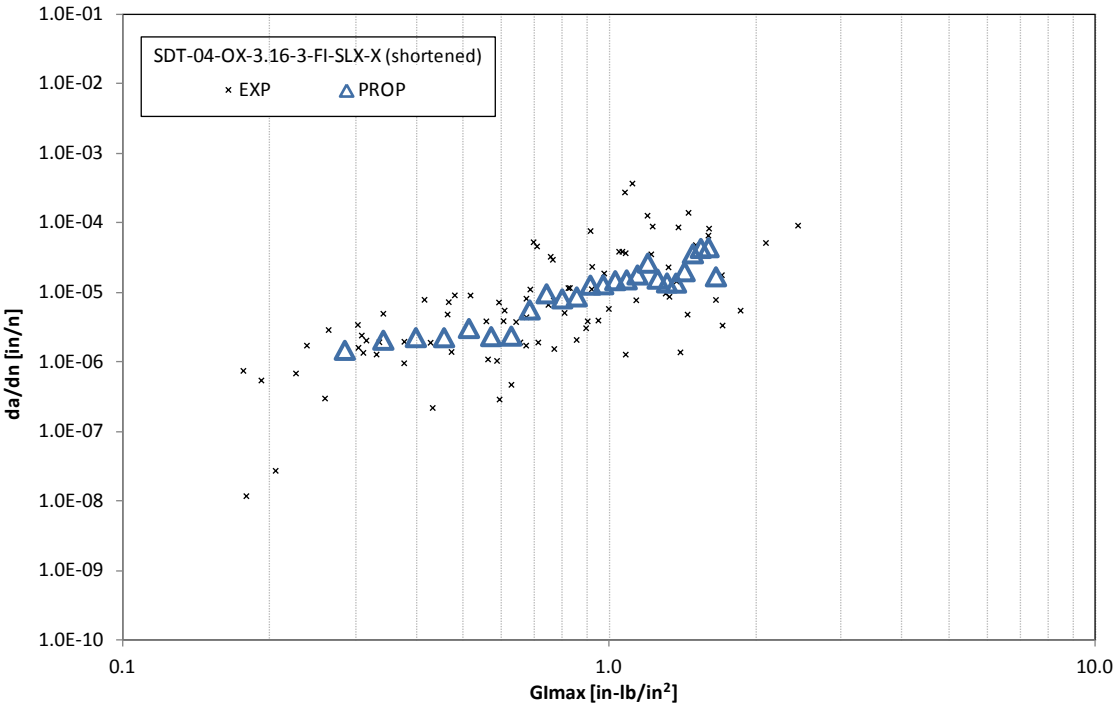

Figure D-6. Fatigue growth da/dn curve for HRH-10/OX–3/16–3.0 fluid ingressed (1.0″ prescribed crack—shortened)

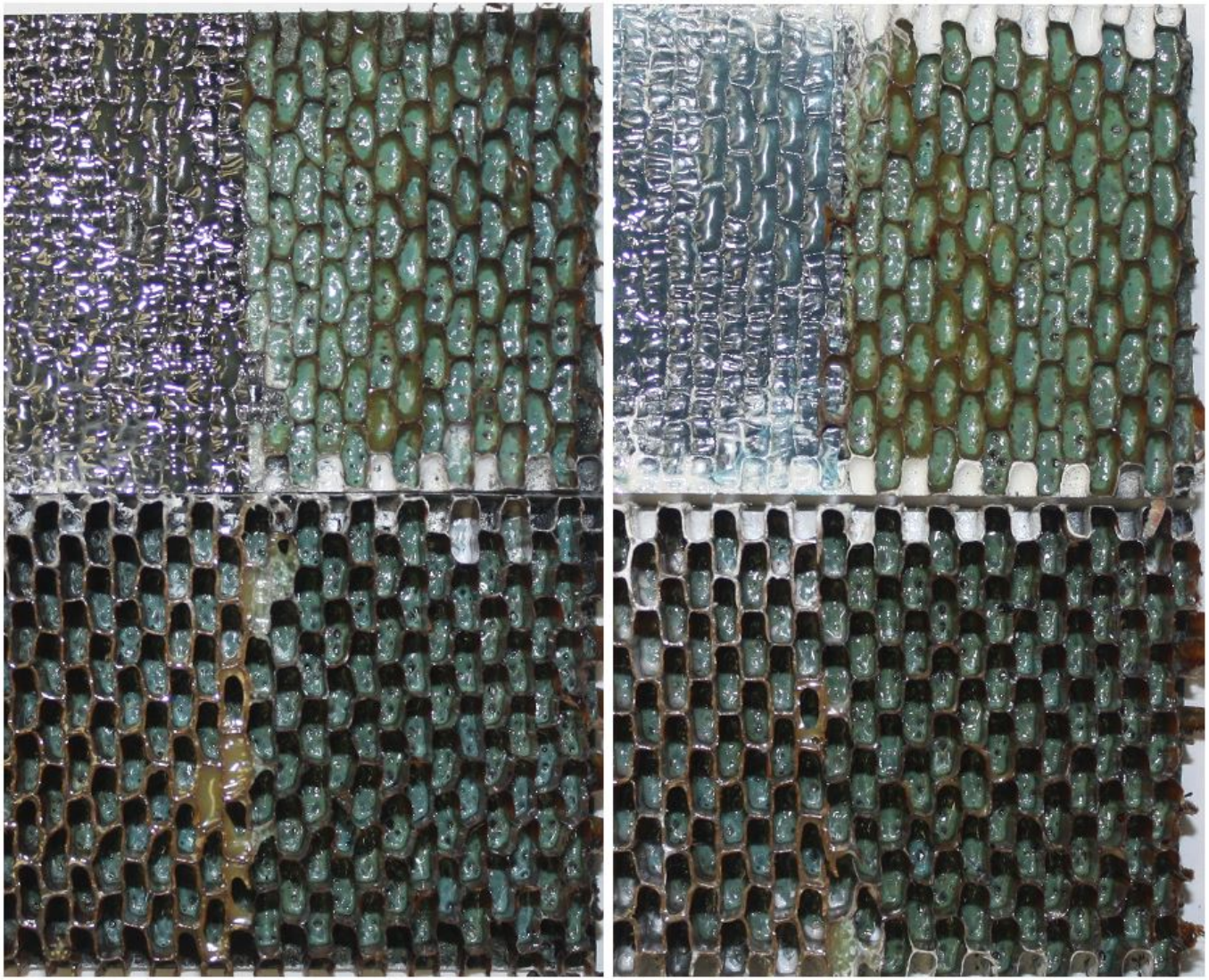

Figure D-7. Failure mode image of SDT-04-OX-3.16-3-FI-SLX-X (shortened) #2 and #3

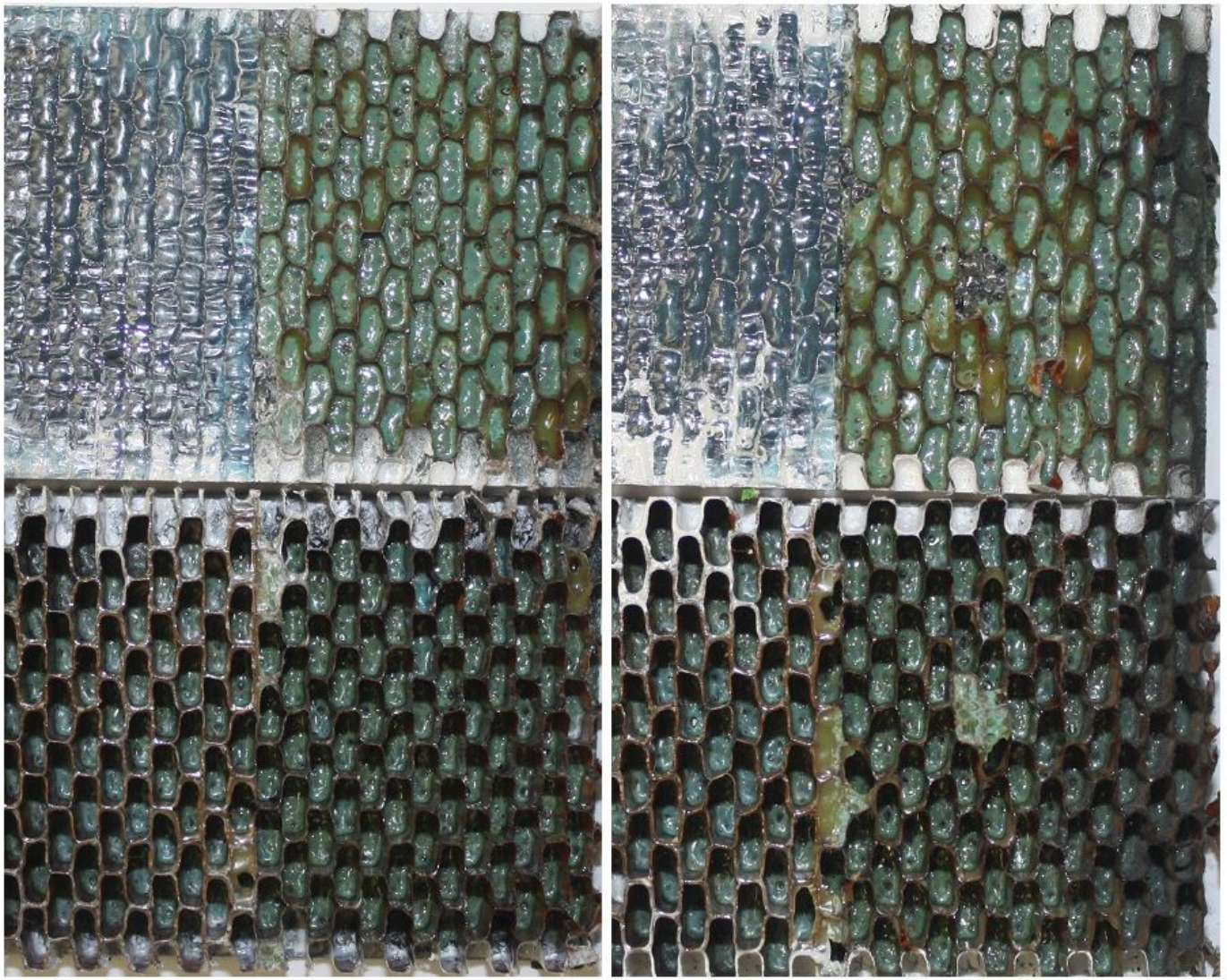

Figure D-8. Failure mode image of SDT-04-OX-3.16-3-FI-SLX-X (shortened) #4 and #5

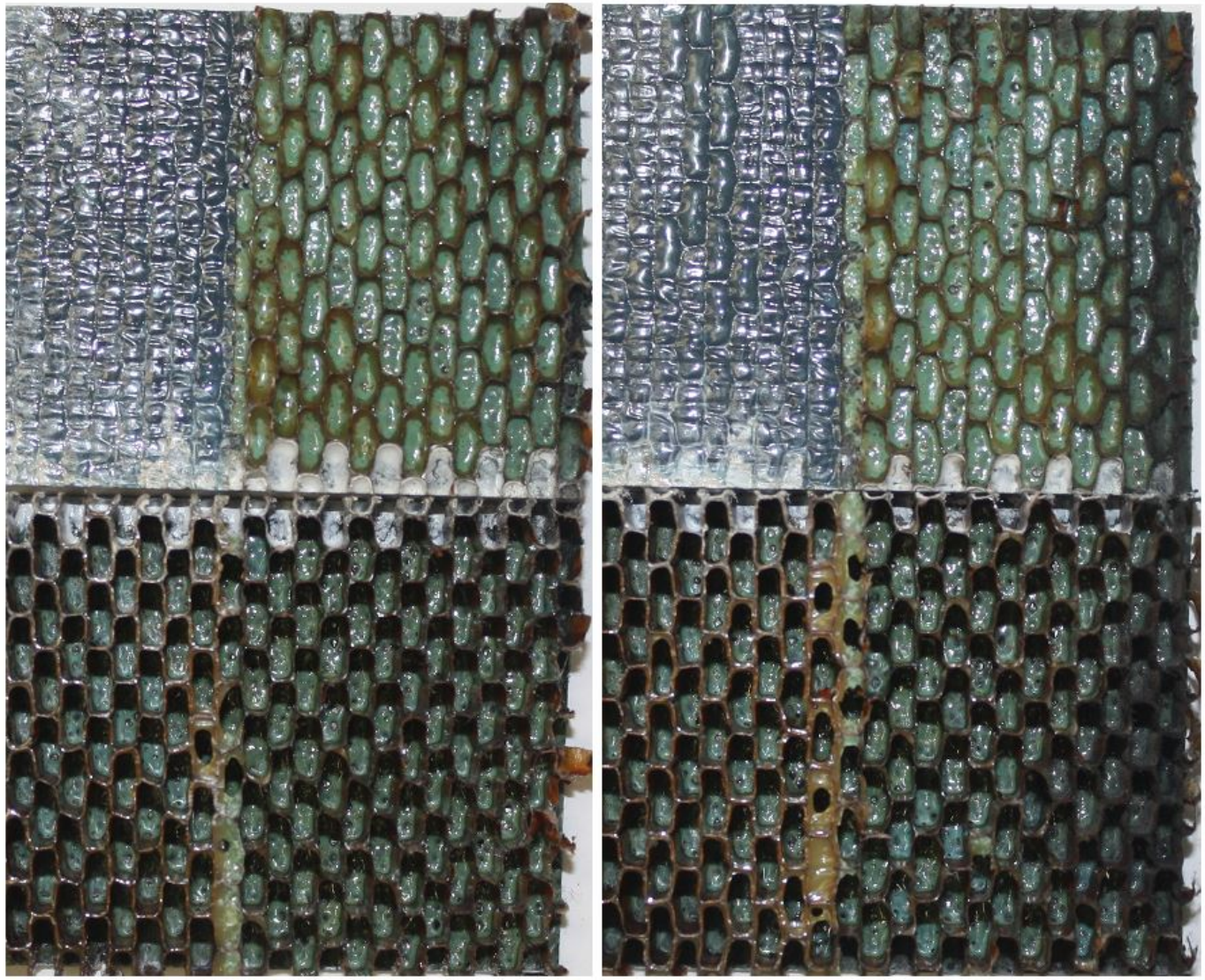

Figure D-9. Failure mode image of SDT-04-OX-3.16-3-FI-SLX-X (shortened) #6 and #7

APPENDIX E—FATIGUE RESULTS FOR THICK FACESHEET (16-PLY) AND HRH-10 OVER-EXPANDED CORE TESTED AS SINGLE-CANTILEVER BEAMS

Note that 16-ply material systems were tested with one prescribed crack length. The baseline and fluid-ingressed specimens were all tested with a 2.5″ prescribed crack.

E.1 HRH-10/OX–3/16–3.0 DATA

E.1.1 HRH-10/OX–3/16–3.0 BASELINE DATA (2.5″ PRESCRIBED CRACK)

Table E-1. Test summary for HRH-10/OX–3/16–3.0 baseline (2.5″ prescribed crack)

Specimen	Shaping Parameter [m] English or SI	Shaping Parameter [B] English	Shaping Parameter [B] SI	Failure Mode
SDT-16-OX-3.16-3-BL-SLX-1	1.976	3.546E-06	3.334E-09	First row split between A and C, then C
SDT-16-OX-3.16-3-BL-SLX-2	4.456	2.521E-06	6.458E-15	First row split between A and C, then C
SDT-16-OX-3.16-3-BL-SLX-3	2.741	7.565E-06	1.366E-10	First row A second row a mix of A and C, then C
SDT-16-OX-3.16-3-BL-SLX-4	2.370	6.865E-06	8.407E-10	Primarily C
SDT-16-OX-3.16-3-BL-SLX-5	2.437	4.011E-06	3.478E-10	First row A, second row a mix of A and C, then C
SDT-16-OX-3.16-3-BL-SLX-6	2.662	5.398E-06	1.463E-10	Primarily C with pocket of A in first three rows
AVERAGE (individual)	2.774	4.984E-06	8.008E-10	
STANDARD DEVIATION	0.867	1.972E-06	1.275E-09	
COEFFICIENT OF VARIATION [%]	31.255	39.572	159.254	
AVERAGE (all)	2.368	4.831E-06	4.140E-08	
AVERAGE (interpolated)	2.316	4.282E-06	6.937E-10	

A = adhesive interface disbond failure; C = tensile core failure

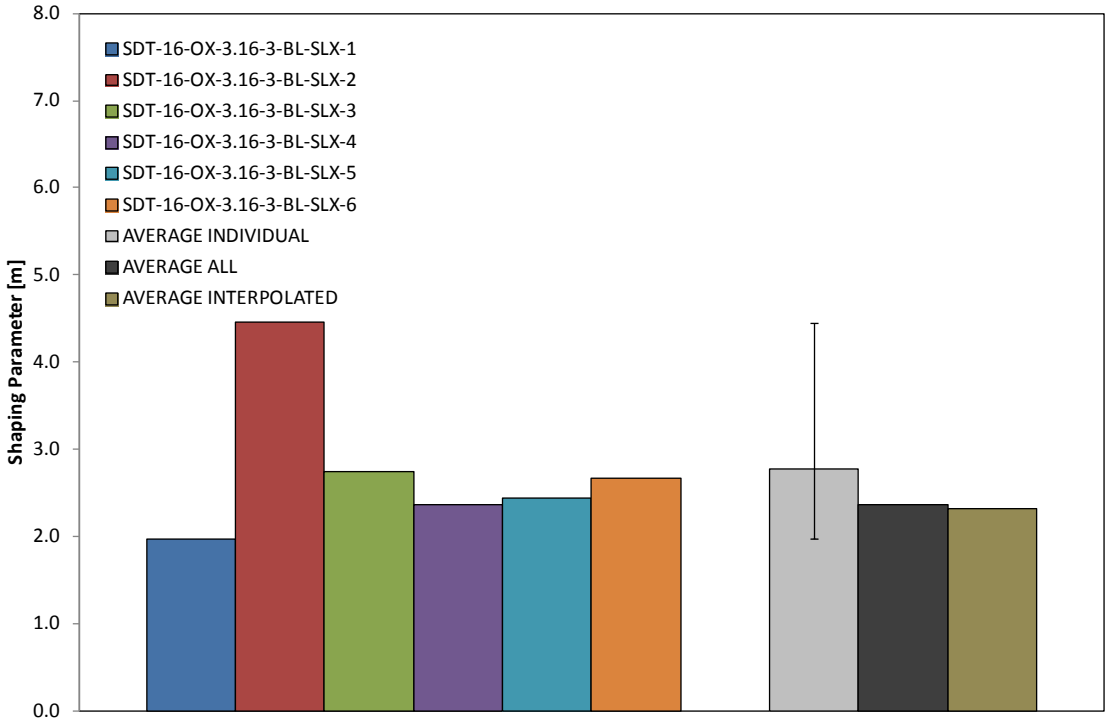

Figure E-1. Shaping parameter (*m*) for HRH-10/OX–3/16–3.0 baseline (2.5″ prescribed crack)

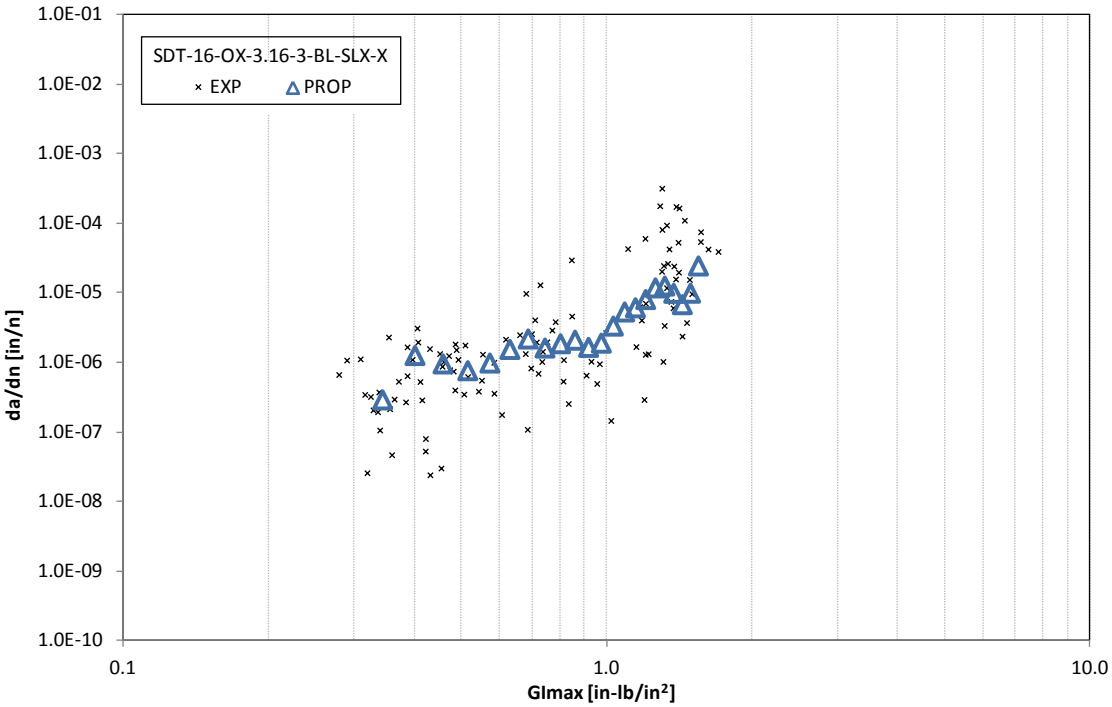

Figure E-2. Fatigue growth da/dn curve for HRH-10/OX–3/16–3.0 baseline (2.5″ prescribed crack)

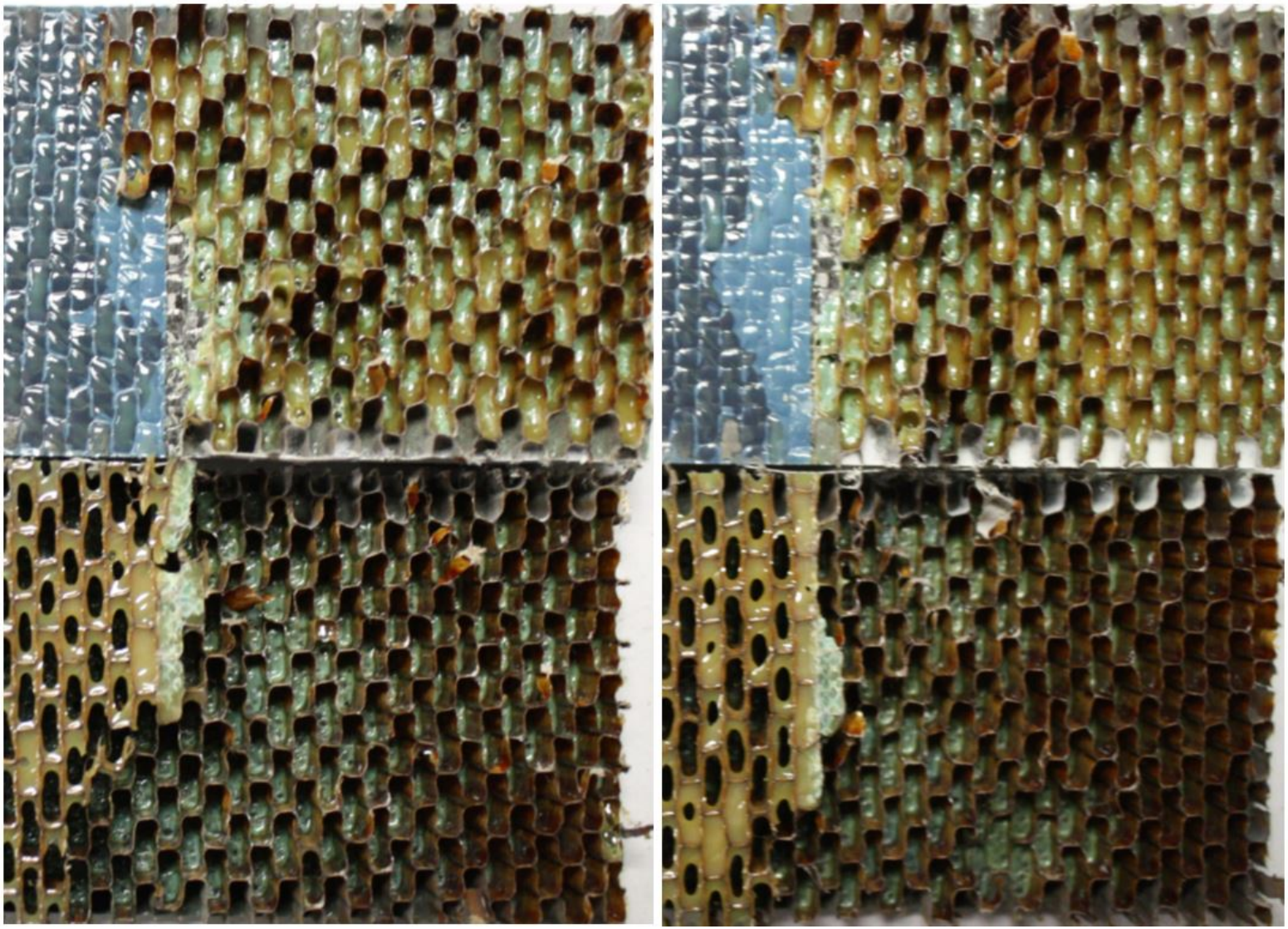

Figure E-3. Failure mode image of SDT-16-OX-3.16-3-BL-SLX-X #1 and #2

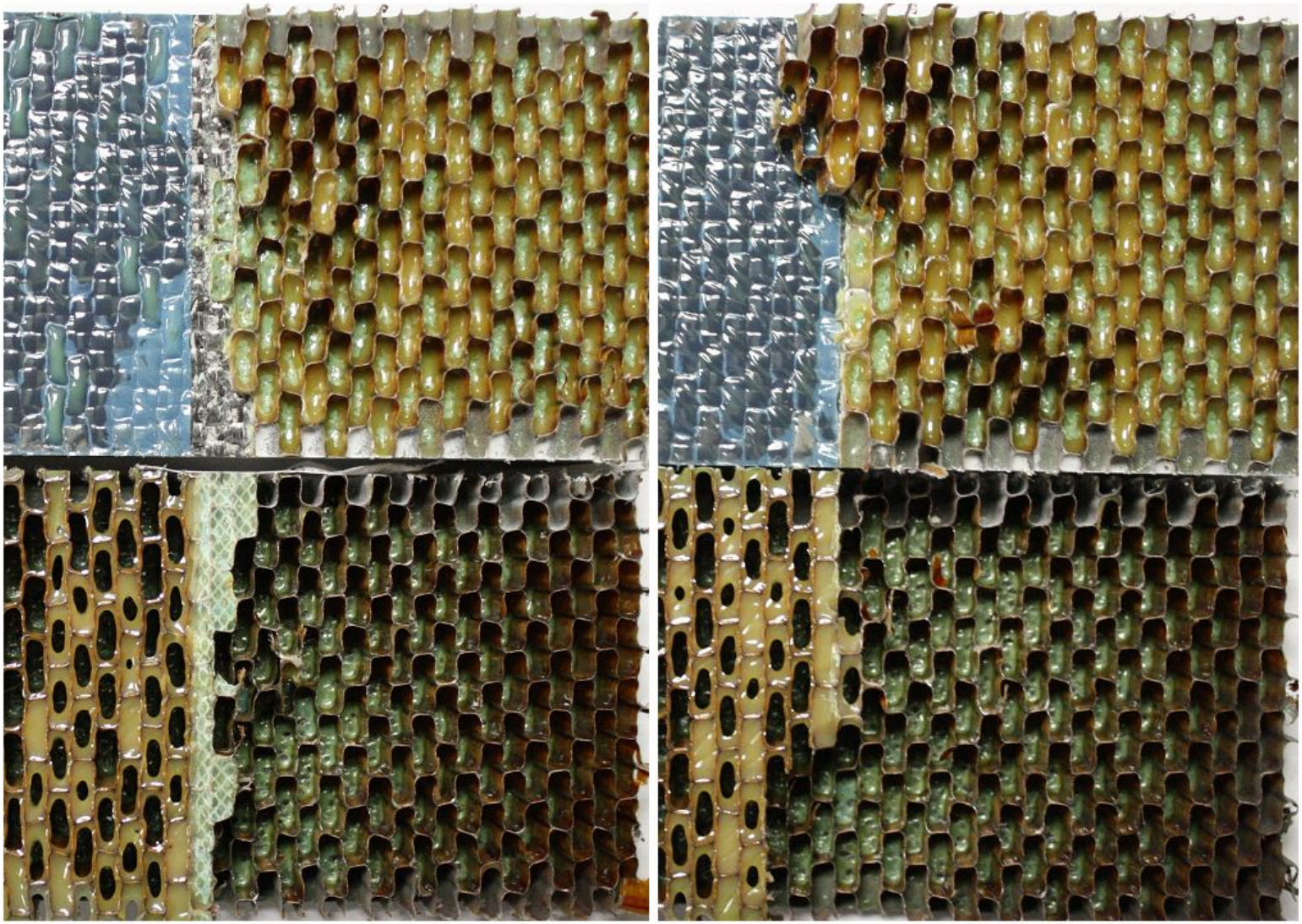

Figure E-4. Failure mode image of SDT-16-OX-3.16-3-BL-SLX-X #3 and #4

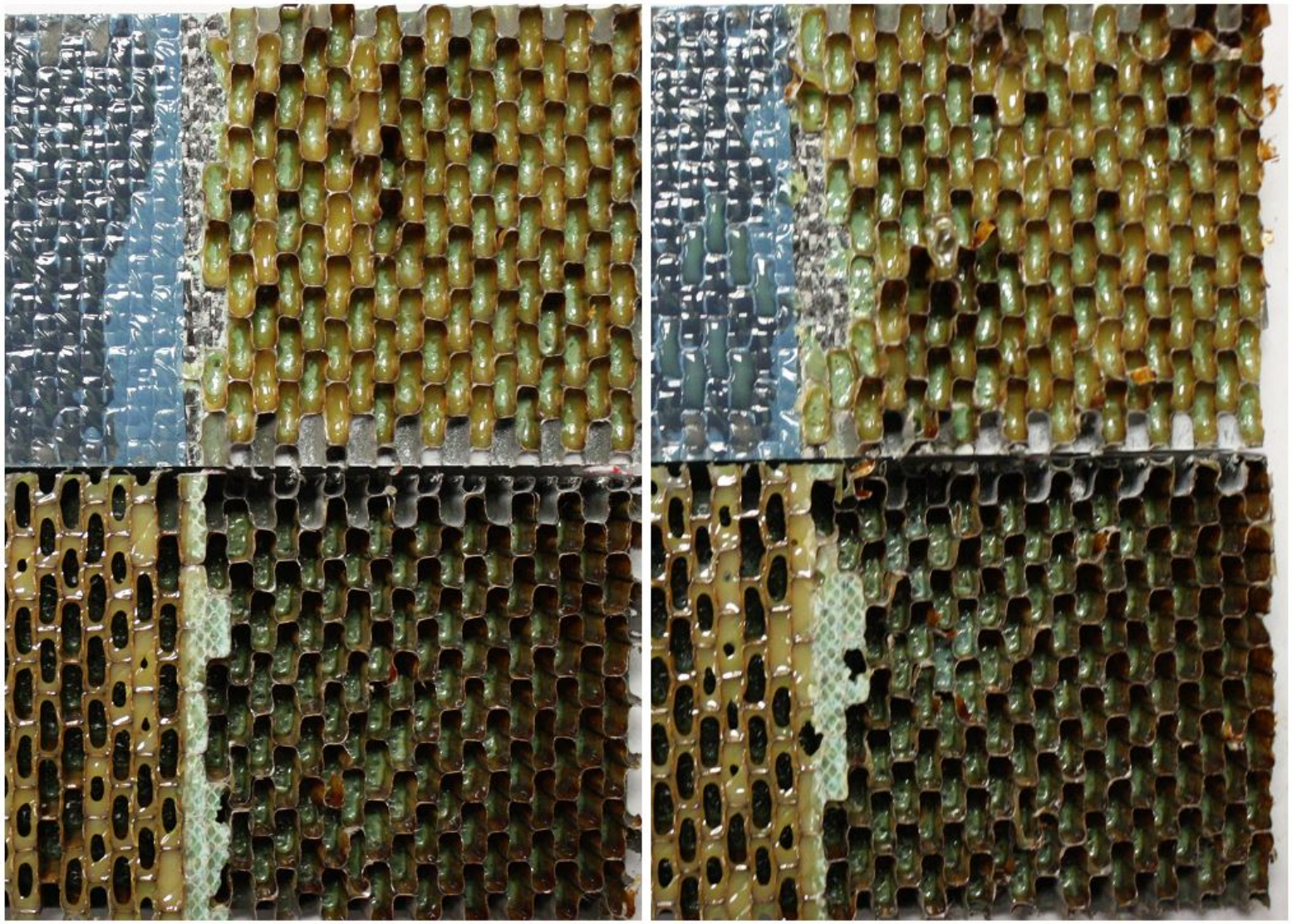

Figure E-5. Failure mode image for SDT-16-OX-3.16-3-BL-SLX-X #5 and #6

E.1.2 HRH-10/OX–3/16–3.0 FLUID-INGRESSED DATA (2.5″ PRESCRIBED CRACK)

Table E-2. Test summary for HRH-10/OX–3/16–3.0 fluid ingressed (2.5″ prescribed crack)

Specimen	Shaping Parameter [m] English or SI	Shaping Parameter [B] English	Shaping Parameter [B] SI	Failure Mode
SDT-16-OX-3.16-3-FI-SLX-1	3.493	6.530E-05	2.419E-11	First row split between A and C, then C
SDT-16-OX-3.16-3-FI-SLX-2	4.441	6.093E-07	1.683E-15	Primarily C
SDT-16-OX-3.16-3-FI-SLX-3	5.721	7.602E-05	2.827E-16	First row primarily A, then C
SDT-16-OX-3.16-3-FI-SLX-4	4.193	2.808E-05	2.805E-13	First row split between A and C, then C
SDT-16-OX-3.16-3-FI-SLX-5	1.745	2.373E-05	7.347E-08	First row split between A and C, then C
SDT-16-OX-3.16-3-FI-SLX-6	3.395	1.113E-05	6.845E-12	First row split between A and C, then C
AVERAGE (individual)	3.831	3.414E-05	1.225E-08	
STANDARD DEVIATION	1.322	3.008E-05	2.999E-08	
COEFFICIENT OF VARIATION [%]	34.494	88.093	244.824	
AVERAGE (all)	1.529	9.791E-06	9.226E-08	
AVERAGE (interpolated)	2.254	1.556E-05	3.480E-09	

A = adhesive interface disbond failure; C = tensile core failure

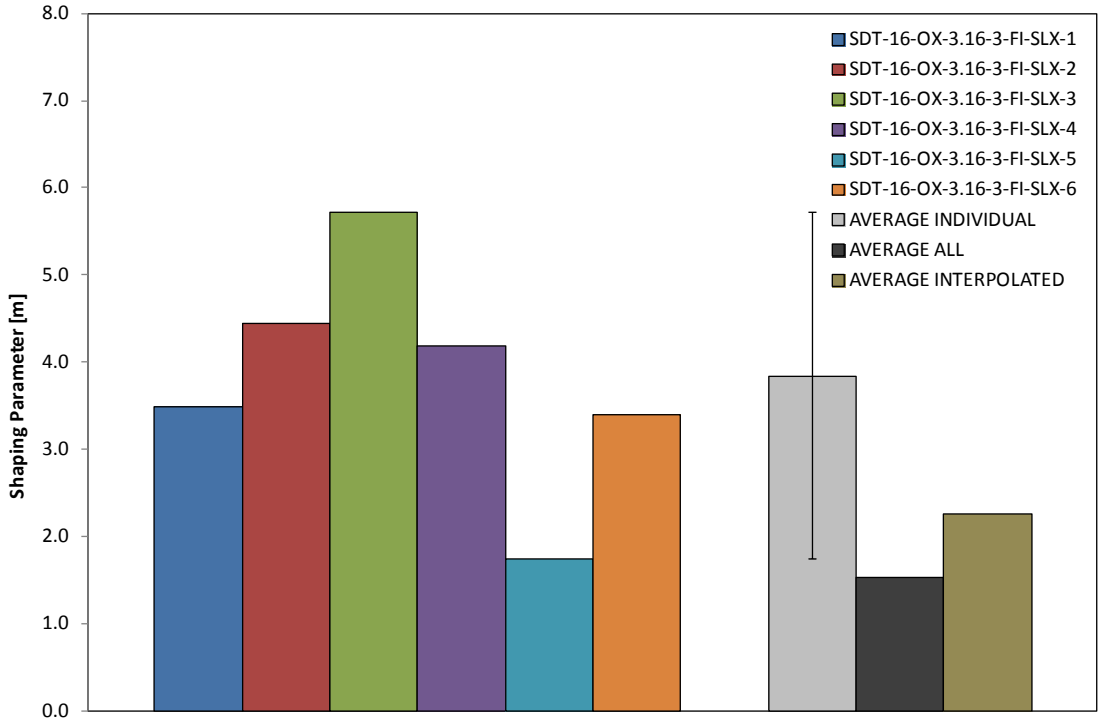

Figure E-6. Shaping parameter (*m*) for HRH-10/OX–3/16–3.0 fluid ingressed (2.5″ prescribed crack)

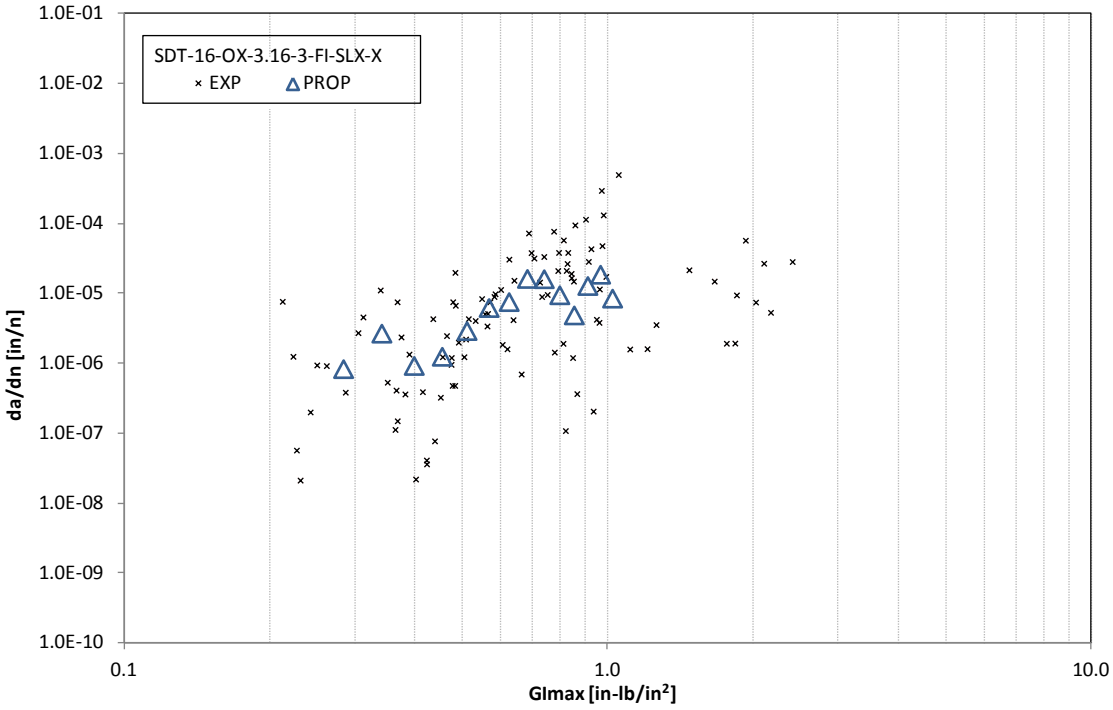

Figure E-7. Fatigue growth da/dn curve for HRH-10/OX–3/16–3.0 fluid ingressed (2.5″ prescribed crack)

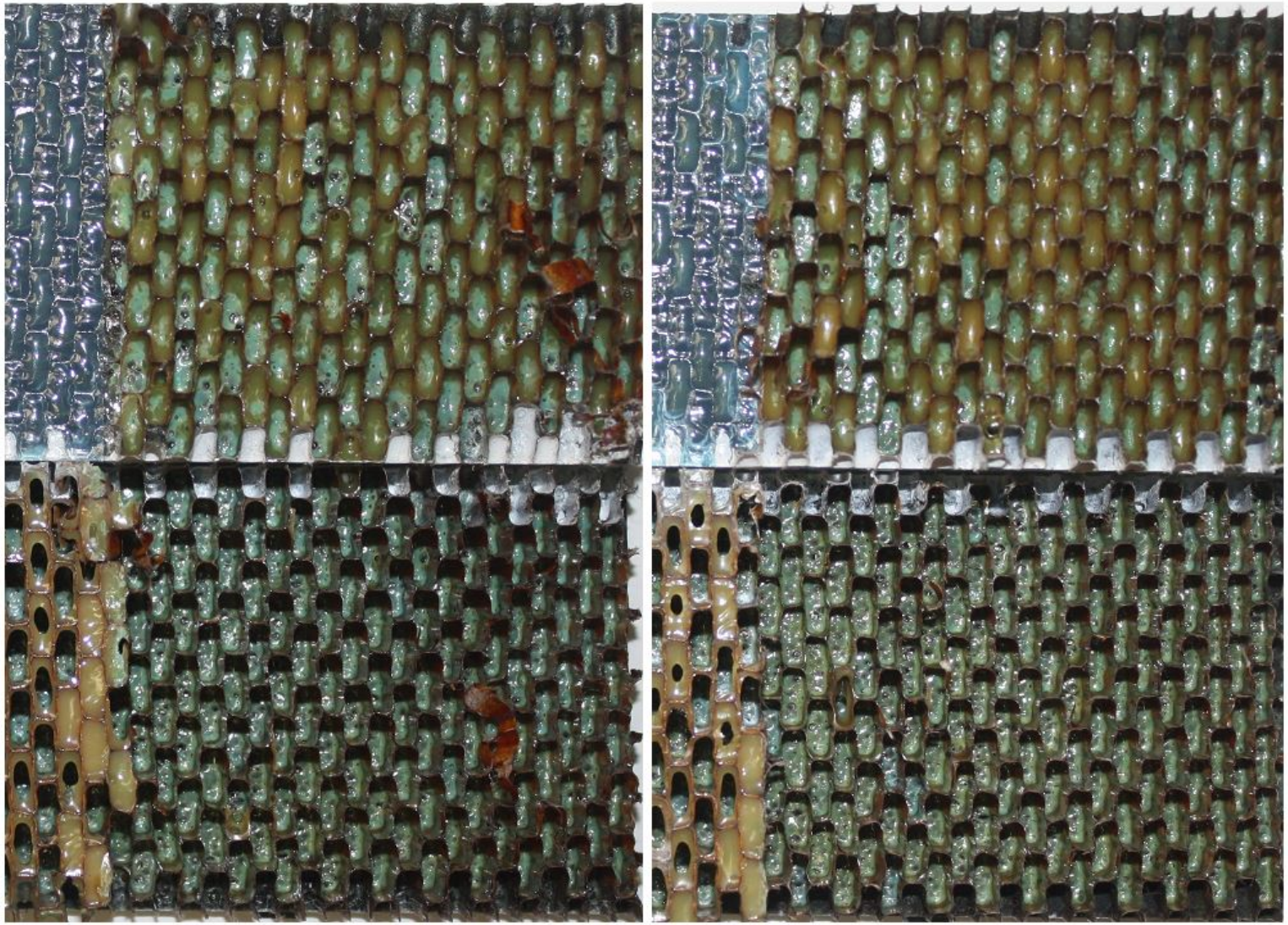

Figure E-8. Failure mode image of SDT-16-OX-3.16-3-FI-SLX-X #1 and #2

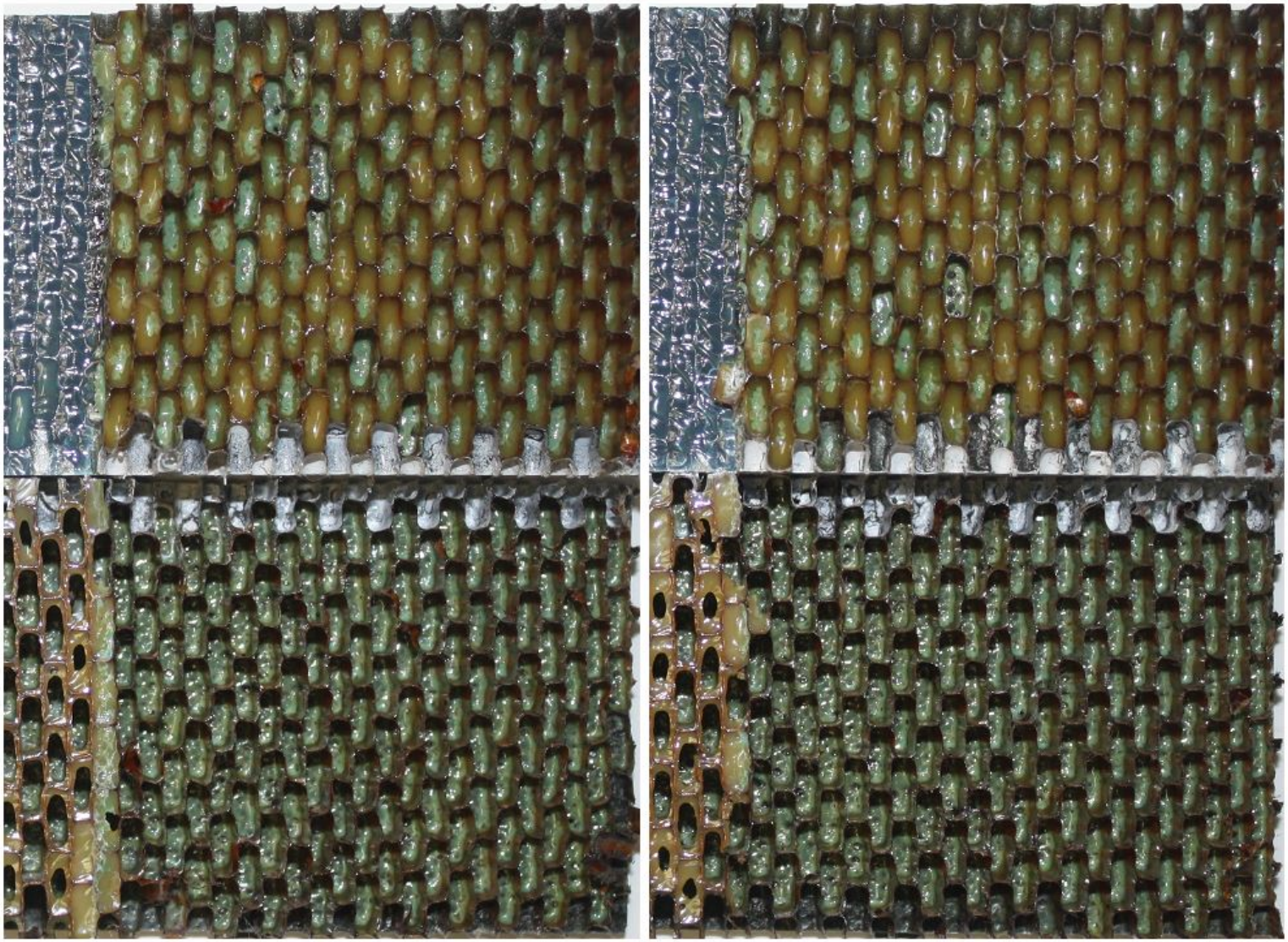

Figure E-9. Failure mode image of SDT-16-OX-3.16-3-FI-SLX-X #3 and #4

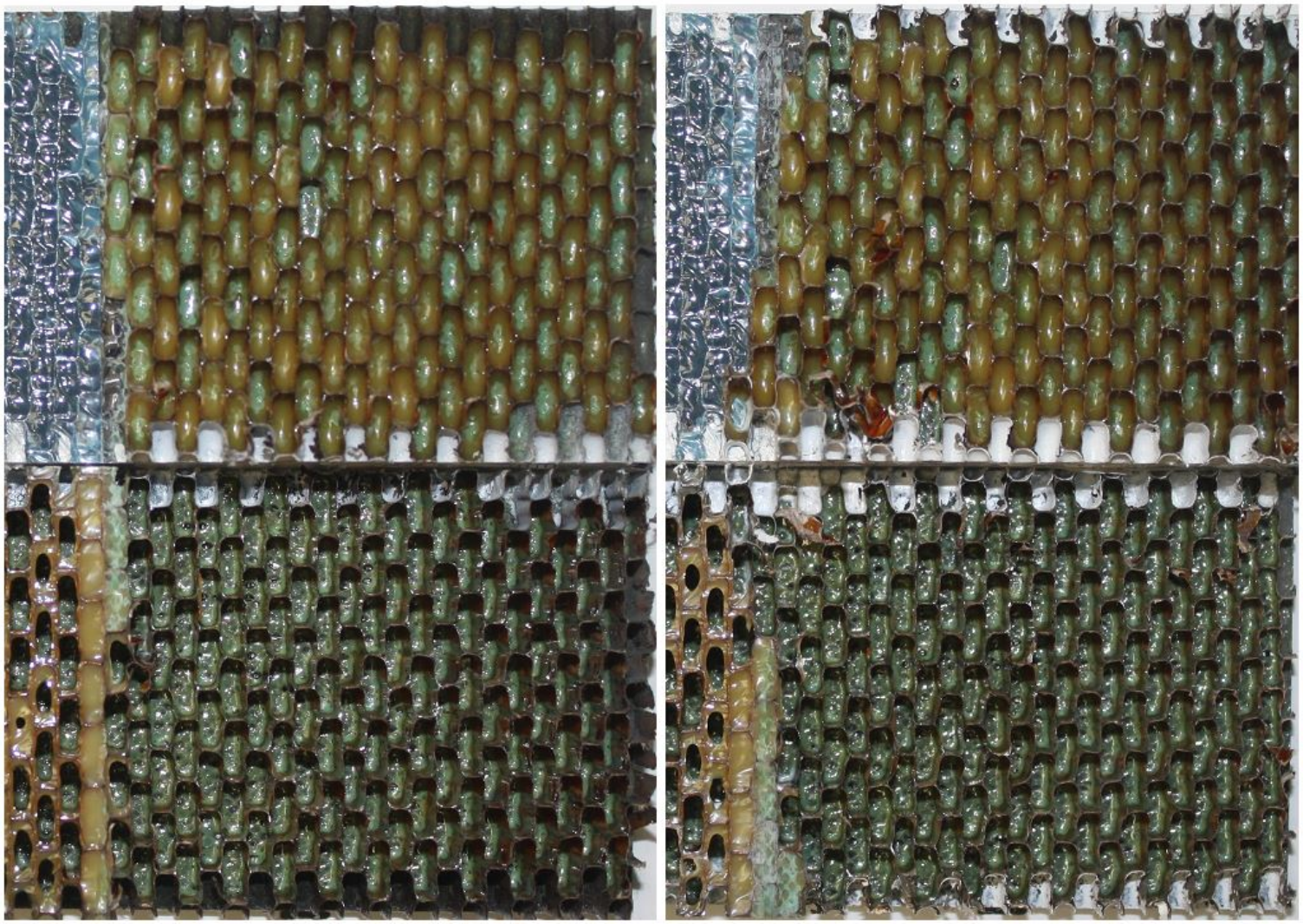

Figure E-10. Failure mode image of SDT-16-OX-3.16-3-FI-SLX-X #5 and #6

APPENDIX F—SUPPLEMENTAL DOUBLE-CANTILEVER BEAMS FATIGUE TESTING OFLAMINATES AND ADHESIVE

Note that double-cantilever beam (DCB) specimens were tested at one temperature (room) and two environmental conditions (baseline and fluid-ingressed).

F.1 DCB DATA

F.1.1 LAMINATE DATA

F.1.1.1 Laminate RTD Baseline Data

Table F-1. Test Summary for Laminate RTD Baseline

Specimen	Shaping Parameter [m] English or SI	Shaping Parameter [B] English	Shaping Parameter [B] SI
SDT-LM-BL-RTD-SLX-1	27.700	3.626E+02	6.647E-59
SDT-LM-BL-RTD-SLX-5	22.626	1.061E+00	4.692E-50
SDT-LM-BL-RTD-SLX-7	27.576	1.374E+03	4.799E-58
SDT-LM-BL-RTD-SLX-8	46.116	1.289E+09	1.148E-93
SDT-LM-BL-RTD-SLX-9	22.830	1.876E+01	2.899E-49
SDT-LM-BL-RTD-SLX-A	19.115	9.824E-01	3.270E-42
AVERAGE (individual)	27.661	2.148E+08	5.449E-43
STANDARD DEVIATION	9.616	5.262E+08	1.335E-42
COEFFICIENT OF VARIATION [%]	34.764	244.949	244.949
AVERAGE (all)	16.673	1.145E-01	1.148E-37
AVERAGE (interpolated)	29.006	3.182E+02	6.865E-62

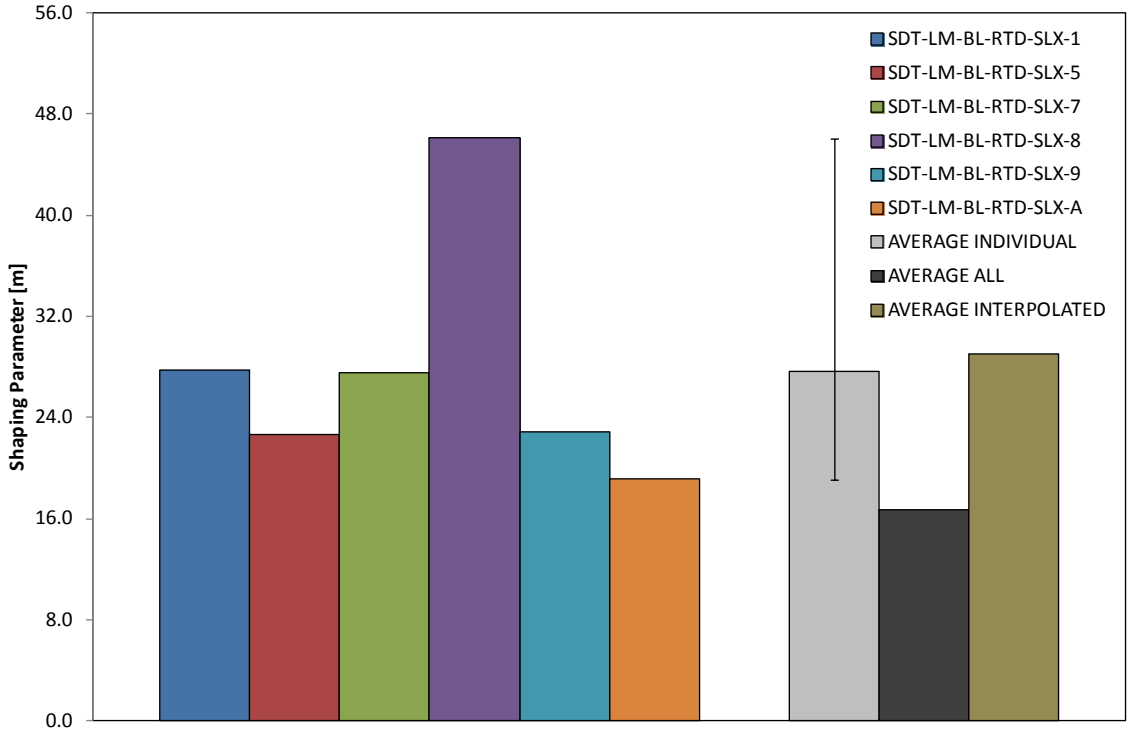

Figure F-1. Shaping parameter (*m*) for laminate RTD baseline

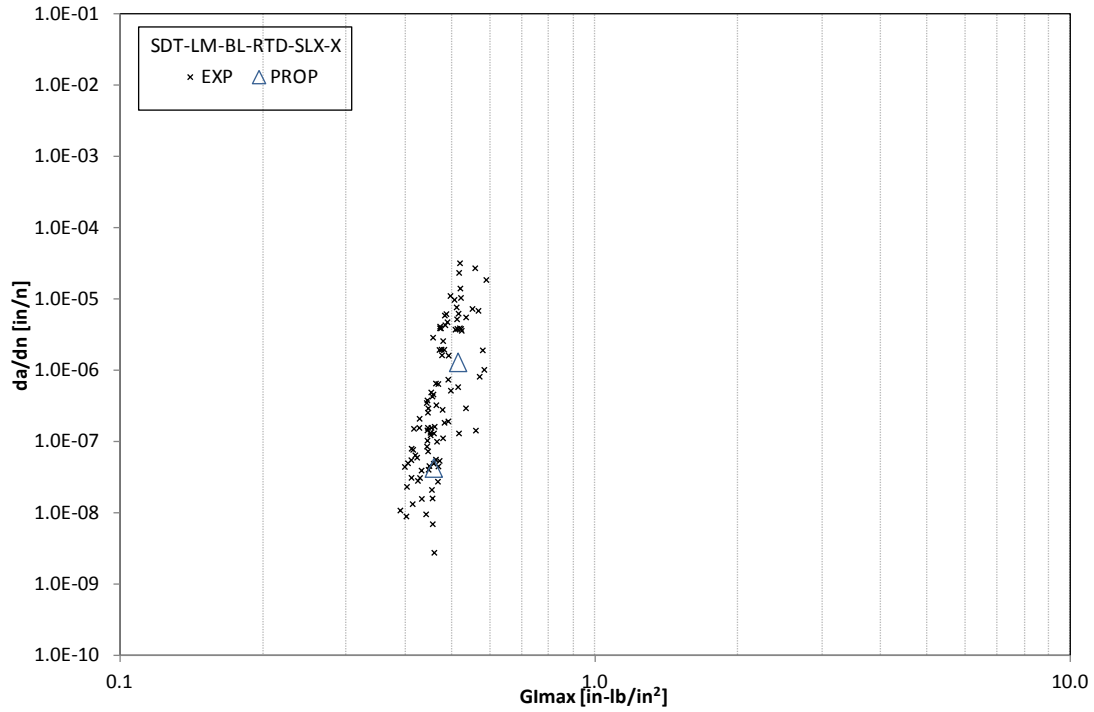

Figure F-2. Fatigue growth da/dn curve for laminate RTD baseline

F.1.1.2 Laminate RTW Fluid-Ingressed Data

Table F-2. Test summary for laminate RTW fluid ingressed

Specimen	Shaping Parameter [m] English or SI	Shaping Parameter [B] English	Shaping Parameter [B] SI
SDT-LM-FI-RTW-SLX-3	51.802	1.030E+09	1.610E-106
SDT-LM-FI-RTW-SLX-4	73.768	4.069E+18	3.366E-146
SDT-LM-FI-RTW-SLX-5	48.264	2.268E+05	3.072E-102
SDT-LM-FI-RTW-SLX-6	32.844	2.163E+01	1.145E-71
SDT-LM-FI-RTW-SLX-7	70.345	1.553E+06	6.133E-151
SDT-LM-FI-RTW-SLX-8	42.597	2.052E+07	1.433E-87
AVERAGE (individual)	53.270	6.781E+17	1.908E-72
STANDARD DEVIATION	15.938	1.661E+18	4.672E-72
COEFFICIENT OF VARIATION [%]	29.919	244.949	244.949
AVERAGE (all)	4.707	1.863E-05	1.303E-14
AVERAGE (interpolated)	31.994	3.312E+01	1.418E-69

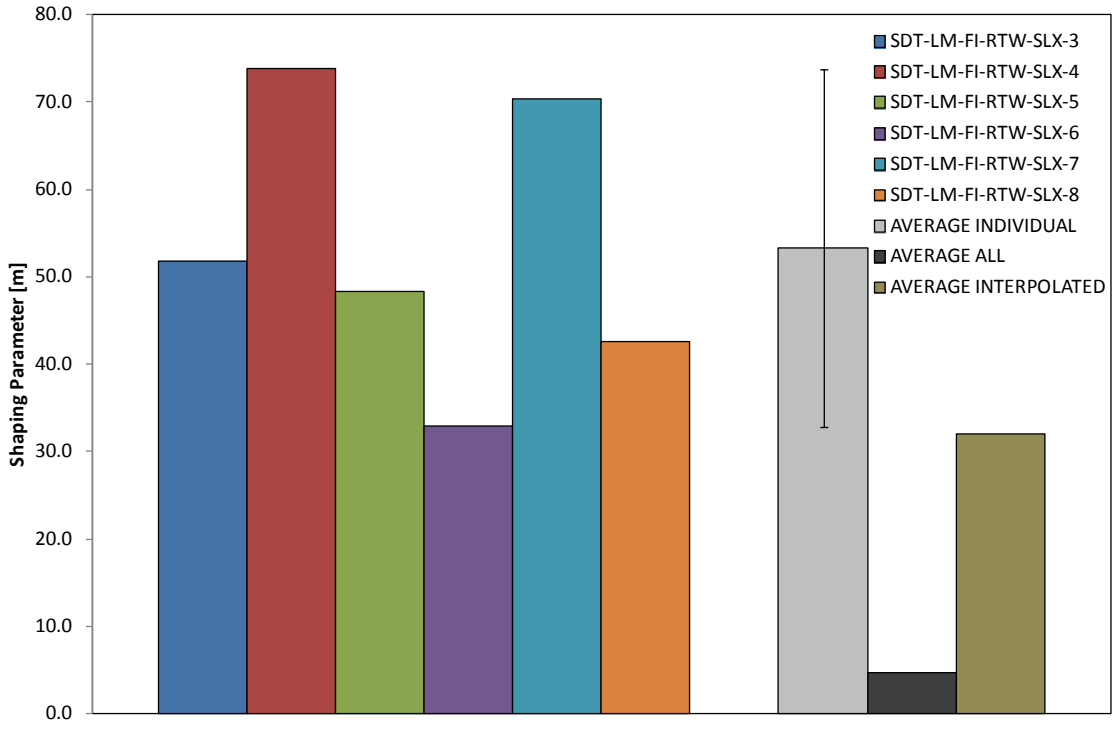

Figure F-3. Shaping parameter (*m*) for laminate RTW fluid ingressed

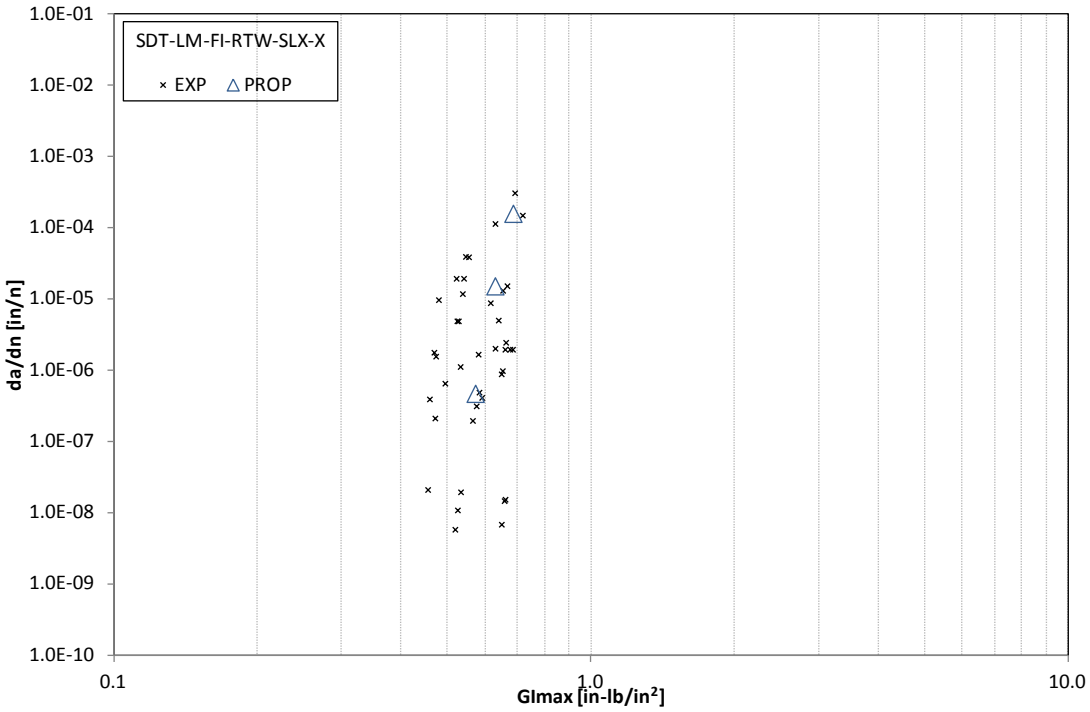

Figure F-4. Fatigue growth da/dn curve for laminate RTW fluid ingressed

F.1.2 ADHESIVE DATA

F.1.2.1 Adhesive RTD Baseline Data

Table F-3. Test summary for adhesive RTD baseline

Specimen	Shaping Parameter [m] English or SI	Shaping Parameter [B] English	Shaping Parameter [B] SI
SDT-AD-BL-RTD-SLX-1	9.234	1.126E-07	5.517E-27
SDT-AD-BL-RTD-SLX-2	6.732	1.877E-07	3.761E-21
SDT-AD-BL-RTD-SLX-3	9.138	7.103E-08	5.707E-27
SDT-AD-BL-RTD-SLX-4	9.857	1.596E-08	3.126E-29
SDT-AD-BL-RTD-SLX-5	8.545	8.532E-08	1.468E-25
SDT-AD-BL-RTD-SLX-6	11.262	4.753E-09	6.579E-33
AVERAGE (individual)	9.128	7.956E-08	6.268E-22
STANDARD DEVIATION	1.495	6.714E-08	1.535E-21
COEFFICIENT OF VARIATION [%]	16.378	8.438E+01	2.449E+02
AVERAGE (all)	7.649	9.626E-08	1.693E-23
AVERAGE (interpolated)	7.789	9.752E-08	8.316E-24

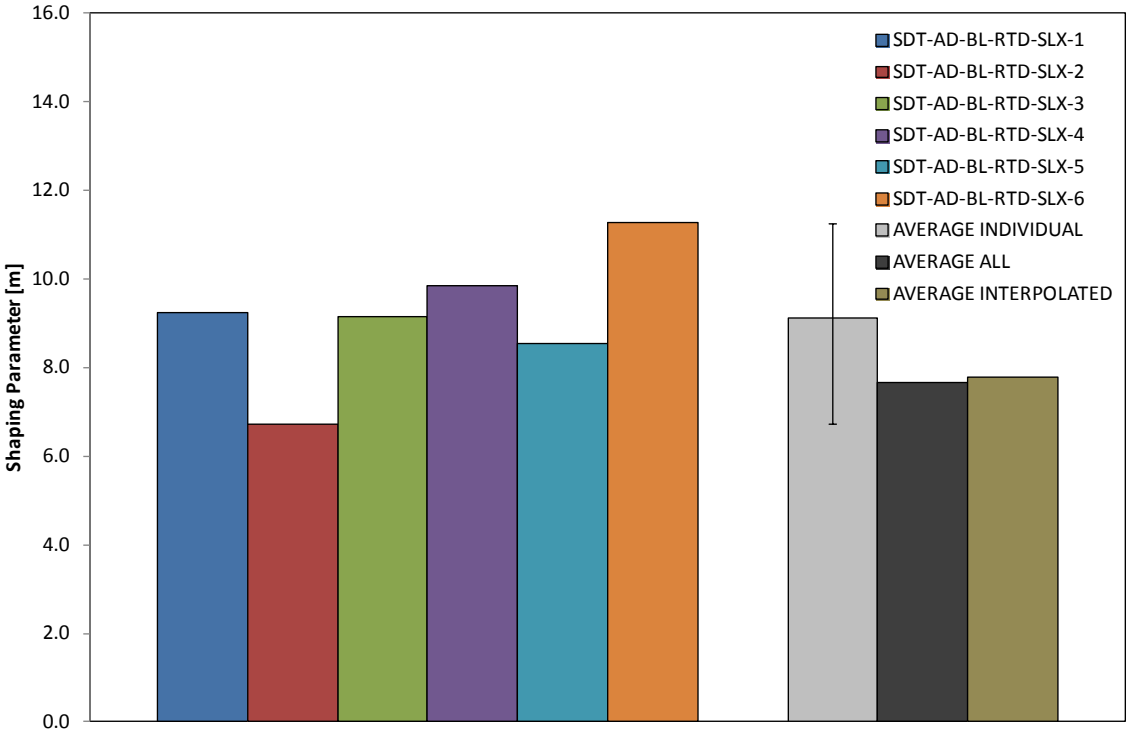

Figure F-5. Shaping parameter (*m*) for adhesive RTD baseline

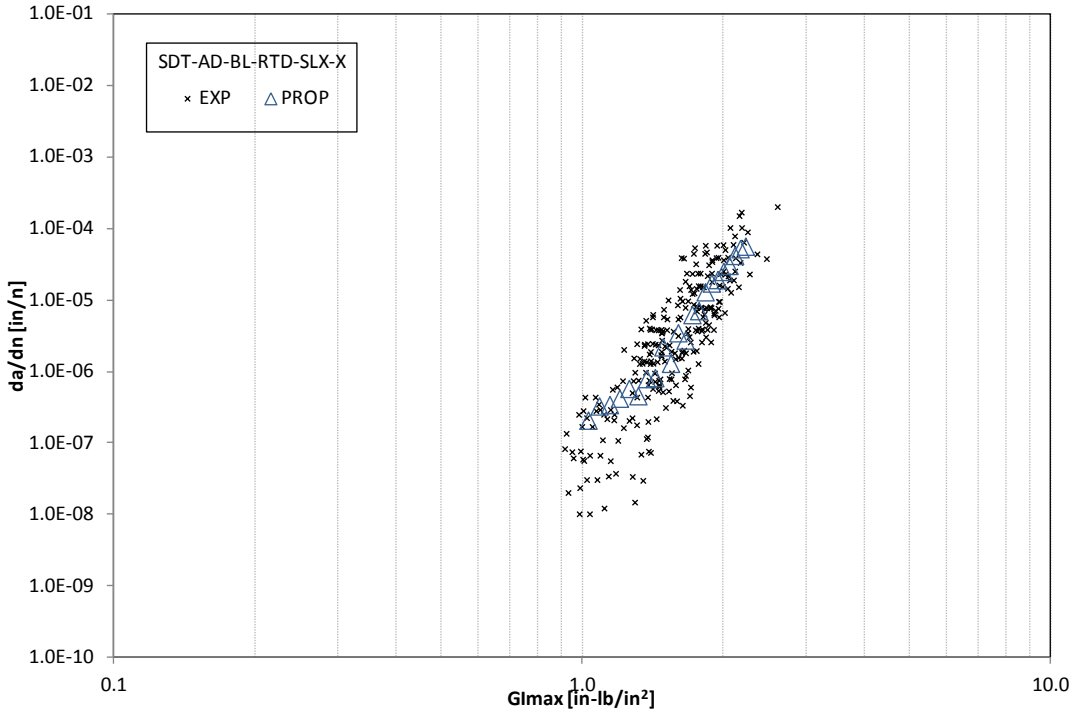

Figure F-6. Fatigue growth da/dn curve for adhesive RTD baseline

F.1.2.2 Adhesive RTW Fluid-Ingressed Data

Table F-4. Test summary for adhesive RTW fluid ingressed

Specimen	Shaping Parameter [m] English or SI	Shaping Parameter [B] English	Shaping Parameter [B] SI
SDT-AD-FI-RTW-SLX-1	14.445	3.358E-10	3.349E-41
SDT-AD-FI-RTW-SLX-2	11.496	5.266E-10	2.171E-34
SDT-AD-FI-RTW-SLX-3	13.809	6.743E-11	1.804E-40
SDT-AD-FI-RTW-SLX-4	13.654	6.543E-10	3.899E-39
SDT-AD-FI-RTW-SLX-5	11.748	7.661E-10	8.608E-35
SDT-AD-FI-RTW-SLX-6	10.505	9.574E-09	6.590E-31
AVERAGE (individual)	12.610	1.987E-09	1.099E-31
STANDARD DEVIATION	1.569	3.725E-09	2.690E-31
COEFFICIENT OF VARIATION [%]	12.444	187.431	244.814
AVERAGE (all)	9.021	8.929E-09	1.310E-27
AVERAGE (interpolated)	10.500	3.946E-09	2.794E-31

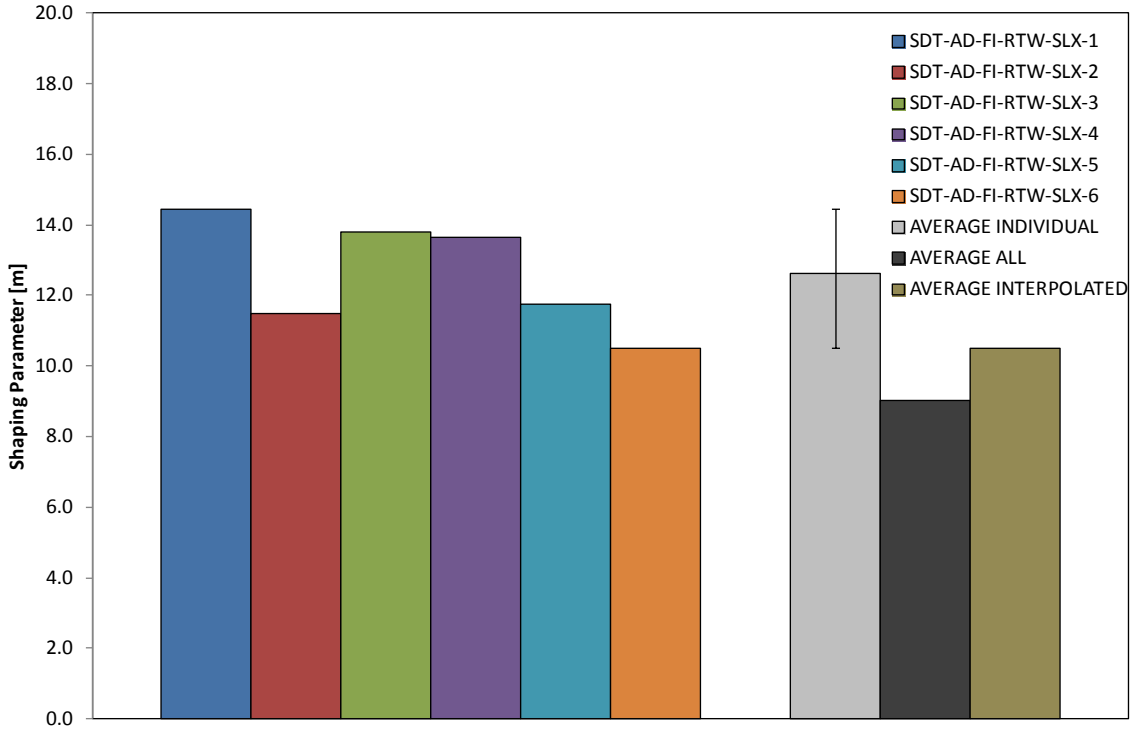

Figure F-7. Shaping parameter (*m*) for adhesive RTW fluid ingressed

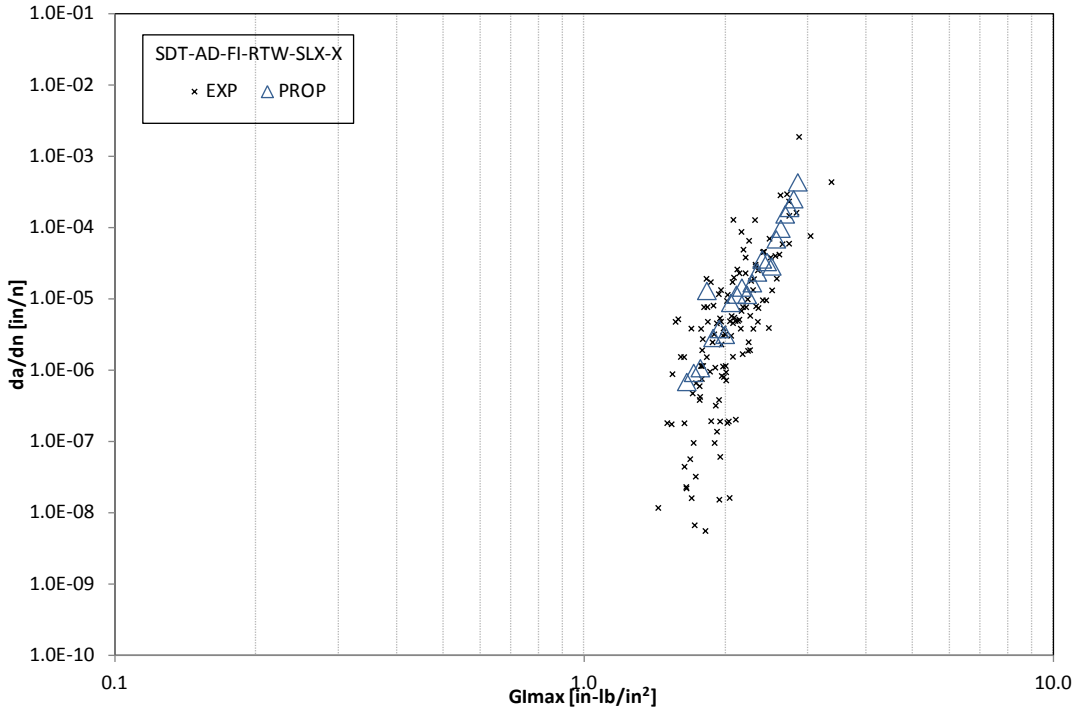

Figure F-8. Fatigue growth da/dn curve for adhesive RTW fluid ingressed